Bacterial Membrane-targeting Cationic-amphiphilic Polymers that Combat Antibiotic Resistance and Neutralize Endotoxins

A Thesis Submitted for the Degree of

Doctor of Philosophy

By

Divakara SS Murthy Uppu

New Chemistry Unit

Jawaharlal Nehru Centre for Advanced Scientific Research

(A Deemed University)

Bangalore - 560064 (INDIA)

January-2016

Dedicated to my Parents

Declaration

I hereby declare that the matter embodied in the thesis entitled "**Bacterial Membrane-targeting Cationic-amphiphilic Polymers that Combat Antibiotic Resistance and Neutralize Endotoxins**" is the result of the investigations carried out by me at the New Chemistry Unit, Jawaharlal Nehru Centre for Advanced Scientific Research, Bangalore, India under the supervision of **Prof. Jayanta Haldar** and that it has not been submitted elsewhere for the award of any degree or diploma.

In keeping with the general practice in reporting the scientific observations, due acknowledgement has been made whenever the work described is based on the findings of other investigators. Any omission that might have occurred due to oversight or error in judgement is regretted.

_____

Mr. Divakara SS Murthy Uppu

(PhD Student)

Certificate

I hereby certify that the matter embodied in this thesis entitled "**Bacterial Membrane-targeting Cationic-amphiphilic Polymers that Combat Antibiotic Resistance and Neutralize Endotoxins**" has been carried out by **Mr. Divakara SS Murthy Uppu** at the New Chemistry Unit, Jawaharlal Nehru Centre for Advanced Scientific Research, Bangalore, India under my supervision and that it has not been submitted elsewhere for the award of any degree or diploma.

_____

Prof. Jayanta Haldar

(Research Supervisor)

Acknowledgments

At the outset, I would take this opportunity to thank each and every one who has contributed directly or indirectly for the completion my thesis. At first, I thank my research supervisor, Prof. Jayanta Haldar for giving me self-confidence I required the most when I joined in his lab. I express my deep sense of gratitude for all his encouragement and inputs during my thesis. I really thank him for instilling the spirit of "Aim High" and he was responsible for my improvement in my presentations. It is from him I learnt to ask the basic and fundamental questions in science. He was instrumental in making me complete as a researcher and I thank him for all that he has done for me.

I came across a wonderful scientist at JNCASR, Prof. C.N.R. Rao F.R.S and I thank him for excellent facilities to carry out world-class research. I really admire him for his talks on the history of science and scientists and it's from him I heard the true meaning of science: observation. I also thank all my course coordinators, Prof. Subi. J. George (JNCASR), Prof. Hemalatha Balaram (JNCASR), Prof P. Balaram (IISc) and Prof. Sidharth Sharma (IISc).

I fail in my duty if I do not express my gratitude to all my collaborators for their excellent cooperation and discussions. I thank Prof. Raju ravikumar and Dr. Jyothi from NIMHANS, Bangalore; Dr. B.R. Shome, Dr. P. Krishnamoorthy and Dr. Sushwetha from ICAR-NIVEDI, Bangalore; Dr. Satyavani V. and Mr. Upayan Baul from IMSc, Chennai; Prof. Leendert W. Hamoen and Mr. Tjalling Siersma from University of Netherlands, Amsterdam; Prof. Octavio L. Franco and his group from Brazil; Prof. Chandrabhas Narayana and Mr. Priyank Singh from CPMU, JNCASR for all their help during this thesis.

I shall never forget the support, encouragement and contribution of my lab members, Padma, Goutham, Jiaul, Venky, Chandradhish, Mohini, Paramita, Swagatam, Dr. Sridhar, Dr. Pinky, Dr. Ashly and Dr. Iqbal. I also thank all the short-term students Nidhi, Ananya, Akshaya, Shanola and Mithun for their help in synthesis of some compounds.

I acknowledge technical staff Dr. R. G. Prakash (Animal house in-charge), Vasu (UV/PL/IR), Mahesh (NMR), Sivakumar (HR-MS) and Selvi (FE-SEM). I am especially thankful to Dr. R. G. Prakash (Animal house in-charge) for helping with animal studies.

I thank my friends Ramana, Suresh, Venky, Saraiah, Nagarjun, Umesh, Arjun, Anand, Chandan, Abishek, Srishti, Dr. Matte, Gangaiah, Dr. Mallikarjun, Murthy, Vijay, Subbareddy, Dr. Avinash, Satya, Dr. Narendra, Dr. Mohit, Pandu, Yugandhar, Shivaprasad, Lakshminarayana reddy, Ramakrishna, Kartheek, Dasari, Soumik, and Lingampalli for making my stay in JNCASR pleasant and enjoyable. I specially thank Dr. Mohit Kumar who has suggested me to join Jayanta's lab at JNCASR.

I would like to express my sincere thanks to all the academic, administrative, security, library, complab and health center staff of JNCASR for making our campus life smooth and easy.

I owe everything to my parents who have always encouraged me to do whatever I want in life and I am indebted to them for being there for me. Next, I thank my chelli and bava for being the most sought-after people for clearing out all my worries. The wonderful thing that happened to me is meeting my soul mate, Manasa. She really is the person who understands me the most and I really thank her for being there throughout the ups and downs of this thesis and of course throughout my life.

Last but not the least I express my gratitude to my guru Bhagwan Sri Sathya Sai Baba who is the sole inspiration for me to carry out research that will be of service to the society. If anyone asks me what is the best phase of my life? I will ever answer that it is my five years of stay at Sri Satyha Sai Institute of Higher Learning and I am what I am today and forever because of that place. I thank all the people from this place who have molded from a nothing to everything. I also thank all my friends and well wishers for their support.

Preface

Flourishing bacterial resistance to antibiotics coupled with languishing antibiotic discovery creates an urgent need for the development of new antimicrobial agents which exert novel mechanisms of action. Conventional antibiotics rely on specific target mechanism of action and hence bacteria can easily develop resistance to them even by single point mutations. Targeting the bacterial cell membrane is a promising approach to combat bacterial resistance to antibiotics. Bacteria have been shown to have fewer tendencies for developing resistance to membrane-targeting agents, for example AMPs. AMPs represent effective therapeutic alternatives to antibiotics but their limited success is due to high cost of production, low stability *in-vivo* and unwanted toxicity to mammalian cells. This thesis aims at design and development of cationic-amphiphilic polymers targeting the bacterial cell membrane and addresses three major problems in bacterial infections namely chronic infections due to biofilms, Gram-negative superbugs and endotoxins.

Optimum amphiphilicity, a tunable balance between cationic charge and hydrophobicity, has been shown to be pivotal for the selective interaction with anionic lipid membranes of bacteria instead of zwitterionic mammalian (human erythrocyte) membranes. However, optimizing this amphiphilicity to selectively target the bacteria sparing the mammalian cells is still an unmet need. **Chapter 2** provides an unprecedented synthetic approach of post-functionalization for the development of cationic amphiphilic antibacterial polymers. The conventional approaches use cationic and hydrophobic monomers as precursors to synthesize amphiphilic antibacterial polymers. On the other hand, our post-functionalization approach incorporates cationic charge and hydrophobicity to a precursor polymer to generate amphiphilic antibacterial polymers. The advantage is that the amphiphilicity can be optimized by merely varying the chemical nature of the side chain alkylating agent used to quaternize the polymer. This novel approach appends different side chain alkylating agents to a precursor polymer (poly(isobutylene-alt-maleic anhydride)) resulting in cationic amphiphilic polymers with tunable amphiphilicity. After identifying the optimum alkyl chain length (C5-C6 i.e. pentyl to hexyl) required for selective antibacterial activity, the side chain chemical structures (ester, amide and ether functional groups) were tuned for further optimization. Hydrophobic alkyl side chain containing polymers showed potent antibacterial efficacy but were toxic to mammalian cells. Hydrophilic ether moiety

containing polymers were neither antibacterial nor toxic to mammalian cells. Although both amide and ester moiety containing polymers were less toxic to mammalian cells, incorporation of amide moieties led to potent antibacterial efficacy compared to ester moieties with membrane-active mechanism of action. Mechanistic studies of these derivatives showed that they depolarized, permeabilized, induced morphological changes in the bacterial membranes, led to leakage of ATP levels and mis-localized essential cell division proteins. This approach of tunable side chemical structure leads to optimal polymers with potent antibacterial efficacy and minimal toxicity to mammalian cells.

Having shown that amide and ester polymers have differences in their antibacterial activity, **Chapter 3** is aimed at understanding these differences. Amide and ester moieties are isosteric in nature and differ in their potency for hydrogen binding. Studies revealed that amide polymers (Q*n*-CmAPs) are potent antibacterial agents with high membrane-disrupting properties compared to their ester counterparts (Q*n*-CmEPs). To understand these differences, bio-physical experiments and molecular dynamics (MD) simulations were performed that showed strong interactions of Q*n*-CmAPs including hydrogen bonding with lipid head groups of bacterial model lipid bilayers, that are absent in Q*n*-CmEPs, make them potent bacterial membrane disruptors. This chapter provides a conceptual advance in understanding the interactions of antibacterial polymers with bacterial cell membranes highlighting the role of hydrogen bonding. Having understood the importance of amide moieties in the strong interactions of cationic amphiphilic polymers with bacterial cell membranes, **Chapter 4** describes the control of hydrophobicity by cyclization, isomerization and unsaturation of amide side chains. Cyclization and unsaturation but not isomerization of side chains resulted in selective antibacterial polymers with low toxicity to mammalian cells. Mechanistic studies indicated the role of tunable hydrophobicity in polymers with different amide side chain architecture. This control of hydrophobicity in amphiphilic polymers drives them selectively towards bacterial cell membranes instead of mammalian membranes. These structural differences in the side chains also led to different interactions with the bacterial cell membranes. Polymers containing chemically different side chains were found to possess variations in their hydrophobicity profiles probably reflecting tunable biological activities. Importantly, unlike antibiotics, bacteria find it difficult to develop resistance to these membrane-active polymers.

Biofilms represent surface attached communities of bacteria that are the underlying cause behind chronic or persistent infections tolerant to antibiotic treatment and host-immune system. It is often difficult to disrupt already established biofilms on surfaces. Bacterial

biofilms accounting for 65-80% of infections in humans place a massive burden on healthcare systems worldwide due to their persistence and chronic nature. Conventional antibiotics are inherently ineffective against biofilms due to various reasons such as slow or non-dividing cells, diffusion barriers and genetic mutations. Targeting the bacterial cell membrane is promising for the eradication of biofilms and also for the elimination of bacterial persisters that constitute biofilms. **Chapter 5** presents the potential of these polymers in disrupting surface established biofilms formed by multi-drug resistant Gram-negative bacteria. Moreover, these polymers kill slow or non-dividing stationary phase and persister bacteria including dispersed cells that release upon biofilm disruption. The membrane-active nature of these polymers was found to be the key of their anti-persister activity. More importantly, these polymers significantly ($p < 0.0001$) decrease the bacterial burden in mice with chronic *A. baumannii* burn wound infection. Bacteria develop rapid resistance to erythromycin and colistin whereas no detectable development of resistance occurs against these polymers even after several passages. These results suggest the potential use of these polymeric biomaterials in disinfecting biomedical device surfaces after the infection has become established and also for the topical treatment of chronic bacterial infections.

Gram-negative 'superbugs' including New Delhi metallo-beta-lactamase-1 ($bla_{\text{NDM-1}}$) producing pathogens have become world's major public health threats. Gram-negative bacteria are inherently resistant to some of the antibiotics and moreover they rapidly acquire resistance to antibiotics through multiple mechanisms of action. The recent havoc of extremely drug-resistant superbugs worldwide is due to Gram-negative bacteria such as carbepenem resistant *Enterobacteriaceae* (CRE), Carbapenemase producing *K. pneumoniae* (KPC) and NDM-1 producing bacteria. Development of molecular strategies that can rehabilitate the 'old antibiotics' and halt the antibiotic resistance is a promising approach to target them. **Chapter 6** describes the ability of these polymers to potentiate (enhancement by >80-1250 fold) antibiotics (tetracyclines and erythromycin) towards Gram-negative superbugs including $bla_{\text{NDM-1}}$ *K. pneumoniae* and $bla_{\text{NDM-1}}$ *E. coli* clinical isolates. More importantly, these polymers potentiate antibiotics to eradicate surface established biofilms formed by Gram-negative bacteria. Further, these membrane-active polymers delay the development of bacterial resistance to antibiotics that highlights the potential of this combination approach in clinical settings. Furthermore, these membrane-active polymers potentiate antibiotic activity in mice models of Gram-negative burn and surgical wound

infections. Organismic studies showed that bacteria had an increased and faster uptake of antibiotics in presence of these polymers which is attributed to the mechanism of re-sensitization. Polymers displayed membrane-active properties such as dissipation of membrane potential and membrane-permeabilization that enabled higher uptake of antibiotics in bacteria. These findings stress the importance of combination approaches of membrane-active molecules and antibiotics to combat MDR Gram-negative superbugs and for the topical treatment of Gram-negative bacterial infections.

Another major problem of Gram-negative infections is harmful and uncontrollable inflammation leading to sepsis that is responsible for a great amount of global mortality. Bacterial endotoxins such as lipopolysaccharide (LPS) released during antibiotic treatment or in response to immune system lead to sepsis. **Chapter 7** deals with the neutralization/detoxification of LPS by cationic amphiphilic polymers. Levels of pro-inflammatory cytokines in human monocytes caused by LPS stimulation were inhibited by more than 80% when co-incubated with these polymers. These reductions were found to be dependent on concentration and more importantly, on the side chain chemical structure due to variations in the hydrophobicity profiles of these polymers. Fluorescence spectroscopy and dynamic light scattering studies delineated that these polymers bind but neither dissociate nor promote LPS aggregation. The binding of polymer to LPS might lead to sort of a pseudo-aggregate formation resulting in LPS neutralization/detoxification. These polymers alone or in combination with antibiotics reduced the inflammation in mouse model of burn wound infections whereas antibiotics alone were ineffective.

In summary, this thesis describes the design and development of cationic amphiphilic polymers that selectively target bacterial cell membrane with low toxicity to mammalian cells. This thesis presents a multi-pronged approach of targeting the bacterial cell membrane namely, the lipid membrane, efflux pumps and endotoxins using a single molecule. These polymers disrupt tough-to-kill bacterial biofilms, combat antibiotic resistance in Gram-negative superbugs and neutralize endotoxins.

Table of Contents

Chapter 1

An Introduction for Targeting the Bacterial Membrane

1.1 Antibiotic resistance - global threat and need

Infectious diseases continue to cause high mortality in global population and are the biggest threat for public health[1]. Infectious diseases contribute for nearly 15 million global deaths every year[1, 2]. The infectious disease burden in India is among the highest in the world[3]. Antimicrobial resistance (AMR) has worsened the global threat of infectious diseases. AMR causes an estimated 700,000 deaths annually and is predicted to cause 10 million deaths annually by 2050. AMR, if left unchecked, will increase the worldwide healthcare costs to $100 trillion by 2050[4,5].

Different classes of antibiotics depending upon their targets have been developed (Fig. 1.1 A). β-lactams and glycopeptides (inhibit cell wall biosynthesis); tetracyclines, aminoglycosides, macrolides, oxazolidinones and lincosamide (inhibit protein synthesis); fluoroquinolones, novobiocin, lincosamide and rifampicin (inhibit RNA/DNA biosynthesis); sulfonamides and trimethoprim (inhibit folate metabolism) and polymyxins (cell membrane, particularly targets lipopolysaccharide (LPS))[6,7]. Development of bacterial resistance to antibiotics is a well studied phenomenon involving various mechanisms (Fig. 1.1 B)[6, 7]. Most of the conventional antibiotics rely on specific receptor-ligand type binding and some of them have to traverse the cell membrane to reach the target. It is this biochemical nature that keeps the bacterial morphology intact and, as a consequence, they can easily develop resistance, for

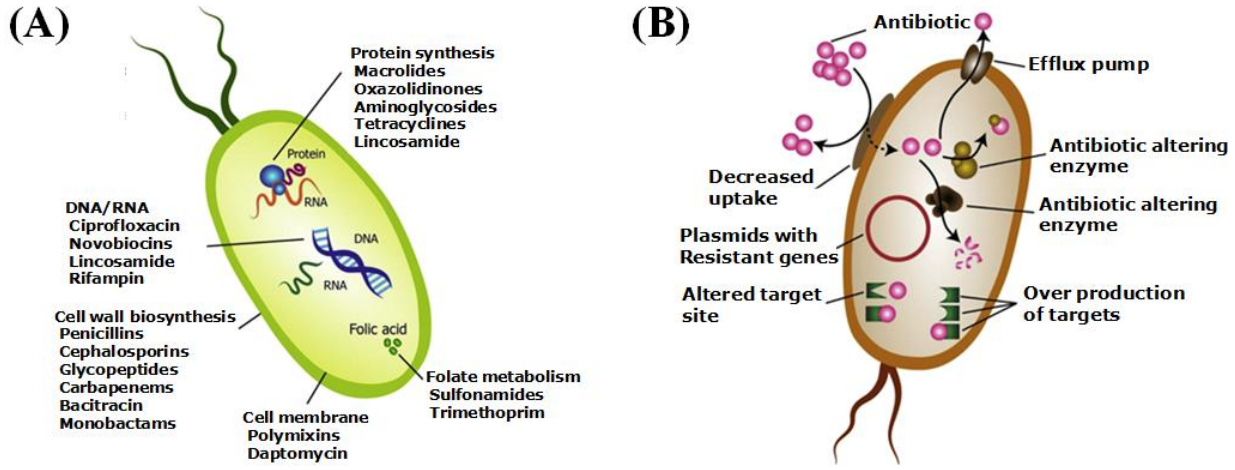

Figure 1.1: Antibiotic targets and antibiotic resistance. (A) Antibiotics have specific targets in bacteria resulting in different classes of antibiotics. (B) Target specific nature of antibiotics leads to various molecular mechanisms of bacterial resistance to antibiotics. Reproduced from reference 105 with the permission from Elsevier Publishing Group.

example through the use of efflux pumps and target mutations or production of drug modifying enzymes. The molecular mechanisms for the development of bacterial resistance to antibiotics include antibiotic altering/degrading enzymes (β-lactams), altered target sites (glycopeptides, fluoroquinolones and protein biosynthesis inhibitors), over production of targets (aminoglycosides), decreased uptake of antibiotics/ exclusion by efflux pumps (tetracyclines, rifampicin, erythromycin, chloramphenicol and novobiocin) and permeability barrier (vancomycin and rifampicin) (Fig. 1.1 B)[6,7].

The WHO Global Report on Surveillance of Antimicrobial Resistance 2014 says that *E. coli* and *K. pneumoniae* have developed more than 50% of resistance to commonly used antibacterial drugs in many settings[8,9]. Of particular concern is the fact that *K. pneumoniae* has developed resistance to carbapenems, a class of β-lactams, last line of available treatment in all WHO regions[8,9]. This ongoing explosion of multi-drug resistant 'superbugs' including the New Delhi metallo-beta-lactamase-1 ($bla_{\text{NDM-1}}$) producing bacteria along with the paucity of antibiotics poses a threat to the global public health (Fig. 1.2 A)[10]. More importantly, carbepenem resistant bacteria such as $bla_{\text{NDM-1}}$ *E. coli* and $bla_{\text{NDM-1}}$ *K. pneumoniae* have become resistant to the highly toxic and the last resort polymyxin antibiotic, colistin[11]. Another antibiotic, tigecycline (tetracycline class) though useful in tissue infections, is less useful in systemic infections[12]. Development of resistance to tigecycline in bacteria being reported in clinical

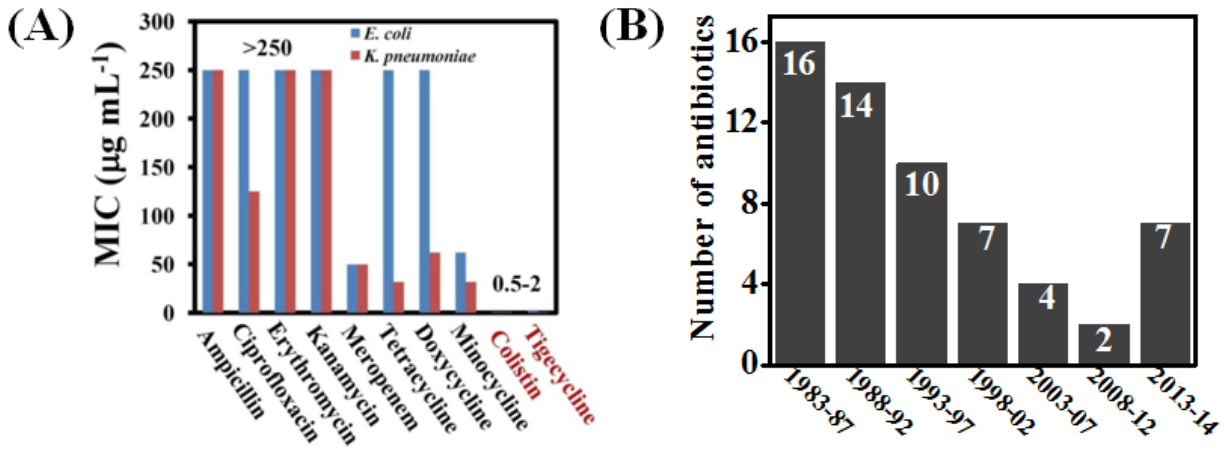

Figure 1.2: Antibiotic resistance and FDA approval of antibiotics. (A) NDM-1 superbugs (*E. coli* and *K. pneumoniae*) have developed resistance to different classes of antibiotics except to colistin and tigeycycline. (B) Approval of antibiotics by FDA has declined rapidly till 2012 and last two years has seen an increase of approved antibiotics.

settings is a matter of worry[12]. Contrary to this situation, the number of antibiotics approved by US FDA (Food and Drug Administration) has declined rapidly from 1983 to 2012[13]. However, the global initiatives to combat AMR have resulted in increase of antibiotics approval in the last two years (Fig. 1.2 B)[14]. The emergence of pan-drug resistant bacteria has become a reality, necessitating the exploration for alternative ammunitions to combat them. This alarming rise of resistant superbugs coupled with the diminishing antibiotic pipeline creates an urgent need for the development of new antimicrobial agents which exert novel mechanisms of action.

1.2 Biofilms and Persisters

Biofilms represent another form of bacterial resistance (inherent and adaptive) to antimicrobial therapy[15-19]. Bacteria live in surface associated communities called biofilms that are the underlying cause behind chronic or persistent infections tolerant to antibiotic treatment and host immune system[20-23]. Biofilms contain a concoction of bacteria and extracellular polymeric substances (EPS) such as polysaccharides, proteins and extracellular DNA (eDNA)[22]. It has been found that nearly 99% of bacteria on earth live in bio-films that are associated with nearly 80% of all bacterial infections in humans[21, 23]. Biofilm formation is found on both abiotic and biotic surfaces ranging from ship hulls to in-dwelling bio-medical devices. Bacteria colonize the surfaces of biomedical devices lead to biofilms and they are also responsible for serious ailments like burn/surgical wound infections, endocarditis, ventilator associated pneumonia (VAP), lung infections in cystic fibrosis (CF) and urinary tract infections (UTI)[20, 24]. To efficiently treat biofilm infections, we need to understand their physiology and pathogenesis.

Infectious biofilms can be divided into surface-related (biotic and abiotic surfaces) and tissue-associated or mucus-embedded cellular aggregates, but it is assumed that all of these involve embedment in a biopolymer matrix that is rich in macromolecular components (Fig. 1.3)[22-24]. Most, if not all, medically important microorganisms can grow in biofilms, including bacteria (Gram-positive and Gram-negative) and fungi. For example, it has been found that biofilms can form without being attached to a surface and that part of the biofilm matrix may originate from the host, such as DNA from the lysis of host cells. The initial stages of biofilm development include the attachment to the surface or to other bacteria by cell surface components such as pili and flagella. As the development takes place or the aggregates grow in size and density, other extracellular components such as lipids, proteins, polysaccharides,

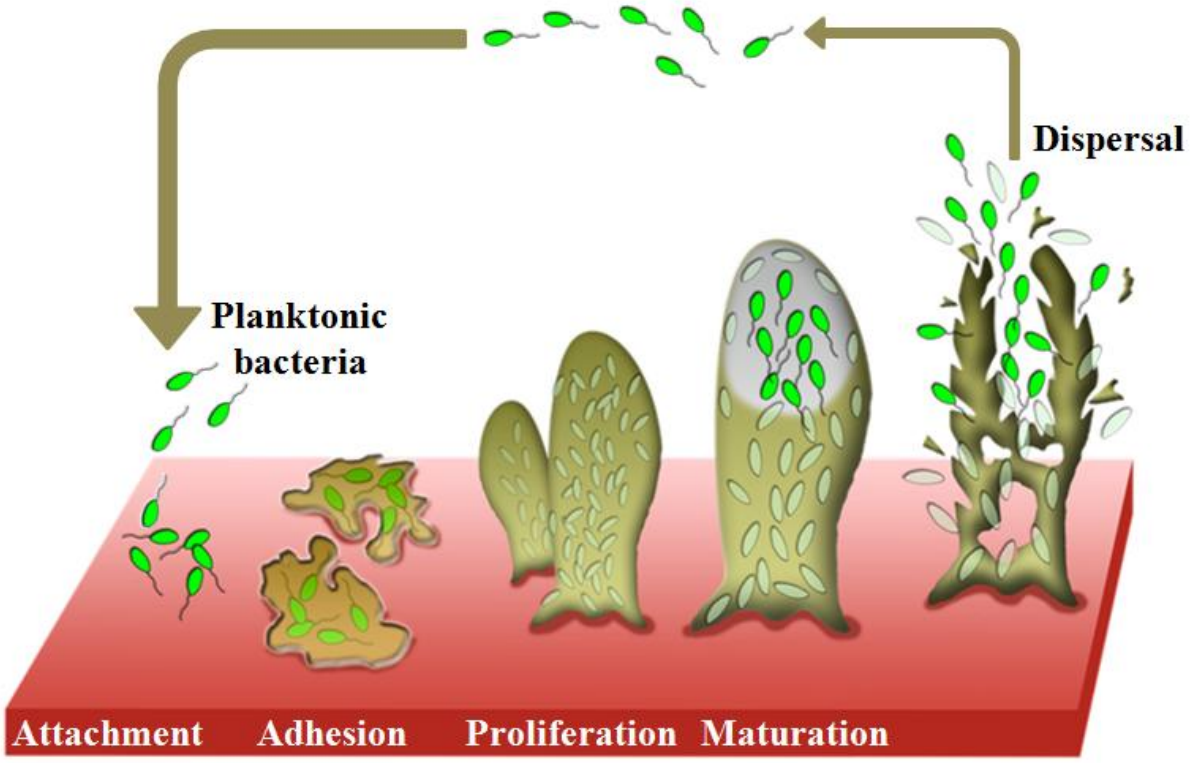

Figure 1.3: Surface establishment of biofilms and their life cycle. Free-floating, or planktonic, bacteria encounter a submerged surface and within minutes can become attached. They begin to produce slimy extracellular polymeric substances (EPS) and to colonize the surface. EPS production allows the emerging biofilm community to develop a complex, three-dimensional structure that is influenced by a variety of environmental factors. Biofilm communities can proliferate and develop within hours to become mature biofilms. Biofilms can propagate through detachment of small or large clumps of cells, or by a type of "seeding dispersal" that releases individual cells. Either type of detachment allows bacteria to attach to a surface or to a biofilm downstream of the original community.

lipopolysaccharides and DNA are excreted to hold the bacteria to maintain the structure and function of biofilms. These extracellular components including the cell surface associated pili and flagella together form the EPS matrix giving the three dimensional structure and stability to the biofilm (Fig. 1.3)[25]. Other than the structure, signaling in biofilms includes production of virulence factors, quorum sensing (a mechanism to communicate to each other)[26, 27] plays an important role in the physiology of the biofilms[22-24]. Due to its structure, not all the cells in the biofilm get equal availability of nutrients[28, 29]. Nutrient availability plays an important part when the layers of the biofilm increase, as gradients of available nutrients and oxygen develop within the biofilms. As a result, bacteria in the inner core of the biofilm do not have access to nutrients

and oxygen, and their growth is halted. It is therefore likely that physiological adaptations such as slow growth have a substantial role in the development of increased antimicrobial tolerance[30].

The important hallmark of chronic, biofilm-based infections is an extreme tolerance or resistance to antibiotics, as well as various other conventional antimicrobial agents, and an extreme capacity to evade the host defense owing to the physical and biological properties of the biofilm[24]. The tolerance of bacteria in biofilms to antimicrobial compounds is multi-factorial, and is an interplay of physical, physiological and adaptive tolerance mechanisms allows biofilm subpopulations to survive, enabling the cells to sustain long-term exposure to antimicrobial agents without loss of viability. Conventional antibiotics are inherently ineffective against biofilms due to various reasons such as slow or non-dividing cells, diffusion barriers and genetic mutations. The physical tolerance mechanism includes limited access to antibiotics. E.g. positively charged antibiotics such as aminoglycosides and polymyxins have physical barriers such as negatively charged EPS containing eDNA or metal cations[24]. Physiological tolerance is determined by the metabolic state of the bacteria. Of late, it is reasoned that the presence of a small sub-population of survivors post antibiotic treatment, called as persisters play a major role in chronic biofilm infections as well as antibiotic resistance[31, 32]. Persister formation is a survival strategy employed by the bacteria to exhibit antibiotic tolerance and they revert to their normal growth conditions after the antibiotic treatment is concluded. These transient phenotypic variants (dormant) of bacteria after growth resumption act as a pool for the development of antibiotic-resistant bacteria and are the underlying cause for relapsing infections. Persister formation was found to be favorable in the presence of stress responses like antibiotic treatment, oxidative stress, nutrient limitation and acidic environment (in macrophages)[31, 33]. Also, these surviving persisters are responsible for the emergence of bacterial resistance to antibiotics. Persisters with reduced metabolic activity exhibit antibiotic-tolerance because the bio-synthetic processes that are the targets for antibiotics are either inactive or corrupt in these cells[32, 34]. Thus, the target-specific mode of action of antibiotics proved unsuccessful for the eradication of chronic infections due to the presence of persisters. In addition to tolerance mechanisms, conventional resistance to antibiotics (independently of biofilm formation) adds to the complexity. Other than the presence of slow or non dividing cells, there are other factors that contribute to the mechanisms of antimicrobial tolerance to biofilms. Thus, targeting dormant persisters, the root-cause, might lead to curbing antibiotic resistance and preventing chronic biofilm infections.

Four main treatment strategies are presented below: prevention, weakening, dispersal and disruption[24, 35, 36]. However, it is likely that a combination of these strategies will be most effective. A promising approach focuses on modifying the biomaterials used in medical devices to make them resistant to biofilm formation[37-43]. If biofilm prevention cannot be achieved, another approach is to disarm bacteria within the biofilm by neutralizing their virulence factors and their biofilm-forming properties. This can be achieved by interfering with virulence factors, quorum sensing[44], siRNAs or iron metabolism. It has been shown *in vitro* that mature biofilms can release antibiotic-susceptible planktonic bacteria or small clusters of bacteria by dispersal. Drugs initiating this process could therefore potentially be used to break up the biofilm. The most efficient approach for treating a biofilm infection is by mechanically or surgically removing the biofilm, but such mechanical removal is obviously only possible on accessible surfaces. Apart from the surgical and mechanical approaches, direct dispersal of biofilms can also be achieved by decreasing the adhesiveness of the bacteria. Importantly, all biofilm dispersal strategies will need to be accompanied by simultaneous antibiotic treatment to eliminate the planktonic bacterial cells that are liberated after dispersion in order to avoid the spread of infection to other parts of the body. Alternative anti-biofilm agents include the use of small molecules, metal nanoparticles[45] and enzymes to disrupt biofilm formation[24]. As discussed above, once a biofilm is established, the bacteria within the biofilms are much more tolerant to microbiocides than planktonic bacteria. Disruption could revert the physical tolerance of bacteria in the biofilm. Given that the matrix stabilizes the biofilm, targeting the production of the matrix or its disruption might weaken the biofilm, leading to improved efficacy of antibiotics, or the release of bacteria from the biofilm. Another approach for disruption strategies could be the application of enzymes that degrade the biofilm matrix (e.g. DNases that target eDNA)[24]. However, there still exists a need for a new approach for developing anti-persister and anti-biofilm strategies which will be useful in targeting the root-cause of antibiotic resistance as well as recalcitrant infections. It is hypothesized that high doses of antibiotics, combined with agents that weaken the biofilm, could enable the effective eradication of biofilms[46-49].

As the target specific action of antibiotics proved unsuccessful to combat the global problem of bacterial resistance to antibiotics (in planktonic as well as biofilm state), there exist a need for the search of novel targets[50, 51]. Targeting the bacterial cell membrane has been found to be a promising approach to combat the development of bacterial resistance to antibiotics and

chronic biofilms[51].

1.3 Bacterial cell membrane: structure and function

The bacteria cell envelope is a complex multilayered structure that protects these organisms from harsh environmental conditions[52,53]. Bacteria on a broad classification fall into two major groups, Gram-negative and Gram-positive bacteria based on a staining procedure developed by Christian Gram in 1884. The differences with respect to the composition, organization, structure and function of the bacterial cell envelope have been very well understood (Fig. 1.4)[52, 54].

Bacteria contain extracellular structures such as fimbriae, pili, S-layers, glycocalyx and flagella that are required for motility, host-tissue interactions, and adhesion to surfaces[52, 53]. The bacterial cell wall differs from that of all other organisms by the presence of peptidoglycan which is located immediately outside of the cytoplasmic membrane (inner membrane, IM). Gram-negative bacteria are surrounded by a thin peptidoglycan (PG) cell wall, which itself is surrounded by an outer membrane (OM) containing lipopolysaccharide (LPS), proteins, enzymes and porins. Gram-positive bacteria lack an outer membrane but are surrounded by layers of peptidoglycan many times thicker than is found in the Gram-negative bacteria. The composition of PG is similar for both Gram-positive bacteria and Gram-negative bacteria and is made up of a polysaccharide backbone consisting of alternating *N*-acetylmuramic acid (NAM) and *N*-acetylglucosamine (NAG) residues in equal amounts cross-linked by short chains of amino acids (peptide). Variations in the linkage of NAM and NAG residues do exist in different species of bacteria. Threading through these layers of peptidoglycan are long anionic polymers, called teichoic acids (TA) which are linear polymers of polyglycerol or polyribitol substituted with phosphates and a few amino acids and sugars in Gram-positive bacteria. The OM is basically stapled to the underlying peptidoglycan by a lipoprotein called Lpp, murein lipoprotein. The OM and IM delimit an aqueous cellular compartment called the periplasm. The periplasm is densely packed with proteins and it is more viscous than the cytoplasm. Cellular compartmentalization allows Gram-negative bacteria to sequester potentially harmful degradative enzymes such as RNAse or alkaline phosphatase. Because of this, the periplasm has been called an evolutionary precursor of the lysosomes of eukaryotic cells. Other proteins that inhabit this compartment include the periplasmic binding proteins, which function in sugar and amino acid transport and chemotaxis, and chaperone-like molecules that function in envelope biogenesis. Gram-positive

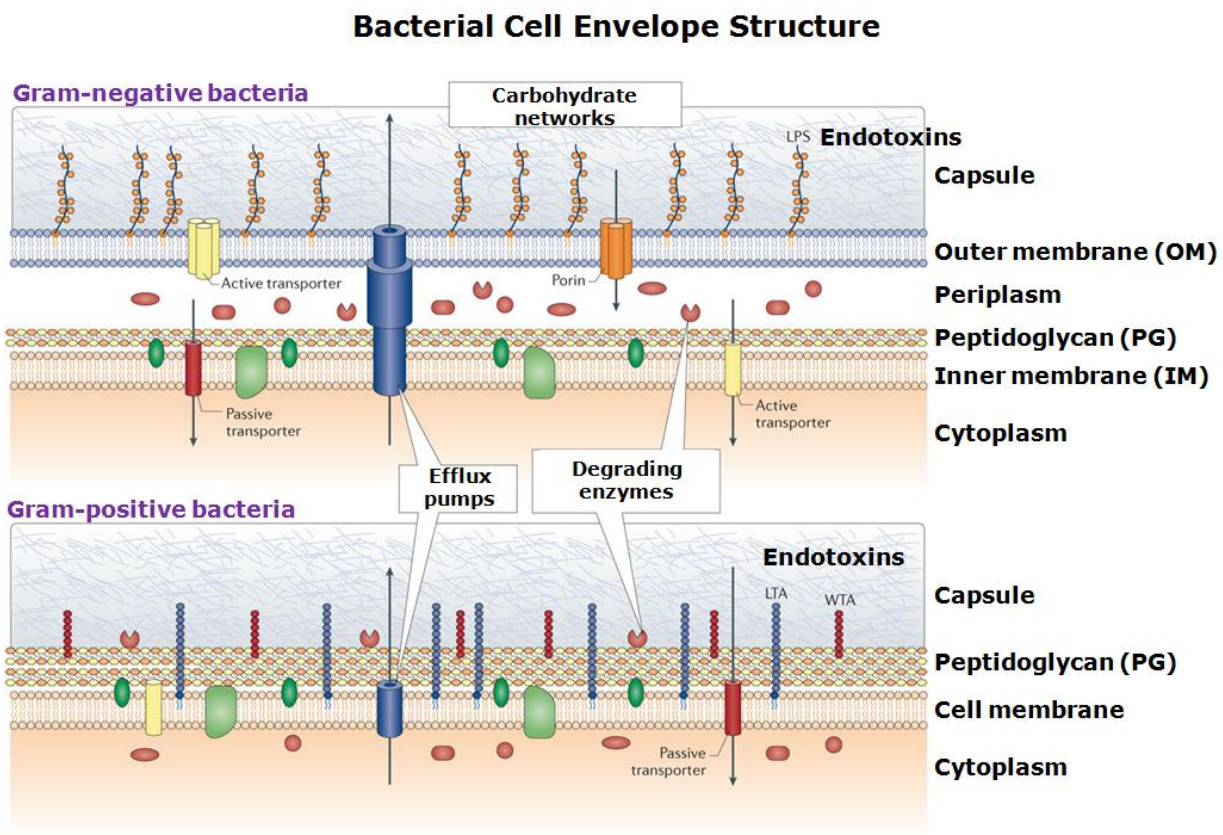

Figure 1.4: Gram-negative and Gram-positive cell walls. Gram-negative bacteria possess both inner and outer membrane surrounding a thin peptidoglycan layer and periplasmic space. Gram-positive bacteria have a thicker peptidoglycan layer to protect a single cytoplasmic membrane. Transport of antibiotics and other extracellular compounds across bacterial membranes occurs both actively and passively, depending on the nature of the transporter. There are numerous components associated with both types of cell walls that limit the ability of antibiotics to penetrate these structures, such as efflux pumps that expunge toxins, defensive enzymes, such as β-lactamases, and complex carbohydrate networks that create a protective capsule coating. Integral and peripheral membrane proteins are shown in light and dark green, respectively. Endotoxins such as LPS (lipopolysaccharide), LTA (lipoteichoic acid) and WTA (wall teichoic acid) contribute to the pathogenecity of both bacteria to a host immune system. Reproduced from reference 54 with the permission from Nature Publishing Group.

bacteria contain lipotechoic acids (LTA) that are anchored to the IM apparently directed outward at right angles to the layers of peptidoglycan. Bacteria lack intracellular organelles, and consequently, all of the necessary functions are performed in the IM which is common for both Gram-positive and Gram-negative bacteria. Its main function is as a selective permeability barrier that regulates the passage of substances into and out of the cell. Bacterial cell membranes are composed of 40% phospholipid and 60% protein. The phospholipids are amphoteric

molecules with a polar hydrophilic glycerol "head" attached via an ester bond to two nonpolar hydrophobic fatty acid tails, which naturally form a bilayer in aqueous environments. Dispersed within the bilayer are various structural and enzymatic proteins which carry out most membrane functions (Fig. 1.4)[52, 53].

As said earlier, most of the essential functions of bacteria are carried out by the cell envelope[52, 53]. The OM of the Gram-negative bacteria contains LPS, proteins, enzymes and porins acting as an additional selective permeability barrier. LPS plays a critical role in the barrier function of the OM. LPS molecules bind each other avidly, especially if cations like Ca^{2+} or Mg^{2+} are present to neutralize the negative charge of phosphate groups present on the molecule. LPS is responsible for the endotoxic shock associated with the septicemia caused by Gram-negative organisms. LTA in Gram-positive bacteria also plays an analogous role as LPS in Gram-negative bacteria. The bacterial cell wall provides structural integrity to the cell. In prokaryotes, the primary function of the cell wall is to protect the cell from internal turgor pressure caused by the much higher concentrations of proteins and other molecules inside the cell compared to its external environment. Peptidoglycan is responsible for the rigidity of the bacterial cell wall and for the determination of cell shape. Since the cell wall is required for bacterial survival, but is absent in eukaryotes, several antibiotics (β-lactams and glycopeptides) stop bacterial infections by interfering with cell wall synthesis, while having no effects on human cells which have no cell wall [6]. Since prokaryotes lack any intracellular organelles for processes such as respiration or photosynthesis or secretion, the cytoplasmic membrane subsumes these processes for the cell and consequently has a variety of functions in energy generation, and biosynthesis. For example, the electron transport system that couples aerobic respiration and ATP synthesis is found in the prokaryotic membrane. The photosynthetic chromophores that harvest light energy for conversion into chemical energy are located in the membrane. Hence, the plasma membrane is the site of oxidative phosphorylation and photophosphorylation in prokaryotes, analogous to the functions of mitochondria and chloroplasts in eukaryotic cells. Besides transport proteins that selectively mediate the passage of substances into and out of the cell, prokaryotic membranes may contain sensing proteins that measure concentrations of molecules in the environment or binding proteins that translocate signals to genetic and metabolic machinery in the cytoplasm. Membranes also contain enzymes involved in many metabolic processes such as cell wall synthesis, septum formation, membrane synthesis, DNA

replication, CO_2 fixation and ammonia oxidation. For e.g. the efflux pumps that pump in essential nutrients and exclude toxins (including antibiotics) from bacteria encompass the whole bacterial cell envelope[6, 7]. The predominant functions of procaryotic membranes are listed here[52].

Functions of the cytoplasmic membrane (IM)

i. Osmotic or permeability barrier
ii. Location of transport systems for specific solutes (nutrients and ions)
iii. Energy generating functions, involving respiratory and photosynthetic electron transport systems, establishment of proton motive force, and transmembranous, ATP-synthesizing ATPase
iv. Synthesis of membrane lipids (including lipopolysaccharide in Gram-negative cells)
v. Synthesis of murein (cell wall peptidoglycan)
vi. Assembly and secretion of extracytoplasmic proteins
vii. Coordination of DNA replication and segregation with septum formation and cell division
viii. Chemotaxis (both motility and sensing functions)
ix. Location of specialized enzyme system

This results in the understanding that the cell envelope contains cell wall, lipid membrane, transport systems, proteins and enzymes (e.g. efflux pumps) and endotoxins that perform a plethora of essential cellular, physiological and pathological processes required for survival of bacteria. Bacterial cell envelope is such an important and integral part of bacteria that it can be considered as "Heart of the bacteria" and can be developed as a new target for novel antibacterial agents[51, 55-57]. Since this thesis largely consists of targeting the parts of the bacterial cell envelope namely lipid membrane, collapsing the efflux energy (efflux pumps) and endotoxins, their structure and function are dealt in detail.

1.3.1 Efflux Pumps

Active efflux systems (efflux pumps) are present in all living cells[58-62]. They participate in the detoxifying process expelling various harmful compounds and xenobiotics. Originally described in mammalian cancer cells, this drug transport was reported among bacteria with tetracycline drugs in the early 1980s. The function of efflux pumps is to transport drugs through the bacterial

envelope and limit the intracellular accumulation of toxic compounds (for example, antibiotics, antimicrobial peptides, metals and detergents). Efflux pumps are one of the major mechanisms of resistance (both inherent and acquired) to antibiotics in bacteria, mainly the Gram-negative bacteria. Efflux pumps, by origin, are important part of the bacteria that they use for the transport of nutrients, throwing out the toxins/waste by-products. However, in the aspect of resistance, bacteria use these pumps as a module to expunge out the antibiotic that is detrimental to their survival. Interestingly, this efflux decreases the antibacterial activity of unrelated drug families and can be considered a 'general' resistance mechanism that cooperates with the target mutations, reduced membrane permeability or drug modifications. Consequently, bacteria become insensitive to antibiotic therapy and the colonization of patients is made easier.

To design new molecules to inhibit the activity of efflux pumps, we need to understand the structure and function of efflux pumps[58, 59, 61]. The envelope of Gram-negative bacteria comprises two membranes: the inner, or cytoplasmic, membrane and the outer membrane, which are separated by the periplasmic space. This organization results in the presence of various proteins that expel different harmful compounds (positively or negatively charged, neutral or zwitterionic). This pumping out due to the activity of the efflux pumps is energized by ATP hydrolysis or by an ion antiport mechanism that contributes to the membrane energy state[58, 59, 61].

ATP-dependent efflux systems. The ATP binding cassette (ABC) transporters comprise a large family of proteins, found in both prokaryotic and eukaryotic systems, which exploit the free energy of ATP hydrolysis to energize transport.

Proton (and sodium) motive force driven multidrug systems. The pmf (also known as the electrochemical proton gradient, Fig. 1.5) (Δp) consists of an electrical potential ($\Delta\Psi$; interior negative) and a chemical proton gradient (ΔpH; interior alkaline). The secondary drug transporters function as antiporters, and therefore mediate drug efflux in exchange with proton (or sodium ion) translocation into the cell (Fig. 1.5). Secondary transporters are sub-divided into distinct families based on similarities in the primary and secondary sequences.

i. Small multidrug resistance (SMR)
ii. Resistance–nodulation–division (RND)
iii. Major facilitator superfamily (MFS)
iv. Multidrug and Toxic compound Extrusion family (MATE)

Efflux pumps can consist of either a single component or multiple components. In Gram-negative bacteria, efflux machineries display a complex arrangement comprising a cytoplasmic membrane-located transporter, a periplasmic-located membrane adaptor protein and an outer-membrane channel protein. Examples of efflux pumps from each family are shown in Fig. 1.5. Efflux pumps of the RND family, which is expressed by Gram-negative bacteria and is associated with clinically significant MDR, is organized as tripartite systems. The well studied

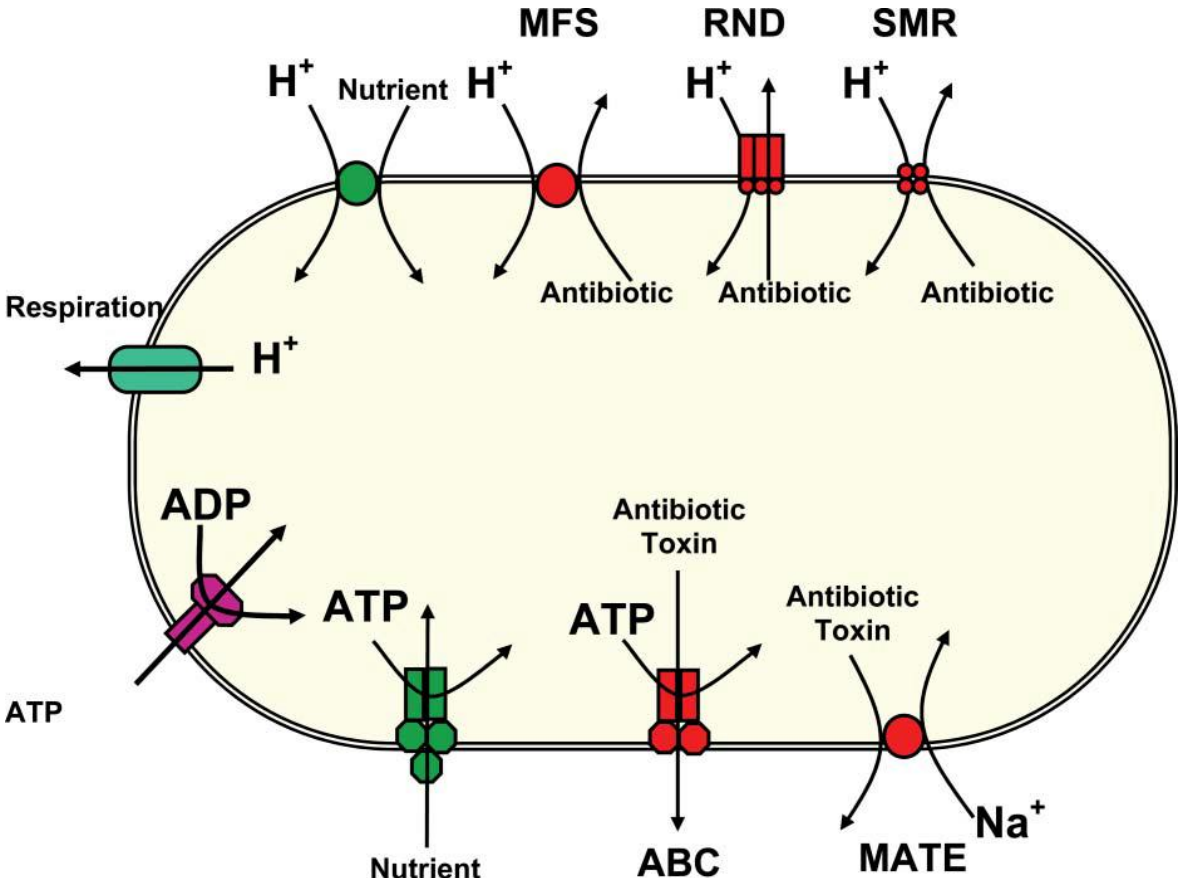

Figure 1.5: Efflux systems and their energisation in bacteria. The large oval represents the cytoplasmic membrane of the microorganism. A transmembrane electrochemical gradient of protons is generated by respiration shown on the left. The gradient may be used to drive ATP synthesis, which is used directly to energise ABC-type transport systems shown bottom left. In bacteria these usually comprise two-five proteins, though the polypeptide elements have become fused in many prokaryotes and eukaryotes. Also shown are examples of the RND, SMR, MATE and MFS types of efflux system. The electrochemical gradient of protons can also be used to energise the MFS proton-nutrient symport and proton/substrate antiport secondary active transport systems shown top left. The gradient of sodium ions may also be used to energise some transport systems, one example of which is shown bottom right. Reproduced from reference 61 with permission from Royal Society of Chemistry.

AcrBTolC and the MexA-OprM are the main (archetype) MDR antibiotic efflux systems of *E. coli* and *P. aeruginosa*. These efflux pumps comprise the following: a transporter (efflux) protein (for example, AcrB), which is located in the inner (cytoplasmic) membrane of the bacterium; an accessory protein (also known as a membrane-fusion protein) (for example, AcrA), which is located in the periplasmic space; and an outer-membrane protein (also known as an outermembrane protein channel) (for example, TolC), which is located in the outer membrane of the bacterium. Using the AcrAB–TolC system (that is, the efflux pump comprising AcrA, AcrB and TolC) as an example, it is thought that the transporter protein AcrB, similar to AcrD, captures its substrates either from within the phospholipid bilayer of the inner membrane or from the cytoplasm, and then transports them to the extracellular medium through TolC, which forms a channel in the outer membrane. The cooperation between AcrB and TolC is mediated by the periplasmic accessory protein AcrA. Efflux through RND-family pumps is driven by the proton motive force, an electrochemical gradient in which the movement of hydrogen ions drives transport of the substrate[58, 59, 61].

It is well established that MDR efflux pumps encoded by bacteria can confer clinically relevant resistance to antibiotics[62]. It is now understood that these efflux pumps also have a physiological role(s). They can confer resistance to natural substances produced by the host, including bile, hormones and host defence molecules. In addition, some efflux pumps of the RND family have been shown to have a role in the colonization and the persistence of bacteria in the host. There is accumulating evidence that efflux pumps that confer clinically relevant antibiotic resistance are important for the pathogenicity of the bacterium. It is also possible that, in some species, efflux pumps that export antimicrobial agents also export virulence determinants, such as adhesins, toxins or other proteins that are important for the colonization and infection of human and animal cells. Taking into account the available data regarding the various efflux pumps in bacteria that cause diverse infections in humans, animals and plants, it is clear that these systems have a fundamental role in allowing bacteria to survive in their ecological niche. With the increasing evidence that MDR efflux pumps have a role in bacterial pathogenicity, research is urgently required to elaborate this role and to investigate whether mutants that overexpress MDR efflux pumps have increased virulence. This knowledge is important for the development of MDR efflux-pump inhibitors, which is an ongoing area of drug development. Our current understanding of MDR efflux pumps indicates that such inhibitors

would be invaluable tools to help clear bacterial infection because of their dual function: restoration of the activity of agents to which efflux pumps confer resistance and reduction in the ability of bacteria to colonize their host or even to cause infections[62].

1.3.2 Endotoxins

As explained earlier, research on septic shock has increased the awareness that this syndrome is caused by a host response to bacterial cell wall components; called pathogen associated molecular patterns (PAMPs) or endotoxins (Fig. 1.6)[63]. Endotoxins have different target receptors on the immune cells of the human body. In the case of Gram-negative bacteria, LPS, a part of the outer membrane, has been identified as the major immunostimulatory component[64]. LPS is released during bacterial growth as well as after lysis of the bacterial cells, for instance, by the actions of antibiotics, although antibiotics may differ in their capacity to cause lysis. The mechanism of how the release of endotoxins upon antibiotic treatment causes deleterious effects on organ function of the human body is more or less clearly understood. LPS is considered to be the most important bacterial factor in the pathogenesis of the Gram-negative septic syndrome. It induces the release of the proinflammatory cytokines (TNF-α, IL-6 etc.). These cytokines activate a cascade of secondary inflammatory mediators, eventually leading to endothelial damage and hemodynamic and metabolic derangements. Analogous to the LPS in Gram-negative bacteria, two cell wall components of the Gram-positive microorganism, *S. aureus*, i.e., PG and LTA are also able to induce the production of proinflammatory cytokines by monocytes *in vitro*. LTA and PG are released spontaneously into the culture medium during growth of Gram-positive bacteria. LPS and LTA have long been known to be the culprits in triggering the inflammation by acing as the TLR4 and TLR2 agonists respectively of human immune cells like macrophages. Both PG and LTA have been shown to stimulate inflammatory responses in a number of *in vivo* and *in vitro* experimental models. Gram-positive bacteria also produce the membrane bound lipopeptides and some secrete exotoxins, such as staphylococcal enterotoxin B (SEB) and toxic shock syndrome toxin (TSST-1). These components are important in the pathophysiological conditions associated with specific infections[63-65].

Adequate antibiotic treatment is thought to be pivotal in the therapy of severe Gram-negative infections, but many *in-vitro* as well as animal and clinical studies have indicated that the endotoxin concentration may increase following bacterial death caused by exposure to

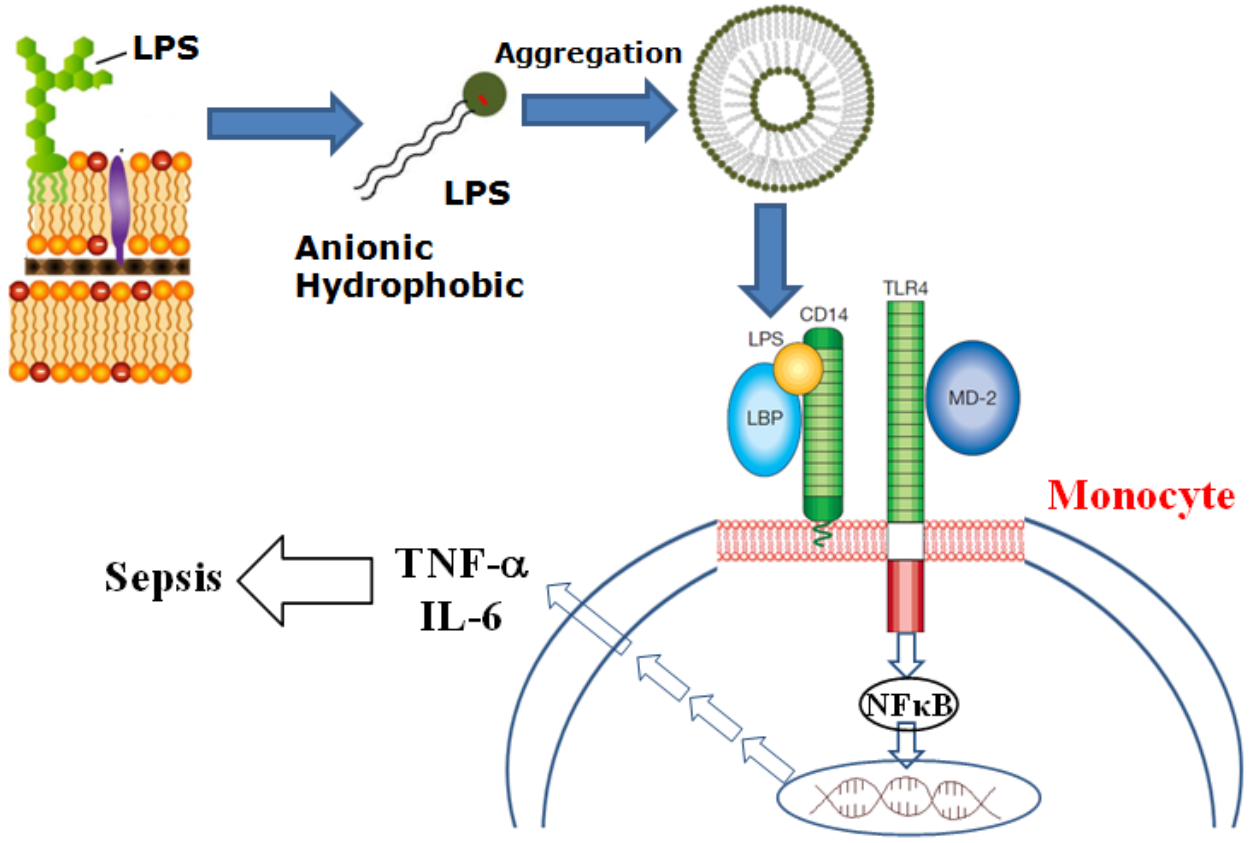

Figure 1.6: Recognition of LPS on the surface of phagocytes. LPS released from Gram-negative bacteria either due to antibiotic treatment or recognition by innume system is opsonized by LBP, and the complex is recognized by the opsonic receptor, CD14, on the macrophage surface. CD14 associates with the cell surface by means of a glycolipid linkage and is not capable of generating a transmembrane signal. It is likely that the LPS–LBP–CD14 ternary complex activates TLR4 in some way, which in turn activates downstream signaling processes to produce the pro-inflammatory cytokines such as TNF-α, IL-6 and that eventually leads to sepsis. Adapted from reference 64 with the permission from Nature Publishing Group.

antibiotics[65]. Moreover, incubation with antibiotics was found to enhance the release of LTA and PG. Three mechanisms can account for this increase: (i) accumulation of bacterial biomass following antibiotic treatment, for instance because of filament formation; (ii) an increase in the accessibility of endotoxin that remains bound to the bacteria, which was demonstrated even when sub-MIC levels of antibiotics were used; or (iii) release of unbound (free) endotoxin. To avoid confusion, the overall increase in the amount of biologically active endotoxin is best described as an increase in endotoxin exposure. Different classes of antibiotics either aggravate or reduce sepsis. Overall, the use of antibiotics instead of causing beneficial effects can lead to

adverse conditions of aggravating the sepsis disease condition rather than treating it. Unfortunately, the current crisis of antibiotic resistance makes even the little beneficial effects of antibiotics unavailable for the sepsis treatment. Over 30% of neonatal sepsis deaths are attributed to antibiotic resistance[65]. There is an urgent need for developing alternative approaches for the treatment of sepsis in the era of antibiotic resistance. Alternative approaches include the bacterial cell membrane targeting molecules that can bind and neutralize the effect of endotoxins have the potential for the treatment of sepsis on their own or in combination with antibiotics.

1.3.3 Lipid membrane

Lipid membrane is an important part of bacteria that performs most of the essential cellular process of bacteria more than just providing the permeability barrier. Thus, targeting the lipid membrane indirectly hampers functions required for the survival of bacteria. More importantly, it has been shown that non-specific targeting of bacterial cell membrane bestows low propensity for the development of bacterial resistance[66, 67]. Since both eukaryotic and prokaryotic cytoplasmic membranes contain phospholipid bilayers, driving the selective interactions of antibacterial agents towards bacterial cell membranes instead of mammalian membranes requires the understanding of differences in their composition. Bacterial cell membranes contain higher proportion of anionic phospholipids (PG: phosphatidylglycerol (-) and CL: cardiolipin (--)) in the outer leaflet including some amount of zwitterionic phosphatidylethanolamine (PE, ±) in the inner leaflet (Table 1.1)[68, 69]. On the other hand, mammalian membranes comprise of a variety of lipids, including, but not limited to, zwitterionic lipids, acidic lipids, glycolipids, and cholesterol (CH). For e.g. human erythrocytes contain majority of zwitterionic (±) phospholipids (PC:phosphatidylcholine, PE:phosphatidylethanolamine, SM:sphingomyelin) in their outer leaflets and has phosphatidylserine (PS, -) in addition to the above in the inner leaflets[68, 69]. Furthermore, the distribution of acidic lipids in eukaryotic membrane is highly disordered and very complex in nature[70]. Conversely, a number of studies using various biochemical approaches and biophysical techniques, including sophisticated solid-state NMR techniques, showed that cholesterol increases the level of membrane order[70, 71]. These differences in the composition of membrane phospholipids provides an understanding that bacterial cell membranes are generally more negatively charged compared to the human erythrocyte counterparts and are less rigid and less ordered due to lack of cholesterol.

Table 1.1: Differences in lipid composition between bacterial and human red blood cells (hRBCs).

Cell Type	PC (±)[a]	PE (±)	PG (-)[b]	PS (-)	SM (±)	CL (--)	CH (0)[c]
E. coli	-	80%	15%	-	-	5%	-
S. aureus	-	-	58%	-	-	42%	-
RBC							
Outer leaflet	33%	9%	-	-	18%	-	25%
inner leaflet	10%	25%	-	10%	5%	-	-

[a,b,c]represent zwitterionic, anionic and neutral phospholipids respectively. PC:phosphatidylcholine, PE:phosphatidylethanolamine, PG: phosphatidylglycerol, PS: phosphatidylserine, SM:sphingomyelin, CL: cardiolipin and CH: cholesterol.

1.4 Targeting the bacterial cell membrane: An under explored target

1.4.1 Membrane-targeting peptide antibiotics

Peptide antibiotics that have specific targets in cell membrane of both Gram-positive and Gram-negative bacteria have been reported in literature (Table 1.2)[55]. Polymyxin B and polymyxin E (colistin) target the LPS of Gram-negative bacteria and hence are not effective against Gram-positive bacteria. Daptomycin is another antibiotic that shows a calcium dependent interaction with PG against Gram-positive bacteria and its target has been found absent in Gram-negative bacteria. Both polymyxins and daptomycin were approved by FDA[55]. Telomycin targets cardiolipin whereas Cinnamycin and Duramycin target phosphatidylethanolamine and Papuamide (A & B) targets phosphatidylserine in the bacterial cell membrane. Recently, Lysocin E has been reported that inhibits the synthesis of menaquinone, an essential component of bacterial cell membrane[55].

Table 1.2: Membrane-targeting peptide antibiotics.

Antibiotic	Target in the cell membrane	Reference
Polymyxin	Lipopolysaccharide (LPS)	Approved by FDA[55]
Daptomycin	Phosphatidylglycerol (PG)	Approved by FDA[55]
Telomycin	Cardiolipin (CL)	[55, 72]
Cinnamycin	Phosphatidylethanolamine (PE)	[73]
Duramycin	Phosphatidylethanolamine (PE)	[73]
Lysocin E	Menaquinone	[74]
Papuamide	Phosphatidylserine (PS)	[55]

1.4.2 Antimicrobial peptides (AMPs)

Taking the advantage of the differences in the lipid composition of bacterial and mammalian cell membranes, two fields of research, polymeric disinfectants[75-79] and antimicrobial peptides (AMPs)[80-85] have emerged in the past few decades targeting the bacterial cell membrane. The major molecular characteristics of these membrane-targeting antibacterial agents are cationic charge and hydrophobicity as the bacterial membranes containing negatively charged phospholipids. In the past two decades, antimicrobial peptides (AMPs) have received increasing attention due to their broad-spectrum activities and ability to combat multi-drug-resistant microbes. In nature, AMPs (about 12-80 amino acid residues) are the key components of innate immune response against infections in eukaryotes (host defense peptides). The mechanisms of action of AMPs are diverse and different from that of the conventional antibiotics. Most of the conventional antibiotics rely on specific receptor-ligand type binding and they have to traverse the cell membrane to reach the target. It is this biochemical nature that keeps the bacterial morphology intact and, as a consequence, they can easily develop resistance, for example through the use of efflux pumps and target mutations or production of drug modifying enzymes. In contrast, AMPs do not have a specific target in microbes, instead bind to bacterial surfaces, insert into cell membranes, thus leading to disruption of membrane integrity and cell death. Alternatively, some AMPs show additional mechanisms of cell death, like binding to cytoplasmic components and inhibition of cell wall synthesis after the insertion into the cell membrane. This biophysical mechanism of action has been shown to be the contributing factor for these peptides to have relatively low propensity for the development of bacterial resistance. Also, it has been recognized that AMPs are involved in immunomodulation wherein they harness the innate immune system to combat bacterial infections (HDPs- host defense peptides)[86-90].

Despite the immense diversity of AMPs, the majority share common structural features like net cationic charge and amphiphilic nature wherein the hydrophilic and hydrophobic residues segregate into the opposite regions of the molecule (facial amphiphilicity)[81-83]. The net positive charge of AMPs ensures their selective binding to the negatively charged lipid membranes of the bacteria compared to the zwitterionic lipid membranes of the mammalian cells (Fig. 1.7). In addition, the inherent or induced amphipathic organization (secondary structure formation) exhibited by some of the AMPs facilitates binding and insertion into the lipid bilayers. During the past few decades, a great deal of effort has gone into the development of

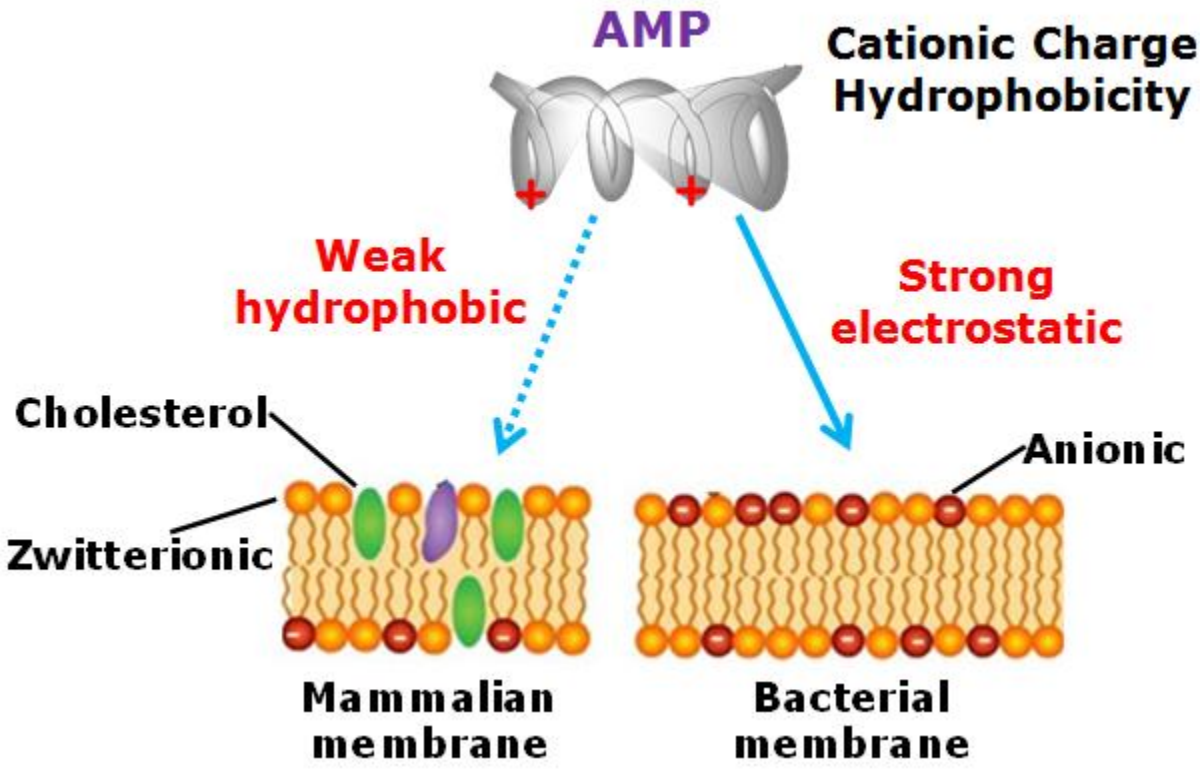

Figure 1.7: Differences in membrane composition between mammalian and bacterial cells providing selectivity of membrane-active antimicrobials. Mammalian cell membrane surface (left) largely contain zwitterionic phospholipids and are rigid due to presence of cholesterol compared to bacterial (right) cell membranes with a majority of anionic phospholipids. Membrane-active molecules such as AMPs interact with bacterial membrane through strong electrostatic interactions and might have weak hydrophobic interactions with the mammalian membranes. Adapted from reference 105 with the permission from Elsevier Publishing Group.

AMPs and only few of them have entered the clinical trials (Plectasin and other AMPs)[91, 92]. AMPs such as Nisin has been used as food preservative, Bacitracin and Gramicidin have been used for topical applications[91]. However, there has been no success for the development of AMPs as systemic therapy[92]. This limited success in clinical applications is due to their high toxicity (for example, hemolysis), rapid *in-vivo* degradation (susceptible to proteases) and more importantly, high manufacturing costs that prevents their large scale industrial production[92]. Furthermore, several studies have reported that pathogenic bacteria are able to elude the action of AMPs, for example, by production of proteolytic enzymes[82, 83].

Mimicry of antimicrobial peptides has been shown to be an attractive approach to overcome the issues that prevent AMPs from reaching the pharmaceutical market[93-95]. The main objective of this biomimetic approach is to incorporate the physiochemical parameters found in AMPs such as their cationic charge, amphiphilicity and induced or inherent amphipathic organization, which play a major role in the mechanism of antimicrobial action. Peptidomimetics including β-peptides[96], peptoids[97], arylamide foldamers[98, 99], oligo acyl lysines (OAKs)[100], γ-peptides[101], aryl alkyl lysines[102] and other small molecules[103, 104] have shown promising success and some are in clinical trials[93]. Although the peptidomimetic design displayed high efficacy and resistance to proteolysis, their cost-intensive preparation and low therapeutic index pose an obstacle to their widespread application.

1.5 Scope of the thesis

Flourishing bacterial resistance to antibiotics coupled with languishing antibiotic discovery creates an urgent need for the development of new antimicrobial agents which exert novel mechanisms of action. Conventional antibiotics rely on specific target mechanism of action and hence bacteria can easily develop resistance to them even by single point mutations. Targeting the bacterial cell membrane is a promising approach to combat bacterial resistance to antibiotics. Bacteria have been shown to have fewer tendencies for developing resistance to membrane-targeting agents, for example AMPs. AMPs represent effective therapeutic alternatives to antibiotics but their limited success is due to high cost of production, low stability *in-vivo* and unwanted toxicity to mammalian cells. This thesis aims at design and development of cationic-amphiphilic polymers targeting the bacterial cell membrane and addresses three major problems in bacterial infections namely chronic infections due to biofilms, Gram-negative superbugs and endotoxins.

Optimum amphiphilicity, a tunable balance between cationic charge and hydrophobicity, has been shown to be pivotal for the selective interaction with anionic lipid membranes of bacteria instead of zwitterionic mammalian (human erythrocyte) membranes. However, optimizing this amphiphilicity to selectively target the bacteria sparing the mammalian cells is still an unmet need. **Chapter 2** provides an unprecedented synthetic approach of post-functionalization for the development of cationic amphiphilic antibacterial polymers. The

conventional approaches use cationic and hydrophobic monomers as precursors to synthesize amphiphilic antibacterial polymers. On the other hand, the post-functionalization approach incorporates cationic charge and hydrophobicity to a precursor polymer to generate amphiphilic antibacterial polymers. The advantage is that the amphiphilicity can be optimized by merely varying the chemical nature of the side chain alkylating agent used to quaternize the polymer. This novel approach appends different side chain alkylating agents to a precursor polymer (poly(isobutylene-alt-maleic anhydride)) resulting in cationic amphiphilic polymers with tunable amphiphilicity. After identifying the optimum alkyl chain length (C5-C6 i.e. pentyl to hexyl) required for selective antibacterial activity, the side chain chemical structures (ester, amide and ether functional groups) were tuned for further optimization. Hydrophobic alkyl side chain containing polymers showed potent antibacterial efficacy but were toxic to mammalian cells. Hydrophilic ether moiety containing polymers were neither antibacterial nor toxic to mammalian cells. Although both amide and ester moiety containing polymers were less toxic to mammalian cells, incorporation of amide moieties led to potent antibacterial efficacy compared to ester moieties with membrane-active mechanism of action. Mechanistic studies of these derivatives showed that they depolarized, permeabilized, induced morphological changes in the bacterial membranes, led to leakage of ATP levels and mis-localized essential cell division proteins. This approach of tunable side chemical structure leads to optimal polymers with potent antibacterial efficacy and minimal toxicity to mammalian cells.

Having shown that amide and ester polymers have differences in their antibacterial activity, **Chapter 3** is aimed at understanding these differences. Amide and ester moieties are isosteric in nature and differ in their potency for hydrogen binding. Studies revealed that amide polymers (Q*n*-CmAPs) are potent antibacterial agents with high membrane-disrupting properties compared to their ester counterparts (Q*n*-CmEPs). To understand these differences, bio-physical experiments and molecular dynamics (MD) simulations were performed that showed strong interactions of Q*n*-CmAPs including hydrogen bonding with lipid head groups of bacterial model lipid bilayers, that are absent in Q*n*-CmEPs, make them potent bacterial membrane disruptors. This chapter provides a conceptual advance in understanding the interactions of antibacterial polymers with bacterial cell membranes highlighting the role of hydrogen bonding. Having understood the importance of amide moieties in the strong interactions of cationic amphiphilic polymers with bacterial cell membranes, **Chapter 4** describes the control of hydrophobicity by cyclization, isomerization and unsaturation of

amide side chains. Cyclization and unsaturation but not isomerization of side chains resulted in selective antibacterial polymers with low toxicity to mammalian cells. Mechanistic studies indicated the role of tunable hydrophobicity in polymers with different amide side chain architecture. This control of hydrophobicity in amphiphilic polymers drives them selectively towards bacterial cell membranes instead of mammalian membranes. These structural differences in the side chains also led to different interactions with the bacterial cell membranes. Polymers containing chemically different side chains were found to possess variations in their hydrophobicity profiles probably reflecting tunable biological activities. Importantly, unlike antibiotics, bacteria find it difficult to develop resistance to these membrane-active polymers.

Biofilms represent surface attached communities of bacteria that are the underlying cause behind chronic or persistent infections tolerant to antibiotic treatment and host-immune system. It is often difficult to disrupt already established biofilms on surfaces. Bacterial biofilms accounting for 65-80% of infections in humans place a massive burden on healthcare systems worldwide due to their persistence and chronic nature. Conventional antibiotics are inherently ineffective against biofilms due to various reasons such as slow or non-dividing cells, diffusion barriers and genetic mutations. Targeting the bacterial cell membrane is promising for the eradication of biofilms and also for the elimination of bacterial persisters that constitute biofilms. **Chapter 5** presents the potential of these polymers in disrupting surface established biofilms formed by multi-drug resistant Gram-negative bacteria. Moreover, these polymers kill slow or non-dividing stationary phase and persister bacteria including dispersed cells that release upon biofilm disruption. The membrane-active nature of these polymers was found to be the key of their anti-persister activity. More importantly, these polymers significantly ($p < 0.0001$) decrease the bacterial burden in mice with chronic *A. baumannii* burn wound infection. Bacteria develop rapid resistance to erythromycin and colistin whereas no detectable development of resistance occurs against these polymers even after several passages. These results suggest the potential use of these polymeric biomaterials in disinfecting biomedical device surfaces after the infection has become established and also for the topical treatment of chronic bacterial infections.

Gram-negative 'superbugs' including New Delhi metallo-beta-lactamase-1 ($bla_{\text{NDM-1}}$) producing pathogens have become world's major public health threats. Gram-negative bacteria are inherently resistant to some of the antibiotics and moreover they rapidly acquire resistance to antibiotics through multiple mechanisms of action. The recent havoc of extremely drug-resistant

superbugs worldwide is due to Gram-negative bacteria such as carbepenem resistant *Enterobacteriaceae* (CRE), Carbapenemase producing *K. pneumoniae* (KPC) and NDM-1 producing bacteria. Development of molecular strategies that can rehabilitate the 'old antibiotics' and halt the antibiotic resistance is a promising approach to target them. **Chapter 6** describes the ability of these polymers to potentiate (enhancement by >80-1250 fold) antibiotics (tetracyclines and erythromycin) towards Gram-negative superbugs including $bla_{\text{NDM-1}}$ *K. pneumoniae* and $bla_{\text{NDM-1}}$ *E. coli* clinical isolates. More importantly, these polymers potentiate antibiotics to eradicate surface established biofilms formed by Gram-negative bacteria. Further, these membrane-active polymers delay the development of bacterial resistance to antibiotics that highlights the potential of this combination approach in clinical settings. Furthermore, these membrane-active polymers potentiate antibiotic activity in mice models of Gram-negative burn and surgical wound infections. Organismic studies showed that bacteria had an increased and faster uptake of antibiotics in presence of these polymers which is attributed to the mechanism of re-sensitization. Polymers displayed membrane-active properties such as dissipation of membrane potential and membrane-permeabilization that enabled higher uptake of antibiotics in bacteria. These findings stress the importance of combination approaches of membrane-active molecules and antibiotics to combat MDR Gram-negative superbugs and for the topical treatment of Gram-negative bacterial infections.

Another major problem of Gram-negative infections is harmful and uncontrollable inflammation leading to sepsis that is responsible for a great amount of global mortality. Bacterial endotoxins such as lipopolysaccharide (LPS) released during antibiotic treatment or in response to immune system lead to sepsis. **Chapter 7** deals with the neutralization/detoxification of LPS by cationic amphiphilic polymers. Levels of pro-inflammatory cytokines in human monocytes caused by LPS stimulation were inhibited by more than 80% when co-incubated with these polymers. These reductions were found to be dependent on concentration and more importantly, on the side chain chemical structure due to variations in the hydrophobicity profiles of these polymers. Fluorescence spectroscopy and dynamic light scattering studies delineated that these polymers bind but neither dissociate nor promote LPS aggregation. The binding of polymer to LPS might lead to sort of a pseudo-aggregate formation resulting in LPS neutralization/detoxification. These polymers alone or in combination with antibiotics reduced the inflammation in mouse model of burn wound infections whereas antibiotics alone were

ineffective.

In summary, this thesis describes the design and development of cationic amphiphilic polymers that selectively target bacterial cell membrane with low toxicity to mammalian cells. This thesis presents a multi-pronged approach of targeting the bacterial cell membrane namely, the lipid membrane, efflux pumps and endotoxins using a single molecule. These polymers disrupt tough-to-kill bacterial biofilms, combat antibiotic resistance in Gram-negative superbugs and neutralize endotoxins.

Chapter 2

Cationic-amphiphilic Polymers with Tunable Side Chain Chemical Structure

Abstract

Cationic amphiphilic polymers which mimic the membrane-active properties of natural AMPs are an emerging class of potential candidates for combating the multidrug resistant microbes. A series of novel cationic amphiphilic polymers based on poly(isobutylene-alt-N-alkyl maleimide)s were developed using an unprecedented synthetic approach of post-functionalization. Amphiphilicity of the polymers was varied by quaternization with alkyl chain lengths ranging from ethyl (C2) to decyl (C10). After identifying the optimum alkyl chain length (C5-C6 i.e. pentyl to hexyl) required for selective antibacterial activity, the side chain chemical structure (ester, amide and ether functional groups) has been tuned for further optimization. These polymers displayed potent antibacterial activities against pathogenic bacteria including multi-drug resistant methicillin-resistant S. aureus (MRSA) and vancomycin resistant E. faecium (VRE). Hydrophobic alkyl side chain containing polymers showed potent antibacterial efficacy but were toxic to mammalian cells. Hydrophilic ether moiety containing polymers were neither antibacterial nor toxic to mammalian cells. Although both amide and ester moiety containing polymers were low toxic to mammalian cells, incorporation of amide moieties led to potent antibacterial efficacy compared to ester moieties. Mechanistic studies of these derivatives showed that they depolarized, permeabilized, induced morphological changes in the bacterial membranes, led to leakage of ATP levels and mis-localized essential cell division proteins. This approach of tunable side chain chemical structure leads to optimal polymers with potent antibacterial efficacy and minimal toxicity to mammalian cells.

(1) Uppu, D. S. *et al.* "Polymers with Tunable Side Chain Amphiphilicity as Non-hemolytic Antibacterial Agents". *Chem. Commun.* **2013**, *49*, 9389.

2.1 Introduction

Mimicking the AMPs has been shown to be an attractive approach to overcome the issues that prevent AMPs from reaching the pharmaceutical market. The main objective of this biomimetic approach is to incorporate the physiochemical parameters found in AMPs such as their cationic charge and amphiphilicity which play a major role in their mechanism of antimicrobial action. More recently, antibacterial polymers[78, 105-107] have been developed to address the problems that limit AMPs from reaching the clinics. Like AMPs, these polymers possess broad spectrum of antibacterial activity but importantly, unlike AMPs, they can be prepared with low cost at large scale. The peptide backbone of AMPs is labile to the proteolytic degradation whereas the stable non-peptide backbone of these polymers makes them more suitable for *in-vivo* use. Amphiphilicity, a key structural feature of AMPs, has been optimized in antibacterial polymers reported so far. This amphiphilicity, a fine balance of hydrophobicity and cationic charge, has been shown to play a key role in the selective interaction of these polymers with the bacterial cell membranes instead of mammalian cell (for e.g. human erythrocyte) membranes. Electrostatic interactions bind the cationic polymers to the bacterial cell membranes that contain negatively charged phospholipids whereas hydrophobic interactions facilitate the binding and insertion into the lipid bilayers. The selective interactions of amphiphilic polymers with bacterial membranes results from the fact that the eukaryotic cell membranes generally contain a higher proportion of zwitterionic phospholipids and are rigid and possess high membrane order due to the presence of cholesterol. Polymers have significant advantages over the low molecular weight peptidomimetics due to the fact that they involve inexpensive synthesis along with the versatility of polymer chemistry, which allows fine tuning of their chemical and structural parameters. To that end, a plethora of cationic and amphiphilic polymers including polyamides[108, 109], polynorbornenes[110], polymethacrylates[111-114], pyridinium copolymers[115], polycarbonates[116, 117], peptidopolysaccharides[118] and others[119-149] have been synthesized over the last decade as synthetic antimicrobial polymers. However, most of the cationic amphiphilic antimicrobial polymers reported in literature still face serious challenges including the use of tedious and expensive synthetic methodologies, low selectivity towards bacteria over mammalian cells. Most of the conventional approaches use cationic and hydrophobic monomers as precursors to synthesize amphiphilic antibacterial polymers. Hence, in these approaches tuning the amphiphilicity requires the synthesis of polymers by varying the feed ratio of cationic and

hydrophobic monomers resulting in less control over the molecular properties of the polymers. A low selectivity towards bacteria over human erythrocytes at *in-vitro* level might impede their success as anti-infective agents for *in-vivo* applications. Critical issues like biocompatibility, biodistribution, renal clearance, *in-vivo* toxicity of the polymers and also their degradation by-products need to be addressed for their early success in clinical applications.

To date, the key structural parameters exploited in designing highly selective cationic antimicrobial polymers are: amphiphilicity (hydrophilic/hydrophobic balance) and backbone structure/sequence (random, block and alternating copolymers or homo polymers) (Fig. 2.1)[105-107]. Optimization of hydrophilic/hydrophobic balance has been achieved by different approaches such as the "segregated monomer approach", the "facially amphiphilic approach" and the "same centered approach" in literature (Fig. 2.1). Synthesis of amphiphilic random copolymers follows the "segregated monomer approach" whereas amphiphilic polymers prepared using the "same centered approach" has a hydrophobic alkyl chain directly attached to the cationic centre within the same repeat unit of the homopolymer. It has been shown that a polymer synthesized using the "segregated monomer approach" was highly hemolytic compared to that of the "same centered approach" having the same alkyl chain length[105, 115]. When it comes to the polymeric backbone structure, Sampson and co-workers have demonstrated that random copolymers were found to be 2-6 fold less active than alternating copolymers towards different bacteria[120]. Kuroda and co-workers have shown that the random copolymers are highly hemolytic compared to block copolymers with similar polymer lengths and monomer compositions but displayed same level of antibacterial activity[112]. Yang and co-workers reported that self-assembling nanoparticles of amphiphilic polycarbonate based triblock copolymers were active towards Gram-positive bacteria but were ineffective towards Gram-negative bacteria[105]. This could be due to the fact that the hydrophobic region of these nanoparticles buried inside their core could not interact with the outermost lipopolysaccharide (LPS) layer of the Gram-negative bacteria. Overall, these reports suggest the importance of structural strategies like the "same centered approach" and an ordered backbone conformation such as alternating/block copolymer structure to achieve optimum selectivity towards bacteria over mammalian cells compared to random copolymers.

In this chapter, amphiphilic alternating quaternized poly (isobutylene-alt-*N*-(*N'*, *N'*–dimethyl *N'*–alkyl aminopropyl)-maleimide) (PIBMI) derivatives were developed and their antibacterial and hemolytic activities were investigated. Following the "same centered

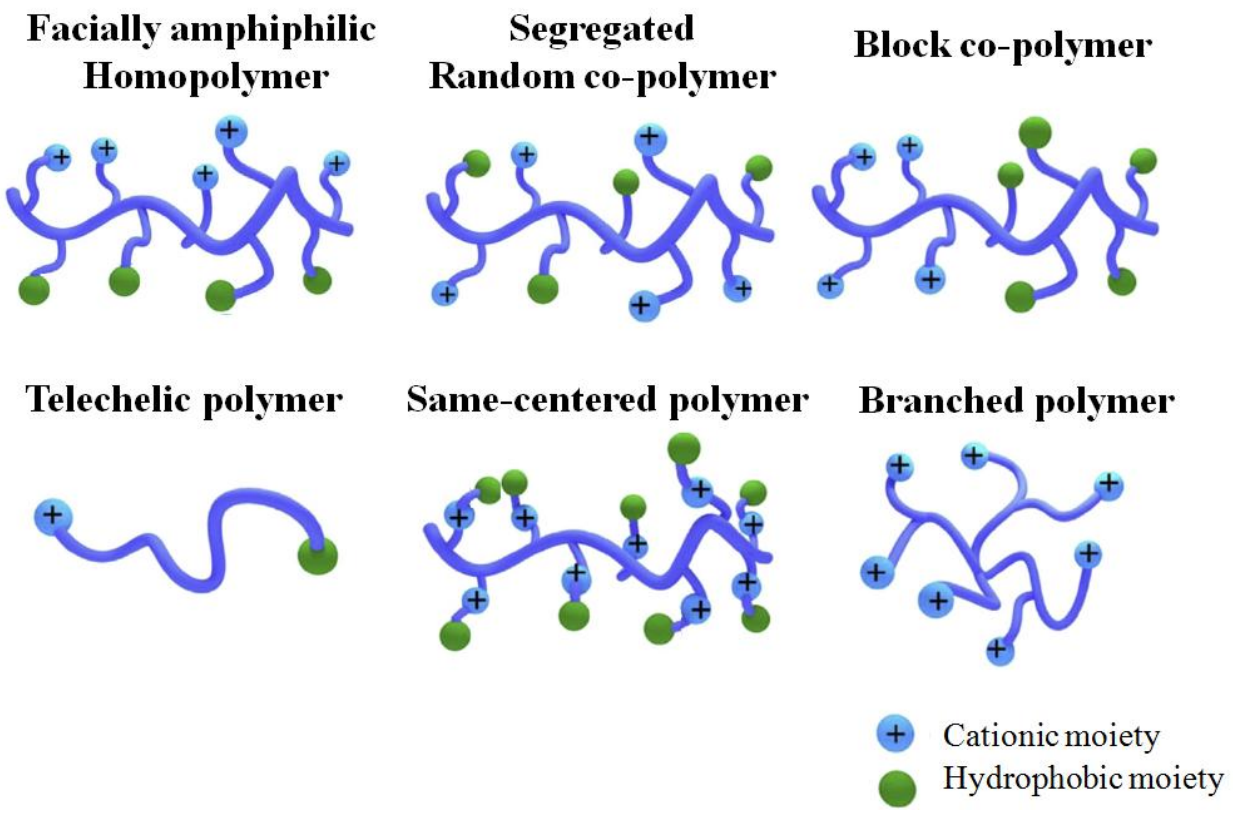

Figure 2.1: Design principles for the development of cationic amphiphilic antibacterial polymers. Variations in backbone structure/sequence and spatial/positional variation of cationic and hydrophobic regions have been elucidated. Reproduced from reference 105 with the permission from Elsevier Publishing Group.

approach", the optimization of amphiphilicity is achieved by varying the alkyl chain lengths. Amphiphilicity was further varied by changing the hydrophilic/hydrophobic nature of the alkylating agent. This eliminates the use of tedious synthetic methodologies as the cationic charge density and the alternating backbone structure were kept invariable. One of the major advantages of the presented synthetic methodology include the use of cheap and commercially available biocompatible polymeric precursor poly (isobutylene-*alt*-maleic anhydride) (PIBMA) with a low average molecular weight of ~6000 Da. More importantly, maleic anhydride copolymers have been shown to be biocompatible with extensive biomedical applications and history of use in humans as well as in approved drug products[150, 151]. Antibacterial efficacy studies in human plasma, effect of culture media conditions towards antibacterial activity and membrane-active mechanism of action were investigated in this chapter.

2.2 Results and discussion

2.2.1 Synthesis

A novel concept of post-functionalization for the facile synthesis of amphiphilic antibacterial polymers has been developed in this chapter. The conventional approaches use cationic and hydrophobic monomers as precursors to synthesize amphiphilic antibacterial polymers. On the other hand, the post-functionalization approach incorporates cationic charge and hydrophobicity to a precursor polymer to generate amphiphilic antibacterial polymers. The advantage is that the amphiphilicity can be optimized by merely varying the chemical nature of the side chain alkylating agent used to quaternize the polymer. A series of water soluble cationic alternating copolymers were synthesized based on quaternized poly (isobutylene-*alt*-*N*-(*N'*, *N'*–dimethyl *N'*–alkyl aminopropyl)-maleimide) (PIBMI) using facile synthetic methodologies from PIBMA. The synthesis of amphiphilic polymers was achieved in a simple two step process of post-functionalization (Scheme 2.1). PIBMA has an average molecular weight of M_w ~ 6000 Da and the polydispersity index (PDI) has been determined by GPC and found to be ~1.2. The nucleophilic ring opening and closure of the highly reactive anhydride with 3-aminopropyldimethylamine was achieved in a single step by heating at 120 °C for 48 h. The complete conversion of PIBMA to PIBMI was investigated by FT-IR and was confirmed by complete disappearance of peaks at 1850 cm^{-1} (C=O asym. str.) and 1785 (C=O sym. str.) for the anhydride ring and appearance of peaks 1767 cm^{-1} (C=O asym. str.), 1696 cm^{-1} (C=O sym. str.) for the imide ring. The complete conversion from PIBMA (soluble in DMSO) to PIBMI (soluble in chloroform) has also been confirmed by ^{1}H NMR. The synthesis of the activated alkyl amide or ester bromide was a facile reaction of the corresponding amine with bromoacetyl bromide in presence of potassium carbonate with quantitative yields devoid of chromatographic separation techniques. The second step was the quaternization of the tertiary nitrogen of PIBMI with the alkyl bromide or activated propyl (amide or ester) bromide at 65-75 °C for 96 h (Scheme 2.1) to give water soluble quaternized polymers (QAPIBMI).

To optimize the length of the alkyl chain required for high selectivity, a series of quaternized polymers with different alkyl chain lengths ranging from ethyl to octyl (C2, C4, C5, C6, C7, C8 and C10) were synthesized. Also, quaternized polymeric derivatives containing alkylating agents with variable hydrophobic/ hydrophilic balance (amide, ester and bis ethylene

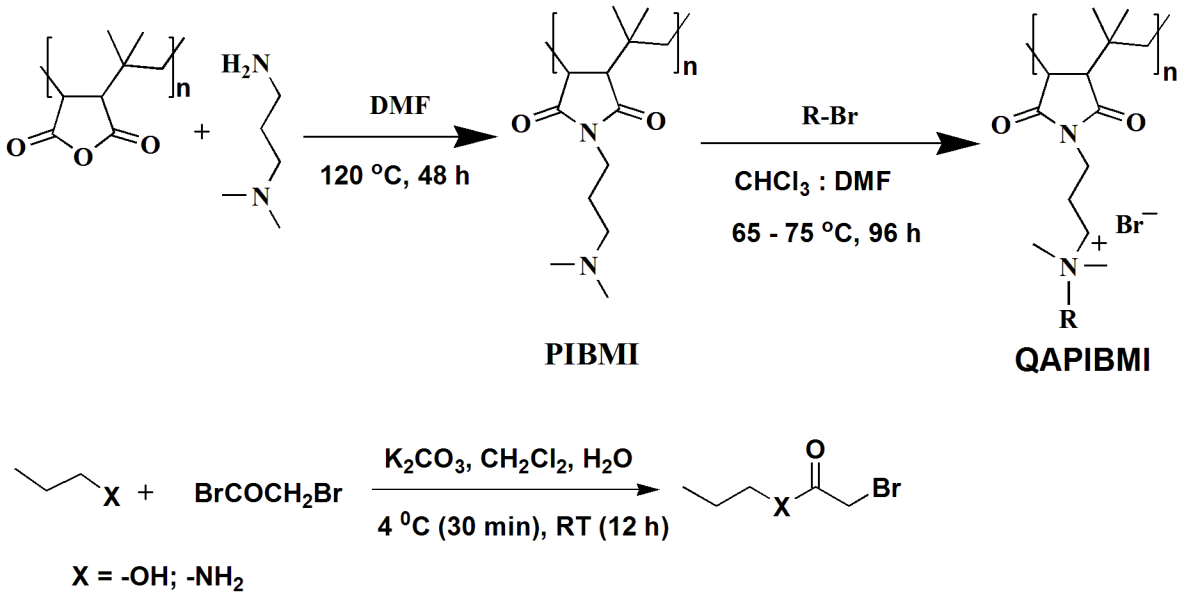

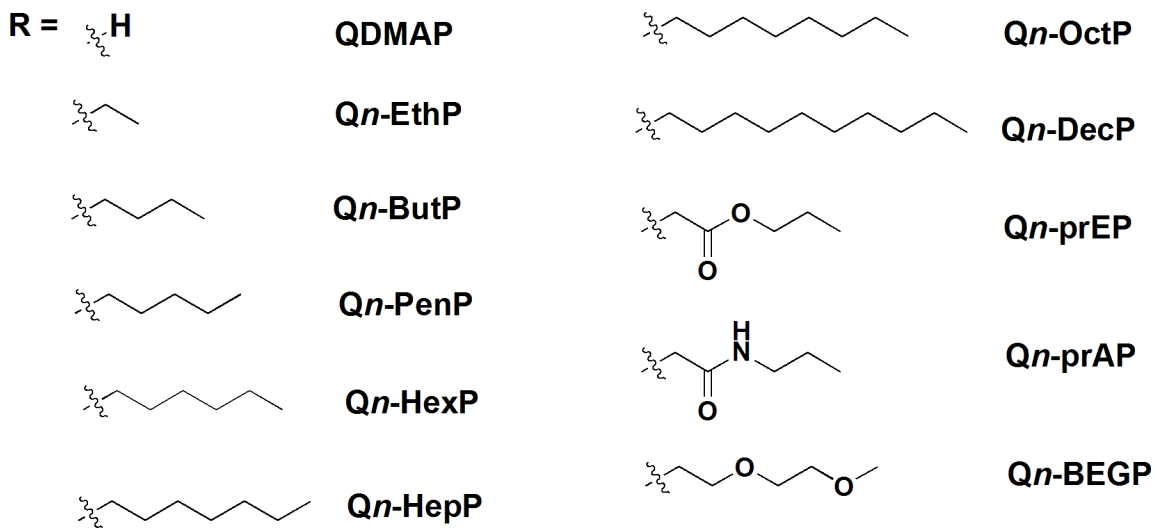

Scheme 2.1: General scheme for the synthesis of cationic amphiphilic polymers using post-functionalization approach with side chains of different chemical structure.

glycol (BEG) moieties) were also synthesized for further optimization of selective toxicity towards bacteria. The quaternized (Q) polymeric (P) derivatives are denoted according to the type of alkylating agent used. QDMAP (dimethylammonium), Q*n*-EthP (*n*-ethyl), Q*n*-ButP (*n*-butyl), Q*n*-PenP (*n*-pentyl), Q*n*-HexP (*n*-hexyl), Q*n*-HepP (*n*-heptyl), Q*n*-OctP (*n*-octyl), Q*n*-DecP (*n*-decyl), Q*n*-prAP (*n*-propyl amide), Q*n*-prEP (*n*-propyl ester), Q*n*-BEGP (bis-

ethyleneglycol) represent the QAPIBMI, quaternized derivatives of PIBMI with alkylating agents containing different alkyl, amide, ester and bis ethylene glycol moieties respectively (Scheme 2.1). All the polymers were characterized using FT-IR and ^{1}H-NMR. The degree of quaternization was calculated by ^{1}H-NMR analysis of the tertiary nitrogen of PIBMI and the quaternized polymer (Fig. 2.2). The $NCH_2(CH_3)_2$ protons shift downfield after quaternization and by integrating the protons corresponding to the unquaternized $NCH_2(CH_3)_2$, the degree of quaternization was calculated (Fig. 2.2). The cationic charge density given by the degree of quaternization was found to be in the range of 92-95% for all the polymers (Table 2.1). The molecular weight (M_n) of all the polymers was found to be in the range of 15-18 KDa.

2.2.2 Degree of quaternization

Degree of quaternization of the polymeric derivatives was calculated using ^{1}H NMR analysis.

Degree of quaternization (x) = (1- y) × 100 %

Wherein y = {([***CH₂***N***(CH₃)₂***]/8)/ ([***CH₂***C$(CH_3)_2$]/2)}

y = {(m/8)/ (n/2)}, m = [***CH₂***N***(CH₃)₂***] and n = [***CH₂***C$(CH_3)_2$]

For e.g. Q*n*-HexP, Degree of quaternization (x) = 1-{(0.32/8) / (2.0/2)} × 100 %

= 96 %

Wherein, [***CH₂***C$(CH_3)_2$] and [***CH₂***N***(CH₃)₂***] are the integrals of the hydrogens (a and b respectively, shown in Fig. 2.2) those are bold and italicized.

The molecular weight (number average molecular weight, M_n) of the final polymers was calculated based on the molecular weight of the precursor polymer, poly(isobutylene-*alt*-maleic anhydride) (average M_w~ 6000 Da, monomer weight was 154 g/mol and n~39) and the degree of quaternization (% of DQ) as described above[152-154].

For e.g. Q*n*-HexP

$M_n = [(m_x \times 0.96) + \{m_y \times (1-0.96)\}] n$

$= [(403.2 \times 0.96) + (238.18 \times 0.04)] 39$

= 18.5 kDa

Where m_x and m_y are the molecular weights of the quaternized and non-quaternized repeating units respectively.

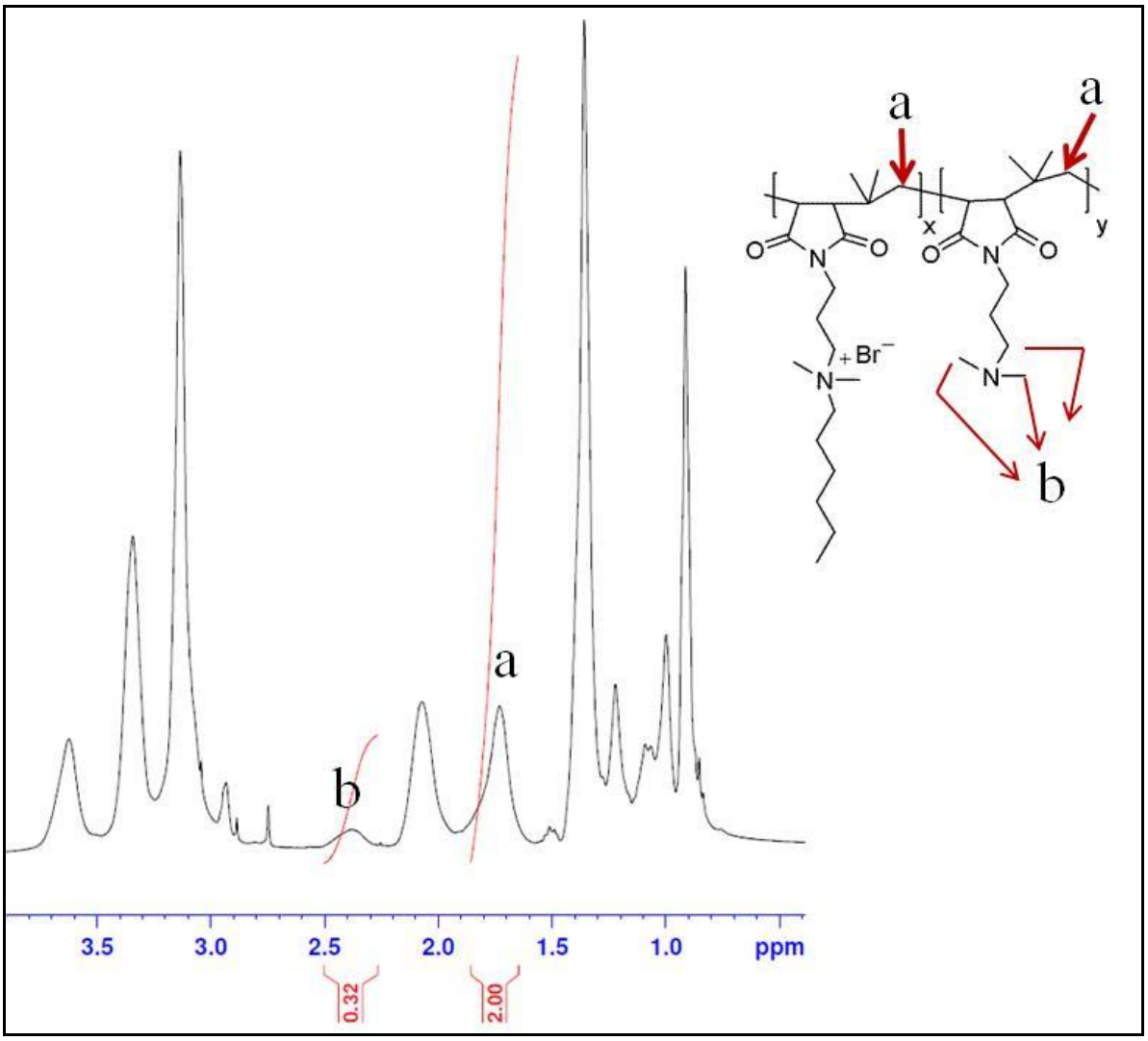

Figure 2.2: ^{1}H-NMR of Q*n*-HexP (in D_2O) indicating the peaks used for the calculation of degree of quaternization (δ/ppm: (a) for 1.7 (br $\boldsymbol{CH_2}C(CH_3)_2$, 2H) and (b) for 2.2-2.5 (br, $NCH_2CH_2\boldsymbol{CH_2}N\boldsymbol{(CH_3)_2}$, 8H).

2.2.3 Antibacterial activity and selectivity

Optimal antibacterial efficacy, minimum toxicity (hemolytic activity) and high selectivity are the important criteria for the use of antibacterial polymers as future antibiotics. To that end,

Table 2.1: Degree of quaternization and molecular weight of the cationic amphiphilic polymers.

Polymer	Degree of Quaternization (DQ) (%)[a]	Molecular Weight (Mn) (KDa)[b]
Q*n*-EthP	95	16.3
Q*n*-ButP	95	17.3
Q*n*-PenP	96	17.9
Q*n*-HexP	96	18.5
Q*n*-HepP	94	18.8
Q*n*-OctP	93	19.2
Q*n*-DecP	94	20
Q*n*-prAP	98	19.2
Q*n*-prEP	96	19.0
Q*n*-BEGP	97	19.2

[a,b] Calculated from ^{1}H NMR analysis.

antibacterial efficacy of these quaternized amphiphilic PIBMI derivatives were tested against *E. coli* (Gram-negative) and *S. aureus* (Gram-positive). Minimum inhibitory concentration (MIC) is measured as the lowest concentration required to completely inhibit the bacterial growth[155]. Also, the issue emerging crisis of antibiotic-resistant infections could mean a "literal return to the preantibiotic era"[156]. Methicillin resistant *S. aureus* (MRSA) has become a global epidemic both in hospital and community-associated settings raising alarms for alternative ammunitions[157]. More than 40 % of *S. aureus* strains are resistant to methicillin[158]. Vancomycin is the "drug of last resort" for MRSA and other antibiotic resistant associated infections[159]. Unfortunately, this wonder drug has also developed resistance with the emergence of vancomycin resistant *Enterococcus* (VRE) and vancomycin resistant *S. aureus* (VRSA)[159,160]. The antibacterial activity of these derivatives was also examined against pathogenic MRSA and VRE. Along with optimum antibacterial efficacy, achieving low toxicity to mammalian cells is of paramount importance for antimicrobial agents to reach the pharmaceutical market. As an initial assessment of mammalian cell toxicity, their hemolytic activities were also studied against human erythrocytes. The polymer concentration that caused 50% hemolysis was considered as HC_{50}. Selectivity or therapeutic index is another criterion for the cationic amphiphilic polymers to

reach clinical applications as antimicrobial drugs. Selectivity is generally defined as the ratio between the concentration at which 50% of RBC lysis occurs and the minimum inhibitory concentration required to inhibit the growth of bacteria (HC_{50}/MIC)[107].

The need for quaternization with different alkylating agents came from the observation that the protonated derivative, QDMAP, did not have optimum antibacterial efficacy (MIC of 105 μg mL^{-1} and 91 μg mL^{-1} against *E. coli* and *S. aureus* respectively). To increase the hydrophobicity, with alternating sequence of isobutylene and *N*-alkylmaleimide as the backbone structure, the amphiphilicity of the derivatives was varied by quaternization with hydrophobic alkyl chain lengths ranging from ethyl (C2) to decyl (C10) (Scheme 2.1). The MIC values of C2-C10 derivatives against *E. coli* and *S. aureus* varied from 3 μg mL^{-1} to >1000 μg mL^{-1} (from C2–C8) and again increased to 100-120 μg mL^{-1} (for C10) (Fig. 2.3 A). Overall, a parabolic relationship was observed between the antibacterial activities of these C2-C10 derivatives (against *E. coli* and *S. aureus*) and their hydrophobic chain lengths (Fig. 2.3 A). Also, their toxicity towards human erythrocytes increased (concentration at which 50% hemolysis occurs, HC_{50} values decreased from >1000 to 4 μg mL^{-1}) as the hydrophobicity increased from C2-C10 (Fig. 2.3 A). Amongst all, Q*n*-PenP (C5) with optimum amphiphilicity showed high selectivity towards bacteria over human erythrocytes (selectivity = HC_{50}/MIC) compared to MSI-78[99, 161], an AMP in phase-III clinical trials as a topical antibacterial agent (Table 2.2). Q*n*-PenP demonstrated a selectivity of 114 whereas MSI-78 had a maximum selectivity of 15 against *S. aureus* (Table 2.2). Q*n*-PenP also showed comparable or better selectivity value of 43, 25, 6 and 4 for *E. faecium*, *E. coli*, *K. pneumoniae* and *P. aeruginosa* respectively compared to the AMP (Table 2.2).

For further optimization of selectivity, the amphiphilicity was varied by quaternizing with alkylating agents containing hydrophilic moieties like ester (Q*n*-prEP), amide (Q*n*-prAP) and ether (Q*n*-BEGP) moieties by keeping the chain length almost constant (Scheme 2.1). Interestingly, these three derivatives did not show 50% hemolysis even up to 1000 μg mL^{-1}, the highest tested concentration ($HC_{50} \geq 1000$ μg mL^{-1}) (Fig. 2.3 B & Table 2.2). Among these, Q*n*-prAP had the highest selectivity of more than 91, 67 and 45 against *S. aureus*, *E. faecium* and *E. coli* respectively compared to MSI-78 and its alkyl chain counter parts Q*n*-HexP (C6) and Q*n*-PenP (C5) (Table 2.2). Q*n*-prEP had less selectivity of more than 15 and 91 towards *E. coli* and *S. aureus* compared to its alkyl chain counterparts Q*n*-HexP (C6) and Q*n*-PenP (C5) as well as

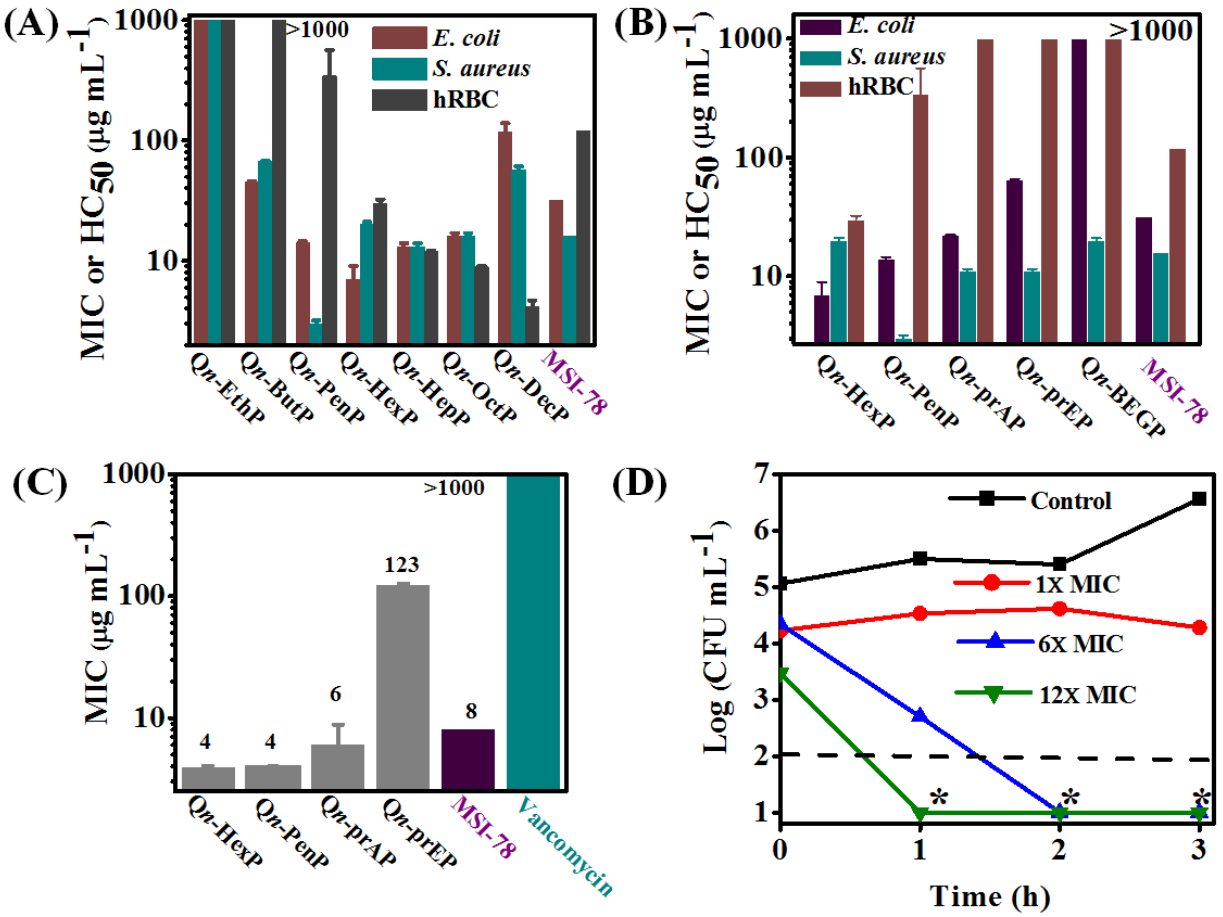

Figure 2.3: Antibacterial activity and hemolysis of cationic amphiphilic polymers. Antibacterial activity against *E. coli* and *S. aureus* and hemolysis against hman red blood cells (hRBC) of polymers of with different alkyl side chains (A) and with side chains of different chemical structure comparing with an AMP, MSI-78 (B); (C) Antibacterial activity of polymers against vancomycin resistant *Enterococci* (VRE); (D) Bactericidal activity of Q*n*-prAP against *S. aureus* (stars represent the detection limit, <50 CFU/mL).

the AMP (Table 2.2). Interestingly, the derivative quaternized with the highly hydrophilic alkylating agent BEG (bisethyleneglycol), (Q*n*-BEGP), showed ‘‘double selectivity’’ towards *S. aureus* over other bacteria and human erythrocytes. These three derivatives also showed comparable or better selectivity towards *K. pneumoniae* and *P. aeruginosa* as well (Table 2.2). Q*n*-HexP, Q*n*-PenP and Q*n*-prAP displayed excellent MICs of 4 μg mL^{-1}, 4 μg mL^{-1}, and 6 μg mL^{-1} respectively against vancomycin resistant *Enterococcus faecium* (VRE), whereas vancomycin was found to be ineffective up to the highest tested concentration of 1000 μg mL^{-1} (Table 2.2 and Fig. 2.3 C). In literature reports, however it has been shown that vancomycin is inactive against VRE even at concentrations above 1000 μg mL^{-1} [162]. Q*n*-PenP and Q*n*-prAP had

the highest selectivity of 86 and >166 against VRE, whereas it has been shown in the literature that MSI-78 has a selectivity of only 15 (Table 2.2)[99, 161]. The derivatives Q*n*-HexP, Q*n*-PenP and Q*n*-prAP had MICs of 113, 104, 224 μg mL^{-1} respectively against MRSA, whereas Q*n*-prEP and (Q*n*-BEGP) were found to be ineffective up to 1000 μg mL^{-1} (Table 2.2). Additionally, Q*n*-prAP showed a rapid 5 $\log_{10}$ of reduction of bacteria within 2 h and 1 h at a concentration of 6 and 12 times the MIC respectively whereas at MIC it rather showed bacteriostatic activity (Fig. 2.3 D). So, by merely varying the side chain amphiphilicity, the overall amphiphilicity of the polymeric mimics of AMPs is varied that resulted in the derivatives with maximum selective toxicity towards bacteria over human erythrocytes. Supporting the hypothesis, these observations suggest the role of optimization of amphiphilicity in selective toxicity to bacteria.

Table 2.2: Antibacterial activity, cytotoxicity and selectivity of amphiphilic polymers.

Polymer	**MIC (μg mL^{-1})**							**HC_{50} (μg mL^{-1})**
	Ec	*Kp*	*Pa*	*Sa*	*Ef*	MRSA[a]	VRE[b]	
Q*n*-HexP	7(4)	36 (1)	62(0.5)	20(1.5)	4(8)	113(0.3)	4(8)	30
Q*n*-PenP	14 (24)	57(6)	94(4)	3(114)	8(43)	104(3.3)	4(86)	343
Q*n*-prAP	22(>45)	59(>17)	101(>10)	11(>91)	15(>67)	224(>5)	6(>166)	>1000
Q*n*-prEP	65(>15)	46(>22)	208(>5)	11(>91)	510(>2)	>1000	123(>8)	>1000
Q*n*-BEGP	>1000	150(>7)	>1000	20(>50)	>1000	>1000	>1000	>1000
MSI-78	32[c] (8)	16[c] (15)	16[c] (15)	16[c] (15)	64[*,c] (2)	32[c] (8)	8[c] (15)	120[d]

[a]Methicillin resistant *Staphylococcus aureus*; [b]Vancomycin resistant *Enterococcus faecium*; [c,d]Literature values[99, 161]; *Literature values for *E. faecalis*[161]; Selectivity (HC_{50}/MIC) is given in parenthesis; *Ec - E. coli, Kp - K. pneumoniae, Pa -P. aeruginosa, Sa -S. aureus, Ef - E. faecium*.

2.2.3.1 Effect of culture media conditions on antibacterial activity

It has been found that antibacterial efficacy of the polymers is dependent on type of culture media used[163]. The animal tissue derived culture media has been shown to decrease the potency of antibacterial polymers[163]. Differences in antibacterial activity were observed between different culture media used for the studies. The MIC of these polymers against MRSA when determined in nutrient broth showed low activity (Table 2.3). However, when performed in Mueller Hinton (MH) broth, the MICs for Q*n*-HexP (4 μg mL^{-1}), Q*n*-PenP (16 μg mL^{-1}), Q*n*-prAP (31 μg mL^{-1}), Q*n*-prEP (250 μg mL^{-1}) and (Q*n*-BEGP) (>1000 μg mL^{-1}) were found to be very low compared to that of nutrient broth (Table 2.3). Also, Q*n*-prAP had MICs of 22 μg mL^{-1} (*E. coli*) and 11 μg

mL^{-1} (*S. aureus*) in LB broth and nutrient broth respectively whereas it had MIC of 31 µg mL^{-1} against both the bacteria when measured in MH broth. Similarily, Q*n*-prEP had MICs of 65 µg mL^{-1} (*E. coli*) and 11 µg mL^{-1} (*S. aureus*) in LB broth and nutrient broth respectively whereas it had MICs of 250 µg mL^{-1} (*E. coli*) and 125 µg mL^{-1} (*S. aureus*) when measured in MH broth.

Table 2.3: Effect of culture media on antibacterial activity of MRSA.

Polymer	**MIC (µg mL^{-1})**	
	MH broth	Nutrient broth
Q*n*-HexP	4	113
Q*n*-PenP	16	104
Q*n*-prAP	31	224
Q*n*-prEP	250	>1000
Q*n*-BEGP	>1000	>1000

2.2.3.2 Antibacterial activity in chemically defined medium

To confirm the fact that the variation in antibacterial activity is indeed due to the differences in chemical structure and not the culture media conditions, antibacterial activity was performed in chemically defined media. The conventional animal extract derived culture media for bacterial growth can affect the antibacterial activity of polymers[163]. Thus, the determination of MIC in these media might give the erroneous understanding of the effect of side chain chemical structure towards antibacterial activity. Also, near the site of infection, it is known that the bacteria are under a nutrient deprived condition[46, 47]. So, the antibacterial activity of the polymers was determined in chemically defined media, M9 minimal medium (contains inorganic salts and glucose) for *E. coli* and minimum essential medium (MEM which contains vitamins, amino acids, inorganic salts and nucleosides) for *S. aureus*[164]. Minimum bactericidal concentration (MBC), determined after 18 h incubation was found to be 2 µg mL^{-1} and 3 µg mL^{-1} for the amide polymer, Q*n*-prAP whereas the corresponding ester polymer, Q*n*-prEP showed 16 µg mL^{-1} and >200 µg mL^{-1} against *S. aureus* and *E. coli* respectively. This observation reiterates the fact that the effect on antibacterial activity is indeed due the differences in their chemical structure and not the culture media conditions.

2.2.3.3 Antibacterial activity in human plasma

One of the major disadvantages of natural AMPs is the loss of antibacterial efficacy because of their susceptibility to proteases in blood plasma. To assess the compound's stability, MIC experiment of Q*n*-PenP and Q*n*-prAP was performed against *S. aureus* as a model bacterium in 50% of human plasma. The MIC of Q*n*-PenP and Q*n*-prAP remained constant even in the presence of 50% of human plasma (MIC = 10 μg mL^{-1} and 12 μg mL^{-1} respectively) (Fig. 2.4). It has been reported in the literature that the MIC of MSI-78 against *S. aureus* increases to two fold in 50% of human serum itself than in the absence of serum (100% media)[161]. The experiment was performed with pre-incubation of the derivatives in 50% of human plasma for 3 h and 6 h. The MIC values (13 μg mL^{-1} and 20 μg mL^{-1} respectively) of Q*n*-PenP and Q*n*-prAP were nearly unchanged even after 3 h of preincubation in human plasma but increased to 2-4 fold after 6 h of pre-incubation in human plasma (26 μg mL^{-1} and 48 μg mL^{-1}) (Fig. 2.4). This suggests that these synthetic antibacterial polymers can be used as systemic therapeutics as they resist the plasma proteases and other plasma components that reduce the efficacy of AMPs.

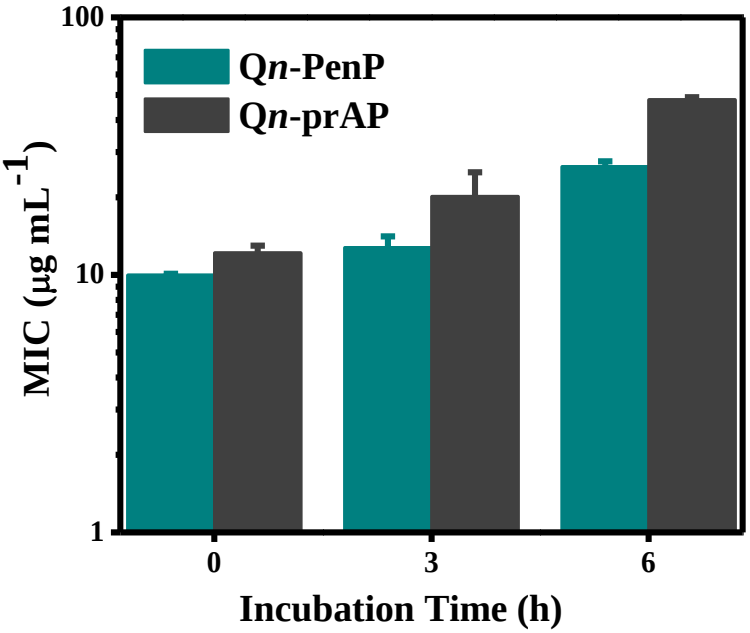

Figure 2.4: Antibacterial efficacy in 50% of human plasma. Polymers were pre-incubated for defined time intervals (0 h, 3 h and 6 h) in 50% of human plasma and then MIC was determined against *S. aureus*.

2.2.4 Mechanism of antibacterial action

As mentioned earlier, the biophysical mechanism of action of natural AMPs and their mimics different from that of conventional antibiotics makes them ideal candidates for the treatment of antibiotic-resistant bacteria. AMPs have different modes of action such as cytoplasmic membrane depolarization, membrane permeabilization, potassium efflux etc[85]. So the aim was to investigate the mechanism of action of our cationic and amphiphilic macromolecules which are designed to mimic the biophysical characteristics of natural AMPs such as cationic charge and amphiphilicity.

2.2.4.1 Cytoplasmic membrane depolarization

Altering the membrane potential across the cytoplasmic cell membrane of the bacteria has been shown to be one of the main mechanisms of action of natural AMPs. Bacterial plasma membrane depolarization by quaternized PIBMI derivatives was measured using a membrane potential sensitive dye, $diSC_3$ (5) ((3, 3'-dipropylthiadicarbocyanine iodide). $DiSC_3$ (5) intercalates into the cytoplasmic membrane of energized cells and initially the fluorescence was quenched. Upon disruption of the potential, the release of the dye into the solution resulted in increase of fluorescence[165]. All the quaternized PIBMI derivatives showed membrane depolarization when tested against *E. coli* (Fig. 2.5 A).

2.2.4.2 Cytoplasmic membrane permeabilization

Cationic and amphiphilic macromolecules can cause membrane permeabilization and disruption causing loss of membrane integrity of the bacteria. Kinetics of membrane permeabilization was studied by measuring the uptake of a fluorescent probe propidium iodide (PI). This dye enters only membrane compromised cells and fluoresces upon binding to nucleic acids[165]. All the three quaternized PIBMI derivatives were shown to cause membrane permeabilization against *S. aureus* (Fig. 2.5 B) and *E. coli* (Fig. 2.5 C).

2.2.4.3 ATP leakage

Dissipation of membrane potential leads to limiting the energy required for metabolic processes in bacteria[94, 166]. Intracellular ATP levels in *E. coli* and *S. aureus* were measured after treatment with Q*n*-prAP and Q*n*-prEP using the luciferin-luciferase bio-luminescence assay to understand

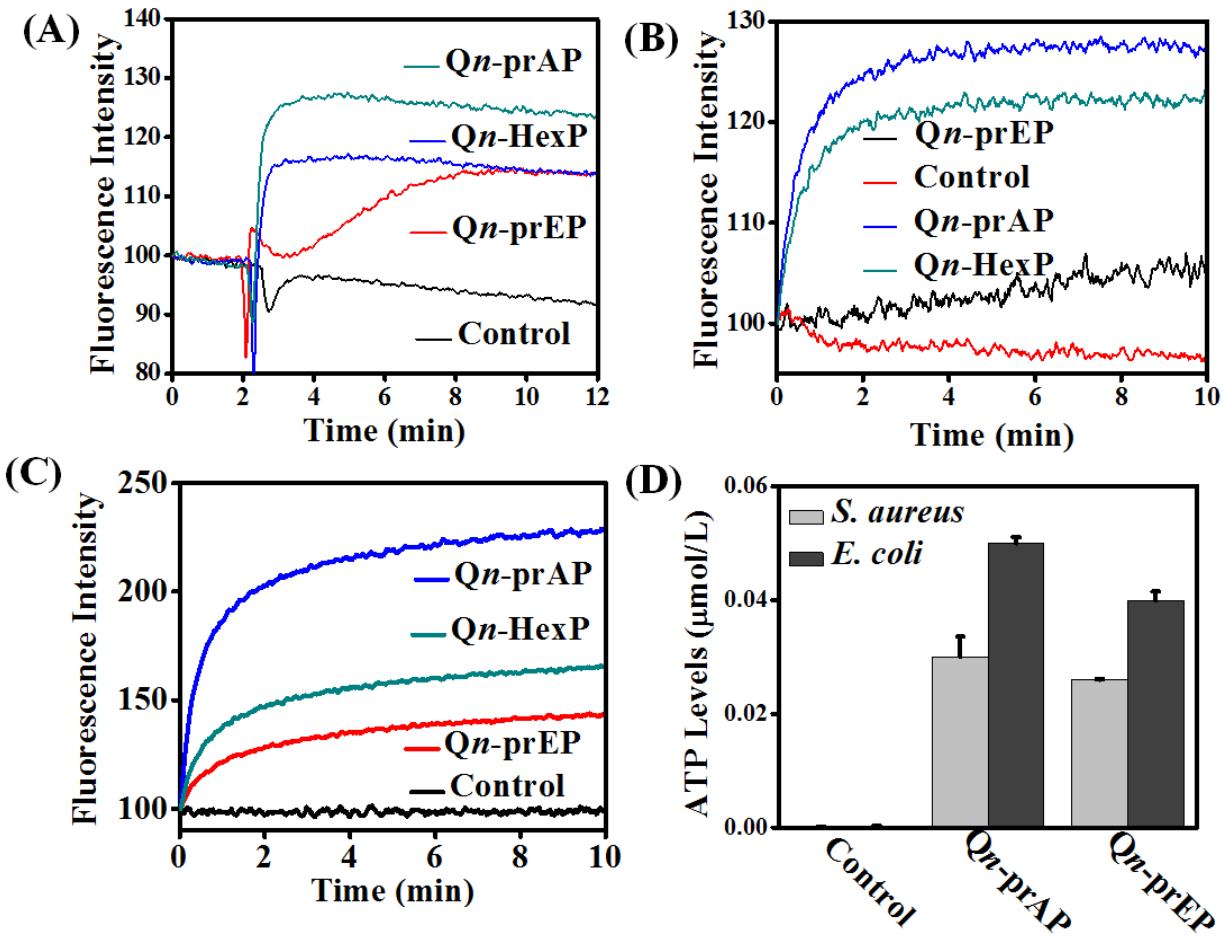

Figure 2.5: Membrane-active properties of cationic-amphiphilic polymers. (A) Cytoplasmic membrane depolarization of *E. coli*, membrane permeabilization of *S. aureus* (B) and *E. coli* (C) treated with polymers having different side chain functionality. (D) Released ATP levels after treatment with polymers for 15 min. Relative ATP levels (mol/L) were determined by subtracting the background ATP levels from the test sample ATP levels. All the polymers were used at a concentration of 50 μg mL^{-1}

the energy limitation conditions. Q*n*-prAP (50 μg mL^{-1}) showed higher release of ATP levels compared to its ester counterpart, Q*n*-prEP (50 μg mL^{-1}) in both *E. coli* and *S. aureus* (Fig. 2.5 D). This supports the fact that the interaction of the amide and ester polymers with the bacterial membrane is different resulting in variable release of ATP levels.

2.2.4.4 Mis-localization of cell division proteins

It has been shown that membrane potential is important for bacterial cell division[166]. Since these polymers dissipate the membrane potential, the localization of three essential cell division

proteins, MinD, MreB and FtsZ were examined using a *B. subtilis* 168 strain carrying the relevant GFP reporter fusions. As shown in Fig. 2.6, within 15 min of addition of Q*n*-prAP and Q*n*-prEP (both at 25 μg mL^{-1}), the dissipation of membrane potential resulted in the complete delocalization of MinD, MreB and FtsZ. The dissipation of membrane potential also affected the membrane staining by the fluorescent probe, Nile Red. The bright fluorescent membrane foci observed upon addition of the polymers probably represents membrane blobs which are a consequence of rapid loss of cell turgor. These results suggested that due to the dissipation of membrane potential in the presence of these cationic polymers key morphological proteins get mis-localized.

2.2.4.5 Morphological membrane disruption by FESEM

Membrane permeabilization/disruption causing loss of membrane integrity of the bacteria is the main mechanism of action of AMPs. Q*n*-prAP at 50 μg mL^{-1} showed cytoplasmic membrane depolarization and permeabilization when tested against both *E. coli* and *S. aureus*. Field emission scanning electron microscopy (FESEM) images of both *S. aureus* and *E. coli* treated with Q*n*-prAP (6 × MIC) for 2 h give visual insights into the morphological membrane disruption (Fig. 2.7). The untreated bacteria showed intact morphology whereas the irregularly shaped morphological membrane was disrupted and thus probably the dead bacteria were found upon treatment with Q*n*-prAP (Fig 2.7). The cationic polymers therefore possibly interact with the mostly negatively charged bacterial cell membrane and disrupt the membrane, which might lead to cell death.

2.3 Conclusions

Taking advantage of the alternating polymeric backbone structure, the amphiphilicity of the quaternized PIBMI derivatives has been optimized by varying the alkyl chain length and their hydrophobic/hydrophilic balance following the "same centered approach". Alternating copolymers quaternized with highly hydrophobic alkylating agents were found to be less selective whereas highly hydrophilic derivatives showed no antibacterial activity as well as were non-toxic to mammalian cells. Although both amide and ester moiety containing polymers were low toxic to mammalian cells, incorporation of amide moieties led to potent antibacterial efficacy compared to ester moieties. Mechanistic studies of these derivatives showed that they

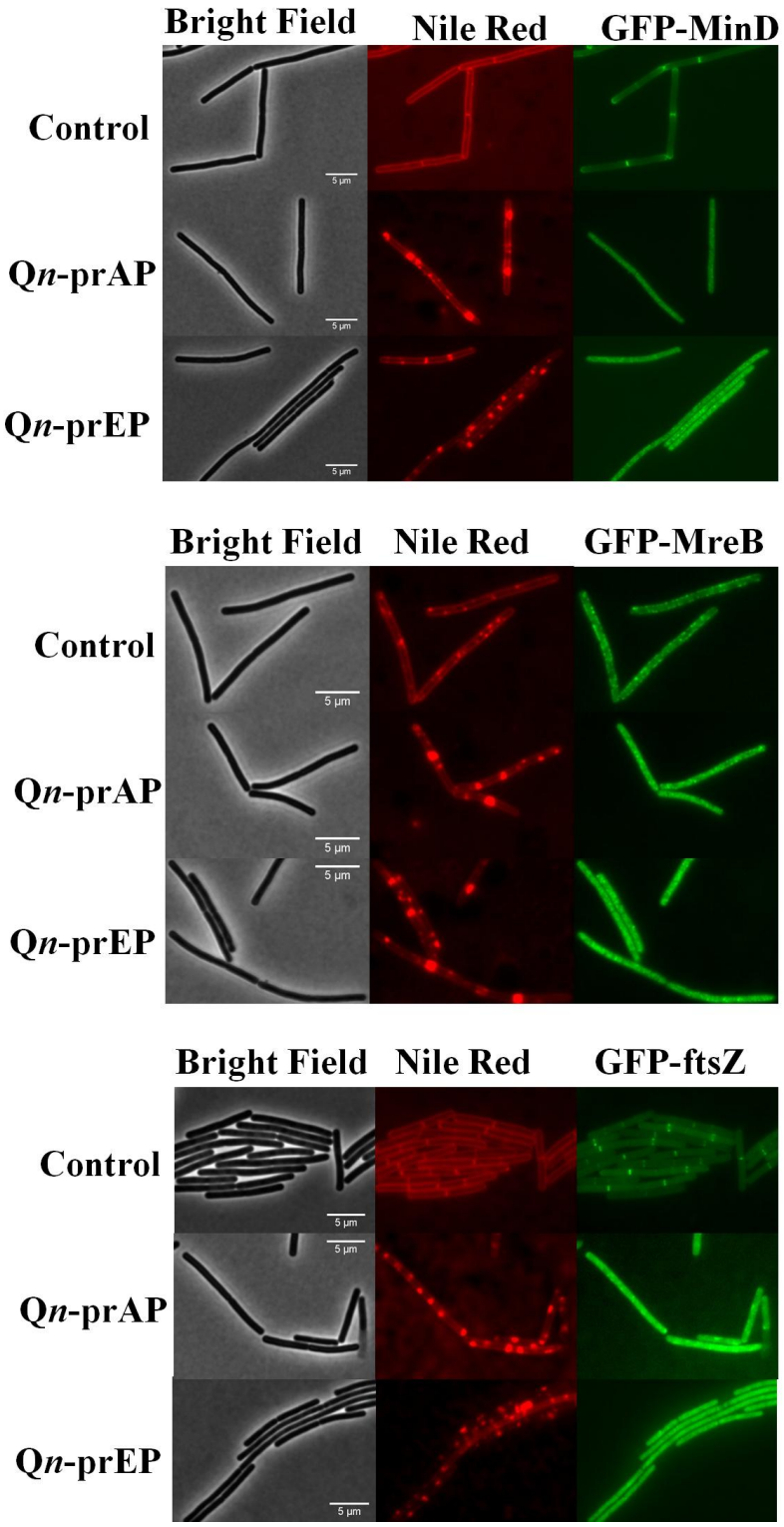

Figure 2.6: Effect on bacterial cell division after the treatment of amide and ester polymers. Mis-localization of cell division-regulating proteins MreB, MinD and FtsZ in *B. subtilis* 168 strain carrying a GFP fusion. Nile red fluorescence represents alteration in membrane lipid staining after the treatment with the polymers. Scale bar is 5 µm.

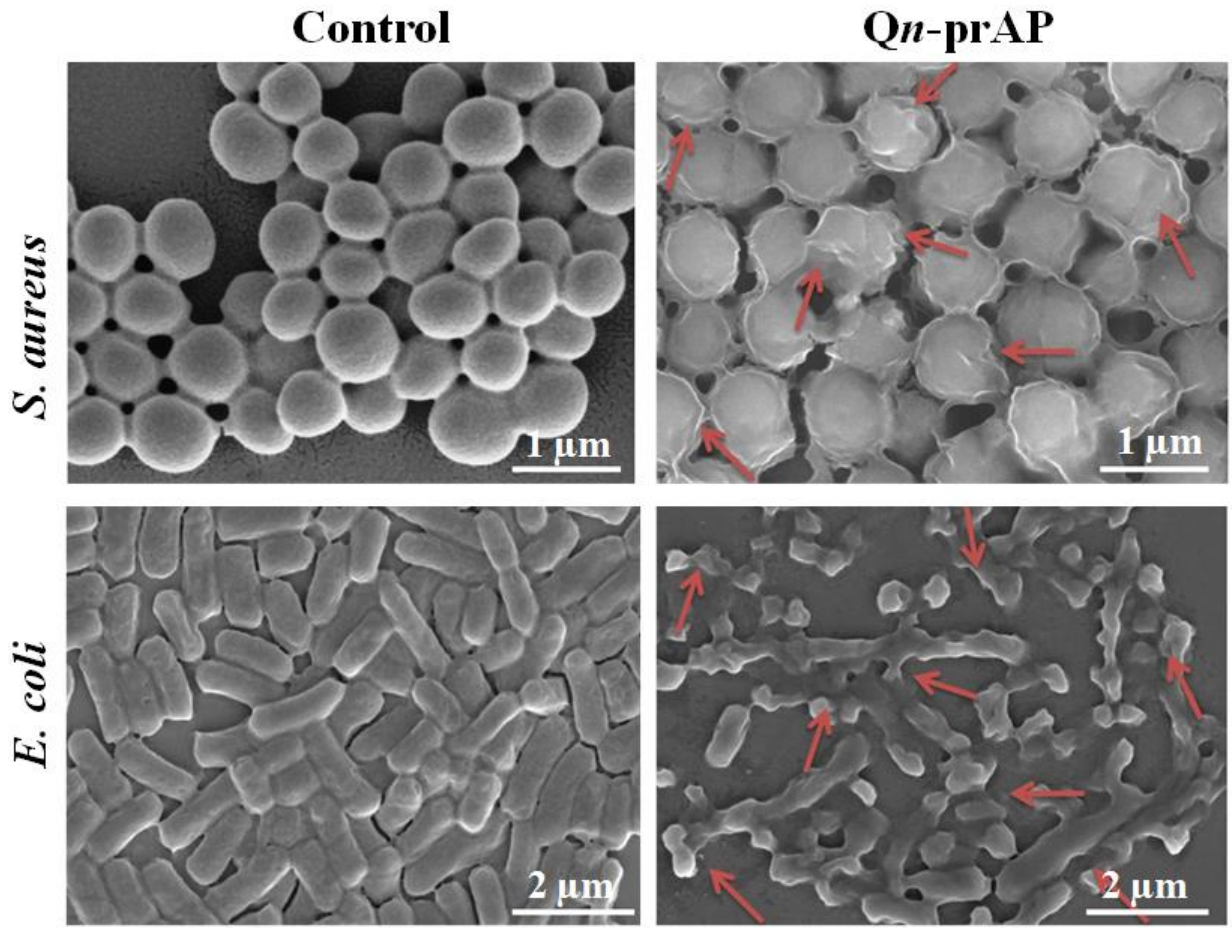

Figure 2.7: FESEM images showing the morphological disruption of the bacteria by Q*n*-prAP (6 × MIC).

depolarized, permeabilized and induced morphological changes in the bacterial membranes. This approach of tunable side chemical structure leads to optimal polymers with potent antibacterial efficacy and minimal toxicity to mammalian cells.

2.4 Experimental section

2.4.1 Materials and methods

All the solvents were of reagent grade and dried prior to use wherever required. Bromoacetyl-bromide, poly(isobutylene-*alt*-maleic anhydride) (Mw~6000 Da, Sigma Catalog no. 531278), 3-aminopropyldimethylamine, 1-Propyl amine, 1-Bromo decane and 1-Bromo-2(2-methoxy

ethoxy) ethane were purchased from Sigma-Aldrich (India) and used as received. 1-Bromo ethane, 1-Bromo butane, 1-Bromo pentane, 1-Bromo heptane and 1-Bromo octane were purchased from Avra chemicals (India) and 1-Propanol and 1-Bromo hexane were obtained from Spectrochem (India) respectively and used as received. Dialysis membrane-150 with a molecular weight cut off of 10 KDa was obtained from HIMEDIA (India). Dialysis tubing, benzoylated with NMWCO of 2 KDa was purchased from Sigma-Aldrich (India). NMR spectra were recorded using Bruker AMX-400 (400 MHz for ^{1}H and 100 MHz for ^{13}C) spectrometer. The chemical shifts (δ) are reported in parts per million downfield from the peak for the internal standard TMS for ^{1}H NMR and ^{13}CNMR. Infrared (IR) spectra of the solid compounds were recorded on Bruker IFS66 V/s spectrometer using KBr pellets. IR spectra of the compounds soluble in low-boiling solvents were recorded with the same instrument using NaCl crystal. Optical density and absorbance were measured by Tecan InfinitePro series M200 Microplate Reader. Bacterial strains, *P. aeruginosa* (MTCC 424), *S. aureus* (MTCC 737) and *E. coli* (MTCC 443) were purchased from MTCC (Chandigarh, India). *E. faecium* (ATCC 19634), β-lactamase producing and drug-resistant *K. pneumoniae* (ATCC 700603), methicillin resistant *S. aureus* (MRSA) (ATCC 33591), vancomycin resistant *E. faecium* (VRE) ((OrlaJensen) Schleifer and Kilpper-Balz, ATCC 51559) were obtained from ATCC (Rockville, Md).

2.4.2 Microorganisms and culture conditions

The antibacterial activity of the polymers was performed against both Gram-negative (*E. coli, P. aeruginosa* and *K. pneumoniae)* and Gram-positive (*S. aureus* and *E. faecium*) bacteria including the drug resistant strains VRE and MRSA. *E. coli* was cultured in Luria Bertani broth (10 g of tryptone, 5 g of yeast extract, and 10 g of NaCl in 1000 mL of sterile distilled water (pH -7) while *S. aureus, P. aeruginosa* and MRSA were grown in Yeast-dextrose broth (1 g of beef extract, 2 g of yeast extract, 5 g of peptone and 5 g of NaCl in 1000 mL of sterile distilled water). Both *E. faecium* and VRE were cultured in Brain Heart Infusion broth (BHI). *K. pneumoniae* was grown in nutrient media (3 g of beef extract and 5 g of peptone in 1000 mL of sterile distilled water). For solid media, 5% agar was used along with above mentioned composition. The bacterial samples were freeze dried and stored at -80°C. 5 μL of these stocks were added to 3 mL of the nutrient broth and the culture was grown for 6 h at 37 °C prior to the experiments.

2.4.3 Synthesis and characterization

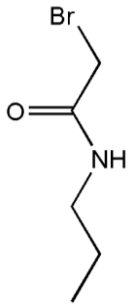

N-propyl-1-bromoethanamide: Propylamine (7 g, 118 mmol) was dissolved in dichloromethane (55 mL). Potassium carbonate, K_2CO_3 (24.55 g, 178 mmol) was dissolved in 60 mL of distilled water and the solution was added to the organic solution. The resulting two phase solution was cooled to 5 °C. A solution of bromoacetyl bromide (35.85 g, 178 mmol) in dichloromethane (55 mL) was carefully added drop wise to the cooled solution while maintaining the temperature at 5 °C for about 30 min. Then the reaction mixture was stirred at room temperature for 12 h. The aqueous solution was separated and washed with dichloromethane (2 × 25 mL). The organic solution was washed with water (2 × 50 mL) and passed over the anhydrous Na_2SO_4 and concentrated to yield an oily liquid quantitatively.

FT-IR: 3250 cm^{-1} (amide N-H str.), 2950-2850 (C-H str.), 1680 cm^{-1} (Amide I, C=O str.), 1560 cm^{-1} (Amide II, N-H ben.), 1470-1410 cm^{-1} (C-C str.), 1290-1110 (C-O str.); ^{1}H-NMR (400 MHz, $CDCl_3$): δ/ppm 0.878 (t, terminal –*CH₃*, 3H), 1.543 (m, -*CH₂*CH_3-, 2H), 3.278 (t, -CONH*CH₂*-, 2H), 3.881 (s, -CO*CH₂*Br, 2H), 6.475 (br s, amide –*NH*CO, 1H); ^{13}C-NMR (100 MHz, $CDCl_3$): δ 14.195, 22.768, 26.904, 29.324, 29.423, 29.588, 29.646, 29.708, 31.995, 40.403, 165.589.

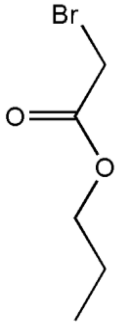

Propyl-1-bromoethanoate: 1-Propanol (7 g, 116.5 mmol) was dissolved in dichloromethane (55 mL). Potassium carbonate, K_2CO_3 (19.32 g, 140 mmol) was dissolved in 60 mL of distilled water and the solution was added to the organic solution. The resulting two phase solution was cooled to 5 °C. A solution of bromoacetyl bromide (28.21 g, 140 mmol) in dichloromethane (55 mL) was carefully added drop wise to the cooled solution while maintaining the temperature at 5 °C for about 30 min. Then the reaction mixture was stirred at room temperature for 12 h. The aqueous solution was separated and washed with dichloromethane (2 × 25 mL). The organic solution was washed with water (2 × 50 mL) and passed over the anhydrous Na_2SO_4 and concentrated to yield an oily liquid quantitatively.

FT-IR: 2950-2850 (C-H str.), 1735 cm^{-1} (C=O str.), 1470-1410cm^{-1} (C-C str.), 1290-1110 (C-O str.); ^{1}H-NMR (400 MHz, $CDCl_3$): δ/ppm 0.85 (t, terminal –*CH₃*, 3H), 1.57 (m, -*CH₂*CH_3-, 2H),

4.0 (t, -COOCH_2-, 2H), 3.7 (s, -COCH_2Br, 2H); ^{13}C-NMR (100 MHz, $CDCl_3$): δ 14.195, 22.768, 26.904, 29.324, 29.423, 29.588, 29.646, 29.708, 31.995, 40.403, 171.19.

Poly(isobutylene-alt-N-(N',N'-dimethylaminopropyl)-maleimide)PIBMI

To a solution of 10 g of poly(isobutylene-*alt*-maleic anhydride) (PIBMA) (Avg. M_w = 6000 g/mol) in 60 ml of DMF, 7.96 g of 3-Aminopropyldimethylamine (1.2 equi. or 78 mmol with respect to the monomer weight of the polymer (154 g/mol)) was added and stirred at 120 °C for 48 h in a screw-top pressure tube. The reaction mixture was cooled, precipitated with 200 mL of distilled water and was centrifuged at 10,000 rpm for 15 min. The polymer was dried at 45 °C for 24 h under vacuum to give a pale yellow solid with 100% yield (complete conversion of the anhydride to imide was confirmed by complete disappearance of peaks at 1850 cm^{-1} (C=O asym. str.) and 1785 (C=O sym. str.) for the anhydride ring and appearance of peaks 1767 cm^{-1} (C=O asym. str.), 1696 cm^{-1} (C=O sym. str.) for the imide ring by FT-IR).

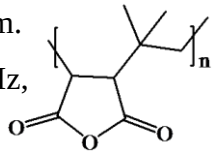

FT-IR: 2950-2850 (C-H str.), 1850 cm^{-1} (C=O asym. str.), 1785 cm^{-1} (C=O sym. str.), 1470-1410cm^{-1} (C-C str.), 1290-1110 (C-O str.); ^{1}H-NMR (400 MHz, $(CD_3)_2SO$): δ/ppm 0.7–1.2 (br $CH_2C(CH_3)_2$, 6H), 1.7 (br $CH_2C(CH_3)_2$, 2H), 2.2 (br, *CH*CH, 1H), 3.1 (br, CH*CH*, 1H).

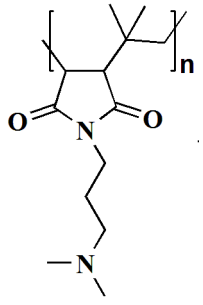

FT-IR: 2950-2850 (C-H str.), 1767 cm^{-1} (C=O asym. str.), 1696 cm^{-1} (C=O sym. str.), 1470-1410cm^{-1} (C-C str.), 1290-1110 (C-O str.); ^{1}H-NMR (400 MHz, $CDCl_3$): δ/ppm 0.7–1.2 (br $CH_2C(CH_3)_2$, 6H), 1.7 (br $CH_2C(CH_3)_2$, 2H), 1.86 (br $NCH_2CH_2CH_2N(CH_3)_2$, 2H), 2.2-2.5 (br $NCH_2CH_2CH_2N(CH_3)_2$, 8H), 2.7–3.1 (br, *CHCH*, 2H), 3.6 (br $NCH_2CH_2CH_2N(CH_3)_2$, 2H); ^{13}C-NMR (100 MHz, $CDCl_3$): 179.9, 179.7, 179.4, 177.4, 177.3, 177.2, 55.5, 45.9, 45.5, 44.1, 40.8, 40.6, 40.2, 40.0, 37.4, 26.2, 25.5, 24.8, 24.7, and 24.6.

Synthesis of QDMAP

0.5 g of PIBMI was dissolved in 10 mL of 2 M HBr solution and stirred at room temperature for 12 h. The product was obtained by dialysing against DI water (benzoylated dialysis tubing with NMWCO of 2 KDa) at 4 °C followed by freeze-drying with 100% yield. FT-IR: 3300 cm^{-1} (N-H

str.), 2950-2850 (C-H str.), 1767 cm^{-1} (C=O asym. str.), 1696 cm^{-1} (C=O sym. str.) 1470-1410cm^{-1} (C-C str.), 1290-1110 (C-O str.); ^{1}H-NMR (400 MHz, D_2O): δ/ppm 0.7–1.2 (br $CH_2C(CH_3)_2$, 6H), 1.7 (br $CH_2C(CH_3)_2$, 2H), 2.0 (br $NCH_2CH_2CH_2N(CH_3)_2$, 2H), 2.8-2.9 (br $NCH_2CH_2CH_2N(CH_3)_2$, 8H), 2.7-3.1 (br, *CHCH*, 2H), 3.6 (br $NCH_2CH_2CH_2N(CH_3)_2$, 2H).

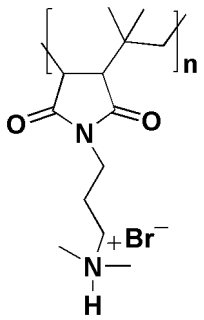

Quaternized PIBMI derivatives-QAPIBMI

To a solution of 0.5 g of PIBMI in 20 mL of DMF/$CHCl_3$ (1:1), 3 equivalents (with respect to the monomer weight of PIBMI (238.18 g/mol)) of 1-bromoalkane (n = 2, 4, 5, 6, 7, 8 and 10) or 1-bromo-2(2-methoxyethoxy) ethane was added and stirred at 75 °C for 96 h in a screw top pressure tube. The solution was cooled, precipitated with 40 mL of *n*-hexane/diethylether and filtered. The white solid was washed with n-hexane (4 × 40 mL) or diethylether and dried at 40 °C for 12 h under vacuum (yield: 100%).

Q*n*-DecP: FT-IR: 2950-2850 (C-H str.), 1767 cm^{-1} (C=O asym. str.), 1696 cm^{-1} (C=O sym. str.) 1470-1410cm^{-1} (C-C str.), 1290-1110 (C-O str.); ^{1}H-NMR (400 MHz, D_2O): δ/ppm 0.85-0.9 (br terminal $-CH_3$, 3H), 0.95–1.2 (br $CH_2C(CH_3)_2$, 6H), 1.3-1.5 (br $CH_2CH_2CH_2CH_2CH_2CH_2CH_2CH_2$, 16H) 1.7 (br $CH_2C(CH_3)_2$, 2H), 2.0 (br $NCH_2CH_2CH_2N(CH_3)_2$, 2H), 2.7–3.1 (br *CHCH*, 2H), 3.1-3.3 (br $NCH_2CH_2CH_2NCH_2(CH_3)_2$, 10H), 3.6 (br $NCH_2CH_2CH_2N(CH_3)_2$, 2H).

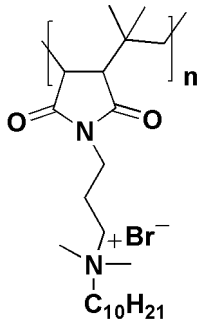

Q*n*-OctP: FT-IR: 2950-2850 (C-H str.), 1767 cm^{-1} (C=O asym. str.), 1696 cm^{-1} (C=O sym. str.) 1470-1410cm^{-1} (C-C str.), 1290-1110 (C-O str.); ^{1}H-NMR (400 MHz, D_2O): δ/ppm 0.85-0.9 (br terminal $-CH_3$, 3H), 0.95–1.2 (br $CH_2C(CH_3)_2$, 6H), 1.3-1.5 (br $CH_2CH_2CH_2CH_2CH_2CH_2$, 12H) 1.7 (br $CH_2C(CH_3)_2$, 2H), 2.0 (br $NCH_2CH_2CH_2N(CH_3)_2$, 2H), 2.7–3.1 (br *CHCH*, 2H), 3.1-3.3 (br $NCH_2CH_2CH_2NCH_2(CH_3)_2$, 10H), 3.6 (br $NCH_2CH_2CH_2N(CH_3)_2$, 2H).

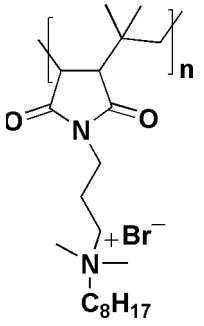

Q*n*-HepP: FT-IR: 2950-2850 (C-H str.), 1767 cm^{-1} (C=O asym. str.), 1696 cm^{-1} (C=O sym. str.) 1470-1410cm^{-1} (C-C str.), 1290-1110 (C-O str.); ^{1}H-NMR (400 MHz, D_2O): δ/ppm 0.85-0.9 (br terminal –*CH_3*, 3H), 0.95–1.2 (br $CH_2C(CH_3)_2$, 6H), 1.3-1.5 (br $CH_2CH_2CH_2CH_2CH_2$, 10H) 1.7 (br $CH_2C(CH_3)_2$, 2H), 2.0 (br $NCH_2CH_2CH_2N(CH_3)_2$, 2H), 2.7–3.1 (br *CHCH*, 2H), 3.1-3.3 (br $NCH_2CH_2CH_2NCH_2(CH_3)_2$, 10H), 3.6 (br $NCH_2CH_2CH_2N(CH_3)_2$, 2H).

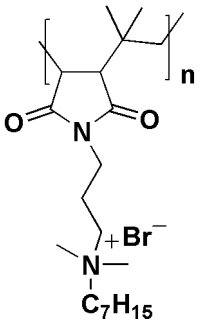

Q*n*-HexP: FT-IR: 2950-2850 (C-H str.), 1767 cm^{-1} (C=O asym. str.), 1696 cm^{-1} (C=O sym. str.) 1470-1410cm^{-1} (C-C str.), 1290-1110 (C-O str.); ^{1}H-NMR (400 MHz, D_2O): δ/ppm 0.85-0.9 (br terminal –*CH_3*, 3H), 0.95–1.2 (br $CH_2C(CH_3)_2$, 6H), 1.3-1.5 (br $CH_2CH_2CH_2CH_2$, 8H) 1.7 (br $CH_2C(CH_3)_2$, 2H), 2.0 (br $NCH_2CH_2CH_2N(CH_3)_2$, 2H), 2.7–3.1 (br *CHCH*, 2H), 3.1-3.3 (br $NCH_2CH_2CH_2NCH_2(CH_3)_2$, 10H), 3.6 (br $NCH_2CH_2CH_2N(CH_3)_2$, 2H).

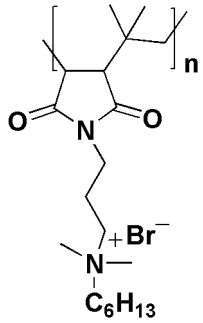

Q*n*-PenP: - FT-IR: 2950-2850 (C-H str.), 1767 cm^{-1} (C=O asym. str.), 1696 cm^{-1} (C=O sym. str.) 1470-1410cm^{-1} (C-C str.), 1290-1110 (C-O str.); ^{1}H-NMR (400 MHz, D_2O): δ/ppm 0.85-0.9 (br terminal –*CH_3*, 3H), 0.95–1.2 (br $CH_2C(CH_3)_2$, 6H), 1.3-1.5 (br $CH_2CH_2CH_2$, 6H) 1.7 (br $CH_2C(CH_3)_2$, 2H), 2.0 (br $NCH_2CH_2CH_2N(CH_3)_2$, 2H), 2.7–3.1 (br *CHCH*, 2H), 3.1-3.3 (br $NCH_2CH_2CH_2NCH_2(CH_3)_2$, 10H), 3.6 (br $NCH_2CH_2CH_2N(CH_3)_2$, 2H).

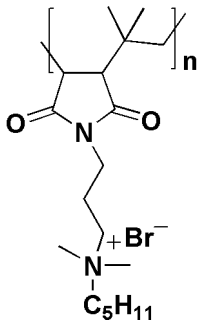

Q*n*-ButP: FT-IR: 2950-2850 (C-H str.), 1767 cm^{-1} (C=O asym. str.), 1696 cm^{-1} (C=O sym. str.) 1470-1410cm^{-1} (C-C str.), 1290-1110 (C-O str.); ^{1}H-NMR (400 MHz, D_2O): δ/ppm 0.85-0.9 (br terminal –*CH_3*, 3H), 0.95–1.2 (br $CH_2C(CH_3)_2$, 6H), 1.3-1.5 (br CH_2CH_2, 4H) 1.7 (br $CH_2C(CH_3)_2$, 2H), 2.0 (br $NCH_2CH_2CH_2N(CH_3)_2$, 2H), 2.7–3.1 (br *CHCH*, 2H), 3.1-3.3 (br $NCH_2CH_2CH_2NCH_2(CH_3)_2$, 10H), 3.6 (br $NCH_2CH_2CH_2N(CH_3)_2$, 2H).

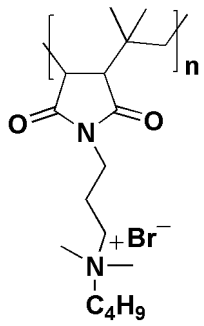

Q*n*-EthP: FT-IR: 2950-2850 (C-H str.), 1767 cm^{-1} (C=O asym. str.), 1696 cm^{-1} (C=O sym. str.) 1470-1410cm^{-1} (C-C str.), 1290-1110 (C-O str.); ^{1}H-NMR (400 MHz, D_2O): δ/ppm 0.85-0.9 (br terminal $–CH_3$, 3H), 0.95–1.2 (br $CH_2C(CH_3)_2$, 6H), 1.7 (br $CH_2C(CH_3)_2$, 2H), 2.0 (br $NCH_2CH_2CH_2N(CH_3)_2$, 2H), 2.7–3.1 (br *CHCH*, 2H), 3.1-3.3 (br $NCH_2CH_2CH_2NCH_2(CH_3)_2$, 10H), 3.6 (br $NCH_2CH_2CH_2N(CH_3)_2$, 2H).

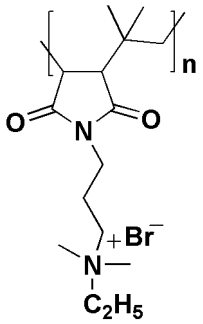

Q*n*-BEGP: FT-IR: 2950-2850 (C-H str.), 1767 cm^{-1} (C=O asym. str.), 1696 cm^{-1} (C=O sym. str.) 1470-1410cm^{-1} (C-C str.), 1290-1110 (C-O str.); ^{1}H-NMR (400 MHz, D_2O): δ/ppm 0.95–1.2 (br $CH_2C(CH_3)_2$, 6H), 1.7 (br $CH_2C(CH_3)_2$, 2H), 2.0 (br $NCH_2CH_2CH_2N(CH_3)_2$, 2H), 2.7–3.1 (br *CHCH*, 2H), 3.1-3.2 (br $NCH_2(CH_3)_2$, 6H), 3.45 (s, terminal $–CH_3$), 3.55-3.8 (br, $NCH_2CH_2CH_2NCH_2(CH_3)_2$ and OCH_2CH_2O, 10H), 4.0 (br $OCH2CH_2N(CH_3)_2$, 2H).

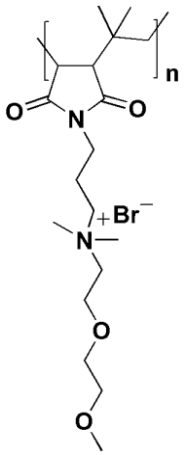

Quaternized PIBMI derivatives-Qn-prEPor Qn-prAP

To a solution of 0.5 g of PIBMI in 20 mL of dry DMF/dry $CHCl_3$ (1:1), 2 equivalents (with respect to the monomer weight of PIBMI (238.18 g/mol)) of propyl-1-bromoethanoate/ *N*-propyl-1-bromoethanamide was added and stirred at 65°C-75°C for 96 h in a screw top pressure tube. The solution was cooled, precipitated with 40 mL of diethylether and filtered. The white solid was washed with diethylether (4 × 40 mL) and dried at 40 °C for 4 h under vacuum (yield: 100%).

Q*n*-prEP: FT-IR: 2950-2850 (C-H str.), 1767 cm^{-1} (imide C=O asym. str.), 1696 cm^{-1} (imide C=O sym. str.), 1735 cm^{-1} (ester C=O str.) 1470-1410cm^{-1} (C-C str.), 1290-1110 (C-O str.); ^{1}H-NMR (400 MHz, D_2O): δ/ppm 0.85 (br, terminal $–CH_3$, 3H), 0.95–1.2 (br, $CH_2C(CH_3)_2$, 6H), 1.57 (br,-$COOCH_2CH_2CH_3$, 2H), 1.7 (br, $CH_2C(CH_3)_2$, 2H), 2.0 (br, $NCH_2CH_2CH_2N(CH_3)_2$, 2H), 2.7–3.1 (br, *CHCH*, 2H), 3.1-3.3 (br, $NCH_2CH_2CH_2N(CH_3)_2$, 8H), 3.6 (br, $NCH_2CH_2CH_2N(CH_3)_2$, 2H), 3.7 (br, -$N(CH_3)_2COCH_2$, 2H) 4.0 (br, -$COOCH_2$-, 2H).

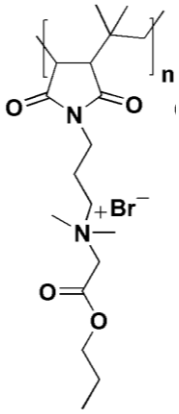

Q*n*-prAP: FT-IR: 3250 cm^{-1} (amide N-H str.), 2950-2850 (C-H str.), 1767 cm^{-1} (imide C=O asym. str.), 1696 cm^{-1} (imide C=O sym. str.) 1680 cm^{-1} (amide I, C=O str.), 1560 cm^{-1} (Amide II, N-H ben.), 1470-1410cm^{-1} (C-C str.), 1290-1110 (C-O str.); ^{1}H-NMR (400 MHz, D_2O): δ/ppm 0.878 (br, terminal –*CH_3*, 3H), 0.95–1.2 (br, $CH_2C(CH_3)_2$, 6H), 1.543 (br, -$CONHCH_2CH_2CH_3$-, 2H), 1.7 (br, $CH_2C(CH_3)_2$, 2H), 2.0 (br, $NCH_2CH_2CH_2N(CH_3)_2$, 2H), 2.7–3.1 (br, *CHCH*, 2H), 3.1-3.3 (br, $NCH_2CH_2CH_2N(CH_3)_2$, 8H), 3.5 (br, -$CONHCH_2$-, 2H), 3.6 (br, $NCH_2CH_2CH_2N(CH_3)_2$, 2H), 3.8 (br, -$N(CH_3)_2COCH_2$, 2H).

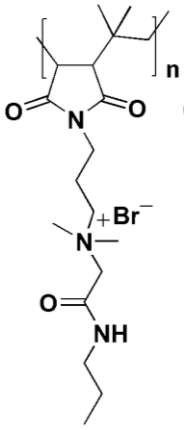

2.4.4 Gel Permeation Chromatography (GPC)

GPC of the water soluble Poly(isobutylene-alt-maleic acid) obtained after hydrolysis of Poly(isobutylene-alt-maleic anhydride) was performed. Experiments were carried out on a Shimadzu-LC 20AD instrument with refractive index (RI) detector using Polysep-GPC-P Linear (300×7.8 mm, Phenomenex, Catalogue no. 00H-3147-K0, Separation Range: 1 KDa-10 MDa) column in sodium acetate buffer (0.2 M, pH = 5.3) with a flow rate of 0.8 mL min^{-1}. Pullulan standards (1.3 KDa, 6 KDa, 10 KDa, 22 KDa and 50 KDa) were used for the experiment to determine the polydispersity index (PDI = M_w/M_n) of the polymer.

2.4.5 Antibacterial assays

2.4.5.1 Antibacterial activity in broth culture media

Antibacterial activity was determined with the slight modifications of standardized protocols[155]. Water-soluble QAPIBMI derivatives were assayed in a modified micro-dilution broth format. Stock solutions of the quaternized PIBMI derivatives were made by serially diluting the compounds using autoclaved Millipore water. Bacteria, to be tested, grown for 6 h in the suitable media contained ~10^9 CFU mL^{-1} (determined by spread plating method), which was then diluted to 10^5 CFU mL^{-1} using nutrient media. 50 µL of serially diluted compound was added to a 96 well plate (Polystyrene) containing 150 µL bacterial solutions. Two controls were made; one containing 150 µL of media and 50 µL of compound and the other containing 150 µL of bacterial solution and 50 µL water . The plate was then incubated at 37 °C for a period of 24 h and the O.D. value was measured at 600 nm using a Tecan InfinitePro series M200 Microplate

Reader. MIC value was determined by taking the average of triplicate O.D. values for each concentration and plotting it against concentration using Origin Pro 8.0 software. The data was then subjected to sigmoidal fitting. From the curve the MIC value was determined, as the point in the curve where the O.D. was similar to that of control having no bacteria. The MIC values and errors are reported as averages and standard errors of mean of three independent experiments respectively. MIC curves for each polymer are representative data from the three independent experiments and each experiment was performed in triplicates.

2.4.5.2 Antibacterial activity in chemically defined media

Bacteria were diluted to ~5×10^5 CFU mL^{-1} in M9 minimal media (as per ATCC Medium: 2511 M9 Minimal Broth containing inorganic salts, glucose and thiamine, pH = 7.4) for *E. coli* and minimum essential medium (MEM which contains vitamins, amino acids, inorganic salts and nucleosides from Life Technologies, USA) for *S. aureus*. 50 μL of compounds (polymers) were added to a 96 well plate (Polystyrene) containing 150 μL bacterial solutions. The plate was then incubated at 37 °C for a period of 18-24 h. 20 μL of bacterial suspension was spot-plated on agar plates. The viable colonies (<100) were counted after 24 h incubation at 37 °C.

2.4.5.3 Bactericidal time-kill kinetics

The bactericidal activity of the polymers was assessed by the kinetics or the rate at which it affects the killing action of the compound. Briefly, *S. aureus* was grown in yeast-dextrose broth at 37 °C for 6 h. Test compound, Q*n*-prAP, having the final concentrations of 1×MIC, 6×MIC and 12×MIC was inoculated with the aliquots of *S. aureus* resuspended in fresh media at approximately 1.8×10^5 CFU mL^{-1}. After specified time intervals (0, 1, 2 and 3 h), 20 μL aliquots were serially diluted 10 fold in 0.9 % saline, plated on sterile yeast-dextrose agar plates and incubated at 37 °C overnight. The viable colonies were counted the next day and represented as $\log_{10}$ (CFU mL^{-1}).

2.4.5.4 Antibacterial efficacy in human plasma

The antibacterial activity of the derivatives was performed in presence of 50% of plasma to assess its susceptibility to plasma proteases. 250 μL of the compound was added to 250 μL of

human plasma (centrifuged from whole blood and collected the blood minus cell fraction) and pre-incubated at 37 °C for 0 and 3 h (final concentration of human plasma is 50% (vol/vol)). After incubation, the compound was diluted two-fold in 0.9% saline, performed the antibacterial assay against *S. aureus* and MIC was determined. Also, a similar MIC experiment against *S. aureus* was performed in the absence of the plasma as control.

2.4.6 Hemolytic assays

The hemolytic activity was determined against human erythrocytes. Erythrocytes were isolated from freshly drawn, heparanized human blood and resuspended to 5 % v/v in PBS (pH 7.4). In a 96-well microtiter plate, 150 µL of erythrocyte suspension was added followed by 50 µL of serially diluted compound to give a final solution of 3.75 % v/v erythrocytes. PBS buffer was added instead of polymer solution as negative hemolysis control and Triton X-100 (1% v/v) was used as positive hemolysis control. The plate was incubated for 1 h at 37°C and was then centrifuged at 3,500 rpm for 5 min. 100 µL of the supernatant was then transferred to a fresh micro titer plate and absorbance at 540 nm was measured using a Tecan InfinitePro series M200 Microplate Reader. Percentage of hemolysis was determined as $(A - A_0)/ (A_{total} - A_0) \times 100$, where A is the absorbance of the test well, A_0 the absorbance of the negative controls, and A_{total} the absorbance of 100% hemolysis wells, all at 540 nm. Hemolysis was plotted as a function of polymer concentration and the HC_{50} was defined as the polymer concentration, which causes 50% hemolysis relative to the positive control. In some cases, hemolysis did not reach 50 % up to the highest polymer concentration tested and the HC_{50} was not determined. The HC_{50} values and errors are reported as averages and standard errors of mean of three independent experiments, respectively. Hemolysis curves for each polymer are representative data from two independent experiments and each experiment was performed in triplicates.

2.4.7 Mechanism of action

2.4.7.1 Cytoplasmic membrane depolarization assay

Mid-log phase bacterial cells were harvested, washed with 5 mM HEPES and 5 mM glucose and resuspended in 5 mM glucose, 5 mM HEPES buffer and 100 mM KCl solution in 1:1:1 ratio ($\sim 10^9$ CFU mL^{-1}). Measurements were made in a cuvette containing 2 mL of bacterial suspension and 2 µM $DiSC_3(5)$. The fluorescence of the dye was monitored using PerkinElmer

LS-55 Luminescence Spectrometer at excitation wavelength of 622 nm and emission wavelength of 670 nm. Dye uptake, and resultant self quenching, was modulated by the membrane potential. After reaching the maximum uptake of the dye by bacteria, which was indicated by a minimum in dye fluorescence, quaternized PIBMI derivatives (50 µg mL^{-1}) were added to the cells, and the decrease in potential was monitored by the increase in fluorescence.

2.4.7.2 Cytoplasmic membrane permeabilization assay

Mid-log phase bacteria were harvested (4000 rpm, 4°C, 10 min), washed, and resuspended in PBS buffer of pH 7.2. Then quaternized PIBMI derivatives were added (50 µg mL^{-1}) to the cuvette containing 2.0 mL of bacterial suspension and 10 µM propidium iodide (PI). Excitation wavelength of 535 nm (slit width: 10 nm) and emission wavelength of 617 nm (slit width: 10 nm) were used. The uptake of PI was measured by the increase in fluorescence of PI as a measure of membrane permeabilization.

2.4.7.3 Release of ATP levels

Mid-log phase bacteria (~10^{8-9} CFU mL^{-1}) were harvested and washed twice with 10 mM TRIS buffer (pH = 7.5) and were resuspended in the same buffer. Then, 150 µl of bacterial suspension and 50 µl of test drugs were added to the microcentrifuge tube and incubated at 37 °C for 15 min. After 15 min, the bacterial suspension was centrifuged and 50 µl of the supernatant was transferred into a Corning 96 well black plate with clear bottom to find out the released ATP levels using ATP Bioluminiscience Assay Kit (Sigma Aldrich) as per the manufacturer's instructions. A standard curve for ATP levels was generated using the ATP standards provided in the kit in the range of 1E-6 to 1E-11 moles of ATP levels. Polymers were used at 50 µg mL^{-1}. Water served as the untreated control. Stock solutions of the polymers were made in water and further diluted in water. Relative ATP levels both in the standard curve and the test sample measurement were measured by subtracting the background ATP levels from the test sample ATP levels as per the manufacturer's instructions. All measurements were performed in duplicates using Tecan InfinitePro series M200 Microplate Reader.

2.4.7.4 Alteration of cell division proteins

B. subtilis strains were cultured in LB medium. Overnight cultures from a single colony were diluted and grown at 30 °C. Xylose (0.1% -0.5%) was added to induce the GFP fusion proteins[164]. At OD_{600} ~0.2, 200 µl of cells were incubated with 25 µg mL^{-1} of polymers for 10 minutes. The last 3 minutes, 1 µg mL^{-1} Nile red (Sigma) was added for membrane staining. Microscope slides were covered with 1% agarose in deionized water. 0.4 µl of cells were spotted onto the agarose layer and excess liquid was allowed to evaporate before a 0.31 mm cover slip (VWR) was placed on top. Cells were observed with a Nikon Eclipse Ti inverted microscope with Nikon plan apo 100x 1.45 oil objective, and Hamamatsu ORCA Flash UBB 3.0 camera. Images were processed using Nikon and ImageJ software.

2.4.7.5 Morphological membrane disruption by FESEM

Bacteria were cultured for 6 h in suitable media (Yeast-dextrose broth for *S. aureus* and LB broth for *E. coli*) at 37°C. The cells were centrifuged and resuspended in respective nutrient media at pH 7.4 (10^8 CFU mL^{-1}). The suspension was divided into two portions (1 mL each). To one portion was added a solution of Q*n*-prAP (6×MIC). The other portion was used as a control and left untreated. The suspensions were then incubated at 37 °C for 2 h (at ~ 250 rpm shaking speed), and the bacteria from both tubes were harvested by centrifugation at 12000 rpm for 1 min. Finally, the cells were sequentially dehydrated with 30, 50, 70, 80, 90, and 100% ethanol. 5 µL of dehydrated cells was then dropped on a small piece of silicon wafer and dried at room temperature. Before being imaged, the silicon wafers containing bacteria were sputter coated with gold. Images were recorded by using Quanta 3D FEG FEI field-emission scanning electron microscopy at 5 kV or 8 kV operating voltage.

Chapter 3

Cationic-amphiphilic Polymers with Isosteric Substitution of Functional Groups in the Side Chains

Abstract

Amphiphilicity, a balance of cationic charge and hydrophobicity, in antibacterial polymers has been shown to be pivotal for their selective interaction with anionic lipid membranes of bacteria instead of zwitterionic mammalian cell (human erythrocyte) membranes. However, it is unclear if and to what extent hydrogen bonding in amphiphilic antibacterial polymers contributes to this membrane binding specificity. To address this, isosteric substitution of ester with amide moieties has been employed that differ in their potency for hydrogen bonding in the side chains of N-alkyl maleimide based amphiphilic polymers. Studies reveal that amide polymers (Qn-CmAPs) are potent antibacterial agents with high membrane-disrupting properties compared to their ester counterparts (Qn-CmEPs). Bio-physical experiments and molecular dynamics (MD) simulations which showed strong interactions of Qn-CmAPs including hydrogen bonding with lipid head groups of bacterial model lipid bilayers, that are absent in Qn-CmEPs, make them potent bacterial membrane disruptors. This work provides a conceptual advance in understanding the interactions of antibacterial polymers with bacterial cell membranes highlighting the role of hydrogen bonding. Thus, these findings have significant implications in efficient design of selective antibacterial polymers.

(1) Uppu, D. S. *et al.* "An Essential Role for Hydrogen Boding in Bacterial Membrane Interactions". Manuscript under review.

3.1 Introduction

Amphiphilicity, a key structural feature of AMPs, has been optimized in antibacterial polymers reported so far[107]. This amphiphilicity which is a fine balance of hydrophobicity and cationic charge has been shown to play a key role in the selective interaction of these polymers with the bacterial cell membranes instead of mammalian cell (for e.g. human erythrocyte) membranes. Electrostatic interactions bind the cationic polymers to the bacterial cell membranes that contain negatively charged phospholipids whereas hydrophobic interactions facilitate the binding and insertion into the lipid bilayers. The selective interactions of amphiphilic polymers with bacterial membranes results from the fact that the eukaryotic cell membranes generally contain a higher proportion of zwitterionic phospholipids and are rigid and possess high membrane order due to the presence of cholesterol [107]. Despite these differences, driving the selective interactions of amphiphilic polymers towards bacteria has remained elusive. An important and yet unexplored question is how hydrogen bonding contributes to the bacterial membrane specific interactions of amphiphilic polymers.

To investigate the role of hydrogen bonding, the concept of isosteric substitution of ester with amide moieties has been introduced in the side chains of poly(isobutylene-*alt*-*N*-alkyl maleimide) based amphiphilic polymers prepared from their maleic anhydride precursor polymer (Scheme 3.1). Substitution of an ester with an amide is isosteric and hence only varies in the potency of hydrogen bonding. It was found that the amide polymers (Q*n*-CmAPs) displayed high antibacterial activity compared to their ester (Q*n*-CmAPs) counterparts. To probe these differences, biophysical experiments and molecular dynamic (MD) simulations were performed on bacterial model lipid bilayers. Collectively, the studies provided the evidence that Q*n*-CmAPs, but not Q*n*-CmAPs, form strong interactions including hydrogen bonding with the phosphate head groups of bacterial model lipid bilayers. Studies performed to understand the mode of action revealed membrane-disruptive activity that led to the dissipation of membrane potential, pore formation and energy depletion. Stability of the polymers in different conditions showed that amide polymers are more stable than ester polymers. Assessment of toxicity studies of polymers and their degradation by-products in mice displayed good safety profiles for *in-vivo* applications.

3.2 Results and Discussion

3.2.1 Rational design

Amide and ester moieties, in general, possess differences in their ability to form hydrogen bonds. This simple replacement of ester with amide moieties, called as isosteric replacement, has been incorporated in the side chains of poly(isobutylene-*alt*-*N*-alkyl maleimide) based amphiphilic polymers (Scheme 3.1). An amide bond is isosteric to an ester because the -O- in the ester is of near-equal size as the -NH- in the amide moiety. Isosteric replacement of an amide by an ester in peptides or proteins has been shown to alter the conformational properties and biological activities[167-169]. The amphiphilic polymers were synthesized as described in Chapter 2 (Scheme 3.1). The cationic charge density given by the degree of quaternization was calculated by ^{1}HNMR analysis as described in Chapter 2 and found to be in the range of 90-95% for all the polymers. This shows that the cationic charge density was more or less constant in all the polymers which facilitated the comparison between them. The polymers (P) shown in Scheme 3.1 are represented as Q*n*-CmAPs and Q*n*-CmEPs for poly(isobutylene-alt-*N*-(*N'*,*N'*-dimethylamino*propyl*)-maleimide) (PIBMI) based quaternized (Q) amide (A) and ester (E) respectively with appended alkyl chains of different lengths (Cm, for number (m) of carbon (C) atoms in the alkyl chain).

3.2.2 Antibacterial activity and mammalian cell toxicity

To understand the effect of isosteric replacement, the antibacterial activity and hemolysis of the polymers were investigated. The amphiphilicity of the polymers was adjusted by varying the length of the alkyl chain appended to them. Both the amide and ester polymers with appended butyl (Q*n*-buAP and Q*n*-buEP) and hexyl (Q*n*-hexAP and Q*n*-hexEP) chains were potent antibacterial agents (MIC = 4-31 μg mL^{-1}) against both *E. coli* and *S. aureus* (Table 3.1). However, even at these longer alkyl chains, the ester polymers (Q*n*-hexEP and Q*n*-buEP) were also hemolytic (HC_{50} = 30 μg mL^{-1} and 124 μg mL^{-1}) but to a lesser extent compared to their amide counterparts (HC_{50} = 12 μg mL^{-1} and 83 μg mL^{-1}). On the other hand, the amide polymers with propyl and ethyl chains (Q*n*-prAP and Q*n*-etAP) have potent antibacterial efficacy with MIC of 31 μg mL^{-1} and 62 μg mL^{-1} respectively, whereas their corresponding ester polymers (Q*n*-prEP and Q*n*-etEP) were weakly antibacterial with MIC = 125-500 μg mL^{-1} against both *E. coli* and *S. aureus* (Fig. 3.1 A & Table 3.1). Minimum bactericidal concentration (MBC) in

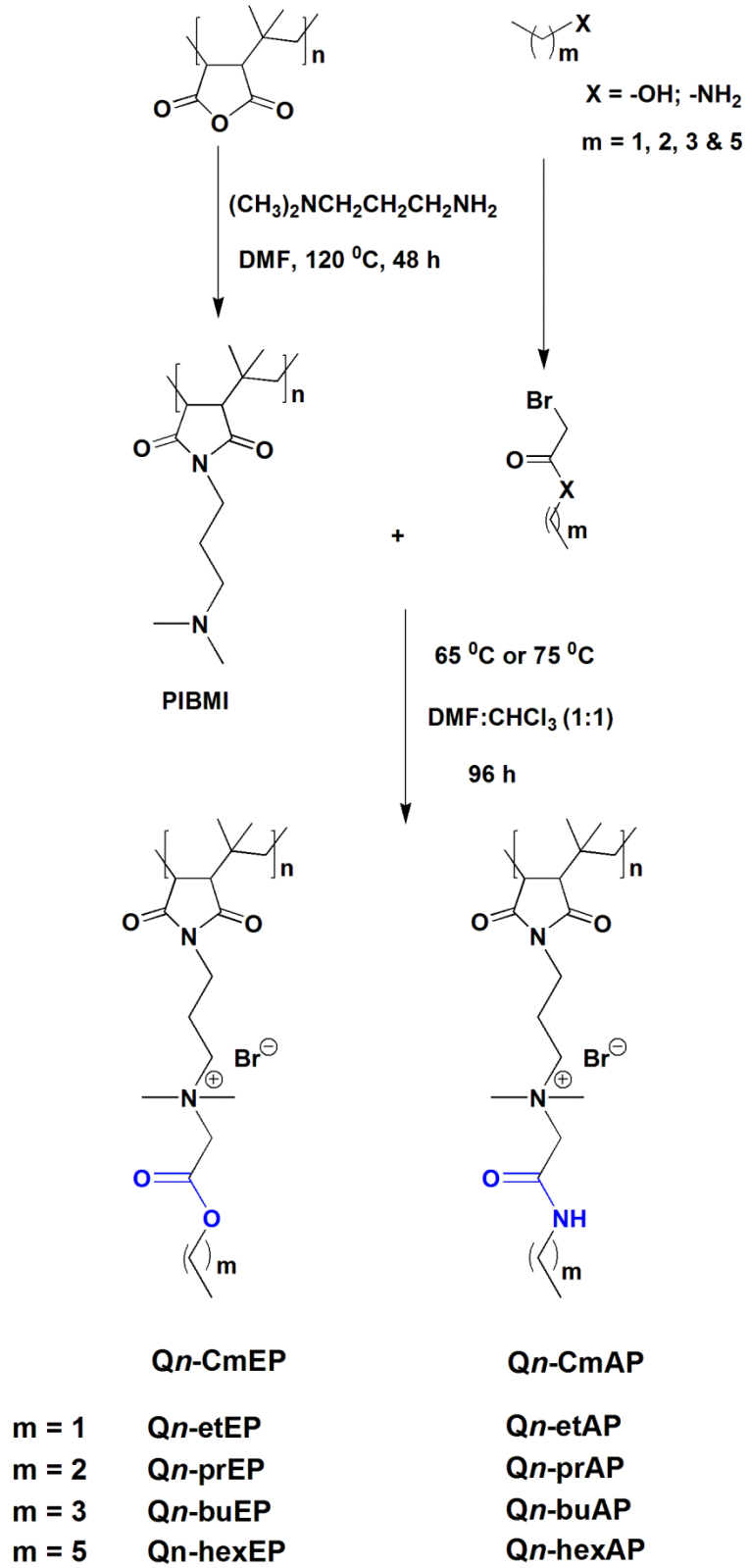

Scheme 3.1: General scheme for the synthesis of isosteric cationic and amphiphilic polymers.

Table 3.1: Antibacterial activity, toxicity and selectivity profiles of cationic polymers

Polymer	MIC[a] (μg mL^{-1})		HC_{50}[b] (μg mL^{-1})	Selectivity[c]	
	E. coli	*S. aureus*		*E. coli*	*S. aureus*
Q*n*-hexAP	31	16	12	0.4	0.8
Q*n*-hexEP	16	8	30	2	4
Q*n*-buAP	31	4	83	3	21
Q*n*-buEP	31	16	124	4	8
Q*n*-prAP	31	31	>1000	>32	>32
Q*n*-prEP	250	125	>1000	>8	>4
Q*n*-etAP	62	62	>1000	>16	>16
Q*n*-etEP	>500	>500	>1000	>2	>2
Q*n*-HexP	7	20	30	4.3	1.5

[a]MIC, minimum inhibitory concentration in cation adjusted Mueller-Hinton broth (CAMHB); [b]HC_{50}, concentration required to cause 50% hemolysis; [c]Selectivity, is defined as HC_{50}/MIC.

chemically defined media was found to be 2 μg mL^{-1} and 3 μg mL^{-1} for Q*n*-prAP whereas Q*n*-prEP showed 16 μg mL^{-1} and >200 μg mL^{-1} against *S. aureus* and *E. coli* respectively. This observation reiterates the fact that the effect of isosteric replacement on antibacterial activity is indeed due the difference in their chemical structure and not the culture media conditions. However, all the lower alkyl chain (C3 and C2) containing amide and ester polymers had HC_{50} > 1000 μg mL^{-1} due to lower hydrophobicity. This resulted in higher selectivity (HC_{50}/MIC) of >16-32 for Q*n*-prAP and Q*n*-etAP whereas their ester counter parts, Q*n*-prEP and Q*n*-etEP had low selectivity of >2-8 against both *E. coli* and *S. aureus* (Table 3.1). The control polymer, Q*n*-HexP though displayed potent antibacterial efficacy but was highly toxic to hRBCs (HC_{50} = 30 μg mL^{-1}) leading to low selectivity (HC_{50}/MIC) (Table 3.1). The amide polymer, Q*n*-prAP with lower hydrophobicity (propyl chain) and the ester polymer, Q*n*-buEP with higher hydrophobicity (butyl chain) showed similar antibacterial activity of 31 μg mL^{-1} against *E. coli*. However, the Q*n*-buEP was found to be more hemolytic (HC_{50} = 124 μg mL^{-1}) than Q*n*-prAP (HC_{50} >1000 μg mL^{-1}). These results suggested that the Q*n*-HexP without any H-bonding moieties in the side chains is highly toxic whereas Q*n*-prAP is less toxic to mammalian cells indicating the importance of amide moiety. The amide containing polymer can be potent antibacterial agent with lower hydrophobicity whereas an ester containing polymer needs relatively higher hydrophobicity to be as effective as its amide counterpart. Thus, optimization of hydrophobicity is required to tune the amphiphilicity as the cationic charge density is more or less constant. However, even at C2 chains, the amide polymer, Q*n*-etAP was more potent in antibacterial

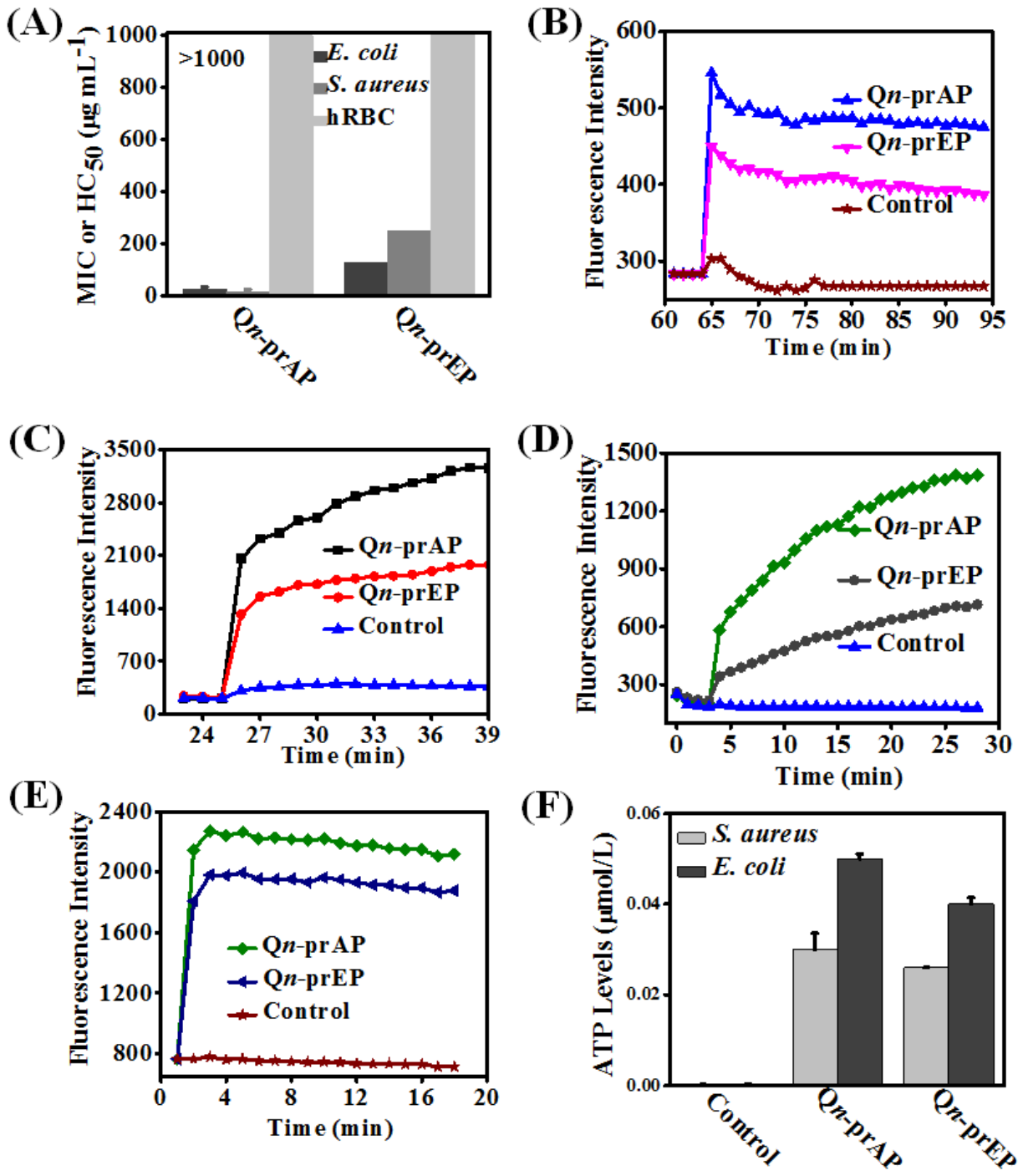

Figure 3.1: Biological activity studies of isosteric amide and ester polymers. (A) Antibacterial and hemolytic activity. The data are expressed as mean ± standard deviation from two independent experiments in triplicate; Membrane depolarization against *E. coli* (B) and *S. aureus* (C); Membrane permeabilization against *E. coli* (D) and *S. aureus* (E); Leakage of ATP levels after treatment for 15 min against against *E. coli* and *S. aureus* (F); Relative ATP levels (mol/L) were determined by subtracting the background ATP levels from the test sample ATP levels.

activity than the Q*n*-etEP supporting the importance of amide than the ester moieties. Therefore, it appears that the amide side chain containing polymers with optimum hydrophobicity selectively kill bacteria compared to their ester counterparts sparing the mammalian cells.

3.2.3 Membrane-active properties

The membrane-active properties of antibacterial polymers were studied in detail to better understand the effects of isosteric replacement towards antibacterial activity against *E. coli* and *S. aureus* at 25 μg mL^{-1}. At longer appended alkyl chains (hexyl, C6) the ester polymers showed similar dissipation of membrane potential than its amide counterparts (Fig. 3.2 A & B). At all the other appended alkyl chains (C2-C4), the amide polymers were always found to possess higher ability to dissipate the membrane potential than their ester counterparts. The optimum alkyl chain amide polymer, Q*n*-prAP has higher depolarization than the corresponding ester, Q*n*-prEP which

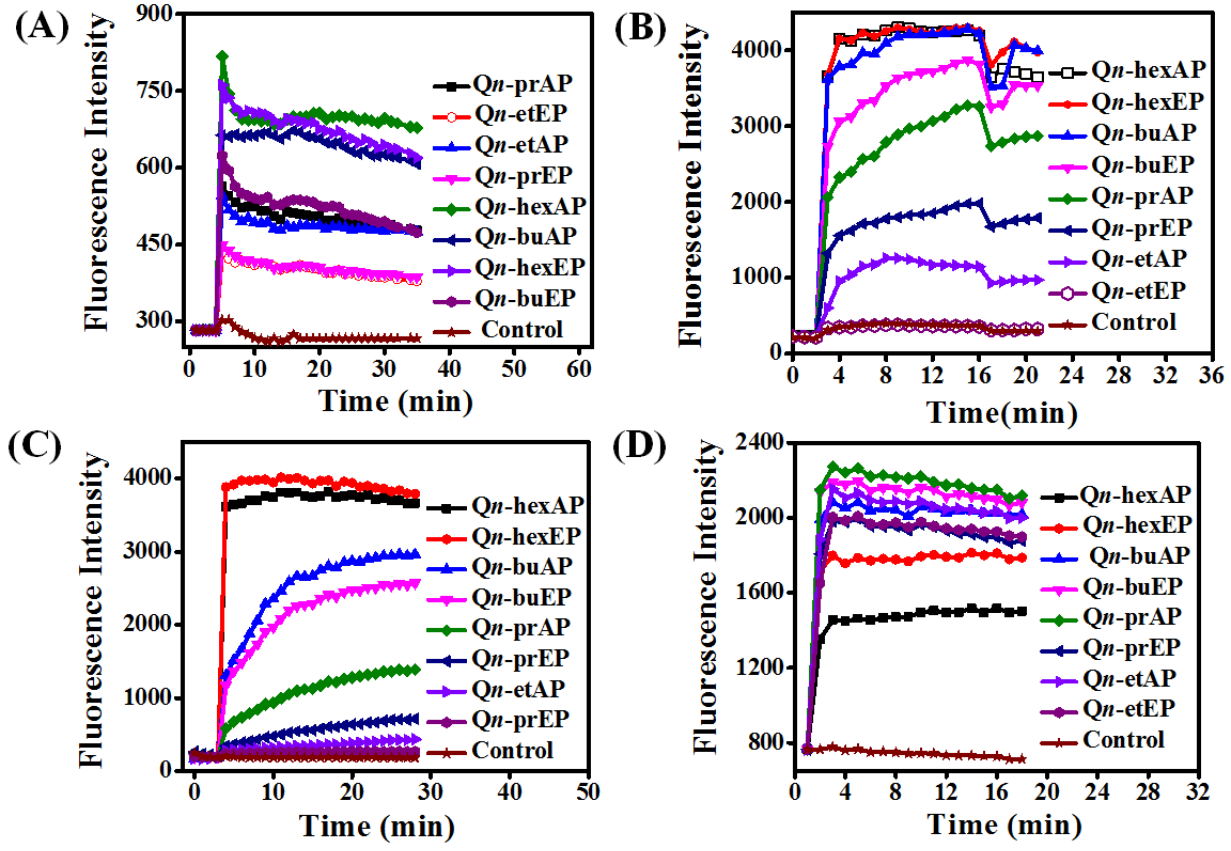

Figure 3.2: Membrane-disrupting properties of isosteric ester and amide polymers. (A) Membrane depolarization of polymers (at 25 μg mL^{-1}) against *S. aureus* (A) and *E. coli* (B); Membrane permeabilization of polymers (at 25 μg mL^{-1}) against *E. coli* (C) and *S. aureus* (D).

could be correlated with the low antibacterial activity of the ester against *E. coli* and *S. aureus* (Fig. 3.1 B & C). EC2P (MIC > 500 µg mL^{-1}) did not have any appreciable effect on membrane potential of *E. coli* and *S. aureus*. Kinetics of membrane permeabilization was studied by measuring the uptake of the fluorescent probe propidium iodide (PI) against *E. coli* and *S. aureus* at 25 µg mL^{-1}. All the amide containing polymers have higher ability to permeabilize the bacterial cell membrane than their ester counterparts at all the appended alkyl chain lengths (Fig. 3.1 D & E, Fig. 3.2 C & D). Lower alkyl chain amide and ester polymers that showed membrane depolarization were devoid of membrane permeabilization. Q*n*-HexP had lower ability than Q*n*-prAP and higher ability than Q*n*-prEP with respect to the membrane-disruptive activity in bacteria as shown in previous chapter (Fig. 2.4 B & C). Dissipation of membrane potential leads to limiting the energy required for metabolic processes in bacteria. Intracellular ATP levels in *E. coli* and *S. aureus* were measured after treatment with Q*n*-prAP and Q*n*-prEP using the luciferin-luciferase bio-luminescence assay to understand the energy limitation conditions. Q*n*-prAP (50 µg mL^{-1}) showed higher release of ATP levels compared to its ester counterpart, Q*n*-prEP (50 µg mL^{-1}) in both *E. coli* (Fig. 3.1 F) and *S. aureus* (Fig. 3.1 G). This supports the fact that the interaction of the amide and ester polymers with the bacterial membrane is different resulting in variable release of ATP levels.

3.2.4 Biophysical experiments using model lipid bilayers

3.2.4.1 Membrane fluidity/viscosity

To emphasize the fact that the interaction of the polymers is indeed with the cell membrane, studies were performed with model lipid bilayers. Bacterial (DPPG:DPPE) and mammalian (DPPC) model lipid bilayers were prepared with Laurdan (6-Dodecanoyl-2-dimethylaminonaphthalene), a hydrophobic dye encapsulated in them. Due to its structure, dipole moment and its fluorescence characteristics, Laurdan is very useful in studies about lipid bilayer dynamics. One of its most important characteristics is its sensitivity to membrane phase transitions as well as other alterations to membrane fluidity such as the penetration of water. Laurdan detects changes in the membrane-phase properties through its sensitivity to the polarity of environment in the lipid bilayer. Polarity changes cause shifts in Laurdan emission spectrum. Interaction of these polymers with the membrane can result in membrane hydration that can be monitored using perturbations in Laurdan dye fluorescence and quantified by calculating general

polarization (GP =(I_{440}- I_{490})/(I_{440}+I_{490})). Lower GP indicates higher fluidity (lower viscosity) of the membrane (Fig. 3.3 A) [170, 171]. The Laurdan GP was calculated after the treatment of DPPG: DPPE (88:12) and DPPC lipid bilayers with the amide (Q*n*-hexAP and Q*n*-prAP) and ester (Q*n*-hexEP and Q*n*-prEP) polymers (lipid: polymer = 7.4:1) (Fig. 3.3 B). The longer alkyl chain amide polymer, Q*n*-hexAP showed the lowest GP followed by similar GP for both Q*n*-prAP and Q*n*-hexEP for DPPG:DPPE lipid system compared to the untreated system. These results suggest that an amide polymer with propyl chain is as effective as an ester polymer with hexyl chain appended to them suggesting the importance of amide moiety. On the other hand, the shorter alkyl chain ester polymer, Q*n*-prEP did not show any reduction in GP for DPPG: DPPE compared to the untreated lipid bilayer. For DPPC bilayer, only the longer alkyl chain amide polymer, Q*n*-hexAP showed reduction in GP compared to the untreated bilayer (Fig. 3.3 B). These observations suggested that Q*n*-prAP displayed selective interaction with the bacterial cell membrane whereas its ester counterpart, Q*n*-prEP was devoid of selectivity between bacterial and mammalian cells.

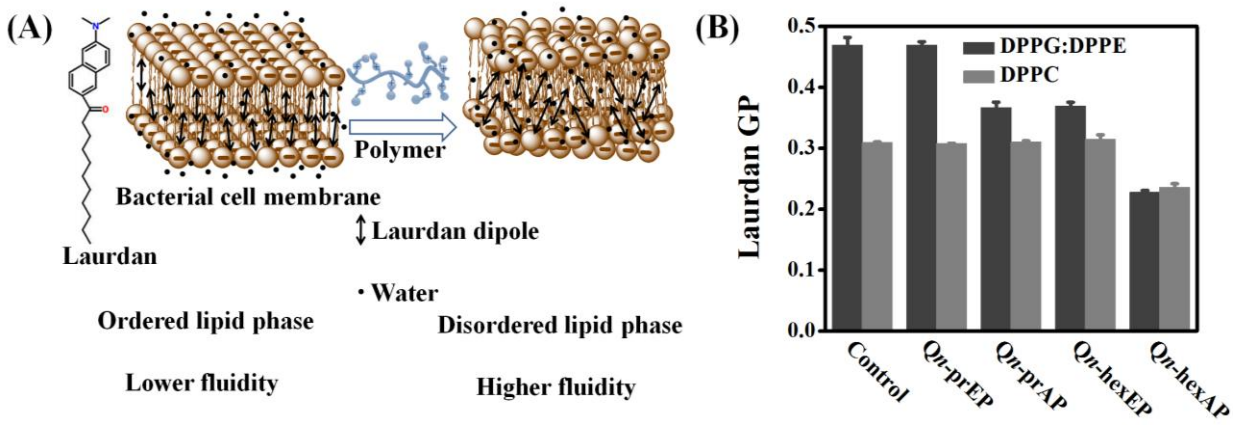

Figure 3.3: Mechanistic studies to understand the interactions of amide and ester polymers with bacterial and mammalian model lipid bilayers. (A) Schematic of membrane-active polymer affecting the membrane hydration/fluidity/viscosity of the membrane. Laurdan, a hydrophobic dye, is sensitive to the membrane bilayer dynamics. Membrane hydration was determined using perturbations in Laurdan dye fluorescence due to the result of hydration of the lipid bilayer and quantified by calculating generalized polarization (GP). (B) Membrane hydration of lipid bilayers at 37 °C consisting of DPPG: DPPE (88:12) and DPPC treated with amide and ester polymers mimicking the bacterial and mammalian cell membranes respectively.

3.2.4.2 Thermodynamic of membrane interactions (ITC)

To delineate the molecular understanding of interactions between the model lipid bilayers and polymers, isothermal titration calorimetry (ITC) was used for obtaining the thermodynamics of interactions. DPPG:DPPE (88:12) or DPPC model lipid bilayers were injected into the polymer solution, i.e. by gradually reducing the concentration of the free polymer in the solution (lipid:polymer = 30:1). The lipid suspensions (1mM) were injected into 50 μg mL^{-1} of polymer at 37 °C in 10 mM HEPES and 0.14M NaCl buffer. The interaction of all four polymers with DPPG:DPPE (88:12) model lipid bilayer was found to be an entropy-driven endothermic process. The longer alkyl chain amide polymer, Q*n*-hexAP had a very fast and complete interaction (within 10 injections) with the DPPG:DPPE (88:12) (Fig. 3.4). The reaction was found to be very spontaneous with ΔG = -10.96 kcal mol^{-1} (Gibbs free energy change) and was entropy-driven with a positive entropy change, ΔS = 63.7 cal mol^{-1} K^{-1} (positive enthalpy change, ΔH = 8.8 kcal mol^{-1}). The shorter alkyl chain amide polymer, Q*n*-prAP also had a complete and spontaneous entropy-driven interaction with the bacterial model lipid bilayer (within 20 injections) having nearly the same ΔG = -11.03 kcal mol^{-1} but with a lower positive ΔS = 43.9 cal mol^{-1} K^{-1} (ΔH = 2.57 kcal mol^{-1}) (Fig. 3.4). The control polymer, Q*n*-HexP had ΔG = -9.8 kcal mol^{-1}, ΔH = 10.75 kcal mol^{-1} and ΔS = 66.3 cal mol^{-1} K^{-1} but did not possess complete interaction (Fig. 3.4). Q*n*-hexEP although had ΔG = -9.3 kcal mol^{-1}, ΔH = 8.94 kcal mol^{-1} and ΔS = 58.8 cal mol^{-1} K^{-1} but still did not have complete interaction by the end of 40 injections. These results suggested that amide polymer with propyl chain, Q*n*-prAP had faster, more spontaneous and complete interaction with the bacterial model lipid bilayer compared to the ester polymer with hexyl chain appended to them (Q*n*-hexEP) stressing the advantage of amide functionality. On the other hand, Q*n*-prEP did produce an endothermic heat of reaction but had an incomplete interaction with DPPG:DPPE (88:12) model lipid bilayer even after 40 injections. With the mammalian model lipid bilayer, DPPC, none of the four cationic polymers (at lipid:polymer = 30:1) displayed any detectable enthalpy changes under the experimental conditions and only the small, nearly constant, and exothermic heat flows suggest a weak or no interaction between the polymers and the lipid bilayer (Fig. 3.4). Positive entropy changes (ΔS) suggest the "hydrophobic effect" explained by the loss of water as the amphipathic molecule enters the lipid bilayer [172-177]. More importantly, membrane-active pore formation/perturbation is also an endothermic entropy-driven process. The culmination of endothermic entropy-driven processes

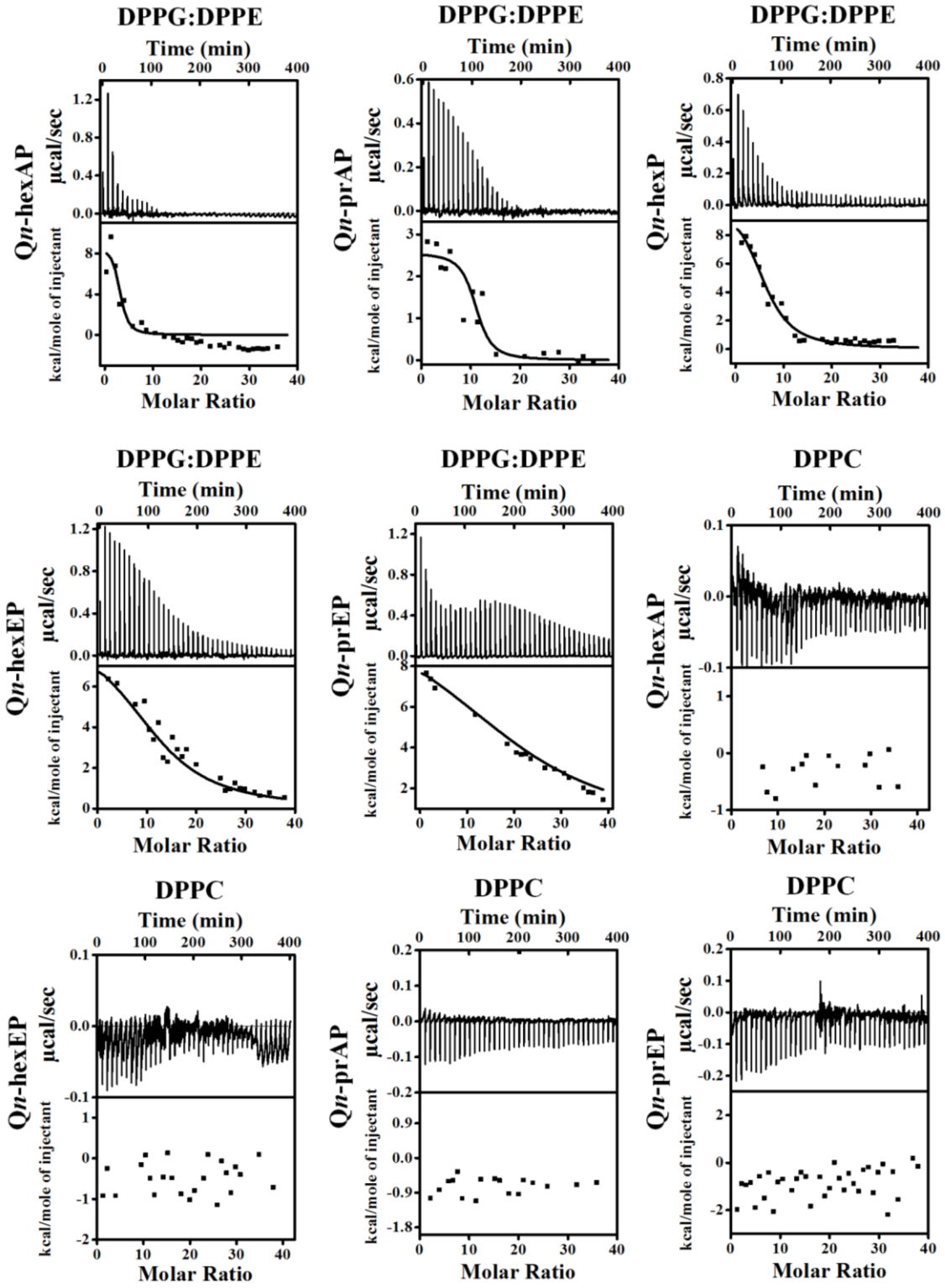

Figure 3.4: Mechanistic studies to understand the interactions of amide and ester polymers with bacterial and mammalian model lipid bilayers. Isothermal titration calorimetry (ITC) thermograms of polymers with DPPG:DPPE(88:12) and DPPC.

such as the hydrophobic effect and membrane perturbation explain the dominating interactions of these polymers with the lipid bilayers. AMPs such as mellitin [172] and PGLa [173] were also found to interact with bacterial cell membranes by endothermic entropy-driven processes such as the hydrophobic effect and membrane pore formation. Hence, the higher entropy change in the interaction of higher hydrophobic Q*n*-hexAP compared to Q*n*-prAP with DPPG:DPPE model lipid bilayer is justified. These results also correlate with higher membrane-active properties and potent antibacterial efficacy of amide containing polymers than their ester counterparts.

3.2.5 Molecular dynamics (MD) simulations

Experimental investigations such as ITC and Laurdan studies did provide the variable interactions of amide and ester polymers with the bacterial cell membranes. However, to gain insight into the nature of interactions that play role in the binding of amide and ester polymers with the bacterial cell membranes all atom molecular dynamics (MD) simulations were studied. The interactions were modeled using a mixture of (POPE: POPG= 7:3) [178, 179]. Each polymer has four representative polymeric chains with 12 monomers each (monomer is an alternating *N*-alkylmaleimide and isobutylene moieties) which were simulated for their interaction with the lipid bilayer. Results after 150 ns simulations of amide and ester polymers with the lipid bilayers showed interesting differences in their membrane-bound conformations as well as their interactions with the lipid head group atoms. The amide polymer, Q*n*-prAP showed greater propensities to adopt extended conformations at the lipid interface, thus maximizing the number of contacts with lipid head groups, while the ester (Q*n*-prEP) polymer adopted considerably more compact conformations (Fig. 3.5A). These results suggest the induced conformational changes in amide polymers similar to what is found in some of the AMPs for e.g. induced secondary structure formation upon interaction with the bacterial cell membranes [83, 84].

Such differences in conformations indicate that these isosteric amide and ester polymers differ in the favorability of their interactions with bilayer lipids. To investigate the same, their interaction energies with the lipid bilayer were computed. The interaction energies have been computed in per sequestered side chain basis to keep them in same footing, since various polymers have different number of sequestered side arms after 150 ns of simulations. It can be seen from Fig. 3.6 A that the electrostatic interaction energies (more negative value indicating stronger interactions) of all the four polymers were statistically equal. This is expected since the

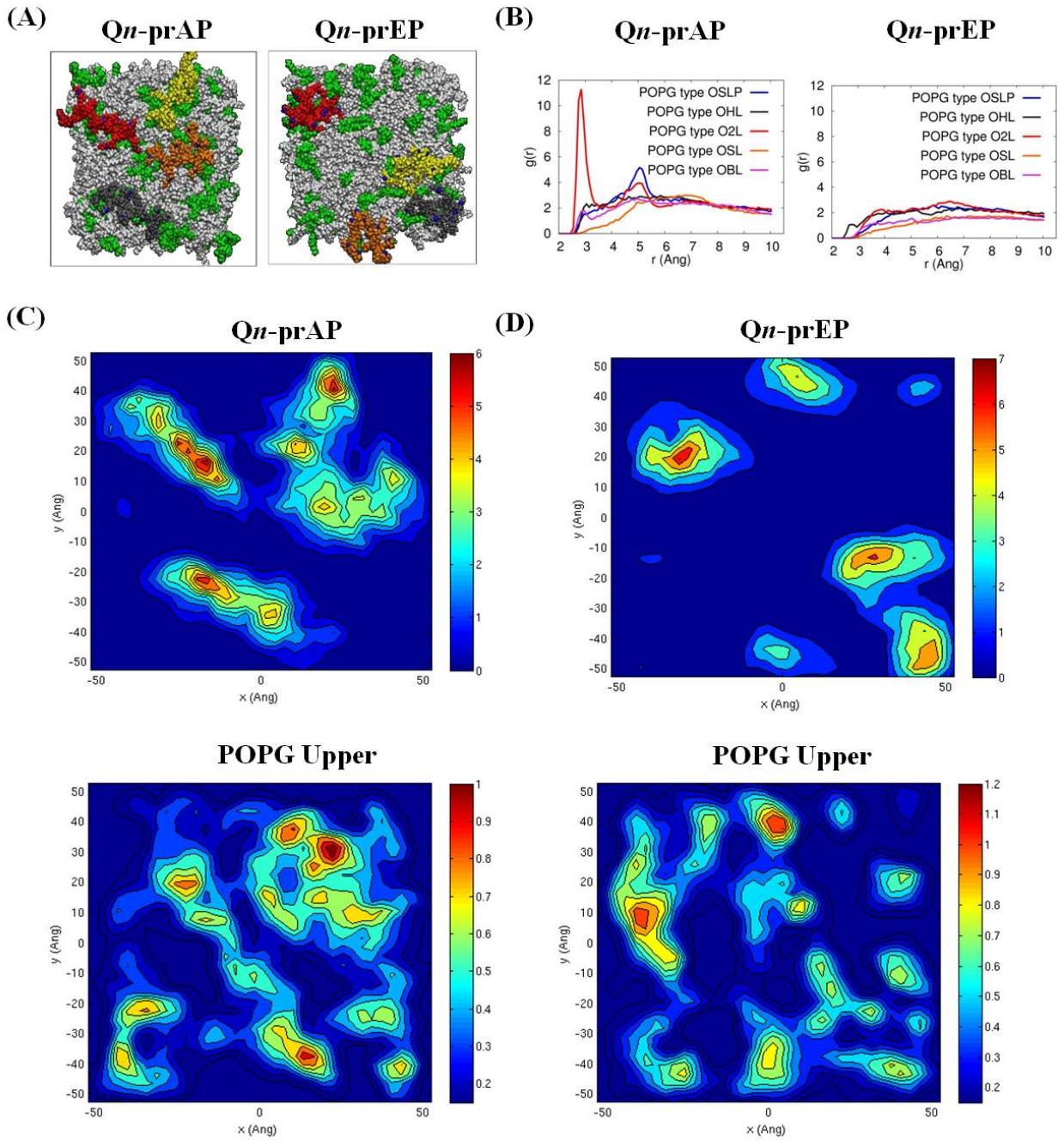

Figure 3.5: Atomistic molecular dynamics (MD) simulations of the polymers and POPE:POPG (7:3) model lipid bilayer. (A) X-Z (top) view of the polymers and bilayer after 150 ns simulations. The POPE and POPG lipid molecules are colored in white and green respectively. The polymer chains (four) of amide and ester polymers are shown in red, yellow, orange and grey. (B) Hydrogen bonding interactions of -NH- of the amide moiety and –C=O of the ester moiety in the amide and ester polymers respectively with the POPG region of the lipid bilayer after 150 ns simulations. 2-D number density plots of amide (C) and ester polymer (D) along with the corresponding POPG molecules in the upper leaflet of the lipid bilayer after 150 ns simulations.

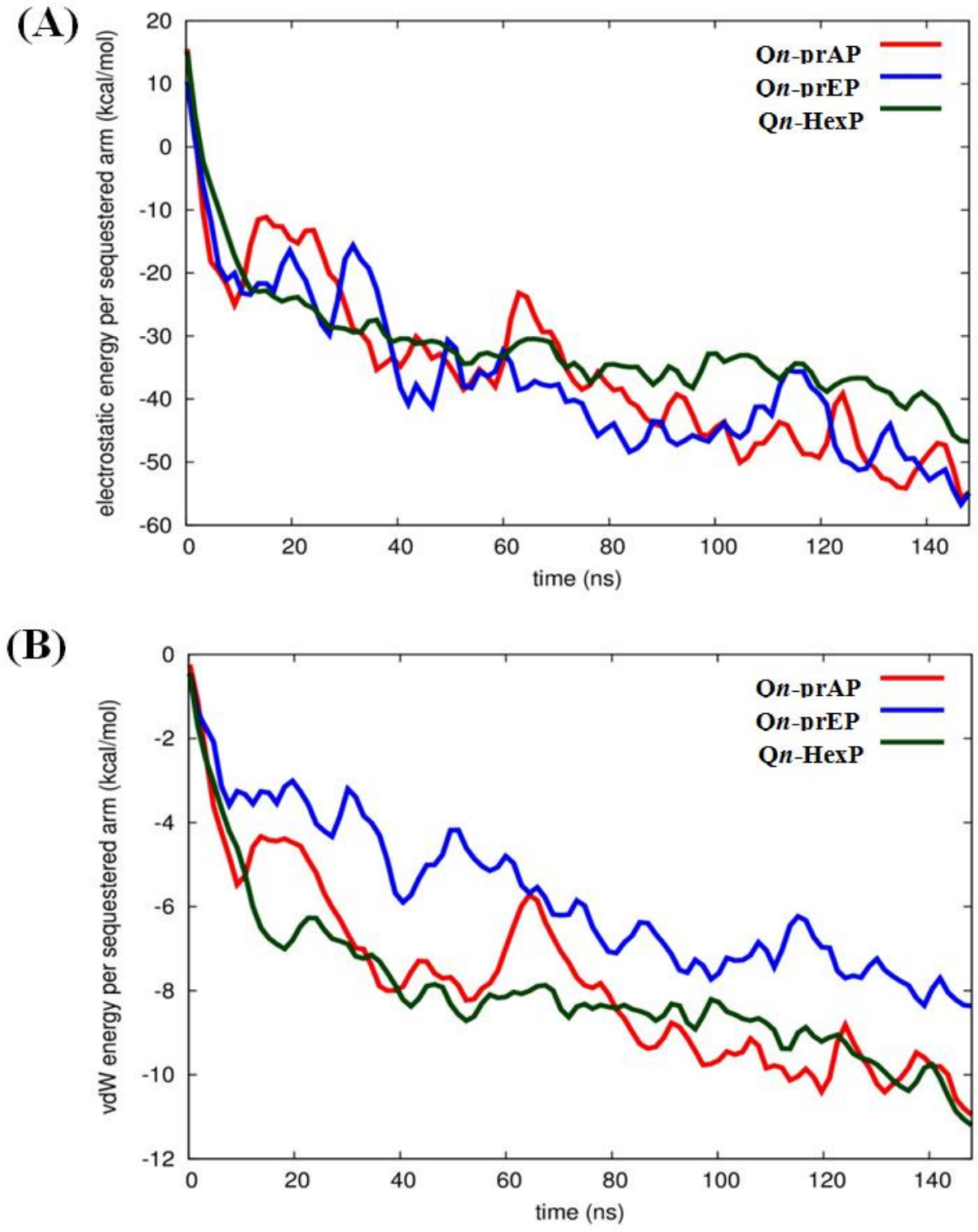

Figure 3.6: Interaction energies of amide and ester polymers with the lipid bilayer (POPG:POPE) after 150 ns atomistic molecular dynamics simulations. The electrostatic (A) and van der Waals' (vdW) (B) interaction energies have been computed in per sequestered side chain basis to keep them in same footing since various polymers have different number of sequestered side arms after 150 ns of simulation.

cationic charge density is constant in the present approach. However, the van der Waals' (vdW) interaction energies, were more negative (hence more attractive) for higher alkyl chain polymers (Q*n*-hexAP and Q*n*-hexEP) than lower alkyl chain polymers (Q*n*-prAP and Q*n*-prEP) (Fig. 3.6 B). Van der Waals' (vdW) interaction energies are likely to incorporate a greater signature of interactions of partitioned side chains of these polymers with the hydrophobic lipid chains. This is consistent with the extent to which the polymers have been inserted into the lipid bilayer.

The differences in the ability of isosteric polymer species to form hydrogen bonds with the lipid head group atoms were probed through direct computations of number of hydrogen bonds. The positional order in the spatial distribution of hydrogen bond forming lipid head group atoms in the neighborhood of amide and ester moieties has also been calculated. Conventionally, in atomistic MD simulations, hydrogen bonds are calculated using geometric criteria and the same was used in the present cases (donor-acceptor distance $\leq$ 4.0 Ang (Å) and donor-H-acceptor angle $\leq 60°$). The amide polymer has displayed a greater propensity to form hydrogen bonds compared to its ester counterpart, both in the overall number of hydrogen bonds formed (34280 & 8343) and the number of sequestered side arms observed to be involved in the formation of said bonds (25537 & 7709). Q*n*-HexP forms the lowest number of hydrogen bonds (4035) and lowest number of sequestered side arms observed to be involved in the formation of said bonds (4000) probably due to the backbone imide groups. The propensity of atomic species' to act as hydrogen bonded partners is portrayed in their radial distribution function or two point density correlation function (g(r)). Radial distribution functions have been computed between the amide and ester groups' hydrogen bond formers and the same from lipid head group atoms and are interpret in the following as their relative affinities in forming hydrogen bonds. The amide group (-NH-) of the amide polymer interacted through strong hydrogen bonds with the oxygen atoms of the phosphate head groups of the POPG lipid molecules as seen in Fig. 3.5 B. On the other hand, the carbonyl group of their ester counterparts has no strong interactions with POPG molecules (Fig. 3.5 B). These results suggest that the amide polymers have strong interactions whereas the ester polymers are devoid of any preferentially favorable interactions with the negatively charged POPG lipids. These results also support the observation of more stretched conformations of amide polymers.

The discernible differences in lipid-amide polymer and lipid-ester polymer interactions described above are further reflected in the relative ability of isosteric polymers in inducing

structural re-organization of the lipid bilayer. The number density distribution of polymers and POPG molecules in the upper leaflet (the leaflet to which the polymers bind to the bilayer) is shown in Fig. 3.5 C & D. It can be seen very clearly that the location of amide polymer and POPG clusters are well correlated and the amide polymer seem to has the ability to reorganize the upper leaflet of the bacterial membrane through favorable interactions between the partitioned side chains and the POPG lipid molecules. These MD simulations support the potent antibacterial efficacy of amide polymers due to the culmination of various stronger interactions with the bacterial cell membrane than their ester counterparts. Random methacrylate polymers bearing primary ammonium groups by Kuroda and co-workers with cationic charge and hydrophobicity have been speculated to show the capability of hydrogen bonding with the phosphate lipid head groups[112].

3.2.6 Raman Spectroscopy

To gain further insight into the hydrogen bonding interactions of polymers with the bacterial lipid bilayers, Raman spectroscopic studies were performed. The full Raman spectra are provided in Fig. 3.7. Since the interest is in the specific interaction of polymers (Q*n*-prAP, Q*n*-prEP, Q*n*-HexP) with the bacterial lipid (DPPG), the modes related to the phosphate region of the lipid (1040 - 1150 cm^{-1}) and the amide (-CONH-) and the ester (-COO-) regions in the polymers (1600-1800 cm^{-1}) were probed. As shown in Fig. 3.8 A, 1064 cm^{-1} vibrational mode is due to -P-O- (DPPG head group), 1100 cm^{-1} is due to PO_2^- and 1129 cm^{-1} is due to -P-O- (DPPG tail group) (blue curve) for DPPG [180]. Upon polymer interaction, all the three modes showed softening (decrease in frequency) indicating that all the three polymers interact with phosphate region of DPPG. It is interesting to note that 1100 cm^{-1} vibrational mode splits into doublet upon interacting with Q*n*-prAP and Q*n*-prEP (Fig. 3.8 B) along with softening. O=P-O^- has the ability to resonate, hence the Fermi resonance (expected in AB_2) doublet does not exist in PO_2^- of DPPG (Fig. 3.8 B). But upon addition of all three polymers, the electrostatic interaction with DPPG would affect the otherwise degenerate PO_2^- vibration leading to splitting. Q*n*-HexP has less chance for hydrogen bonding with DPPG and hence the non-directional electrostatic interaction is weaker with no splitting of PO_2^- vibration (Fig. 3.8 B). The hydrogen bonding ability of Q*n*-prAP and Q*n*-prEP with DPPG gets the cationic nitrogen localized in space leading to strong interactions with the PO_2^- group resulting in its splitting. The lower frequency mode

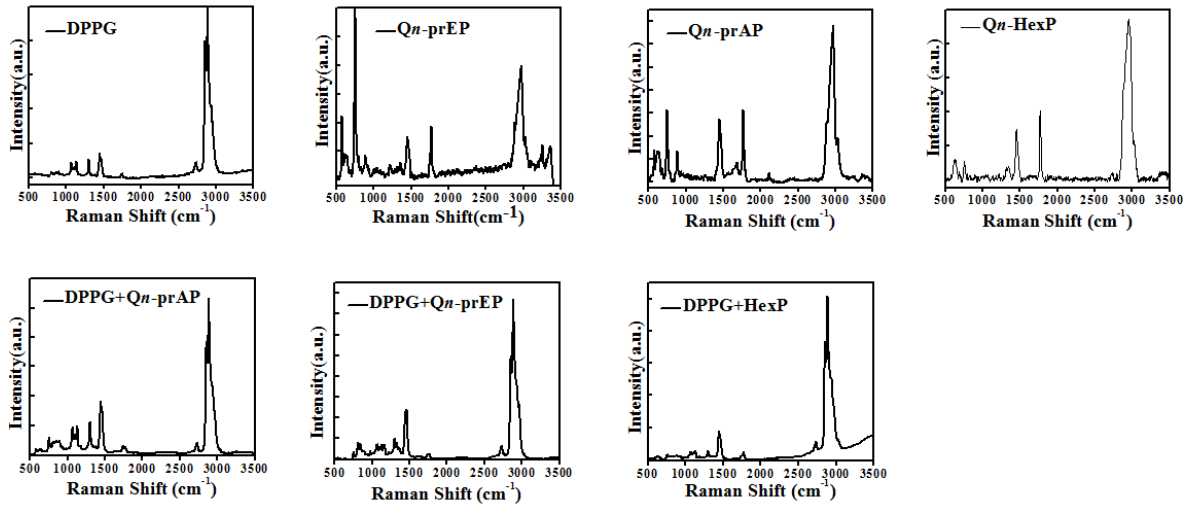

Figure 3.7: Full region Raman spectra of DPPG alone, polymer alone and DPPG + polymer.

is due to the PO^- group (1096 cm^{-1}) and the higher frequency mode is due to the P=O group (1100 cm^{-1}). Interestingly, the relative intensities of the two peaks in doublet is higher in Q*n*-prAP + DPPG than in Q*n*-prEP + DPPG suggesting the strong interactions of amide polymer with the lipid compared to the ester polymer (Fig. 3.8 B).

The polymer region (1600-1800 cm^{-1}) of the spectra as shown in Fig. 3.8 C is dominated by the side chain amide I vibration (1680 cm^{-1}) and the side chain ester C=O vibrational mode (1740 cm^{-1}). This region is affected by the presence of a strong signature from the long chain ester C=O of DPPG (black curve Fig. 3.8 C) and also from the polymer backbone C=O (imide) at around 1770 cm^{-1} [180, 181]. It is interesting to see that amide I mode (1680 cm^{-1}) disappears in DPPG + Q*n*-prAP (green curve Fig. 3.8 C) and looks very similar to the DPPG + Q*n*-prEP spectrum (dark blue curve Fig. 3.8 C). This is very important because it shows there is a strong hydrogen bonding between the amide moiety of Q*n*-prAP and DPPG. It is interesting to see that the spectrum for DPPG + Q*n*-HexP (purple curve Fig. 3.8 C) more or less looks like the convolution of DPPG (black curve, Fig. 3.8 C) and Q*n*-HexP (magenta curve Fig. 3.8 C). The long chain lipid ester (1740 cm^{-1}) peak has shifted showing some weak interaction between DPPG and Q*n*-HexP as observed earlier. In order to confirm the hydrogen bonding, the Raman spectra for DPPG + Q*n*-prAP was recorded on heating up to 40 $^{\circ}C$ (Phase transition temperature (T_m) of DPPG is 41 $^{\circ}C$) (Fig. 3.8 D). The emergence of amide (1680 cm^{-1}) band above 35 $^{\circ}C$ suggested the breaking of hydrogen bond. The strong 1740 cm^{-1} also shows the emergence of

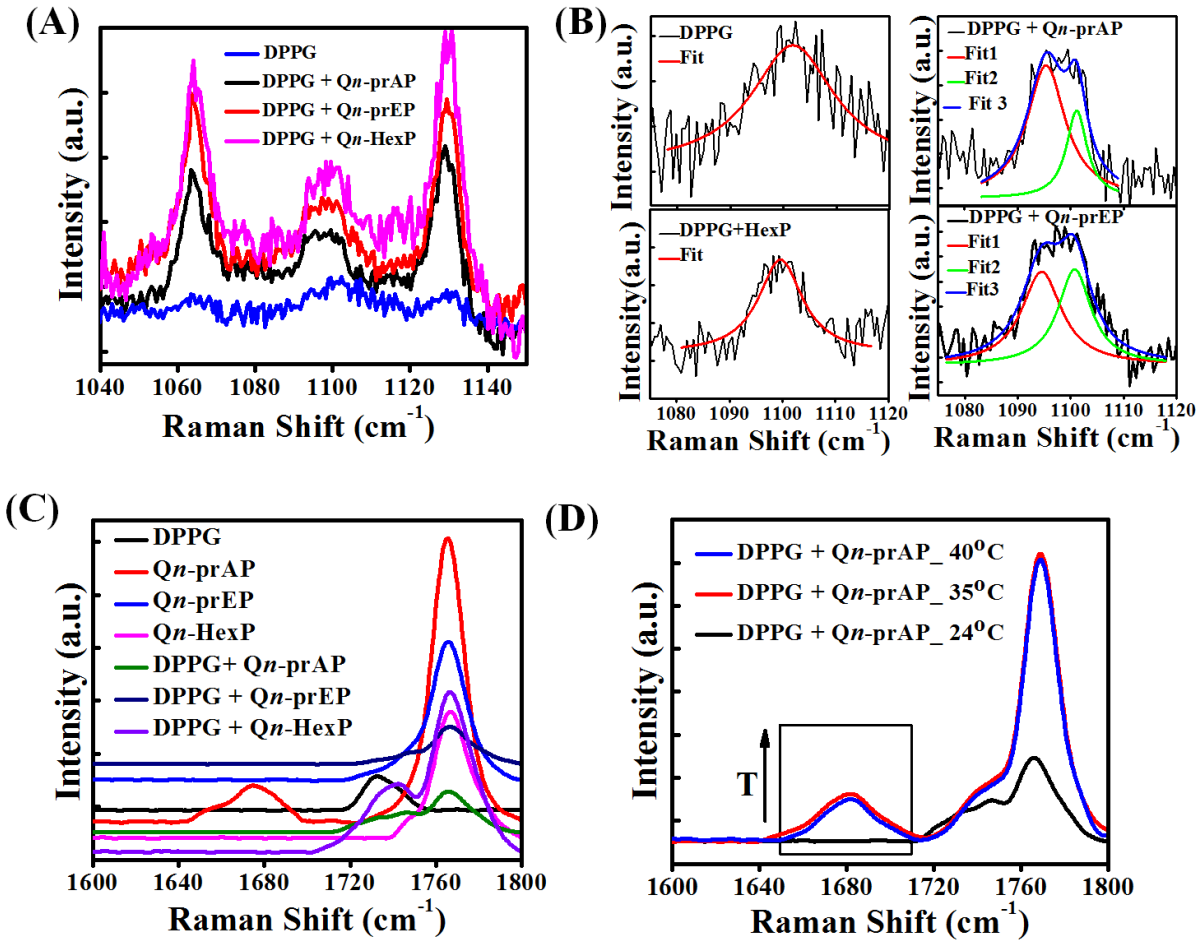

Figure 3.8: Polymer interactions with bacterial membrane lipid, DPPG using Raman spectroscopy. (A) Lipid phosphate vibrational modes (1064 cm^{-1}, -P-O- (DPPG head group), 1100 cm^{-1}, PO_2^- and 1129 cm^{-1}, -P-O- (DPPG tail group) DPPG and polymer + DPPG indicate softening (decrease in frequency) of all three modes. (B) Splitting of PO_2^- mode into a doublet (loss of degeneracy) due to strong interactions of amide polymer with DPPG, followed by weak interactions of ester polymer with DPPG and weaker interaction of Q*n*-HexP with DPPG. (C) Spectra in the region of 1600-1800 cm^{-1} showing side chain amide I vibration (1680 cm^{-1}) and the side chain ester C=O vibrational mode (1740 cm^{-1}), long chain ester C=O of DPPG (black curve) and polymer backbone C=O (imide) at around 1770 cm^{-1}. Upon interaction with DPPG, amide I mode (1680 cm^{-1}) of Q*n*-prAP (red curve) disappears in DPPG + Q*n*-prAP (green curve). (D) Temperature dependent spectra (arrow showing increase in temperature, T) of DPPG + Q*n*-prAP showing the emergence of amide I mode at high temperatures showing the strong hydrogen bonding between Q*n*-prAP and DPPG.

long chain ester C=O vibration of the lipid. Similar experiments in the DPPG + Q*n*-prEP spectrum bring the emergence of a strong 1740 cm^{-1} similar to DPPG + Q*n*-prAP indicated the breaking of ester polymer C=O hydrogen bond with DPPG (Fig. 3.9). Heating effect on the 1100 cm^{-1} mode showed no changes in DPPG and DPPG + Q*n*-HexP, but in DPPG + Q*n*-prAP as well

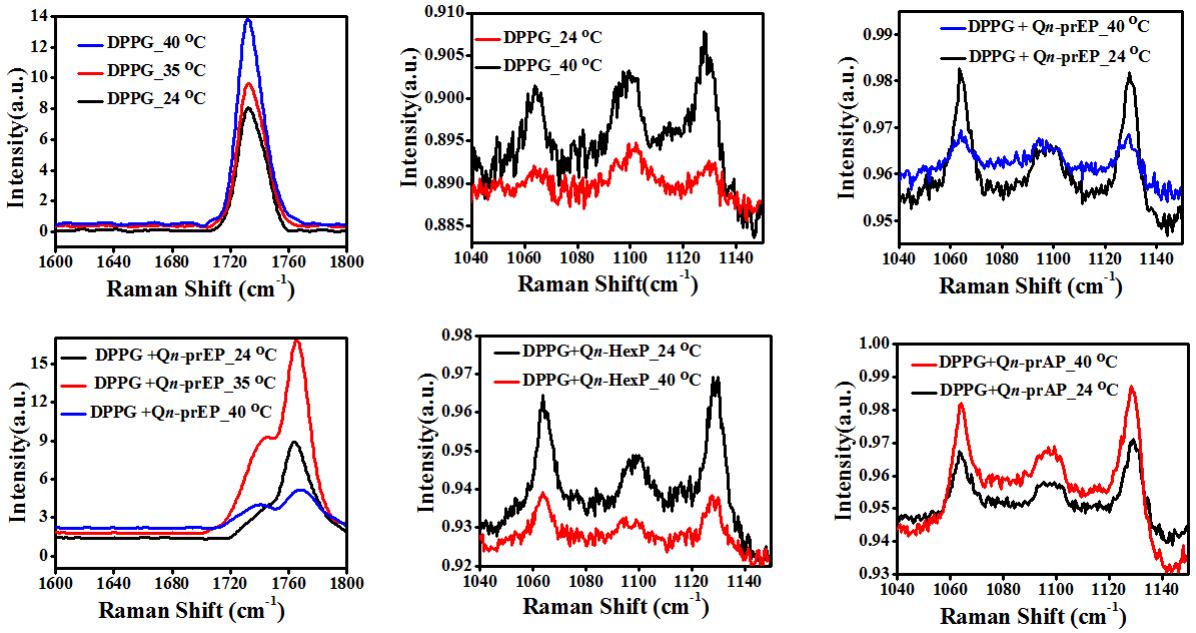

Figure 3.9: Temperature dependent Raman spectra of DPPG alone and DPPG + polymer.

as DPPG + Q*n*-prEP, the splitting still persisted suggesting that the molecules are still weakly hydrogen bonded and in position (Fig. 3.9).

The above results clearly suggest that the difference between the interaction of Q*n*-prAP and Q*n*-prEP with DPPG is that the amide provides strong hydrogen bonding interactions with DPPG compared to Q*n*-prEP probably through the two hydroxyl groups of the DPPG head group. These results also correlated with MD simulations which showed the hydrogen bonding interactions of amide polymers with the hydroxyl and phosphate oxygen atoms of POPG in bacterial model lipid bilayers. Taken together, these data suggested that despite similar electrostatic and hydrophobic interactions, the lack of strong hydrogen bonding interactions can render weaker binding of ester polymers with lipid bilayers compared to amide polymers (Fig. 3.10).

3.2.7 *In-vivo* toxicity of polymers

One of the most important setbacks of antibacterial polymers is their high toxicity towards mammalian systems. Experiments performed to assess the *in-vivo* toxicity of Q*n*-prAP and Q*n*-prEP after single-dose intravenous (i.v.) administration to mice (n = 5-6) resulted in LD_{50} values of 20 and 37 mg kg^{-1}, respectively. This compares favorably with clinically approved antibiotics such as polymixins, which work by a comparable cell-lytic mechanism as AMPs, and have lower

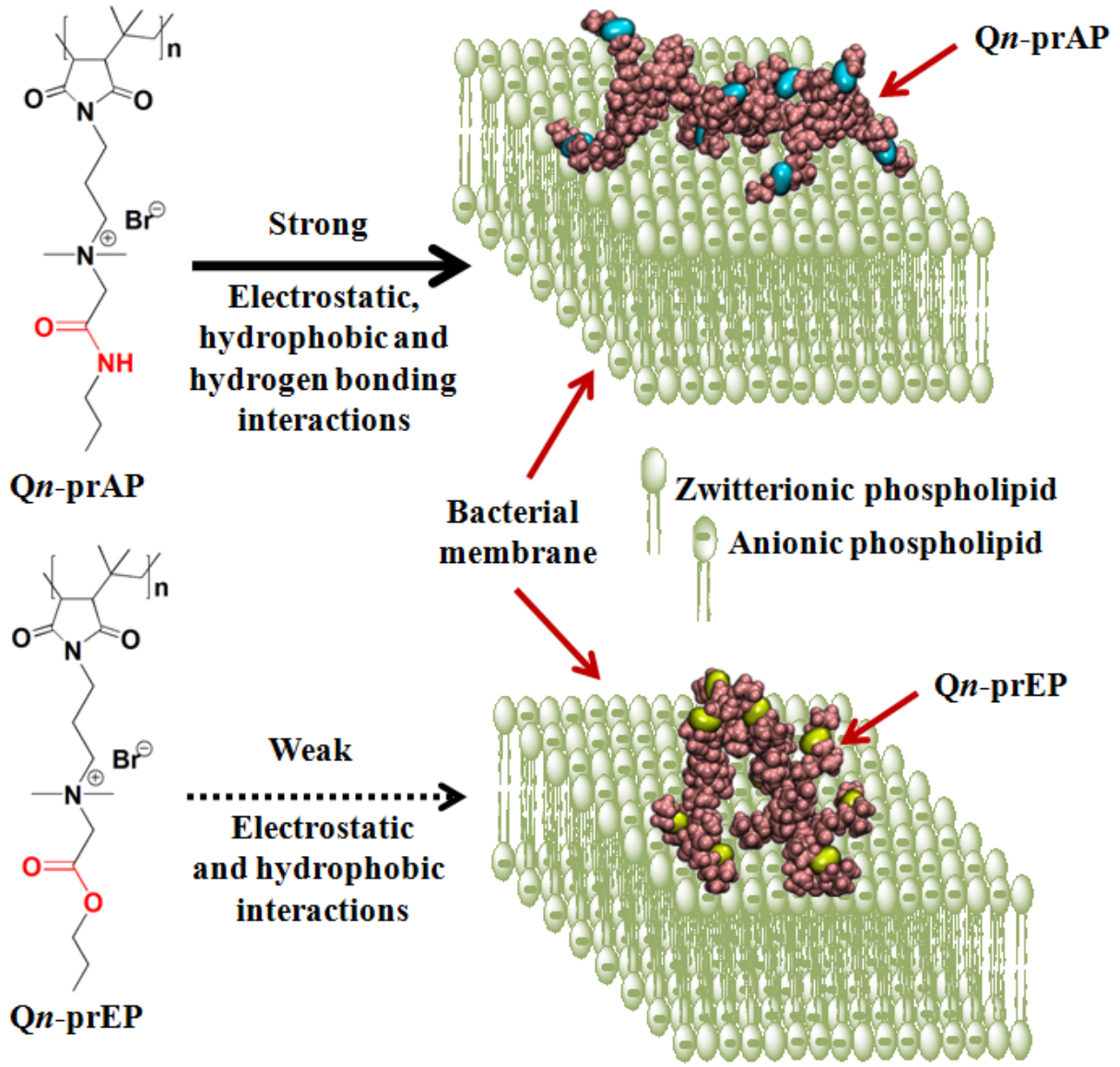

Figure 3.10: Schematic representation of effect isosteric replacement in amphiphilic polymers towards the interaction with bacterial cell membrane. A prototypical bacterial cell membrane consists of higher proportion of anionic compared to zwitterionic phospholipids. Amphiphilic amide polymers, unlike the ester polymers, possess strong interactions involving in hydrogen bonding accompanied by conformational changes with the bacterial cell membrane.

LD_{50} levels of approximately 8-10 mg kg^{-1} with reported neuro- and nephro-toxicity [182]. The *in-vivo* toxicity of the Q*n*-prAP has been evaluated through single dose intraperitoneal (i.p.) and subcutaneous (s.c.) injection into the mice and found no lethal effects up to 17.5 mg kg^{-1} and 55 mg kg^{-1} respectively. Next, the sub-chronic toxicity to major organs in mice has been investigated by evaluating the clinical biochemistry parameters in the blood after a single-dose

i.v. administration of Q*n*-prAP and Q*n*-prEP (at a dosage of 2 mg kg^{-1}). Neither of the derivatives induced any adverse toxicity to major organs like liver and kidney and did not interfere with the balance of electrolytes in the blood of mice 2 days and 14 days post treatment compared to vehicle control and laboratory parameters (Table 3.2).

Table 3.2: Effect of polymers on the liver and kidney functional parameters and balance of electrolytes in the blood of mice 48 h and 14 days post-treatment.

Treatment	Liver Function	Kidney Function		Electrolyte Balance		
	ALP ($IU\ L^{-1}$)	Creatinine ($mg\ dL^{-1}$)	Urea Nitrogen ($mg\ dL^{-1}$)	Sodium ion ($mg\ dL^{-1}$)	Potassium ion ($mg\ dL^{-1}$)	Chloride ($mg\ dL^{-1}$)
PBS	150 ± 57	0.23 ± 0.07	18.4 ± 3.4	143 ± 1.6	7.2 ± 0.7	111.5 ± 2
Q*n*-prAP (48 h)	157 ± 64 (P > 0.05)	0.19 ± 0.06 (P > 0.05)	16.4 ± 2.2 (P > 0.05)	143 ± 1.7 (P > 0.05)	7.3 ± 0.5 (P > 0.05)	109 ± 2.4 (P < 0.05)
Q*n*-prAP (14 days)	157.4 ± 60 (P > 0.05)	0.14 ± 0.07 (P > 0.05)	16.7 ± 3.1 (P < 0.05)	137.5 ± 1.1 (P < 0.05)	8.2 ± 1 (P < 0.05)	105.3 ± 2 (P < 0.05)
Q*n*-prEP (48 h)	140 ± 43 (P > 0.05)	0.25 ± 0.11 (P > 0.05)	19.1 ± 4.4 (P > 0.05)	146.1 ± 0.8 (P < 0.05)	6.0 ± 0.5 (P < 0.05)	114 ± 2.1 (P < 0.05)
Q*n*-prEP (14 days)	175 ± 44 (P > 0.05)	0.13 ± 0.05 (P > 0.05)	15 ± 2 (P > 0.05)	139.6 ± 4.2 (P < 0.05)	6.5 ± 0.5 (P < 0.05)	106.8 ± 5 (P < 0.05)
Laboratory Range*	209.3 ± 72	0.38 ± 0.12	16 ± 7.2	152.3 ± 17	8.9 ± 1.5	119.3 ± 13.5

The data are expressed as mean ± standard deviation, based on values obtained from 10 mice (n = 10). Statistical analysis was performed using student's *t-test*. Differences are considered statistically significant with probability $p < 0.05$. ALP, alkaline phosphatase; I.U, international unit. *Source: Charles River Laboratories.

3.2.8 Degradation of amide and ester polymers and toxicity of degradation by-products

The degradation properties of both the amide and ester-bearing polymers were studied under acidic, alkaline and enzymatic hydrolytic conditions using ^{1}H NMR at 37 °C for 10 days. Amide-containing polymer (Q*n*-prAP) was found to hydrolyze only under alkaline conditions whereas the ester-containing polymer (Q*n*-prEP) hydrolyzed under all the three conditions (Fig. 3.11).

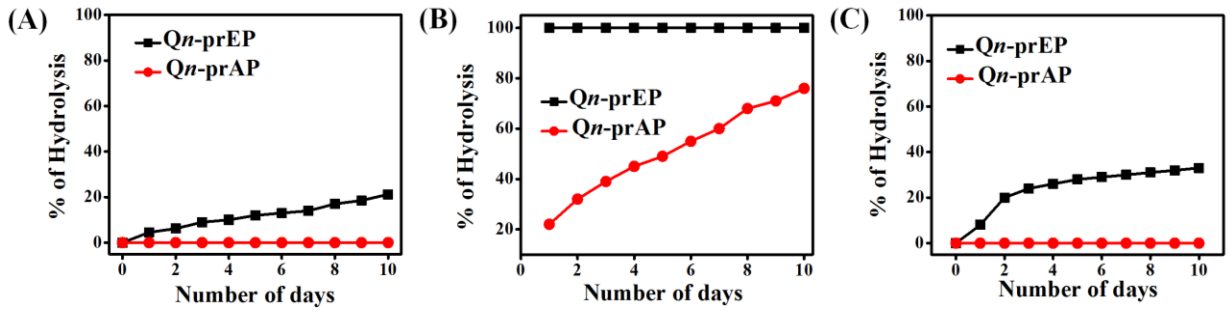

Figure 3.11: *In-vitro* degradation profiles of Q*n*-prAP and Q*n*-prEP. Rate of hydrolysis of amide and ester-containing polymers in presence of acidic, basic and enzymatic conditions. % of hydrolysis of Q*n*-prAP and Q*n*-prEP in presence of 0.2 M DCl in D_2O (A), 0.2 M NaOD in D_2O (B) and 5 U/mL lipase (C).

Amide-group being chemically more stable did not get hydrolyzed in presence of acid even till day 10. On the other hand, hydrolysis of ester-containing polymer started at day 1 and increased gradually with time. The degree of hydrolysis of ester-containing polymer was 20-22% after day 10 in presence of acidic conditions under the experimental conditions (Fig. 3.11 A). However, amide-containing polymer was found to hydrolyze in the presence of the base. Hydrolysis of amide-containing polymer started at day 1 and increased with time. The degree of hydrolysis of was 71-76% after day 10 inpresence of base under the experimental conditions. On the other hand, ester-containing polymer degraded completely (100% hydrolysis) just after day 1 which again proves that the polymers having ester groups are more susceptible towards both acid and base treatment than the amide containing polymers (Fig. 3.11 B). When tested the susceptibility of these polymer towards enzyme lipase (particularly known to hydrolyze ester and in some cases amide groups), the ester containing polymer was found to hydrolyze in presence of lipase whereas the amide-containing polymer remained un-hydrolyzed till day 10 under the experimental conditions. Hydrolysis of ester-containing polymer started at day 1 and increased gradually with time in presence of lipase. The degree of hydrolysis of ester-containing polymer was 25-28% after day 10 under the experimental conditions (Fig. 3.11 C). These preliminary *in-vitro* degradation results suggest that the amide polymers are relatively more stable than their ester counterparts under given experimental conditions that is required for their long lasting antibacterial activity but certainly need further investigations in detail.

Toxicity due to by-products from degradation of polymers is another safety issue that needs to be addressed. As a preliminary study, the toxicity of the chemically degraded (pH)

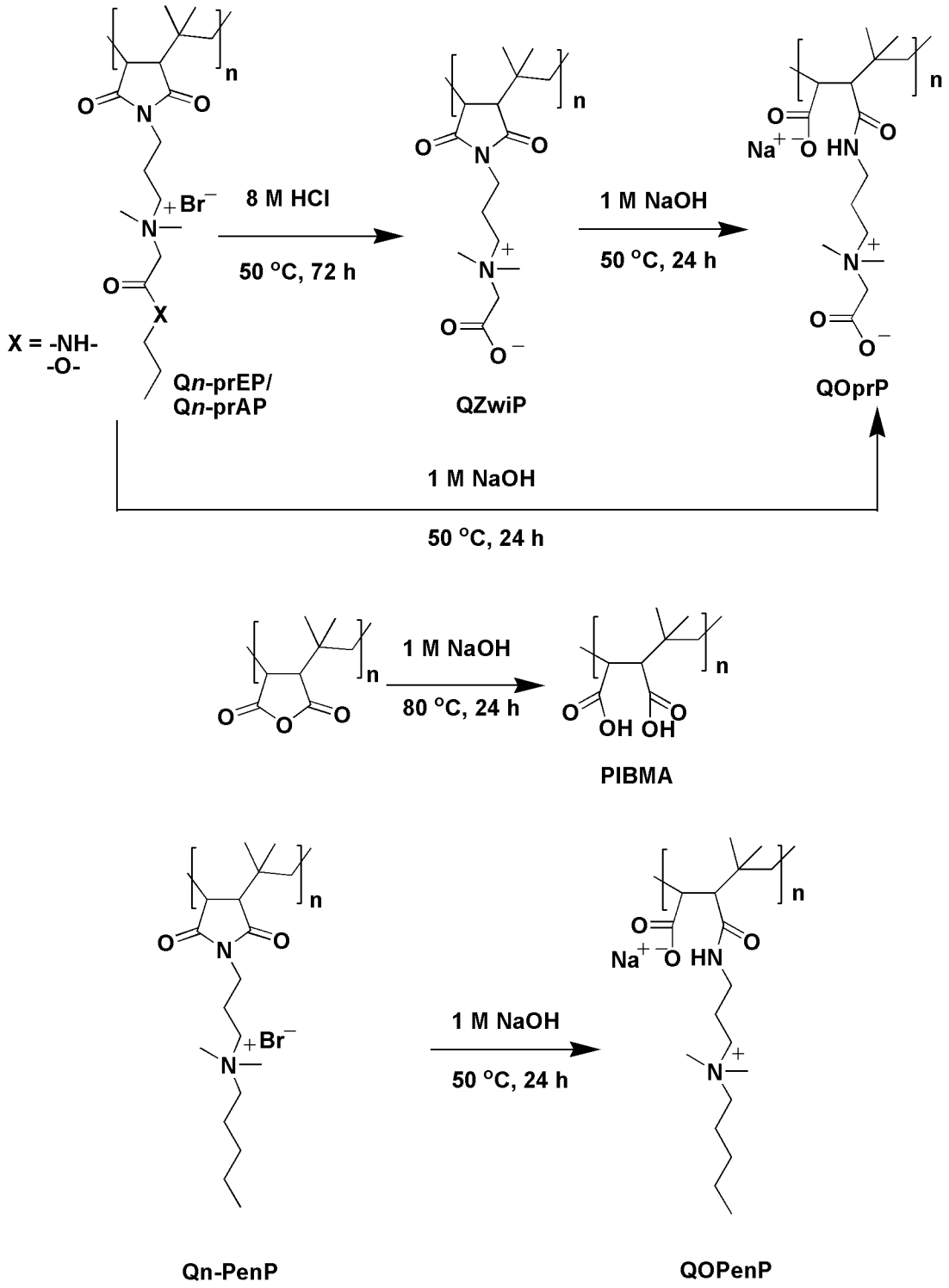

Figure 3.12: Synthesis of degradation by-products of Q*n*-prEP/Q*n*-prAP and Q*n*-PenP.

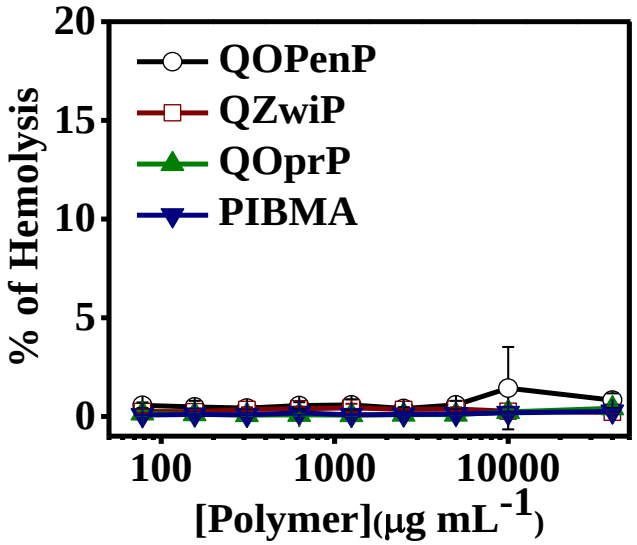

Figure 3.13: Hemolysis of degraded polymeric by-products.

polymeric by-products of the derivatives Q*n*-PenP, Q*n*-prEP/Q*n*-prAP was studied against human erythrocytes (Fig. 3.12). All the polymeric by-products were found to be significantly non-hemolytic up to 10000 μg mL^{-1}, the highest tested concentration. The *in-vivo* systemic toxicity of the polymeric by-products QZwiP and QOprP (Fig. 3.13) of Q*n*-prAP or Q*n*-prEP has been investigated and found that they did not induce any mortality in mice up to 400 mg kg^{-1}, the highest tested dose. Moreover, the molecular weight of all the derivatives and the polymeric by-products is in the range of 6-20 KDa, which is much below the threshold for renal clearance (<50 KDa) [183]. More importantly, the degradation-by products were found to devoid of antibacterial activity even up to 1000 μg mL^{-1}. Some of the conventional antibiotics are released into the environment in their active form contributing to the development of bacterial resistance [107]. However, these non-active degradation by-products will have less or no chance for the development of bacterial resistance thus suggesting their safety for the environment. These results indicate the good safety profiles of the polymers for use *in-vivo*.

3.3 Conclusions

In conclusion, with the unique concept of amide and ester moiety bearing polymers, it has been shown that hydrogen bonding plays an important role in bacterial membrane interactions. This understanding will aid in efficient specificity driven design of membrane-active molecules in

future. These polymeric analogs of AMPs appear to offer several advantages over AMPs with regard to stability due to non-peptide backbone and low cost of production. The low propensity for the development of bacterial resistance to these polymers certainly proves the importance of targeting bacterial cell membrane. Moreover, the degradation by-products of these polymers were non-toxic in mice. This work provides a conceptual advance in understanding the interactions of antibacterial polymers with bacterial cell membranes highlighting the role of hydrogen bonding. Thus, these findings have significant implications in efficient design of selective antibacterial polymers.

3.4 Experimental section

3.4.1 Synthesis and characterization

Synthesis of the amide, ester based alkylating agents and quaternized polymers were carried out as described in Chapter 2.

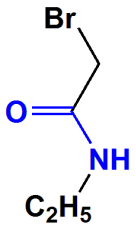

***N-ethyl-1-bromoethanamide*:** FT-IR: 3250 cm^{-1} (amide N-H str.), 2950-2850 (C-H str.), 1680 cm^{-1} (Amide I, C=O str.), 1560 cm^{-1} (Amide II, N-H ben.), 1470-1410 cm^{-1} (C-C str.), 1290-1110 (C-O str.); ^{1}HNMR (400 MHz, $CDCl_3$): δ/ppm 1.185 (t, terminal –*CH₃*, 3H), 3.336 (q, -CONH*CH₂*-, 2H), 3.874 (s, -CO*CH₂*Br, 2H), 6.475 (br s, amide –*NH*CO, 1H)); ^{13}C NMR (100 MHz, $CDCl_3$): δ 14.195, 22.768, 26.904, 29.324, 29.423, 29.588, 29.646, 29.708, 31.995, 40.403, 165.589; HR-MS: *m/z* 165.98 (observed): 165.98 (calculated for $[M+H]^+$).

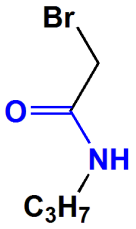

***N-propyl-1-bromoethanamide*:** FT-IR: 3250 cm^{-1} (amide N-H str.), 2950-2850 (C-H str.), 1680 cm^{-1} (Amide I, C=O str.), 1560 cm^{-1} (Amide II, N-H ben.), 1470-1410 cm^{-1} (C-C str.), 1290-1110 (C-O str.); ^{1}HNMR (400 MHz, $CDCl_3$): δ/ppm 0.878 (t, terminal –*CH₃*, 3H), 1.543 (m, -CONHCH₂*CH₂*CH₃-, 2H), 3.278 (t, -CONH*CH₂*-, 2H), 3.881 (s, -CO*CH₂*Br, 2H), 6.475 (br s, amide –*NH*CO, 1H)); ^{13}C NMR (100 MHz, $CDCl_3$): δ 14.195, 22.768, 26.904, 29.324, 29.423, 29.588, 29.646, 29.708, 31.995, 40.403, 165.589; HR-MS: *m/z* 180.00 (observed): 179.99 (calculated for $[M+H]^+$).

***N-butyl-1-bromoethanamide*:** FT-IR: 3250 cm^{-1} (amide N-H str.), 2950-2850 (C-H str.), 1680 cm^{-1} (Amide I, C=O str.), 1560 cm^{-1} (Amide II, N-H ben.), 1470-1410 cm^{-1} (C-C str.), 1290-1110 (C-O str.); ^{1}HNMR (400 MHz, $CDCl_3$): δ/ppm 0.878 (t, terminal –*CH₃*, 3H), 1.543 (m, $CONHCH_2CH_2$ CH_2CH_3, 4H), 3.278 (t, -$CONHCH_2$-, 2H), 3.881 (s, -$COCH_2Br$, 2H), 6.475 (br s, amide –*NH*CO, 1H)); ^{13}C NMR (100 MHz, $CDCl_3$): δ 14.195, 22.768, 26.904, 29.324, 29.423, 29.588, 29.646, 29.708, 31.995, 40.403, 165.589 ; HR-MS: *m/z* 194.00 (observed): 194.01 (calculated for $[M+H]^+$).

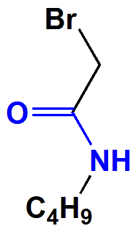

***N-hexyl-1-bromoethanamide*:** FT-IR: 3250 cm^{-1} (amide N-H str.), 2950-2850 (C-H str.), 1680 cm^{-1} (Amide I, C=O str.), 1560 cm^{-1} (Amide II, N-H ben.), 1470-1410 cm^{-1} (C-C str.), 1290-1110 (C-O str.); ^{1}HNMR (400 MHz, $CDCl_3$): δ/ppm 0.878 (t, terminal –*CH₃*, 3H), 1.543 (m, - $CONHCH_2CH_2CH_2CH_2$ CH_2CH_3-, 8H), 3.278 (t, -$CONHCH_2$-, 2H), 3.881 (s, -$COCH_2Br$, 2H), 6.475 (br s, amide –*NH*CO, 1H)); ^{13}C NMR (100 MHz, $CDCl_3$): δ 14.195, 22.768, 26.904, 29.324, 29.423, 29.588, 29.646, 29.708, 31.995, 40.403, 165.589; HR-MS: *m/z* 222.05 (observed): 222.04 (calculated for $[M+H]^+$).

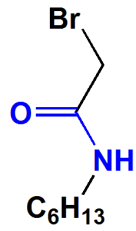

Ethyl-1-bromoethanoate: FT-IR: 2950-2850 (C-H str.), 1735 cm^{-1} (C=O str.), 1470-1410cm^{-1} (C-C str.), 1290-1110 (C-O str.); ^{1}HNMR (400 MHz, $CDCl_3$): δ/ppm 1.18 (t, terminal –*CH₃*, 3H), 4.0 (q, -$COOCH_2$-, 2H), 3.7 (s, -$COCH_2Br$, 2H); ^{13}C NMR (100 MHz, $CDCl_3$): δ 14.195, 22.768, 26.904, 29.324, 29.423, 29.588, 29.646, 29.708, 31.995, 40.403, 171.19 ; HR-MS: *m/z* 166.05 (observed): 165.96 (calculated for M^+).

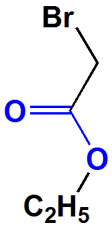

Propyl-1-bromoethanoate: FT-IR: 2950-2850 (C-H str.), 1735 cm^{-1} (C=O str.), 1470-1410cm^{-1} (C-C str.), 1290-1110 (C-O str.); ^{1}HNMR (400 MHz, $CDCl_3$): δ/ppm 0.85 (t, terminal –*CH₃*, 3H), 1.57 (m, -$COOCH_2CH_2CH_3$, 2H), 4.0 (t, -$COOCH_2$-, 2H), 3.7 (s, -$COCH_2Br$, 2H); ^{13}C NMR (100 MHz, $CDCl_3$): δ 14.195, 22.768, 26.904, 29.324, 29.423, 29.588, 29.646, 29.708, 31.995, 40.403, 171.19; HR-MS: *m/z* 180.10 (observed): 179.98 (calculated for M^+).

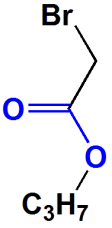

Butyl-1-bromoethanoate: FT-IR: 2950-2850 (C-H str.), 1735 cm^{-1} (C=O str.), 1470-1410cm^{-1} (C-C str.), 1290-1110 (C-O str.); ^{1}HNMR (400 MHz, $CDCl_3$): δ/ppm 0.85 (t, terminal –*CH₃*, 3H), 1.57 (m, $COOCH_2CH_2CH_2CH_3$, 4H), 4.0 (t, -$COOCH_2$-, 2H), 3.7 (s, -$COCH_2Br$, 2H); ^{13}C NMR (100 MHz, $CDCl_3$): δ 14.195, 22.768, 26.904, 29.324, 29.423, 29.588, 29.646, 29.708, 31.995, 40.403, 171.19 ; HR-MS: *m/z* 194.10 (observed): 193.99 (calculated for M^+).

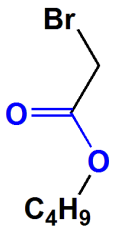

Hexyl-1-bromoethanoate: FT-IR: 2950-2850 (C-H str.), 1735 cm^{-1} (C=O str.), 1470-1410cm^{-1} (C-C str.), 1290-1110 (C-O str.); ^{1}HNMR (400 MHz, $CDCl_3$): δ/ppm 0.85 (t, terminal –*CH₃*, 3H), 1.57 (m, $COOCH_2CH_2CH_2CH_2$ CH_2CH_3, 8H), 4.0 (t, -$COOCH_2$-, 2H), 3.7 (s, -$COCH_2Br$, 2H); ^{13}C NMR (100 MHz, $CDCl_3$): δ 14.195, 22.768, 26.904, 29.324, 29.423, 29.588, 29.646, 29.708, 31.995, 40.403, 171.19 ; HR-MS: *m/z* 222.10 (observed): 222.03 (calculated for M^+).

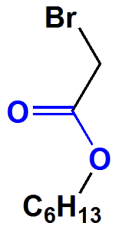

Q*n*-etEP: FT-IR: 2950-2850 (C-H str.), 1767 cm^{-1} (imide C=O asym. str.), 1696 cm^{-1} (imide C=O sym. str.), 1735 cm^{-1} (ester C=O str.) 1470-1410cm^{-1} (C-C str.), 1290-1110 (C-O str.); ^{1}HNMR (400 MHz, D_2O): δ/ppm 0.95–1.2 (br, $CH_2C(CH_3)_2$, 6H), 1.57 (br, $COOCH_2CH_3$, 3H), 1.7 (br, $CH_2C(CH_3)_2$, 2H), 2.0 (br, $NCH_2CH_2CH_2N(CH_3)_2$, 2H), 2.7–3.1 (br, *CHCH*, 2H), 3.1-3.3 (br, $NCH_2CH_2CH_2N(CH_3)_2$, 8H), 3.6 (br, $NCH_2CH_2CH_2N(CH_3)_2$, 2H), 3.7 (br, -$N(CH_3)_2CH_2CO$, 2H), 4.0 (br, -$COOCH_2$-, 2H).

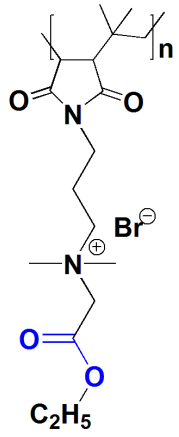

Q*n*-prEP: FT-IR: 2950-2850 (C-H str.), 1767 cm^{-1} (imide C=O asym. str.), 1696 cm^{-1} (imide C=O sym. str.), 1735 cm^{-1} (ester C=O str.) 1470-1410cm^{-1} (C-C str.), 1290-1110 (C-O str.); ^{1}HNMR (400 MHz, D_2O): δ/ppm 0.85 (br, terminal –*CH₃*, 3H), 0.95–1.2 (br, $CH_2C(CH_3)_2$, 6H), 1.57 (br,-$COOCH_2CH_2CH_3$, 2H), 1.7 (br, $CH_2C(CH_3)_2$, 2H), 2.0 (br, $NCH_2CH_2CH_2N(CH_3)_2$, 2H), 2.7–3.1 (br, *CHCH*, 2H), 3.1-3.3 (br, $NCH_2CH_2CH_2N(CH_3)_2$, 8H), 3.6 (br, $NCH_2CH_2CH_2N(CH_3)_2$, 2H), 3.7 (br, -

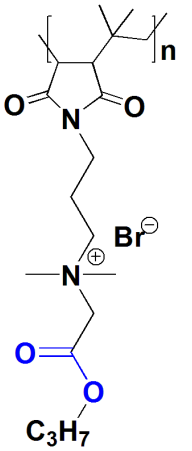

$N(CH_3)_2CH_2CO$, 2H) 4.0 (br, -$COOCH_2$-, 2H).

Q*n*-buEP: FT-IR: 2950-2850 (C-H str.), 1767 cm^{-1} (imide C=O asym. str.), 1696 cm^{-1} (imide C=O sym. str.), 1735 cm^{-1} (ester C=O str.) 1470-1410cm^{-1} (C-C str.), 1290-1110 (C-O str.); ^{1}HNMR (400 MHz, D_2O): δ/ppm 0.85 (br, terminal –CH_3, 3H), 0.95–1.2 (br, $CH_2C(CH_3)_2$, 6H), 1.57 (br,-$COOCH_2CH_2CH_2CH_3$, 4H), 1.7 (br, $CH_2C(CH_3)_2$, 2H), 2.0 (br, $NCH_2CH_2CH_2N(CH_3)_2$, 2H), 2.7–3.1 (br, *CHCH*, 2H), 3.1-3.3 (br, $NCH_2CH_2CH_2N(CH_3)_2$, 8H), 3.6 (br, $NCH_2CH_2CH_2N(CH_3)_2$, 2H), 3.7 (br, -$N(CH_3)_2CH_2CO$, 2H) 4.0 (br, -$COOCH_2$-, 2H).

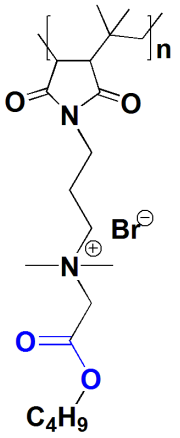

Q*n*-hexEP: FT-IR: 2950-2850 (C-H str.), 1767 cm^{-1} (imide C=O asym. str.), 1696 cm^{-1} (imide C=O sym. str.), 1735 cm^{-1} (ester C=O str.) 1470-1410cm^{-1} (C-C str.), 1290-1110 (C-O str.); ^{1}HNMR (400 MHz, D_2O): δ/ppm 0.85 (br, terminal –CH_3, 3H), 0.95–1.2 (br, $CH_2C(CH_3)_2$, 6H), 1.57 (br,-$COOCH_2CH_2CH_2CH_2CH_2CH_3$, 8H), 1.7 (br, $CH_2C(CH_3)_2$, 2H), 2.0 (br, $NCH_2CH_2CH_2N(CH_3)_2$, 2H), 2.7–3.1 (br, *CHCH*, 2H), 3.1-3.3 (br, $NCH_2CH_2CH_2N(CH_3)_2$, 8H), 3.6 (br, $NCH_2CH_2CH_2N(CH_3)_2$, 2H), 3.7 (br, -$N(CH_3)_2CH_2CO$, 2H) 4.0 (br, -$COOCH_2$-, 2H).

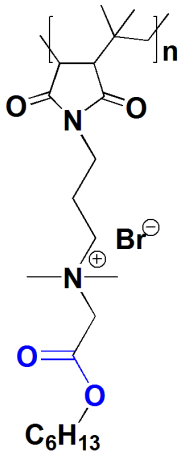

Q*n*-etAP: FT-IR: 3250 cm^{-1} (amide N-H str.), 2950-2850 (C-H str.), 1767 cm^{-1} (imide C=O asym. str.), 1696 cm^{-1} (imide C=O sym. str.) 1680 cm^{-1} (amide I, C=O str.), 1560 cm^{-1} (Amide II, N-H ben.), 1470-1410cm^{-1} (C-C str.), 1290-1110 (C-O str.); ^{1}HNMR (400 MHz, D_2O): δ/ppm 0.95–1.2 (br, $CH_2C(CH_3)_2$, 6H), 1.543 (br, -$CONHCH_2CH_3$, 3H), 1.7 (br, $CH_2C(CH_3)_2$, 2H), 2.0 (br, $NCH_2CH_2CH_2N(CH_3)_2$, 2H), 2.7–3.1 (br, *CHCH*, 2H), 3.1-3.3 (br, $NCH_2CH_2CH_2N(CH_3)_2$, 8H), 3.5 (br, -$CONHCH_2$-, 2H), 3.6 (br, $NCH_2CH_2CH_2N(CH_3)_2$, 2H), 3.8 (br, -$N(CH_3)_2CH_2CO$, 2H).

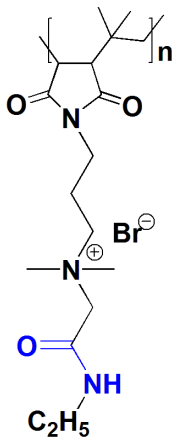

Q*n*-prAP: FT-IR: 3250 cm^{-1} (amide N-H str.), 2950-2850 (C-H str.), 1767 cm^{-1} (imide C=O asym. str.), 1696 cm^{-1} (imide C=O sym. str.) 1680 cm^{-1} (amide I, C=O str.), 1560 cm^{-1} (Amide II, N-H ben.), 1470-1410cm^{-1} (C-C str.), 1290-1110 (C-O str.); ^{1}HNMR (400 MHz, D_2O): δ/ppm 0.878 (br, terminal –*CH_3*, 3H), 0.95–1.2 (br, $CH_2C(CH_3)_2$, 6H), 1.543 (br, -$CONHCH_2CH_2CH_3$, 2H), 1.7 (br, $CH_2C(CH_3)_2$, 2H), 2.0 (br, $NCH_2CH_2CH_2N(CH_3)_2$, 2H), 2.7–3.1 (br, *CHCH*, 2H), 3.1-3.3 (br, $NCH_2CH_2CH_2N(CH_3)_2$, 8H), 3.5 (br, -$CONHCH_2$-, 2H), 3.6 (br, $NCH_2CH_2CH_2N(CH_3)_2$, 2H), 3.8 (br, -$N(CH_3)_2CH_2CO$, 2H).

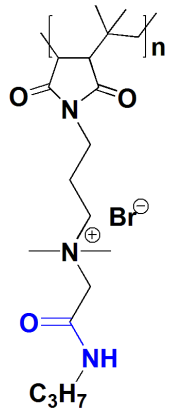

Q*n*-buAP: FT-IR: 3250 cm^{-1} (amide N-H str.), 2950-2850 (C-H str.), 1767 cm^{-1} (imide C=O asym. str.), 1696 cm^{-1} (imide C=O sym. str.) 1680 cm^{-1} (amide I, C=O str.), 1560 cm^{-1} (Amide II, N-H ben.), 1470-1410cm^{-1} (C-C str.), 1290-1110 (C-O str.); ^{1}HNMR (400 MHz, D_2O): δ/ppm 0.878 (br, terminal –*CH_3*, 3H), 0.95–1.2 (br, $CH_2C(CH_3)_2$, 6H), 1.543 (br, -$CONHCH_2CH_2$ CH_2CH_3, 4H), 1.7 (br, $CH_2C(CH_3)_2$, 2H), 2.0 (br, $NCH_2CH_2CH_2N(CH_3)_2$, 2H), 2.7–3.1 (br, *CHCH*, 2H), 3.1-3.3 (br, $NCH_2CH_2CH_2N(CH_3)_2$, 8H), 3.5 (br, -$CONHCH_2$-, 2H), 3.6 (br, $NCH_2CH_2CH_2N(CH_3)_2$, 2H), 3.8 (br, -$N(CH_3)_2CH_2CO$, 2H).

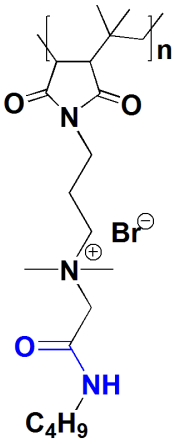

Q*n*-hexAP: FT-IR: 3250 cm^{-1} (amide N-H str.), 2950-2850 (C-H str.), 1767 cm^{-1} (imide C=O asym. str.), 1696 cm^{-1} (imide C=O sym. str.) 1680 cm^{-1} (amide I, C=O str.), 1560 cm^{-1} (Amide II, N-H ben.), 1470-1410cm^{-1} (C-C str.), 1290-1110 (C-O str.); ^{1}HNMR (400 MHz, D_2O): δ/ppm 0.878 (br, terminal –*CH_3*, 3H), 0.95–1.2 (br, $CH_2C(CH_3)_2$, 6H), 1.543 (br, -$CONHCH_2CH_2CH_2CH_2CH_2CH_3$,8H), 1.7 (br, $CH_2C(CH_3)_2$, 2H), 2.0 (br,$NCH_2CH_2CH_2N(CH_3)_2$, 2H), 2.7–3.1 (br, *CHCH*, 2H), 3.1-3.3 (br, $NCH_2CH_2CH_2N(CH_3)_2$, 8H), 3.5 (br, -$CONHCH_2$-, 2H), 3.6 (br, $NCH_2CH_2CH_2N(CH_3)_2$, 2H), 3.8 (br, -$N(CH_3)_2CH_2CO$, 2H).

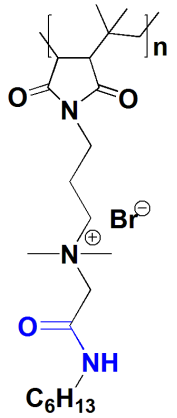

3.4.2 Chemical degradation of polymers

The hydrolysis of the Q*n*-prEP/Q*n*-prAP was done using 8 M HCl at 50 °C for 72 h to give the zwitterionic derivative QZwiP. Treatment of either the Q*n*-prEP or QZwiP with 1 M NaOH at 50

°C for 24 h degraded the succinimide ring yielding the corresponding open ring by-product with net anionic charge. Similarly, the succinimide ring opening of Q*n*-PenP was achieved after heating in 1 M NaOH at 50 °C for 24 h. All these by-products were obtained after dialyzing against DI water at room temperature using a dialysis membrane (Mol. wt. cut off =10 KDa) followed by freeze-drying. Poly(isobutylene-*alt*-maleic acid) was synthesized by treatment of poly(isobutylene-*alt*-maleic anhydride) with 1 M NaOH at 80 °C for 24 h followed by dialysis against DI water (benzoylated dialysis tubing with NMWCO of 2 KDa) at 4 °C and freeze-drying. With respect to all the derivatives, the complete conversion from the reactant to the product was confirmed quantitatively by FT-IR.

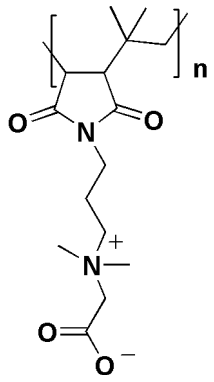

QZwiP: FT-IR: 2950-2850 (C-H str.), 1767 cm^{-1} (imide C=O asym. str.), 1696 cm^{-1} (imide C=O sym. str.) 1634 cm^{-1} (carboxylate C=O str.), (1470-1410 cm^{-1} (C-C str.), 1290-1110 (C-O str.) ; ^{1}HNMR (400 MHz, D_2O): δ/ppm 0.95–1.2 (br, $CH_2C(CH_3)_2$, 6H), 1.7 (br, $CH_2C(CH_3)_2$, 2H), 2.0 (br, $NCH_2CH_2CH_2N(CH_3)_2$, 2H), 2.7–3.1 (br, *CHCH*, 2H), 3.1-3.3 (br, $NCH_2CH_2CH_2N(CH_3)_2$, 8H), 3.6 (br, $NCH_2CH_2CH_2N(CH_3)_2$, 2H), 4.1-4.3 (br, $-N(CH_3)_2COCH_2$, 2H).

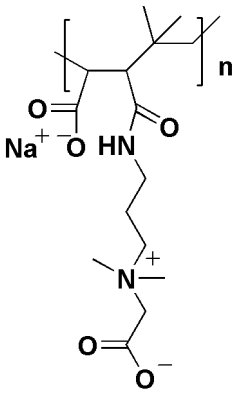

QOprP: FT-IR: 3250 cm^{-1} (amide N-H str.), 2950-2850 (C-H str.), 1680 cm^{-1} (amide I, C=O str.), 1634 cm^{-1} (zwitterionic carboxylate C=O str.), 1580 cm^{-1} (sodium carboxylate C=O str), 1560 cm^{-1} (Amide II, N-H ben.), (1470-1410 cm^{-1} (C-C str.), 1290-1110 (C-O str.).

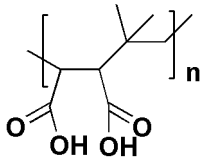

PIBMA: FT-IR: 2950-2850 (C-H str.), 1720 cm^{-1} (C=O str.), (1470-1410 cm^{-1} (C-C str.), 1290-1110 (C-O str.).

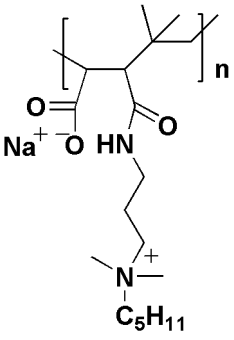

QOPenP: FT-IR: 3250 cm^{-1} (amide N-H str.), 2950-2850 (C-H str.), 1680 cm^{-1} (amide I, C=O str.), 1580 cm^{-1} (sodium carboxylate C=O str), 1560 cm^{-1} (Amide II, N-H ben.), (1470-1410 cm^{-1} (C-C str.), 1290-1110 (C-O str.).

3.4.3 *In-vitro* degradation of the polymers

The degradation study (chemical hydrolysis) was performed for both amide and ester-containing polymers in the presence of acid (0.2 M DCl in D_2O), base (0.2 M NaOD in D_2O) and enzyme lipase (from *Candida antarctica*) (5 U/mL in D_2O). 500 µL of polymer solution (4 mg/mL) in the above mentioned acid, base or enzyme solution was added to a 5 mm NMR tube and proton NMR spectra were recorded immediately. Then the tubes were held in a water bath at 37 °C and proton NMR spectra were recorded every day for 10 days on Bruker AMX 400 MHz NMR spectrometer. The degree of hydrolysis at different times was calculated from the relative integrals originating from β−CH_2− protons (1.5 ppm) of the hydrolysed product $HOCH_2\mathit{CH_2}CH_3$ for ester containing polymer or from α−CH_2− protons (2.5 ppm) of the hydrolysed product $NH_2\mathit{CH_2}CH_2CH_3$ for the amide containing polymer and from β−CH_2− protons (δ 2.0 ppm) of the $NCH_2\mathit{CH_2}CH_2N^+(Me_2)$– for the polymer. Degradation of these polymers will generate 1-aminopropane or 1-propanol. Thus the degree of hydrolysis at different times was calculated from the relative integrals originating from β−CH_2− protons (1.5 ppm) of the hydrolysed product $HOCH_2\mathit{CH_2}CH_3$ for ester containing polymer or from α−CH_2− protons (2.5 ppm) of the hydrolysed product $NH_2\mathit{CH_2}CH_2CH_3$ for the amide containing polymer and from β−CH_2− protons (δ 2.0 ppm) of the $NCH_2\mathit{CH_2}CH_2N^+(Me_2)$– for the polymer. The appearance of the peaks at 1.48-1.51 and 3.3-3.4 ppm that correspond to the β–CH_2− and α–CH_2− groups of 1-propanol confirmed the hydrolysis of the ester-containing polymer. On the other hand, the appearance of the peaks at 1.49-1.52 and 2.4-2.5 ppm that correspond to the β–CH_2− and α–CH_2− groups of 1-aminopropane confirmed the hydrolysis of the amide-containing polymer.

3.4.4 Biophysical experiments with model lipid bilayers

3.4.4.1 Liposome preparation

Lipids (0.5 mM of DPPC or 0.5 mM DPPG:DPPE (88:12)) and Laurdan dye (5 µM) were taken in round-bottom glass vials in chloroform. Thin films were made under dry argon gas, and films were dried under vacuum for complete drying. Lipid films were hydrated with 1x PBS (pH = 7.4) for overnight. Hydrated films were then processed for 10 freeze thaw cycles from 70 to 4 °C with intermittent vortexing. Multilamellar vesicles were then sonicated at 70 °C for 15 min to get unilamellar vesicles.

3.4.4.2 Membrane hydration. 2 ml of laurdan embedded liposome dispersion (lipid: dye = 100:1) containing the polymer solution (lipid: polymer = 7.4:1) in PBS (pH = 7.4) was taken in a fluorescence cuvette. The fluorescence emission intensity was measured at 440 nm and 490 nm by using the excitation wavelength at 350 nm. The measurements were performed at 37 °C using Water Peltier system attached PerkinElmer LS-55 Luminescence Spectrometer. Laurdan, a hydrophobic dye detects changes in the membrane-phase properties through its sensitivity to the polarity of environment in the lipid bilayer. Polarity changes are shown by shifts in the Laurdan emission spectrum, which are quantified by calculating the generalized polarization (GP). Then, membrane hydration was determined using perturbations in Laurdan dye fluorescence due to the result of hydration of the lipid bilayer and quantified by calculating general polarization (GP). GP was calculated by using the following equation.

$$GP = (I_{440} - I_{490})/ (I_{440} + I_{490})$$

Wherein I_{440} and I_{490} represent the fluorescent emission intensity at 440 nm and 490 nm respectively.

3.4.4.3 Isothermal titration calorimetry (ITC)

All experiments were performed at 37 °C using isothermal titration calorimeter (Micro Cal Inc.). Reference cell was filled with double distilled water. All the experiments were performed in 10mM HEPES and 0.14M NaCl (pH = 7.4) buffer. The liposomal suspensions (DPPC or DPPG:DPPE (88:12)) were made in the above buffer at 1mM and polymers were also dissolved in the same buffer and used at a concentration of 50 µg mL^{-1}. The lipid to polymer ratio was kept at 30:1. All the samples were degassed before the titrations. The lipid suspensions were taken in the syringe and the polymer solution was filled in the calorimetric cell. The experiment consisted of 40 injections of 5 µL each (2 µL of first injection) with 10 min intervals to ensure that the titration peak returned to the baseline before the next injection was done. Each injection lasted for 10 s and the stirring speed was kept at 307 rpm for homogenous mixing. A background titration was performed under same conditions with the buffer placed in the calorimetric cell instead of the polymer solution. This result was subtracted from each polymeric sample titration to account for the heat of dilution.The change in enthalpy (ΔH) and the association constant (K_a) were obtained by fitting the data to one set of sites model using Origin 7 software from Micro Cal Inc. The Gibbs free energy change (ΔG) and change in entropy (ΔS) were calculated using

the following equation

$$\Delta G = -RT \ln(55.5K_a) = \Delta H - T\,\Delta S$$

Wherein, R is the universal gas constant (1.986 cal mol^{-1} K^{-1}), factor 55.5 is to account for the molar concentration of water and T is the absolute temperature.

3.4.5 Atomistic molecular dynamics simulations

Classical atomistic molecular dynamics (MD) simulations were performed using simulation package NAMD (versions 2.8 and 2.9)[184] to investigate the interaction of the individual polymer species with a model POPE-POPG bacterial membrane patch consisting of 90 POPE and 38 POPG lipid molecules (Table 3.4). The bilayer configuration used to construct the polymer-bilayer systems was taken from a fully hydrated, 300 ns equilibrated membrane patch used in a previous published work[179]. Owing to such long equilibration, the last 50 ns (250 - 300 ns) of the simulation was used as control study to compute observables in absence of polymers. CHARMM forcefield CHARMM 36[185], optimized to simulate tension less bilayers was used for the lipid (POPE, POPG) molecules and force field parameters for the polymers were derived using the CGenFF program[186, 187]. TIP3P model was used for water and standard CHARMM parameters[188] for ions (Na^+, Cl^-). Equilibrium structures of the 12-monomer length polymers in aqueous environment were obtained by simulating single polymers in 150 mM NaCl solutions for 50 ns. Initial system sizes for such simulations were ~68x68x68 A^3 containing ~9500 water molecules. Polymer properties in aqueous environment were computed over the last 30 ns (20 - 50 ns) of simulation data (data not shown). The polymer configurations at the end of 50 ns were extracted, replicated and used to construct the polymer-bilayer systems. To construct each of the polymer-bilayer systems, four polymers (of same chemical composition) were placed dispersed in the bilayer plane ~(12-18) Å away along the bilayer normal from one of the bilayer leaflets (referred to as "upper leaflet"). Additional water molecules were added so as to prevent the polymers from interacting strongly with the other bilayer leaflet (referred to as "lower leaflet"), at least at the initial stages of simulations. Further, Na^+ and Cl^- ions were added to neutralize the excess charges in the systems and set salt concentration at 150 mM. The number of atoms for the polymer-bilayer systems simulated was ~86000. These systems were each simulated for 150 ns and stationary properties were computed over the last 20 ns (130 - 150 ns) of simulation, unless stated otherwise. All simulations were performed under isothermal-isobaric (NPT) conditions at

a temperature of 310.15 K. Pressure was maintained at 1 atm using Langevin Piston[189]. Time step for all simulations was 2.0 fs. Long range electrostatic interactions were computed using particle-mesh Ewald (PME) and Lennard-Jones interactions were truncated beyond 12 Å using a switching function between 10 Å and 12 Å.

Table 3.4 Parameters used for MD Simulations.

System	N(polymers)	N(POPE)/ Leaflet	N(POPG)/ Leaflet	N(atoms)	Simulation time (ns)
Control	0	90	38	62945	300
Bilayer-Q*n*-prAP	4	90	38	86138	150
Bilayer-Q*n*-hexAP	4	90	38	89282	150
Bilayer-Q*n*-prEP	4	90	38	87672	150
Bilayer-Q*n*-hexEP	4	90	38	88641	150

3.4.6 Raman spectroscopy

Measurements were performed using WiTec Raman spectrometer (UHTS600 SMFC) equipped with CCD (CCD-17531). The excitation source was 532 nm with a power of ~ 20 mW at the sample. A 60x objective (Nikon make) with a numerical aperture (NA) 0.8 was used for normal Raman and 50x ultra long working distance objective with 0.45 NA was used for temperature dependent studies for focusing the laser and collecting scattered light in 180° back scattering geometry. The typical accumulation times were 600 seconds. Temperature dependent measurements were performed using Linkam cryostage (Linkam Scientific Instrument). 20 µL of methanolic solution (400 µg mL^{-1}) of sample was drop coated onto Sapphire substrate and dried under vacuum.

3.4.7 Animal studies

Animal studies were performed according to the protocols approved by Institutional Animal Ethics Committee (IAEC) of Jawaharlal Nehru Centre for Advanced Scientific Research (JNCASR) and National Institute of Veterinary Epidemiology and Disease Informatics (NIVEDI). Acute and sub-chronic toxicity studies were performed at JNCASR, Bengaluru (CPCSEA/201) in accordance with institutional ethical guidelines. Infection studies were performed at NIVEDI. The animal experiments were approved by the IAEC of NIVEDI, Bengaluru (881/GO/ac/05/CPCSEA) and carried out as per the guidelines of Committee for the

purpose of Supervision and Experiments on Animals (CPCSEA), Ministry of Environment and Forests, New Delhi, India. The mice were housed in individually ventilated cages (IVC) maintained with controlled environment as per the standards. They are: housing – pathogen free conventional caging system, bedding material– Corn Cob. The husbandry conditions: -Light: dark cycle- 12:12 hours, Animal Room Temp: 22 ± 2 °C, Relative humidity: 30-40 %, Access to feed and water: *ad libitum* and Water: RO Water. Animals were randomly selected, marked to permit individual identification and kept in their cages for at least 5 days before the experiment to allow for acclimatization to the experimental conditions. Animal handling and experimentation protocols were followed according to OECD Guidelines for the Testing of Chemicals (OECD 425). All care was taken to cause no pain to the animals. Humane endpoints were used to avoid unnecessary distress and suffering in animals following an experimental intervention that would lead to death.

3.4.7.1 *In-vivo* toxicity

The experimentation protocols for the determination of dosage, number of animals per groups etc. were followed according to the OECD Guidelines for the Testing of Chemicals (OECD 425). Female Balb/c mice (6-8 weeks, 18-22 g) were used for systemic toxicity studies. Mice were randomized into control and test groups with 5 mice per group. Control groups received 200 μL of sterilized PBS (pH = 7.4). Different doses (5.5, 17.5, 55 and 175 mg kg^{-1}) of the test drugs were used as per the OECD guidelines. 200 μL of the test drug solution in sterilized PBS (pH = 7.4) was injected into each mouse (5 mice per group) through intravenous (i.v.) (tail vein) route of administration. The mice in the high dose group (175 mg kg^{-1}) immediately post-injection of the drug, showed clinical signs of tremors, recumbency, sever distress and convulsions, which were indicative of the impending death or moribund condition. Therefore, some which were in moribund condition were humanely euthanized using Isoflurane (Halothane) inhalant anaesthetic. For the intraperitoneal (i.p.) and subcutaneous (s.c.) (over the flank) routes of administration, the high dose (175 mg kg^{-1}) was not injected to reduce the animal lethality. All the mice were monitored for 14 days post-treatment. Different routes of administration were used to find out the best method of administration of test drugs with minimal pain or lethality to the animals. The animals were closely monitored for the first 30 min to 4 hr for the first 24 hours of the initiation of the experiment. And then onwards, they were monitored daily for 14 days.

During the observation period of 14 days, no onset of abnormality was found. The 50 % lethal dose (LD_{50}) was estimated according to the up- and -down method[190]. The remaining animals, post-experimentation, were euthanized using the same procedure.

3.4.7.2 *In-vivo* sub-chronic toxicity studies

Parameters analyzed in subchronic toxicity studies were chosen as per the FDA guidelines of Subchronic Toxicity Study in Rodents. Female Balb/c mice (6-8 weeks, 18-22 g) were used for both acute and subchronic toxicity studies. 200 μL of the polymer solution in sterilized PBS (pH = 7.4) was injected into each mouse. For evaluating the subchronic toxicity-clinical biochemistry parameters, four groups of 10 mice each were given intravenous (i.v.) injection of Q*n*-prAP (20 mice) and Q*n*-prEP (20 mice) at a dosage of 2 mg kg^{-1} in 200 μL of sterilized PBS (pH = 7.4) and 10 mice were used for the control group. After 48 h, blood was collected from 30 mice (10 mice for Q*n*-prAP, 10 mice for Q*n*-prEP and 10 mice for control) and analyzed for different parameters like alkaline phosphatase (ALP), creatinine, blood urea nitrogen, and electrolytes like sodium, potassium ions and chloride. Also, after 14 days, blood was collected from the remaining mice and analyzed for the above mentioned parameters. Similarly, all the above parameters were analyzed for the control group as well. The data are expressed as mean ± standard deviation, based on values obtained from 10 mice (n = 10 for the data from this report). Statistical analysis was performed using student's *t-test*. Differences are considered statistically significant with probability $p < 0.05$. Post experimentation, mice were euthanized using Isoflurane (Halothane) inhalant anaesthetic.

Chapter 4

Cationic-amphiphilic Polymers with Tunable Hydrophobicity of the Amide Side Chains

Abstract

Controlling the hydrophobicity of amphiphilic polymers modulates their molecular behavior as well as biological activity profiles. Most of the conventional approaches modulate hydrophobicity in amphiphilic polymers by varying the number of carbon atoms (for e.g. alkyl chain length). Here, a novel approach of tuning the hydrophobicity in amphiphilic polymers is reported by varying the chemical architecture of amide side chains. Isomerisation, cyclisation and unsaturation of amide side chains has been employed in amphiphilic polymers keeping a constant number of carbons. It has been observed that cyclic and unsaturated hydrophobic side chain containing polymers outperform their isomeric counterparts with respect to potent antibacterial activity and reduced mammalian toxicity. This control of hydrophobicity in amphiphilic polymers drives them selectively towards bacterial cell membranes instead of mammalian membranes. These structural differences in the side chains also led to different interactions with the bacterial cell membranes. It has been found that polymers containing chemically different side chains possess variations in their hydrophobicity profiles probably reflecting tunable biological activities. Such design of amphiphilic polymers with diverse side chain structures can be used to develop functional polymers for biological applications.

(1) Uppu, D. S. *et al.* Cyclization and Unsaturation rather than Isomerization of Side Chains Governs the Selective Antibacterial Activity of Cationic-amphiphilic Polymers. *Chem. Commun.* **2016**. Under Revision.

4.1 Introduction

Antibacterial polymers inspired from natural AMPs possess amphiphilicity (cationic/hydrophobic balance) as one of their major structural determinants [107]. The positive charge ensures their selective binding to the negatively charged lipid membranes of bacteria compared to the zwitterionic lipid membranes of mammalian cells whereas the hydrophobic interactions further strengthen membrane disintegration. Optimum amphiphilicity is required to selectively target the bacteria sparing the mammalian cells. This selectivity is tuned by improving the antibacterial activity while reducing the mammalian toxicity which is generally measured from the hemolysis of red blood cells (HC_{50}/MIC). However, the Holy Grail of the field is how to improve this selectivity to target specifically the bacterial cells [107].

To date, optimization of cationic/hydrophobic balance has been achieved either by varying the cationic charge or side chain hydrophobicity (generally by altering the carbon number) in a variety of polymers. More important is the spatial/positional variation of cationic charge and hydrophobic side chain. Two approaches are generally used for this spatial variation: the cationic and hydrophobic groups are either on opposite sides (facial) of a homopolymer or spatially segregated from one another in a co-polymer. Another approach of attaching the hydrophobic side chain to the cationic centre in co-polymers (same centered) has also been shown to be effective [107]. In this chapter, a different approach of varying the chemical structure of the amide side chain appended to the cationic centre by keeping a constant positive charge as well as fixed carbon number. An important, yet unexplored, question is how this variation in just the side chain chemical structure can tune the selective antibacterial activity of amphiphilic polymers. A novel approach of controlling the hydrophobicity of amphiphilic systems has been introduced by chemical structure variations such as cyclization, isomerization and unsaturation of the amide side chains in quaternized polymers. The advantage of this approach lies in tuning the hydrophobicity by keeping the fixed number of carbons in the side chains unlike the conventional strategies that use the concept of varying the number of carbons. Molecular weight of the polymer affects its properties enormously including the biological activity profiles. The molecular weight of the polymers prepared using the present approach (isomerization, cyclization and unsaturation at fixed carbon number) remains nearly constant whereas changing the length of the carbon chain drastically increases the molecular weight thereby making it difficult to decipher the role of hydrophobicity. How this control of hydrophobicity in

amphiphilic polymers influences antibacterial activity and mammalian cell toxicity has been studied. An important question investigated in this report is the role of hydrophobicity in directing the amphiphilic polymers selectively to bacterial cell membranes instead of mammalian membranes.

4.2 Results and Discussion

4.2.1 Synthesis

The synthetic protocols were followed as described in Chapter 2 (Scheme 4.1). Appending the amide side chains with different side chemical structure such as cyclization, isomerization and unsaturation resulted in the polymers as shown in Scheme 4.1. The cationic charge density given

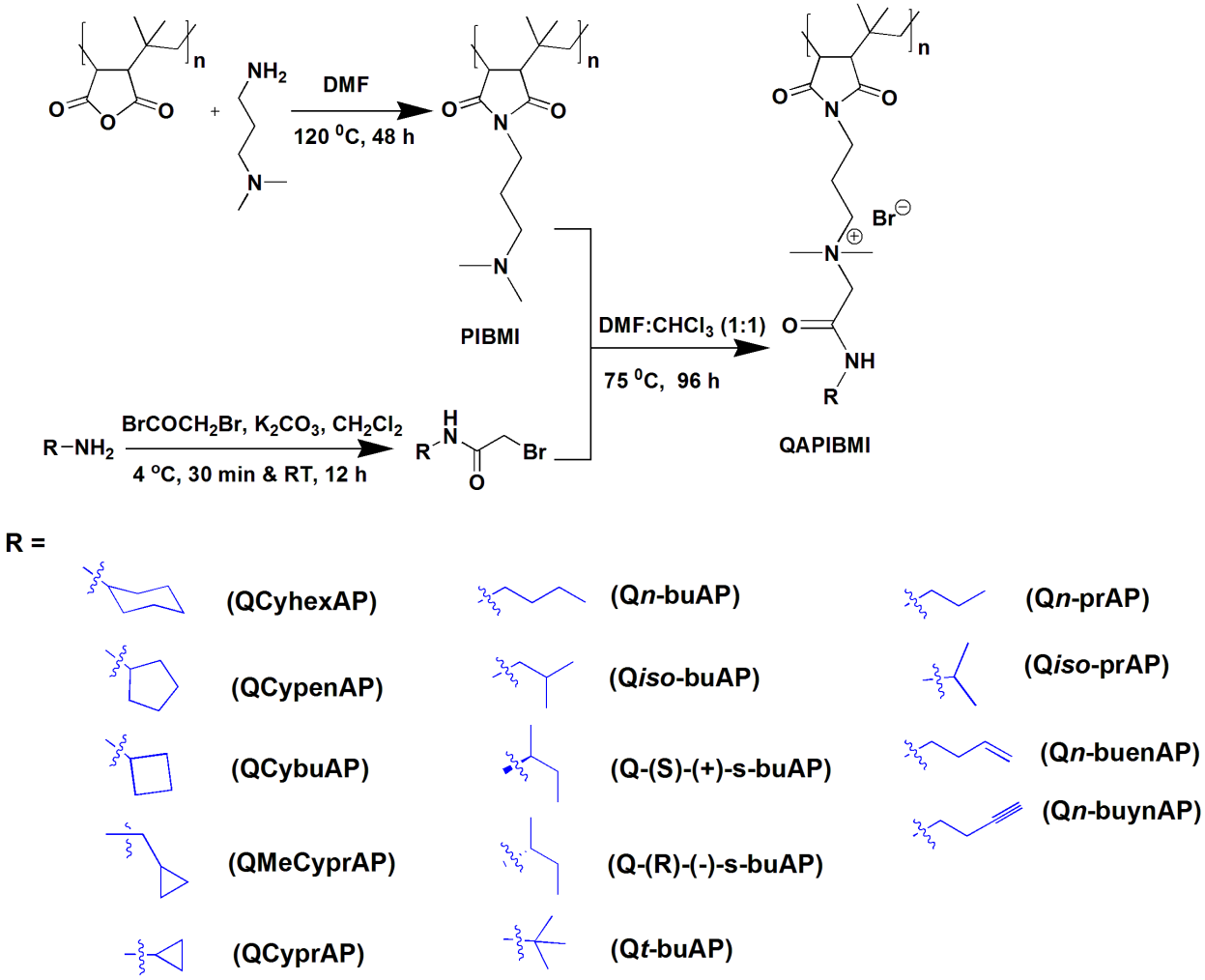

Scheme 4.1: General synthetic approach for the synthesis of cationic amphiphilic polymers with appended amide side chains of different chemical structures.

by the degree of quaternization was calculated by ^{1}HNMR analysis as described in Chapter 2 and found to be in the range of 90-95% for all the polymers (Table 4.1). The molecular weight of all the polymers was found to be in the range of 15-18 kDa (Table 4.1). This shows that the cationic charge density was more or less constant in all the polymers which facilitated the comparison between them. The polymers (P) shown in scheme 4.1 are represented as Q*n*-CmAPs or QCyCmAPs for poly(isobutylene-alt-*N*-(*N'*,*N'*-dimethylamino*propyl*)-maleimide) (PIBMI) based quaternized (Q) amide (A) with appended acyclic or cyclic (Cy) side chains.

Table 4.1: Degree of quaternization and molecular weight of cationic amphiphilic polymers.

Polymer	Degree of Quaternization (DQ, %)[a]	Molecular Weight (M_n) (KDa)[b]
QCyhexAP	94	17.3
QCypenAP	93	16.7
Q*n*-buAP	94	16.4
QCybuAP	91	17.6
Q*iso*-buAP	93	16.3
Q(S)-(+)-*s*-buAP	93	16.3
Q(R)-(-)-*s*-buAP	92	16.2
Q*t*-buAP	93	16.3
QMeCyprAP	95	16.4
Q*n*-buenAP	93	16.2
Q*n*-buynAP	92	16
Q*n*-prAP	95	16.1
QCyprAP	93	15.7
Q*i*-prAP	95	18.0

[a,b] Calculated using ^{1}H NMR analysis.

4.2.2 Antibacterial activity and mammalian cell toxicity

To understand the influence of side chain architecture, the antibacterial activity and mammalian cell toxicity of polymers with both cyclic and acyclic side chains were investigated. The antibacterial activity of cationic polymers has been evaluated in *E. coli*, *A. baumannii* and *S. aureus* as well as drug resistant bacteria such as MRSA and VRE. Next, the mammalian cell toxicity has been investigated by the release of lactate dehydrogenase (LDH) as a measure of membrane permeabilization from human endothelial kidney (HEK) cells. The concentration required for 50% release of LDH was designated as IC_{50}.

To start with, amphiphilic polymers with varying number of carbons were prepared and then the polymers with variations in side chain chemical structures at a fixed carbon number were synthesized. At first, to fix the carbon number, synthesis of polymers with cyclic side chains of variable hydrophobicity (different carbon number) such as QCyhexAP (six carbons), QCypenAP (five carbons), QCybuAP, QMeCyprAP (four carbons) and QCyprAP (three carbons) was achieved (Scheme 4.1). The higher cyclic side chain polymers, QCyhexAP, QCypenAP, QCybuAP and QMeCyprAP displayed minimum inhibitory concentration (MIC) and minimum bactericidal concentration (MBC) in the range of 4-16 μg mL^{-1} against *E. coli* and *S. aureus* (Table 4.2). The lower cyclic side chain, QCyprAP had moderate activity against (MIC and MBC = 16-31 μg mL^{-1}) against *E. coli* and *S. aureus* (Table 4.2). Even against multi-drug resistant bacteria such as methicillin resistant *Staphyloccus aureus* (MRSA) and Vancomycin resistant *Enterococcus faecium* (VRE), QCyhexAP, QCypenAP, QCybuAP and QMeCyprAP showed MIC of 4-16 μg mL^{-1} whereas QCyprAP had very low activity (MIC = 125 μg mL^{-1}) (Table 4.2).

Table 4.2: Antibacterial activity and toxicity profiles of amphiphilic polymers.

Polymer	**MIC**[a] (μg mL^{-1})				**HC_{50}**[b] (μg mL^{-1})	**IC_{50}**[c] (μg mL^{-1})
	E. coli	*S. aureus*	MRSA	VRE		
QCyhexAP	16	8	8	8	45	65
QCypenAP	16	4	8	8	80	65
Q*n*-buAP	31	4	8	4	83	65
QCybuAP	16	8	16	8	250	95
Q*iso*-buAP	16	4	8	4	80	65
Q(S)-(+)-*s*-buAP	16	16	31	8	125	77
Q(R)-(-)-*s*-buAP	16	16	31	16	150	83
Q*t*-buAP	16	16	31	8	125	65
QMeCyprAP	31	16	16	8	250	100
Q*n*-buenAP	31	31	62	16	>1000	>100
Q*n*-buynAP	31	31	125	62	>1000	>100
Q*n*-prAP	31	8	31	31	1000	100
QCyprAP	31	16	125	125	>1000	>100
Q*i*-prAP	31	62	125	62	>1000	>100

[a]Minimum inhibitory concentration (MIC); [b]Concentration required for 50% hemolysis of human red blood cells (hRBCs); [c]Concentration required for 50% of lactate dehydrogenase (LDH) release from human endothelial kidney (HEK) cells.

Table 4.3: Antibacterial activity, toxicity and selectivity profiles of cationic polymers.

Polymer	MBC[a] (μg mL^{-1})		HC_{50}[b] (μg mL^{-1})	Selectivity[c]	
	E. coli	*S. aureus*		*E. coli*	*S. aureus*
QCyhexAP	5	2.5	45	9	18
QCypenAP	5	2.5	80	16	32
Q*n*-buAP	5	2.5	83	16	33
QCybuAP	5	2.5	250	50	100
Q*iso*-buAP	5	2.5	80	16	33
Q(S)-(+)-*s*-buAP	5	2.5	125	25	50
Q(R)-(-)-*s*-buAP	5	2.5	150	30	60
Q*t*-buAP	5	2.5	125	25	50
QMeCyprAP	5	2.5	250	51	102
Q*n*-buenAP	10	2.5	>1000	100	>400
Q*n*-buynAP	>10	2.5	>1000	>100	>400
Q*n*-prAP	5	2.5	1000	200	400
QCyprAP	>10	2.5	>1000	>100	>400
Q*i*-prAP	>10	2.5	>1000	>100	>400

[a]Minimum bactericidal concentration (MBC) after 24 h; [b]Concentration required for 50% hemolysis; [c]Selectivity = HC_{50}/MBC.

It has been found that antibacterial efficacy of the polymers is dependent on type of culture media used [163]. Thus, the antibacterial activity has been determined in chemically defined media against *E. coli* and *S. aureus*. QCyhexAP, QCyPenAP, QCybuAP and QMeCyprAP showed potent antibacterial activity with MBC of 5 μg mL^{-1} and 2.5 μg mL^{-1} against *E. coli* and *S. aureus* respectively (Table 4.3). QCyprAP, although showed good activity against *S. aureus* (MBC = 2.5 μg mL^{-1}), displayed low activity against *E. coli* (MBC >10 μg mL^{-1}). These results suggest that the antibacterial activity depends on the type of culture media conditions.

Though highly effective against bacteria, QCyhexAP and QCypenAP were highly toxic to mammalian cells. The HC_{50} and IC_{50} values decreased as the carbon number of the cyclic side chains decrease from six to three (Table 4.2). The smaller ring derivative, QCyprAP showed very low mammalian cell toxicity (HC_{50} and IC_{50} >1000 μg mL^{-1} and 100 μg mL^{-1} respectively). QCybuAP and QMeCyprAP with potent antibacterial activity displayed low toxicity to mammalian cells. Selectivity factor (HC_{50}/MBC) gives the measure of how much selective is the agent to bacteria over mammalian cells. QCybuAP and QMeCyprAP had a high selectivity of 50-100 towards bacteria over mammalian cells (Table 4.3). These results suggested the carbon number of four being the optimum required for selective toxicity to bacteria.

Next, the cyclic side chain polymers were compared with their acyclic counterparts to understand the influence of cyclization towards tuning the selective antibacterial activity. The higher hydrophobic side chain polymers, Q*n*-buAP (*n*-butyl) and QCybuAP (cyclobutyl) displayed MIC in the range of 4-31 μg mL^{-1} whereas the less hydrophobic counterparts Q*n*-prAP (*n*-propyl) and QCyprAP (cyclopropyl) had MIC of 16-31 μg mL^{-1} against *E. coli* and *S. aureus* (Table 4.2). Interestingly, these polymers displayed potent antibacterial efficacy against *A. baumannii* (MTCC 1425) including the multi-drug resistant clinical isolates (*A. baumannii* R674 and R676). All the four polymers showed MIC in the range of 3.9-7.8 μg mL^{-1} against all the three strains of *A. baumannii*. Against the drug resistant bacteria, MRSA and VRE, Q*n*-buAP and QCybuAP had MIC in the range of 4-16 μg mL^{-1}. Q*n*-prAP showed MIC of 8 μg mL^{-1} and 31 μg mL^{-1} whereas QCyprAP lost the activity with MIC of 125 μg mL^{-1} against VRE and MRSA respectively (Table 4.2). Even in chemically defined media, Q*n*-buAP, QCybuAP and Q*n*-prAP showed potent antibacterial activity with same MBC of 5 μg mL^{-1} and 2.5 μg mL^{-1} against *E. coli* and *S. aureus* respectively (Table 4.3). QCyprAP, although showed good activity against *S. aureus* (MBC = 2.5 μg mL^{-1}), displayed low activity against *E. coli* (MBC >10 μg mL^{-1}). Against *A. baumannii* all the polymers had MBC in the range of 3.9-7.8 μg mL^{-1}.

Q*n*-buAP showed toxicity to hRBCs with HC_{50} of 83 μg mL^{-1} whereas QCybuAP had HC_{50} of 250 μg mL^{-1}. Q*n*-prAP and QCyprAP showed low toxicity with HC_{50} = 1000 and >1000 μg mL^{-1} respectively (Table 4.2). QCybuAP and Q*n*-prAP with potent antibacterial activity and low toxicity to mammalian cells had the high selectivity (HC_{50}/MBC) of 50-100 and 200-400 respectively towards bacteria over mammalian cells (Table 4.3). Thus, at higher hydrophobicity, the cyclic side chain polymer (QCybuAP) was found to be better than its acyclic counterpart (Q*n*-buAP) in these amphiphilic polymers with respect to selective toxicity to bacteria. However, at lower hydrophobicity, the cyclic side chain polymer (QCyprAP) has lower antibacterial activity as well as non-toxic to mammalian cells. Q*n*-prAP showed potent antibacterial activity and low-toxicity to mammalian cells. These results suggest the role of optimum hydrophobicity and cyclization of side chains in tuning the selective toxicity to bacteria.

Next, the role of the side chain architecture towards antibacterial activity and toxicity was studied by keeping the four carbon number constant, the optimum side chain as described above. Regio- and stereo-isomerization was employed in the acyclic side chains of the polymers to investigate their effect on antibacterial activity and mammalian cell toxicity. The isomeric side

chain containing polymers (Scheme 4.1) such as Q*n*-buAP (*n*-butyl), Q*iso*-buAP (isobutyl), Q-(S)-(+)-*s*-buAP (sec-butyl), Q-(R)-(-)-*s*-buAP (sec-butyl) and Q*t*-buAP (t-butyl) displayed MIC in the range of 4-31 μg mL^{-1} against *E. coli*, *S. aureus*, MRSA and VRE (Table 4.2) comparable to the corresponding cyclic side chain polymers, QCybuAP and QMeCyprAP (methylcyclopropane) (Table 4.2). However, all these five isomeric side chain containing polymers displayed more or less similar cytotoxicity and selectivity values (Table 4.2). These observations resulted in the understanding that isomerization in the hydrophobic side chains does not improve the selective antibacterial activity of these cationic amphiphilic polymers.

Moreover, unsaturation of side chains was used to further tune the selective toxicity to bacteria. The double bond containing polymer, Q*n*-buenAP (but-3-enyl) showed an MIC of 16-62 μg mL^{-1} against both *E. coli* and *S. aureus*, MRSA and VRE. However, the triple bond containing polymer, Q*n*-buynAP (but-3-ynyl) though was active against *E. coli* and *S. aureus* but lost the activity against MRSA and VRE (Table 4.2). Nevertheless, both the unsaturated side chain containing polymers were non-hemolytic even up to 1000 μg mL^{-1}. But the corresponding Q*n*-buAP (HC_{50} = 83 μg mL^{-1}), QCybuAP and QMeCyprAP (HC_{50} = 250 μg mL^{-1}) were more toxic to red blood cells. The amphiphilic polymers with structural variations in their side chains such as Q*n*-buAP, QCybuAP, QMeCyprAP, Q*n*-buenAP and Q*n*-buynAP also had different toxicity profiles to HEK cells (Table 4.2). Q*n*-buAP, QCybuAP and QMeCyprAP were found to be more toxic to HEK cells than Q*n*-buenAP and Q*n*-buynAP. Q*n*-buenAP and Q*n*-buynAP showed the highest selectivity of >100 and >400 to bacteria over mammalian cells amongst all the polymers (Table 4.3).

4.2.3 Membrane-active mode of action

The membrane-active properties of polymeric materials were determined by measuring the cytoplasmic membrane depolarization, permeabilization and ATP leakage against *E. coli* and *S. aureus*. All the experiments were performed at a concentration of 25 μg mL^{-1}. Q*n*-buAP, QCybuAP, Q*n*-prAP and QCyprAP showed significant and similar extent of membrane depolarization against both *E. coli* and *S. aureus* (Fig. 4.1 A & 4.1 B). Q*n*-buAP, QCybuAP and QMeCyprAP had similar whereas both Q*n*-buenP and Q*n*-buynAP showed lower effect on membrane depolarization of *S. aureus*. On contrary, against *E. coli*, Q*n*-buAP showed a very high capability to dissipate the membrane potential compared to QCybuAP, QMeCyprAP, Q*n*-

buenAP and Q*n*-buynAP. However, against *A. baumannii*, Q*n*-buAP had higher dissipation of membrane potential than other three polymers (Fig. 4.2 A). Concentration dependent effect of QCybuAP on membrane depolarization of *E. coli* was investigated (Fig. 4.3 A). Starting from 5 μg mL^{-1}, QCybuAP showed increased membrane depolarization up to 20 μg mL^{-1}. Even at 5 μg mL^{-1}, the lowest concentration used, QCybuAP showed high extent of depolarization that would have eventually led to cell death (MBC = 5 μg mL^{-1}, Table 4.3).

Q*n*-buAP had the highest ability followed by QCybuAP, Q*n*-prAP and QCyprAP to permeabilize the membranes of *E. coli* (Fig. 4.1 C) and *A. baumannii* (Fig. 4.2 B). The membrane permeabilization of *E. coli* follows an increasing trend with Q*n*-buAP showing the highest permeabilization whereas Q*n*-buynAP had the lowest permeabilization. Concentration dependent effect of QCybuAP on membrane permeabilization of *E. coli* was determined (Fig. 4.3 B). Unlike membrane depolarization, QCybuAP had increased membrane permeabilization from 10 μg mL^{-1} up to 20 μg mL^{-1}. However, at 5 μg mL^{-1} no effect of membrane permeabilization was found whereas a great extent of membrane depolarization at the same concentration was observed against *E. coli*.

Dissipation of membrane potential leads to limiting the energy required for the metabolic processes in bacteria. Leakage of ATP levels in *E. coli* (Fig. 4.1 D) and *S. aureus* (Fig. 4.4 A) were measured after treatment with the polymers using the luciferin-luciferase bioluminescence assay to understand the energy limitation conditions. Q*n*-buAP had higher levels of ATP leakage followed by QCybuAP, Q*n*-prAP and QCyprAP against *E. coli*. However, against *S. aureus*, all the four polymers showed significant but similar levels of ATP leakage. Against *S. aureus*, Q*n*-buynAP had lower whereas Q*n*-buenAP, QMeCyprAP and Q*n*-buAP had more or less similar levels of ATP leakage. Q*n*-buAP had the highest whereas QMeCyprAP, Q*n*-buenAP and Q*n*-buynAP had similar leakage of ATP levels in *E. coli*. The above mechanistic studies suggest that these polymers exert their antibacterial activity through membrane-active mechanism of action. The differences in the membrane-active profiles of the polymers were more apparent against *E. coli* (Gram-negative bacteria) that possesses an additional outer lipid membrane compared to *S. aureus* (Gram-positive bacteria). The potent antibacterial activity of Q*n*-buAP, QCybuAP and Q*n*-prAP and lower activity of QCyprAP got evident in the membrane-active profiles of these polymers against *E. coli*. Against *S. aureus*, all the polymers displayed similar membrane-active properties that also correlate with their similar antibacterial activity profiles.

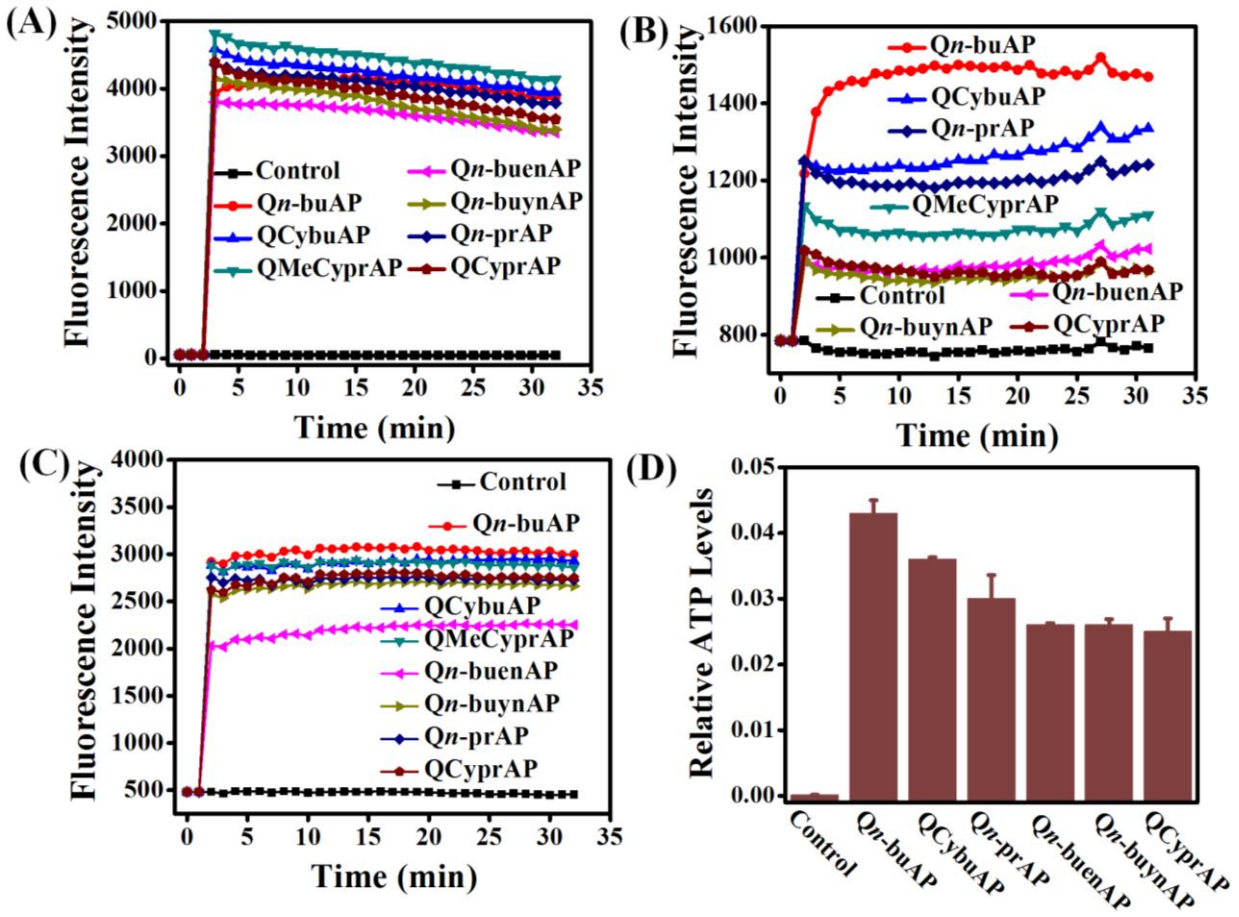

Figure 4.1: Membrane-disrupting properties of polymers. (A) Membrane depolarization of polymers against *S. aureus* (A) and *E. coli* (B); Membrane permeabilization of polymers against *E. coli* (C); Released ATP levels after treatment with polymers for 15 min against *E. coli* (D). Relative ATP levels (µmol/L) were determined by subtracting the background ATP levels from the test sample ATP levels.

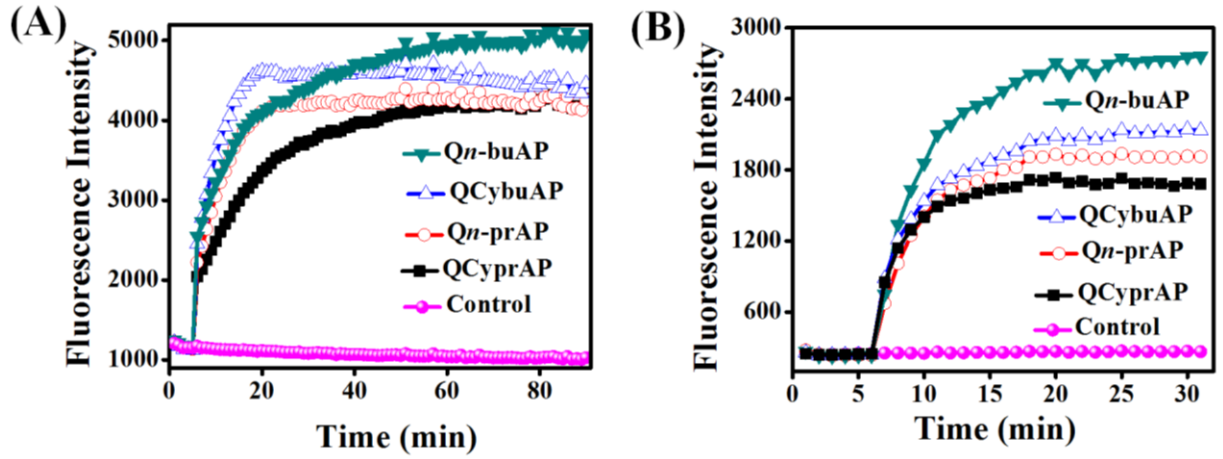

Figure 4.2: Membrane-disrupting properties of polymers in *A. baumannii*. (A) Membrane depolarization and (B) Membrane permeabilization.

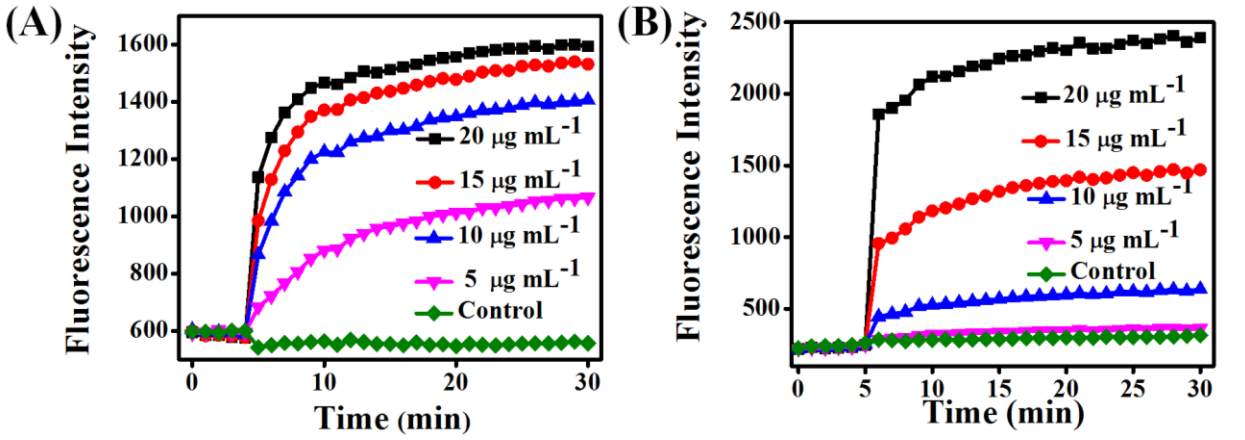

Figure 4.3: Concentration dependent membrane-activity of QCybuAP against *E. coli*. (A) Membrane depolarization and (B) membrane permeabilization after treatment with various concentrations of QCybuAP.

4.2.4 Membrane hydration

To present a physical picture as to how this control of hydrophobicity directs the polymers selectively to bacterial cell membranes instead of mammalian membranes, model lipid bilayers were used. Bacterial (DPPG:DPPE) and mammalian (DPPC) model lipid bilayers were prepared with Laurdan (6-Dodecanoyl-2-dimethylaminonaphthalene), a hydrophobic dye encapsulated in them. The membrane hydration/fluidity experiments were calculated as described in Chapter 3. The Laurdan GP was calculated after the treatment of DPPG: DPPE (88:12) and DPPC lipid bilayers with polymers (lipid: polymer = 7.4:1) (Fig. 4.4 B). GP values decreased upon interaction of the amphiphilic polymers with the bacterial but not the mammalian model lipid bilayers (Fig. 4.4 B). Q*n*-buAP showed lower GP followed by QCybuAP, Q*n*-buenAP and Q*n*-buynAP compared to untreated bacterial lipid bilayer (DPPG:DPPE). These results suggested that Q*n*-buAP caused maximum bacterial membrane perturbations (disordered lipid phase-higher fluidity) followed by QCybuAP, Q*n*-buenAP and Q*n*-buynAP compared to the untreated lipid bilayer (ordered lipid phase-lower fluidity).

4.2.5 Hydrophobicity profiles

To test the hypothesis that variations in side chain chemical structures such as cyclization and unsaturation tune the hydrophobicity, chromatographic profiles of these polymers were studied on a C-18 column (using reverse phase high performance liquid chromatography (RP- HPLC),

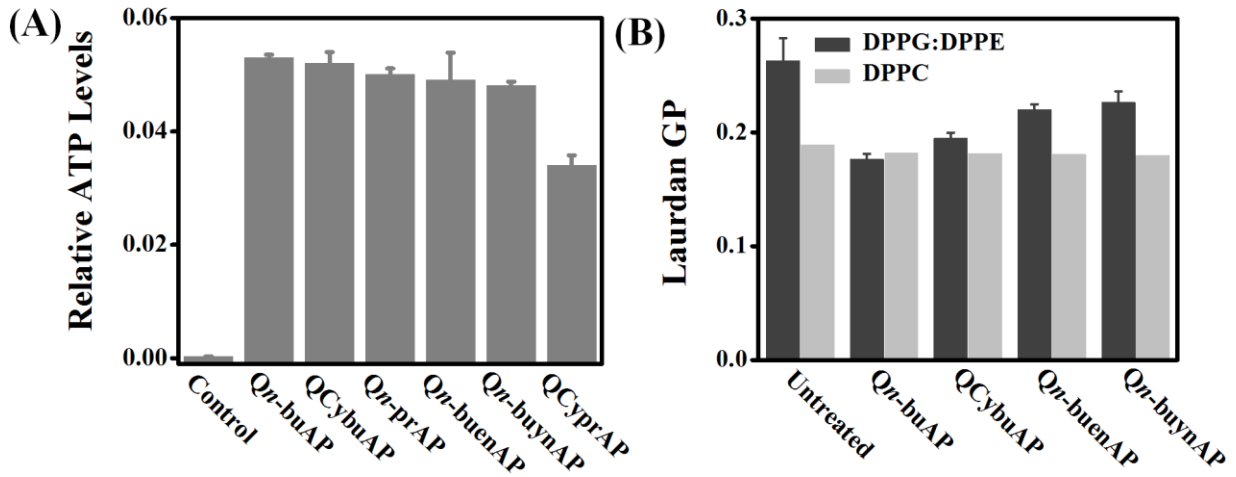

Figure 4.4: Membrane-disrupting properties of polymers. (A) Released ATP levels after treatment with polymers for 15 min against *S. aureus*. Relative ATP levels (µmol/L) were determined by subtracting the background ATP levels from the test sample ATP levels; (B) Mechanistic studies to understand the interactions of polymers with bacterial and mammalian model lipid bilayers. Membrane hydration of lipid bilayers at 37 °C consisting of DPPG: DPPE (88:12) and DPPC treated with polymers mimicking the bacterial and mammalian cell membranes respectively. Membrane hydration was determined using perturbations in Laurdan dye fluorescence due to the result of hydration of the lipid bilayer and quantified by calculating generalized polarization (GP).

absorbance at 220 nm). The retention time (RT in min) of the polymers varied with respect to differences in hydrophobicity as well as side chain chemical structure. Four carbon number polymers, Q*n*-buAP had RT of 22.2 min compared to its cyclic analogue, QCybuAP with RT of 21.2 min (Fig. 4.5). Similarly, the lower hydrophobic polymers, Q*n*-prAP had RT of 19.8 min whereas QCyprAP had the lowest RT of 18.5 min. Variation in the carbon number of the side chain reduced the overall hydrophobicity of the polymers. Interestingly, these observations suggested that cyclization of the appended side chains decreased the overall hydrophobicity of these polymers even when the number of carbons remained same. The differences in the hydrophobicity profiles of these polymers also correlate with the antibacterial activity, mammalian cell toxicity and membrane-active properties. Higher hydrophobic polymer, Q*n*-buAP (RT = 22.2) was more toxic to mammalian cells than QCybuAP (RT = 21.2) although both had more or less similar antibacterial activity and membrane disruption. The differences were more apparent with three carbon number side chain polymers. Q*n*-prAP (RT = 19.8) had higher antibacterial activity and potent membrane-disruption properties compared to QCyprAP (RT = 18.5) despite both being low toxic to mammalian cells. Overall, optimum hydrophobicity in

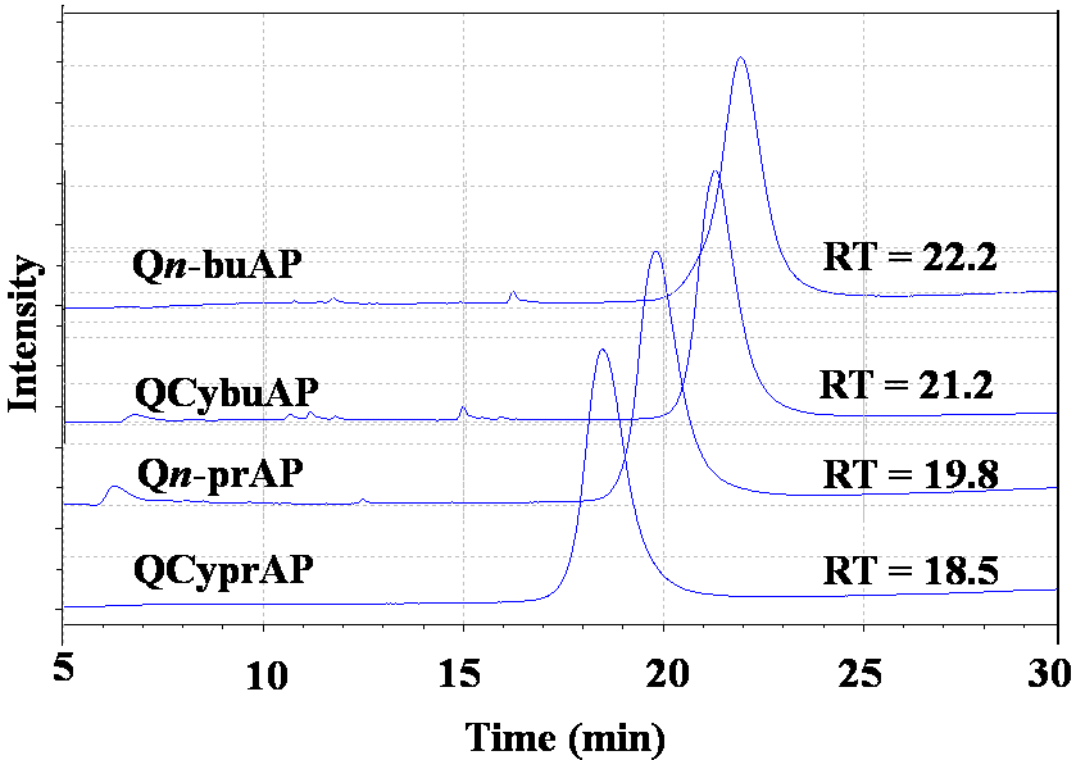

Figure 4.5: Chromatograms (reverse phase-high performance liquid chromatography, RP-HPLC) of amphiphilic polymers having cyclic and acyclic side chains displaying varied retention times (RT).

acyclic side chains (Q*n*-prAP) and cyclization (QCybuAP) resulted in amphiphilic polymers with potent antibacterial activity and minimal toxicity to mammalian cells. Upon unsaturation, the hydrophobicity decreased in the order of Q*n*-buAP, QCybuAP, Q*n*-buenAP, QMeCyprAP and Q*n*-buynAP. It was found that Q*n*-buenAP had RT of 20.5 and Q*n*-buynAP displayed the lowest RT of 19.4 (Fig. 4.6 B). These results indicated that overall hydrophobicity of the polymers changes due to variation in their side chain chemical structure. It also suggested that it is indeed the changes in hydrophobicity that lead to tunable antibacterial activity as well as reduced mammalian cell toxicity of these polymers. The well known differences in the polarizability[191] of saturated (acyclic and cyclic) and unsaturated hydrocarbons might lead to variations in hydrophobicity. Recently, Gellman and co-workers showed that in nylon-3 co-polymers, cyclic subunits close to the backbone selectively targets the bacteria compared to acyclic subunits due to assumed changes in local backbone flexibility [108, 192]. On the other hand, the data provided evidence that cyclization of hydrophobic side chains appended to the cationic centre far from the polymeric backbone selectively kills the bacteria compared to their acyclic counterparts because

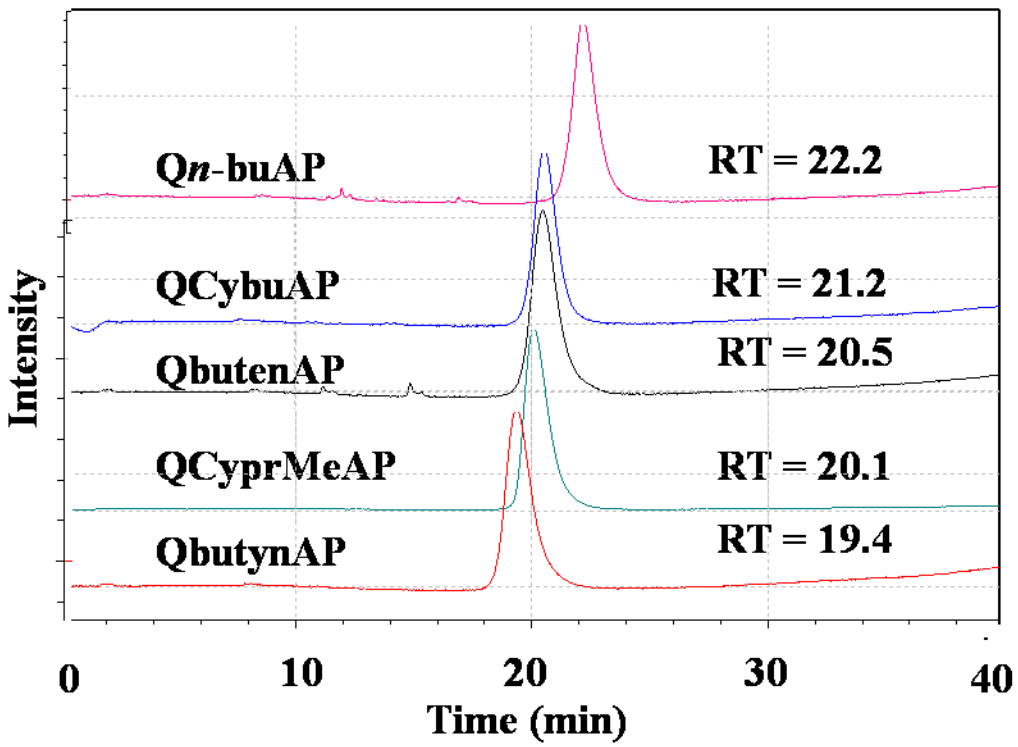

Figure 4.6: Chromatograms (reverse phase-high performance liquid chromatography, RP-HPLC) of amphiphilic polymers having side chains with different chemical structures of four carbon number displaying varied retention times (RT).

of changes in hydrophobicity.

Overall, the acyclic saturated hydrophobic side chains in these polymers yield less selectivity compared to their cyclic counterparts. In addition, the unsaturated hydrophobic side chains yield better selectivity compared to the corresponding saturated acyclic and cyclic side chains in these polymers. However, the isomerization in the hydrophobic side chains (branched hydrophobicity) did not result in drastic changes both in antibacterial activity and toxicity thus displaying more or less similar selectivity. Literature reports [78, 105, 107] show that increasing either the cationic charge density or hydrophobicity (by increasing alkyl chain length) or molecular weight (up to a certain limit) improves antibacterial activity but results in greater extent of hemolysis. In the present approach nearly constant cationic charge density serves to be the primary driving force towards anionic bacterial cell membranes. Most of the reported antibacterial polymers have uncontrollable variations in their molecular weight making it difficult to draw the conclusions. On the other hand, the present strategy allows precise control of molecular weight in amphiphilic polymers thereby leading to better comparison amongst

them. For e.g. the isomeric and structurally different (Q*n*-buAP, QCybuAP, QMeCyprAP, Q*n*-buenAP and Q*n*-buynAP) side chain containing polymers have nearly same molecular weights (Table 4.1). More importantly, varying the hydrophobicity has been achieved by increasing the alkyl chain length in amphiphilic antibacterial polymers reported so far. This approach tunes hydrophobicity by varying the chemical structure of the side chains (isomerization, cyclization and unsaturation) wherein the number of carbons was kept constant. Also, the spatial/positional variation of cationic and hydrophobic moieties in amphiphilic polymers such as on different monomers (segregated) [112], on same monomers (facially amphiphilic/same centered) [115] [110] and on different polymeric segments (block co-polymers) [116] influences the activity and toxicity profiles. The present concept provided a conceptual understanding that in same centered amphiphilic polymers varying the side chain chemical structure such as cyclization, isomerization and unsaturation influences the antibacterial activity and mammalian cell toxicity with nearly constant cationic charge density and precise control of molecular weight. Tuning the hydrophobicity of the polymers with variations in side chain chemical structure led to specific membrane driven interactions thereby reflecting in their antibacterial activity and mammalian cell toxicity. Q*n*-buAP having the highest interaction with the bacterial cell membranes showed the potent activity whereas QCybuAP, QMeCyprAP and Q*n*-buenAP with optimum membrane interactions resulted in optimum antibacterial activity. Q*n*-buynAP with the lowest membrane-active profiles displayed lower antibacterial activity against all the bacteria. However, Q*n*-buAP was found to be equally toxic to both bacteria as well as mammalian cells. QCybuAP, QMeCyprAP and Q*n*-buenAP showed optimum antibacterial activity and minimal mammalian toxicity resulting in selective antibacterial activity. Q*n*-buynAP was low toxic to bacteria and non-toxic to mammalian cells. It is known that a highly constrained cyclopropyl group can often mimic the properties of alkene and alkyne groups (π-character) and this may be the reason behind why the cyclopropyl derivatives show such similar activity profiles to the unsaturated derivatives. The present strategy of controlling the hydrophobicity significantly advances the understanding of how to direct the amphiphilic antibacterial polymers selectively to bacteria instead of mammalian cells.

4.3 Conclusions

In conclusion, a novel approach of tuning the hydrophobicity has been demonstrated by cyclization and unsaturation of side chains in amphiphilic polymers. It has been found that optimal hydrophobicity dependent on the side chain chemical structure of these polymers dictate the selective toxicity to bacteria. This control of hydrophobicity led to driving the selective interactions of amphiphilic polymers towards bacteria instead of mammalian cells thereby suggesting its influence on biological activity profiles. Such design of tunable hydrophobicity and diverse side chain structures can be used to tailor the functionality of amphiphilic polymers such as their molecular behavior and biological interactions.

4.4 Experimental section

4.4.1 Synthesis and characterization

The synthesis and characterization of the small molecules and polymers has been carried out as mentioned in the Chapter 2 and Chapter 3.

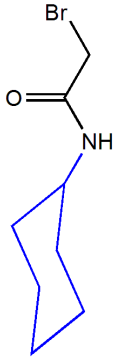

***N-(cyclohexyl)-1-bromoethanamide*:** FT-IR: 3250 cm^{-1} (amide N-H str.), 2950-2850 (C-H str.), 1680 cm^{-1} (Amide I, C=O str.), 1560 cm^{-1} (Amide II, N-H ben.), 1470-1410 cm^{-1} (C-C str.), 1290-1110 (C-O str.); ^{1}H-NMR (400 MHz, $CDCl_3$): δ/ppm 1.195 (m, cyCH_2, 2H), 1.383 (m, cyCH_2, 2H), 1.621 (m, cyCH_2, 2H), 1.721 (m, cyCH_2, 2H), 1.917 (m, cyCH_2, 2H), 3.761 (m, cyCH, 1H), 3.861 (s, -COCH_2Br, 2H), 6.475 (br s, amide –*NH*CO, 1H)); HR-MS: *m/z* 220.03 (observed): 220.03 (calculated for $[M + H]^+$).

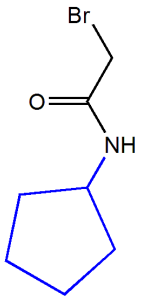

***N-(cyclopentyl)-1-bromoethanamide*:** FT-IR: 3250 cm^{-1} (amide N-H str.), 2950-2850 cm^{-1} (C-H str.), 1680 cm^{-1} (Amide I, C=O str.), 1560 cm^{-1} (Amide II, N-H ben.), 1470-1410 cm^{-1} (C-C str.), 1290-1110 cm^{-1} (C-O str.); ^{1}H-NMR (400 MHz, $CDCl_3$): δ/ppm 1.428 (m, cyCH_2, 2H), 1.657 (m, cy$(CH_2)_2$, 4H), 2.013 (m, cyCH_2, 2H), 3.856 (s, -COCH_2Br, 2H), 4.19 (m, cyCH, 1H), 6.385 (br s, amide –*NH*CO, 1H)); HR-MS: *m/z* 206.01 (observed): 206.01 (calculated for $[M + H]^+$).

***N-(cyclobutyl)-1-bromoethanamide*:** FT-IR: 3250 cm^{-1} (amide N-H str.), 2950-2850 cm^{-1} (C-H str.), 1680 cm^{-1} (Amide I, C=O str.), 1560 cm^{-1} (Amide II, N-H ben.), 1470-1410 cm^{-1} (C-C str.), 1290-1110 cm^{-1} (C-O str.); ^{1}H-NMR (400 MHz, $CDCl_3$): δ/ppm 1.747 (m, cyCH_2, 2H), 1.924 (m, cyCH_2, 2H), 2.357 (m, cyCH_2, 2H), 3.843 (s, -COCH_2Br, 2H), 4.373 (m, cyCH, 1H), 6.576 (br s, amide –NHCO, 1H)); HR-MS: *m/z* 192.00 (observed): 191.99 (calculated for $[M + H]^+$).

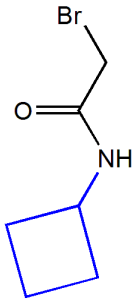

***N-(iso-butyl)-1-bromoethanamide*:** FT-IR: 3250 cm^{-1} (amide N-H str.), 2950-2850 cm^{-1} (C-H str.), 1680 cm^{-1} (Amide I, C=O str.), 1560 cm^{-1} (Amide II, N-H ben.), 1470-1410 cm^{-1} (C-C str.), 1290-1110 cm^{-1} (C-O str.); ^{1}H-NMR (400 MHz, $CDCl_3$): δ/ppm 0.929 (d, terminal -$(CH_3)_2$, 6H), 1.813 (m, -$CH_2CH(CH_3)_2$, 1H), 3.113 (d, -CH_2CH$(CH_3)_2$, 2H), 3.887 (s, -COCH_2Br, 2H), 6.475 (br s, amide –NHCO, 1H)); HR-MS: *m/z* 194.02 (observed): 194.01 (calculated for $[M + H]^+$).

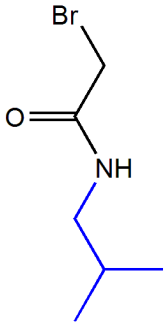

***N-((S)-(+)-sec-butyl)-1-bromoethanamide*:** FT-IR: 3250 cm^{-1} (amide N-H str.), 2950-2850 cm^{-1} (C-H str.), 1680 cm^{-1} (Amide I, C=O str.), 1560 cm^{-1} (Amide II, N-H ben.), 1470-1410 cm^{-1} (C-C str.), 1290-1110 cm^{-1} (C-O str.); ^{1}H-NMR (400 MHz, $CDCl_3$): δ/ppm 0.921 (t, -CHCH$_2CH_3$, 3H), 1.162 (d, -CH_2CHCH_3, 3H), 1.511 (m, -CHCH_2CH$_3$, 2H), 3.905 (m, -CHCH$_2$CH$_3$, 1H), 3.869 (s, -COCH_2Br, 2H), 6.475 (br s, amide –NHCO, 1H)); HR-MS: *m/z* 194.01 (observed): 194.01 (calculated for $[M + H]^+$).

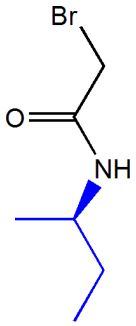

***N-((R)-(-)-sec-butyl)-1-bromoethanamide*:** FT-IR: 3250 cm^{-1} (amide N-H str.), 2950-2850 cm^{-1} (C-H str.), 1680 cm^{-1} (Amide I, C=O str.), 1560 cm^{-1} (Amide II, N-H ben.), 1470-1410 cm^{-1} (C-C str.), 1290-1110 cm^{-1} (C-O str.); ^{1}H-NMR (400 MHz, $CDCl_3$): δ/ppm 0.921 (t, -CHCH$_2CH_3$, 3H), 1.162 (d, -CH_2CHCH_3, 3H), 1.511 (m, -CHCH_2CH$_3$, 2H), 3.869 (s, -COCH_2Br, 2H), 3.905 (m, -CHCH$_2$CH$_3$, 1H), 6.475 (br s, amide –NHCO, 1H)); HR-MS: *m/z* 194.01 (observed): 194.01 (calculated for $[M + H]^+$).

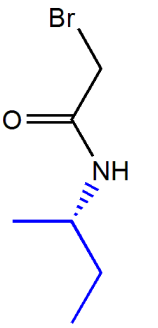

***N-(t-butyl)-1-bromoethanamide*:** FT-IR: 3250 cm^{-1} (amide N-H str.), 2950-2850 cm^{-1} (C-H str.), 1680 cm^{-1} (Amide I, C=O str.), 1560 cm^{-1} (Amide II, N-H ben.), 1470-1410 cm^{-1} (C-C str.), 1290-1110 cm^{-1} (C-O str.); ^{1}H-NMR (400 MHz, $CDCl_3$): δ/ppm 1.3 (s, terminal -C$(CH_3)_3$, 9H), 3.845 (s, -COCH_2Br, 2H), 6.475 (br s, amide –*NH*CO, 1H)); HR-MS: *m/z* 194.02 (observed): 194.01 (calculated for $[M + H]^+$).

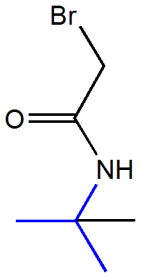

***N-(methylcyclopropyl)-1-bromoethanamide*:** FT-IR: 3250 cm^{-1} (amide N-H str.), 2950-2850 cm^{-1} (C-H str.), 1680 cm^{-1} (Amide I, C=O str.), 1560 cm^{-1} (Amide II, N-H ben.), 1470-1410 cm^{-1} (C-C str.), 1290-1110 cm^{-1} (C-O str.); ^{1}H-NMR (400 MHz, $CDCl_3$): δ/ppm 0.236 (m, cyCH_2, 2H), 0.547 (m, cyCH_2, 2H), 0.986 (m, cy*CH*, 1H), 3.155 (dd, -CH_2CH$(CH_2)_2$, 2H), 3.891 (s, -COCH_2Br, 2H), 6.576 (br s, amide –*NH*CO, 1H)); HR-MS: *m/z* 192.00 (observed): 191.99 (calculated for $[M + H]^+$).

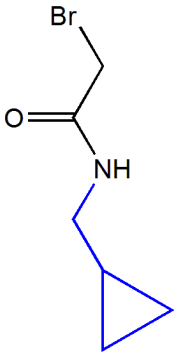

***N-(cyclopropyl)-1-bromoethanamide*:** FT-IR: 3250 cm^{-1} (amide N-H str.), 2950-2850 cm^{-1} (C-H str.), 1680 cm^{-1} (Amide I, C=O str.), 1560 cm^{-1} (Amide II, N-H ben.), 1470-1410 cm^{-1} (C-C str.), 1290-1110 cm^{-1} (C-O str.); ^{1}H-NMR (400 MHz, $CDCl_3$): δ/ppm 0.565 (m, cyCH_2, 2H), 0.822 (m, cyCH_2, 2H), 2.734 (m, cy*CH*, 1H), 3.8 (s, -COCH_2Br, 2H), 6.475 (br s, amide –*NH*CO, 1H)); HR-MS: *m/z* 177.98 (observed): 177.98 (calculated for $[M + H]^+$).

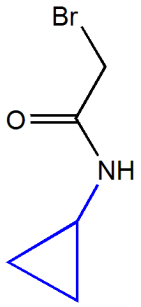

***N-(but-3-enyl)-1-bromoethanamide*:** FT-IR: 3250 cm^{-1} (amide N-H str.), 3049 cm^{-1} (C-H str.), 1680 cm^{-1} (Amide I, C=O str.), 1642 cm^{-1} (C=C str.), 1560 cm^{-1} (Amide II, N-H ben.), 1470-1410 cm^{-1} (C-C str.), 1290-1110 cm^{-1} (C-O str.); ^{1}H-NMR (400 MHz, $CDCl_3$): δ/ppm 2.3 (m, -CONHCH$_2$$CH_2$-, 2H), 3.2 (t, -CONH$CH_2CH_2$-, 2H), 3.8 (s, -CO$CH_2$Br, 2H), 5.138 (dq, CH_2CH_2CH=CH_2, J_{cis} = 10.52 Hz, 1H), 5.192 (dq, CH_2CH_2CH=CH_2, J_{trans} = 17.27 Hz, 1H), 5.85 (m, CH_2CH_2CH=CH_2, 1H), 6.475 (br s, amide –*NH*CO, 1H) ; HR-MS: *m/z* 190.98 (observed); 190.99 (calculated for $[M + H]^+$).

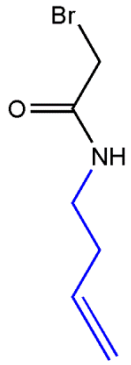

***N-(but-3-ynyl)-1-bromoethanamide*:** FT-IR: 3250 cm^{-1} (amide N-H str.), 3310 cm^{-1} (≡C-H str.), 2857-2942 cm^{-1} (-C-H str.), 2119 cm^{-1} (C≡C str.), 1680 cm^{-1} (Amide I, C=O str.), 1642 cm^{-1} (C=C str.), 1560 cm^{-1} (Amide II, N-H ben.), 1470-1410 cm^{-1} (C-C str.), 1290-1110 cm^{-1} (C-O str.); ^{1}H-NMR (400 MHz, $CDCl_3$): δ/ppm 1.82 (t, -$CH_2C{\equiv}CH$, 1H), 2.29 (m, -$CONHCH_2CH_2$-, 2H), 3.37 (t, -$CONHCH_2CH_2$-, 2H), 3.8 (s, -$COCH_2Br$, 2H), 6.475 (br s, amide –*NH*CO, 1H)); HR-MS: *m/z* 188.98 (observed); 188.97 (calculated for $[M + H]^+$).

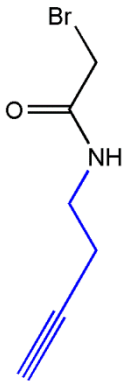

QCyhexAP: FT-IR: 3250 cm^{-1} (amide N-H str.), 2950-2850 cm^{-1} (C-H str.), 1767 cm^{-1} (imide C=O asym. str.), 1696 cm^{-1} (imide C=O sym. str.) 1680 cm^{-1} (amide I, C=O str.), 1560 cm^{-1} (Amide II, N-H ben.), 1470-1410 cm^{-1} (C-C str.), 1290-1110 cm^{-1} (C-O str.); ^{1}H-NMR (400 MHz, D_2O): δ/ppm 0.95–1.2 (br, $CH_2C(CH_3)_2$, 6H), 1.19 (br, cyCH_2, 2H), 1.38 (br, cyCH_2, 2H), 1.62 (br, cyCH_2, 2H), 1.7 (br, $CH_2C(CH_3)_2$, 2H), 1.72 (br, cyCH_2, 2H), 1.82 (br, cyCH_2, 2H), 2.0 (br, $NCH_2CH_2CH_2N(CH_3)_2$, 2H), 2.7–3.1 (br, *CHCH*, 2H), 3.1-3.3 (br, $NCH_2CH_2CH_2N(CH_3)_2$, 6H), 3.5 (br, $NCH_2CH_2CH_2N(CH_3)_2$, 2H), 3.6 (br, $NCH_2CH_2CH_2N(CH_3)_2$, 2H), 3.6 (br, -$N(CH_3)_2CH_2CO$, 2H), 4.04 (br, cy*CH*, 1H).

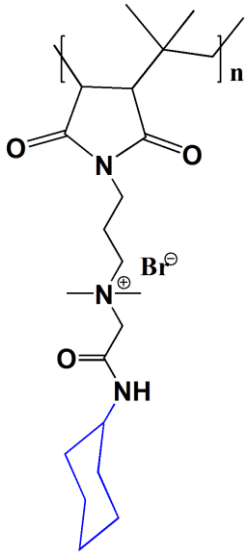

QCypenAP: FT-IR: 3250 cm^{-1} (amide N-H str.), 2950-2850 cm^{-1} (C-H str.), 1767 cm^{-1} (imide C=O asym. str.), 1696 cm^{-1} (imide C=O sym. str.) 1680 cm^{-1} (amide I, C=O str.), 1560 cm^{-1} (Amide II, N-H ben.), 1470-1410 cm^{-1} (C-C str.), 1290-1110 cm^{-1} (C-O str.); ^{1}H-NMR (400 MHz, D_2O): δ/ppm 0.95–1.2 (br, $CH_2C(CH_3)_2$, 6H), 1.43 (br, cyCH_2, 2H), 1.66 (br, cy$(CH_2)_2$, 4H), 1.7 (br, $CH_2C(CH_3)_2$, 2H), 1.98 (br, cyCH_2, 2H), 2.1 (br, $NCH_2CH_2CH_2N(CH_3)_2$, 2H), 2.7–3.1 (br, *CHCH*, 2H), 3.1-3.3 (br, $NCH_2CH_2CH_2N(CH_3)_2$, 6H), 3.5 (br, $NCH_2CH_2CH_2N(CH_3)_2$, 2H), 3.6 (br, $NCH_2CH_2CH_2N(CH_3)_2$, 2H), 4.13 (br, -$N(CH_3)_2CH_2CO$, 2H), 4.13 (m, cy*CH*, 1H).

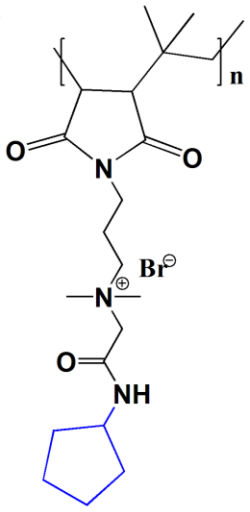

QCybuAP: FT-IR: 3250 cm^{-1} (amide N-H str.), 2950-2850 cm^{-1} (C-H str.), 1767 cm^{-1} (imide C=O asym. str.), 1696 cm^{-1} (imide C=O sym. str.) 1680 cm^{-1} (amide I, C=O str.), 1560 cm^{-1} (Amide II, N-H ben.), 1470-1410 cm^{-1} (C-C str.), 1290-1110 cm^{-1} (C-O str.); ^{1}H-NMR (400 MHz, D_2O): δ/ppm 0.92–1.4 (br, $CH_2C(CH_3)_2$, 6H), 1.7 (br, -$CH_2C(CH_3)_2$, 2H), 1.77 (br, cyCH_2, 2H), 2.0 (br, cyCH_2, 2H), 2.1 (br, $NCH_2CH_2CH_2N(CH_3)_2$, 2H), 2.29 (br, -$CH(CH_2)_3$, 2H), 2.8–3.2 (br, *CHCH*, 2H), 3.2-3.4 (br, $NCH_2CH_2CH_2N(CH_3)_2$, 6H), 3.6 (br, $NCH_2CH_2CH_2N(CH_3)_2$, 2H), 3.6 (br, $NCH_2CH_2CH_2N(CH_3)_2$, 2H), 4.06 (br, -$N(CH_3)_2CH_2CO$, 2H), 4.24 (br, cy*CH*, 1H).

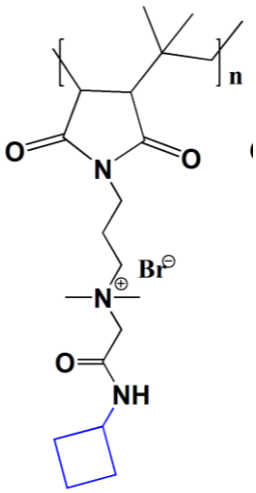

QMeCyprAP: FT-IR: 3250 cm^{-1} (amide N-H str.), 2950-2850 cm^{-1} (C-H str.), 1767 cm^{-1} (imide C=O asym. str.), 1696 cm^{-1} (imide C=O sym. str.) 1680 cm^{-1} (amide I, C=O str.), 1560 cm^{-1} (Amide II, N-H ben.), 1470-1410 cm^{-1} (C-C str.), 1290-1110 cm^{-1} (C-O str.); ^{1}H-NMR (400 MHz, D_2O): δ/ppm 0.236 (br, cyCH_2, 2H), 0.547 (br, cyCH_2, 2H), 0.986 (br, cy*CH*, 1H), 0.92–1.4 (br, $CH_2C(CH_3)_2$, 6H), 1.7 (br, $CH_2C(CH_3)_2$, 2H), 2.1 (br, $NCH_2CH_2CH_2N(CH_3)_2$, 2H), 2.8–3.2 (br, *CHCH*, 2H), 3.1 (br, -$CH_2CH(CH_2)_2$, 2H), 3.2-3.4 (br, $NCH_2CH_2CH_2N(CH_3)_2$, 6H), 3.6 (br, $NCH_2CH_2CH_2N(CH_3)_2$, 2H), 3.6 (br, $NCH_2CH_2CH_2N(CH_3)_2$, 2H), 4.06 (br, -$N(CH_3)_2CH_2CO$, 2H).

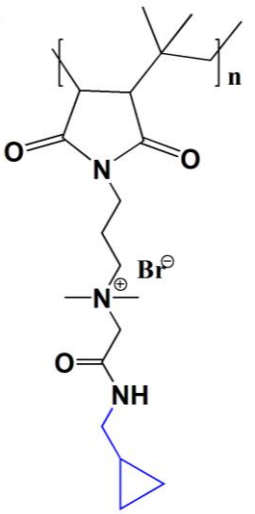

QCyprAP: FT-IR: 3250 cm^{-1} (amide N-H str.), 2950-2850 cm^{-1} (C-H str.), 1767 cm^{-1} (imide C=O asym. str.), 1696 cm^{-1} (imide C=O sym. str.) 1680 cm^{-1} (amide I, C=O str.), 1560 cm^{-1} (Amide II, N-H ben.), 1470-1410 cm^{-1} (C-C str.), 1290-1110 cm^{-1} (C-O str.); ^{1}H-NMR (400 MHz, D_2O): δ/ppm 0.64 (br, cyCH_2, 2H), 0.86(br, cyCH_2, 2H), 0.92–1.4 (br, $CH_2C(CH_3)_2$, 6H), 1.7 (br, $CH_2C(CH_3)_2$, 2H), 2.1 (br, $NCH_2CH_2CH_2N(CH_3)_2$, 2H), 2.73 (m, cy*CH*, 1H), 2.8–3.2 (br, *CHCH*, 2H), 3.2-3.4 (br, $NCH_2CH_2CH_2N(CH_3)_2$, 6H), 3.6 (br, $NCH_2CH_2CH_2N(CH_3)_2$, 2H), 3.6 (br, $NCH_2CH_2CH_2N(CH_3)_2$, 2H), 4.1 (br, -$N(CH_3)_2CH_2CO$, 2H).

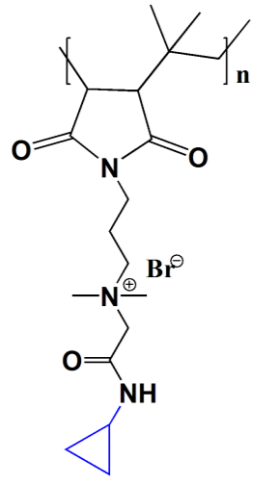

Q*iso*-buAP: FT-IR: 3250 cm^{-1} (amide N-H str.), 2950-2850 cm^{-1} (C-H str.), 1767 cm^{-1} (imide C=O asym. str.), 1696 cm^{-1} (imide C=O sym. str.) 1680 cm^{-1} (amide I, C=O str.), 1560 cm^{-1} (Amide II, N-H ben.), 1470-1410 cm^{-1} (C-C str.), 1290-1110 cm^{-1} (C-O str.); ^{1}H-NMR (400 MHz, D_2O): δ/ppm 0.92 (br, terminal -$(CH_3)_2$, 6H), 0.96–1.38 (br, $CH_2C(CH_3)_2$, 6H), 1.7 (br, $CH_2C(CH_3)_2$, 2H), 1.82 (br, $-CH_2CH(CH_3)_2$, 1H), 2.1 (br, $NCH_2CH_2CH_2N(CH_3)_2$, 2H), 2.7–3.1 (br, *CHCH*, 2H), 3.13 (br, $-CH_2CH(CH_3)_2$, 2H), 3.2-3.4 (br, $NCH_2CH_2CH_2N(CH_3)_2$, 6H), 3.6 (br, $NCH_2CH_2CH_2N(CH_3)_2$, 2H), 3.6 (br, $NCH_2CH_2CH_2N(CH_3)_2$, 2H), 4.1 (br, $-N(CH_3)_2CH_2CO$, 2H).

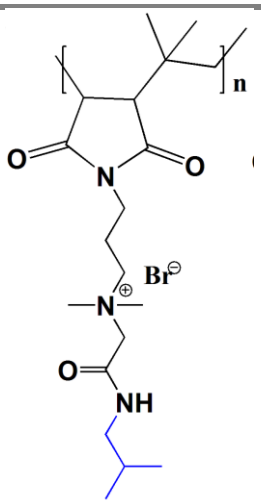

Q(S)-(+)-*s*-buAP: FT-IR: 3250 cm^{-1} (amide N-H str.), 2950-2850 cm^{-1} (C-H str.), 1767 cm^{-1} (imide C=O asym. str.), 1696 cm^{-1} (imide C=O sym. str.) 1680 cm^{-1} (amide I, C=O str.), 1560 cm^{-1} (Amide II, N-H ben.), 1470-1410 cm^{-1} (C-C str.), 1290-1110 cm^{-1} (C-O str.); ^{1}H-NMR (400 MHz, D_2O): δ/ppm 0.89 (br, $-CHCH_2CH_3$, 3H), 0.96–1.27 (br, $CH_2C(CH_3)_2$, 6H), 1.2 (br, $-CH_2CHCH_3$, 3H), 1.5 (br, $-CHCH_2CH_3$, 2H), 1.7 (br, $CH_2C(CH_3)_2$, 2H), 2.1 (br, $NCH_2CH_2CH_2N(CH_3)_2$, 2H), 2.7–3.1 (br, *CHCH*, 2H), 3.2-3.4 (br, $NCH_2CH_2CH_2N(CH_3)_2$, 6H), 3.6 (br, $NCH_2CH_2CH_2N(CH_3)_2$, 2H), 3.6 (br, $NCH_2CH_2CH_2N(CH_3)_2$, 2H), 3.8 (br, $-CHCH_2CH_3$, 1H), 4.09 (br, $-N(CH_3)_2CH_2CO$, 2H).

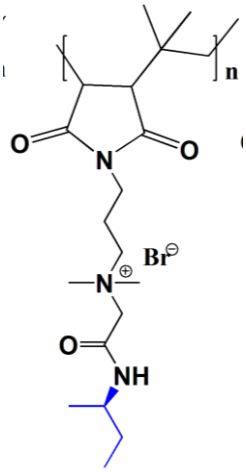

Q(R)-(-)-*s*-buAP: FT-IR: 3250 cm^{-1} (amide N-H str.), 2950-2850 cm^{-1} (C-H str.), 1767 cm^{-1} (imide C=O asym. str.), 1696 cm^{-1} (imide C=O sym. str.) 1680 cm^{-1} (amide I, C=O str.), 1560 cm^{-1} (Amide II, N-H ben.), 1470-1410 cm^{-1} (C-C str.), 1290-1110 cm^{-1} (C-O str.); ^{1}H-NMR (400 MHz, D_2O): δ/ppm 0.88 (br, $-CHCH_2CH_3$, 3H), 0.96–1.27 (br, $CH_2C(CH_3)_2$, 6H), 1.2 (br, $-CH_2CHCH_3$, 3H), 1.5 (br, $-CHCH_2CH_3$, 2H), 1.7 (br, $CH_2C(CH_3)_2$, 2H), 2.1 (br, $NCH_2CH_2CH_2N(CH_3)_2$, 2H), 2.7–3.1 (br, *CHCH*, 2H), 3.2-3.4 (br, $NCH_2CH_2CH_2N(CH_3)_2$, 6H), 3.6 (br, $NCH_2CH_2CH_2N(CH_3)_2$, 2H), 3.6

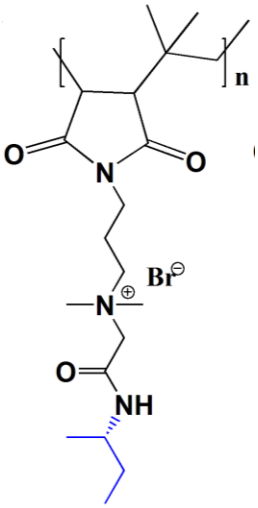

(br, N*CH*$_2$CH$_2$CH$_2$N(CH$_3$)$_2$, 2H), 3.8 (br, -*CH*CH$_2$CH$_3$, 1H), 4.09 (br, -N(CH$_3$)$_2$*CH*$_2$CO, 2H).

Q*t*-buAP: FT-IR: 3250 cm^{-1} (amide N-H str.), 2950-2850 cm^{-1} (C-H str.), 1767 cm^{-1} (imide C=O asym. str.), 1696 cm^{-1} (imide C=O sym. str.), 1680 cm^{-1} (amide I, C=O str.), 1560 cm^{-1} (Amide II, N-H ben.), 1470-1410 cm^{-1} (C-C str.), 1290-1110 cm^{-1} (C-O str.); ^{1}H-NMR (400 MHz, D$_2$O): δ/ppm 0.96–1.27 (br, CH$_2$C*(CH$_3$)$_2$*, 6H), 1.35 (br, terminal -C*(CH$_3$)$_3$*, 9H), 1.7 (br, *CH*$_2$C(CH$_3$)$_2$, 2H), 2.1 (br, NCH$_2$*CH*$_2$CH$_2$N(CH$_3$)$_2$, 2H), 2.7–3.1 (br, *CHCH*, 2H), 3.2-3.4 (br, NCH$_2$CH$_2$CH$_2$N*(CH$_3$)$_2$*, 6H), 3.6 (br, NCH$_2$CH$_2$*CH*$_2$N(CH$_3$)$_2$, 2H), 3.6 (br, N*CH*$_2$CH$_2$CH$_2$N(CH$_3$)$_2$, 2H), 3.98 (br, -N(CH$_3$)$_2$*CH*$_2$CO, 2H).

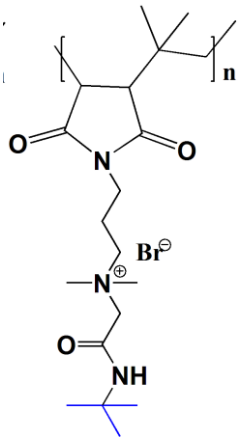

Q*n*-buenAP: FT-IR: 3250 cm^{-1} (amide N-H str.), 3049 cm^{-1} (C-H str.), 1767 cm^{-1} (imide C=O asym. str.), 1696 cm^{-1} (imide C=O sym. str.),1680 cm^{-1} (Amide I, C=O str.), 1642 cm^{-1} (C=C str.), 1560 cm^{-1} (Amide II, N-H ben.), 1470-1410 cm^{-1} (C-C str.), 1290-1110 cm^{-1} (C-O str.); ^{1}H-NMR (400 MHz, D$_2$O): δ/ppm 0.96–1.27 (br, CH$_2$C*(CH$_3$)$_2$*, 6H), 1.7 (br, *CH*$_2$C(CH$_3$)$_2$, 2H), 2.0 (br, NCH$_2$*CH*$_2$CH$_2$N(CH$_3$)$_2$, 2H), 2.3 (br, -CONHCH$_2$*CH*$_2$-, 2H), 2.7–3.1 (br, *CHCH*, 2H), 3.29 (br, NCH$_2$CH$_2$CH$_2$N*(CH$_3$)$_2$*, 6H), 3.35 (br, -CONH*CH*$_2$CH$_2$-, 2H), 3.6 (br, NCH$_2$CH$_2$*CH*$_2$N(CH$_3$)$_2$, 2H), 3.6 (br, N*CH*$_2$CH$_2$CH$_2$N(CH$_3$)$_2$, 2H), 4.10 (br, -N(CH$_3$)$_2$*CH*$_2$CO, 2H), 5.17 (br, CH$_2$CH$_2$CH=*CH*$_2$, 2H), 5.85 (m, CH$_2$CH$_2$*CH*=CH$_2$, 1H).

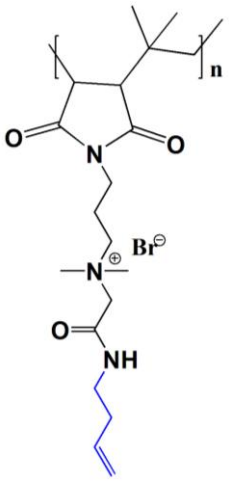

Q*n*-buynAP: FT-IR: 3250 cm^{-1} (amide N-H str.), 3310 cm^{-1} (≡C-H str.), 2857-2942 cm^{-1} (-C-H str.), 2119 cm^{-1} (C≡C str.), 1767 cm^{-1} (imide C=O asym. str.), 1696 cm^{-1} (imide C=O sym. str.), 1680 cm^{-1} (Amide I, C=O str.), 1642 cm^{-1} (C=C str.), 1560 cm^{-1} (Amide II, N-H ben.), 1470-1410 cm^{-1} (C-C str.), 1290-1110 cm^{-1} (C-O str.); ^{1}H-NMR (400 MHz, D$_2$O): δ/ppm 0.96–1.27 (br, CH$_2$C*(CH$_3$)$_2$*, 6H), 1.7 (br, *CH*$_2$C(CH$_3$)$_2$, 2H), 1.82 (br, -CH$_2$C≡*CH*, 1H), 2.1 (br, NCH$_2$*CH*$_2$CH$_2$N(CH$_3$)$_2$, 2H), 2.29 (br, -CONHCH$_2$*CH*$_2$-, 2H),

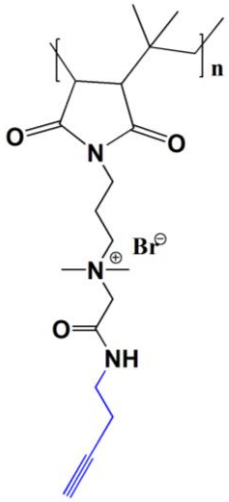

2.7–3.1 (br, *CHCH*, 2H), 3.2-3.4 (br, $NCH_2CH_2CH_2N(CH_3)_2$, 6H), 3.37 (br, -$CONHCH_2CH_2$-, 2H), 3.6 (br, $NCH_2CH_2CH_2N(CH_3)_2$, 2H), 3.6 (br, $NCH_2CH_2CH_2N(CH_3)_2$, 2H), 4.16 (br, -$N(CH_3)_2CH_2CO$, 2H).

4.4.2 *In-vitro* mammalian cell toxicity

CytoTox 96 Non-Radioactive Cytotoxicity Assay (Promega) kit was used for determining the cytotoxicity of the compounds. In brief, HEK293 cells that were maintained in complete DMEM media (Gibco) supplemented with 10% FBS (Gibco) and Penicillin-Streptomycin solution (Gibco) were seeded in 96 well plates at a concentration of 10^4 cells/well. They were allowed to adhere to the plate overnight. 0.5% Triton-X and media were used as positive and untreated controls respectively. The cells were treated with respective test compound solutions. After 24 hrs of treatment, the plates were centrifuged at 1100 rpm for 5 min. The supernatants from respective wells were transferred and the assay was performed according to the manufacturer's instructions. 100 µL of the supernatant was then transferred to a fresh micro titer plate and absorbance at 490 nm was measured using a Tecan InfinitePro series M200 Micro plate Reader. Percentage of cell death was determined as $(A - A_0)/ (A_{total} - A_0) \times 100$, where A is the absorbance of the test well, A_0 the absorbance of the negative controls, and A_{total} the absorbance of triton-X treated wells, all at 490 nm. Percentage of LDH release was plotted as a function of polymer concentration and the IC_{50} was defined as the polymer concentration, which causes 50% LDH release relative to the positive control. In some cases, LDH release did not reach 50% up to the highest polymer concentration tested and IC_{50} was not determined.

4.4.3 Reverse-phase high performance liquid chromatography (RP-HPLC)

Chromatographic profiles were analyzed by reverse phase HPLC using 0.1% trifluoroacetic acid (TFA) in water/acetonitrile (0−100%) as mobile phase. HPLC analysis was performed on a Shimadzu-LC 8 Å liquid chromatography instrument (C18 column, 10 mm diameter, 250 mm length) with UV detector monitoring at 220 nm. The data was acquired from 0-40 min.

Chapter 5

Amide Side Chain Amphiphilic Polymers Target Bacterial Biofilms

Abstract

Bacterial biofilms accounting for 65-80% of infections in humans place a massive burden on healthcare systems worldwide due to their persistence and chronic nature. Conventional antibiotics are inherently ineffective against biofilms due to various reasons such as slow or non-dividing cells, diffusion barriers and genetic mutations. Targeting the bacterial cell membrane is promising for the eradication of biofilms and also for the elimination of bacterial persisters that constitute biofilms. In this chapter, cationic-amphiphilic polymers have been shown to eradicate surface established biofilms formed by multi-drug resistant Gram-negative bacteria. Moreover, these polymers kill slow or non-dividing stationary phase and persister bacteria including dispersed cells that release upon biofilm disruption. The membrane-active nature of these polymers was found to be the key of their anti-persister activity. More importantly, these polymers significantly ($p < 0.0001$) decrease the bacterial burden in mice with chronic A. baumannii burn wound infection. Bacteria develop rapid resistance to erythromycin and colistin whereas no detectable development of resistance occurs against these polymers even after several passages. These results suggest the potential use of these polymeric biomaterials in disinfecting biomedical device surfaces after the infection has become established and also for the topical treatment of chronic bacterial infections.

(1) Uppu, D. S. *et al.* Amide Side Chain Amphiphilic Polymers Disrupt Surface Established Bacterial Bio-films and Protect Mice from Chronic *Acinetobacter baumannii* Infection. *Biomaterials.* **2016**, *74*, 131.

(2) Uppu, D. S. *et al.* "Membrane-active Polymers Kill Bacterial Persisters and Potentiate Antibiotics to Biofilms". Manuscript under preparation.

5.1 Introduction

Chronic bacterial infections often encountered after antibiotic treatment is a major worry in health care [21]. Bacteria live in surface associated communities called bio-films that are the underlying cause behind chronic or persistent infections tolerant to antibiotic treatment and host immune system. Biofilms contain a concoction of bacteria and extracelluar polymeric substances (EPS) such as polysaccharides, proteins and extracellular DNA (eDNA). It has been found that nearly 99% of bacteria on earth live in bio-films that are associated with nearly 80% of all bacterial infections in humans[22,23]. Bio-film formation is found on both abiotic and biotic surfaces ranging from ship hulls to in-dwelling bio-medical devices. Bacteria colonize the surfaces of biomedical devices such as catheters, pace makers, orthopedic implants etc. leading to extra burden on health care costs. Also, bio-films are responsible for serious ailments like burn-wound infections, endocarditis, ventilator associated pneumonia (VAP), lung infections in cystic fibrosis (CF) and urinary tract infections (UTI)[20,37,38].

Conventional antibiotics are inherently ineffective against biofilms due to various reasons such as slow or non-dividing cells, diffusion barriers and genetic mutations[17,24,35]. Of late, it is reasoned that the presence of a small sub-population of survivors post antibiotic treatment, called as persisters play a major role in chronic infections as well as antibiotic resistance. Persisters with reduced metabolic activity exhibit antibiotic-tolerance because the bio-synthetic processes that are the targets for antibiotics are either inactive or corrupt in these cells[28-32,193]. Thus, the target-specific mode of action of antibiotics proved unsuccessful for the eradication of infections due to the presence of persisters. Hence, there exists a need for a new approach for developing anti-persister strategies which will be useful in targeting the root-cause of antibiotic resistance as well as recalcitrant infections. The bacterial cell membrane is a vital part of bacteria and is required for maintaining the viability in their active and metabolically inactive (dormant) state. This vital nature of bacterial cell membrane makes it an interesting target for developing anti-persister strategies[51]. Membrane-targeting compounds are also interesting due to their low tendency for bacterial resistance development.

Alternative anti-biofilm agents include the use of quorum sensing inhibitors [44], small molecules [194-196], metal nanoparticles [45, 197], combination approaches [46-48, 198], enzymes [24] and so on to inhibit or disrupt biofilm formation. A promising approach focuses on modifying the biomaterials used in medical devices to make them resistant to biofilm formation[37, 38]. However,

it is often difficult to sterilize the surface after the infection has become established due to the formation of biofilms. Antibacterial polymers with cationic charge and hydrophobicity offer a potential solution for targeting or disrupting biofilms. These cationic polymers might interact with the negatively charged EPS matrix leading to disruption of biofilms. Further, the membrane-active mode of action of these polymers might target slow or non-dividing as well as antibiotic tolerant bacteria in biofilms resulting in their eradication. Cationic charge of these polymers drive them towards the negatively charged lipid membrane of bacteria and the hydrophobicity further strengthens membrane disintegration. Their selective interaction with bacteria results from the fact that mammalian cell (for e.g. human erythrocyte) membranes generally contain higher proportion of zwitterionic lipids. Although a variety of antibacterial polymers has been reported, the ability of polymers to disrupt surface established biofims have been scarce. Melander *et al.* reported methacrylate polymers containing 2-aminoimidazle subunit that inhibit *A. baumannii* biofilm formation [199]. Hedrick and co-workers reported antimicrobial polymeric hydrogels that can disrupt bacterial and fungal biofilms[200, 201]. Gellman and his group showed that nylon-3 polymers can inhibit and disrupt fungal biofilms [202].

In this chapter, cationic-amphiphilic polymers have been shown to disrupt established *A. baumannii* biofilms on surfaces *in-vitro* and protect mice from chronic *A. baumannii* burn wound infections. These polymers were found to kill the slow or non-dividing stationary phase as well as persister bacteria. In addition, the membrane-active mechanism and ability to stall bacterial resistance have been reported.

5.2 Results and Discussion

5.2.1 Synthesis

Two optimized polymers, Q*n*-prAP and QCybuAP (Fig. 5.1) resulted from the structure-activity relationship studies from Chapter 4 were used for studies in this chapter.

5.2.2 Antibacterial activity against stationary phase and persister cells

The stationary phase bacteria represent slow-growing or non-dividing populations that are tolerant to antibiotic treatment. More important are the small sub-population of bacterial survivors exhibiting antibiotic-tolerance in the stationary phase cultures called as persister cells[32, 33]. Thus, the antibacterial efficacy of these polymers has been investigated against

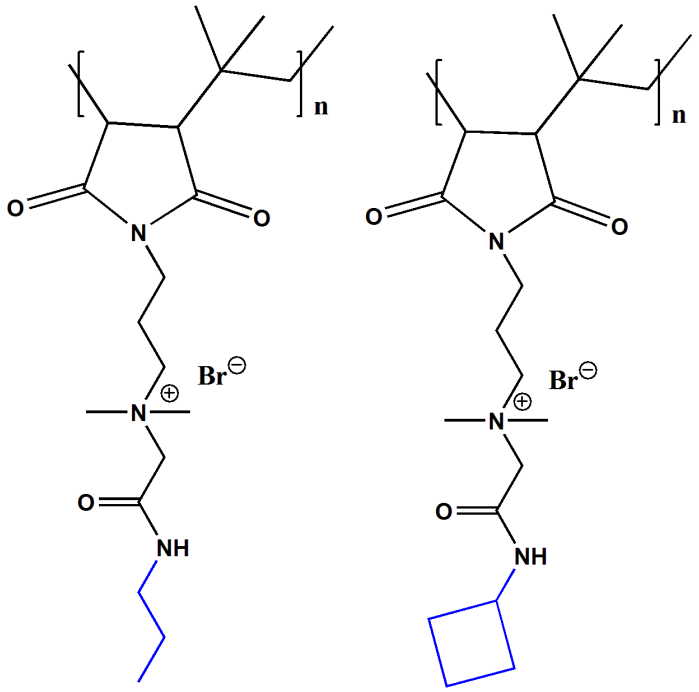

Q*n*-prAP **QCybuAP**

Figure 5.1: Chemical structures of amide side chain cationic-amphiphilic polymers.

stationary phase and persister cells. The antibacterial activity was evaluated by determining the reduction in bacterial counts of actively growing, stationary phase and persister cells after 2 h treatment in chemically defined media, M9 complete medium (*E. coli*) and minimal essential media (MEM) (*S. aureus*). QCybuAP showed concentration dependent reduction in bacterial counts against stationary phase *E. coli* with complete killing at 10 µg mL^{-1} (Fig. 5.2). On the other hand, antibiotics like ampicillin and kanamycin at 100 µg mL^{-1} and membrane active drug colistin even at 30 µg mL^{-1} did not result in any bactericidal activity against stationary phase *E. coli* cells (Fig. 5.2).

Persisters were isolated by treating the stationary phase cultures of *E. coli* and *S. aureus* with ampicillin as reported in literature[46,47]. The surviving persisters of *E. coli* and *S. aureus* were isolated and used for the activity studies. The cationic polymer, QCybuAP showed concentration dependent reduction in bacterial count with complete elimination of bacteria at 5 µg mL^{-1} whereas ampicillin (100 µg mL^{-1}), kanamycin (100 µg mL^{-1}) and colistin (even at 30 µg mL^{-1}) were devoid of any activity against *E. coli* persisters (Fig. 5.3 A & B). Q*n*-prAP also showed concentration dependent killing of *E. coli* persisters (Fig. 5.4). However, all the

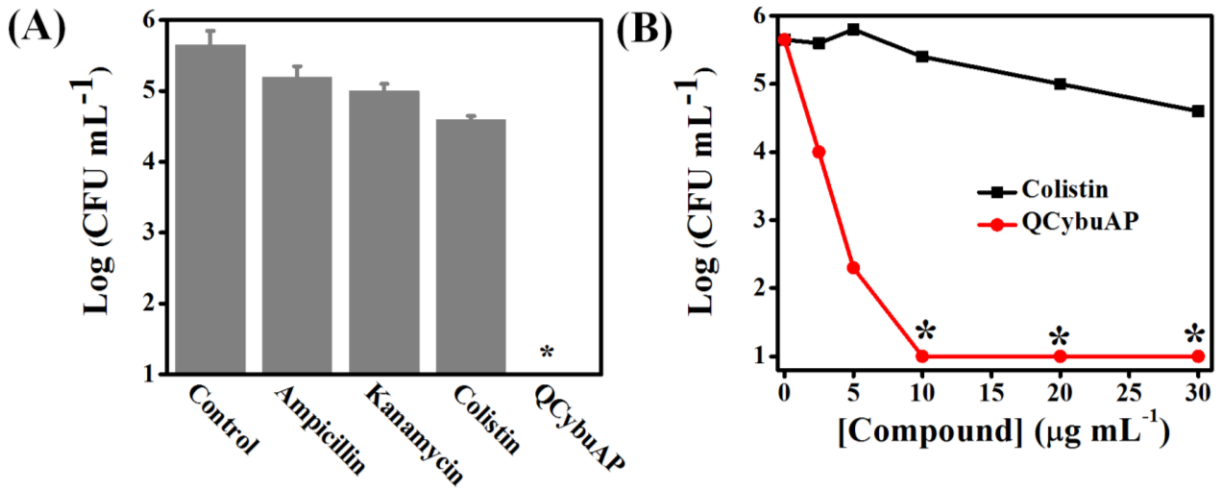

Figure 5.2: Antibacterial activity of antibiotics and cationic polymer (QCybuAP) against stationary phase cells of *E. coli*. (A) Ampicillin (100 µg mL^{-1}), kanamycin (100 µg mL^{-1}) and colistin (30 µg mL^{-1}) do not kill whereas QCybuAP (10 µg mL^{-1}) completely eliminates the bacteria. (B) Concentration dependent killing of stationary phase *E. coli* in presence of QCybuAP and colistin. Stars represent the limit of detection in the experiment (<50 CFU/mL).

antibiotics (ampicillin, kanamycin and colistin) and the cationic polymer, QCybuAP were highly effective against the actively growing cells of *E. coli* (Fig. 5.3 C & D) and *S. aureus* (Fig. 5.5 A). When tested against *S. aureus* persisters, QCybuAP was found to completely eradicate the bacteria at 2.5 µg mL^{-1} whereas ampicillin (20 µg mL^{-1}), kanamycin (20 µg mL^{-1}) and ciprofloxacin (5 µg mL^{-1}) had no reduction in bacterial counts when tested against *S. aureus* persisters (Fig. 5.5 B). These results suggest that the antibiotics are ineffective against the metabolically inactive persisters. Interestingly, colistin (Polymixin E), the Gram-negative membrane (LPS) targeting antibiotic was also ineffective against stationary phase and persister cells of *E. coli* at a concentration of 30 µg mL^{-1}[134]. Polymixin B was reported to have reduced activity (200-1500 fold increase in MIC) towards stationary phase *S. typhimirium*[203]. It was also reported that the stationary phase cells of *A. baumannii* have reduced surface charge and more hydrophobicity compared to wild-type cells that might contribute to the increased resistance towards colistin[204]. In contrast, the cationic polymer, QCybuAP displayed good activity against actively growing, stationary phase as well as the persister cells of Gram-positive and Gram-negative bacteria at low concentrations. This led us to probe the mechanism of antibacterial activity of this class of cationic polymer against persister cells.

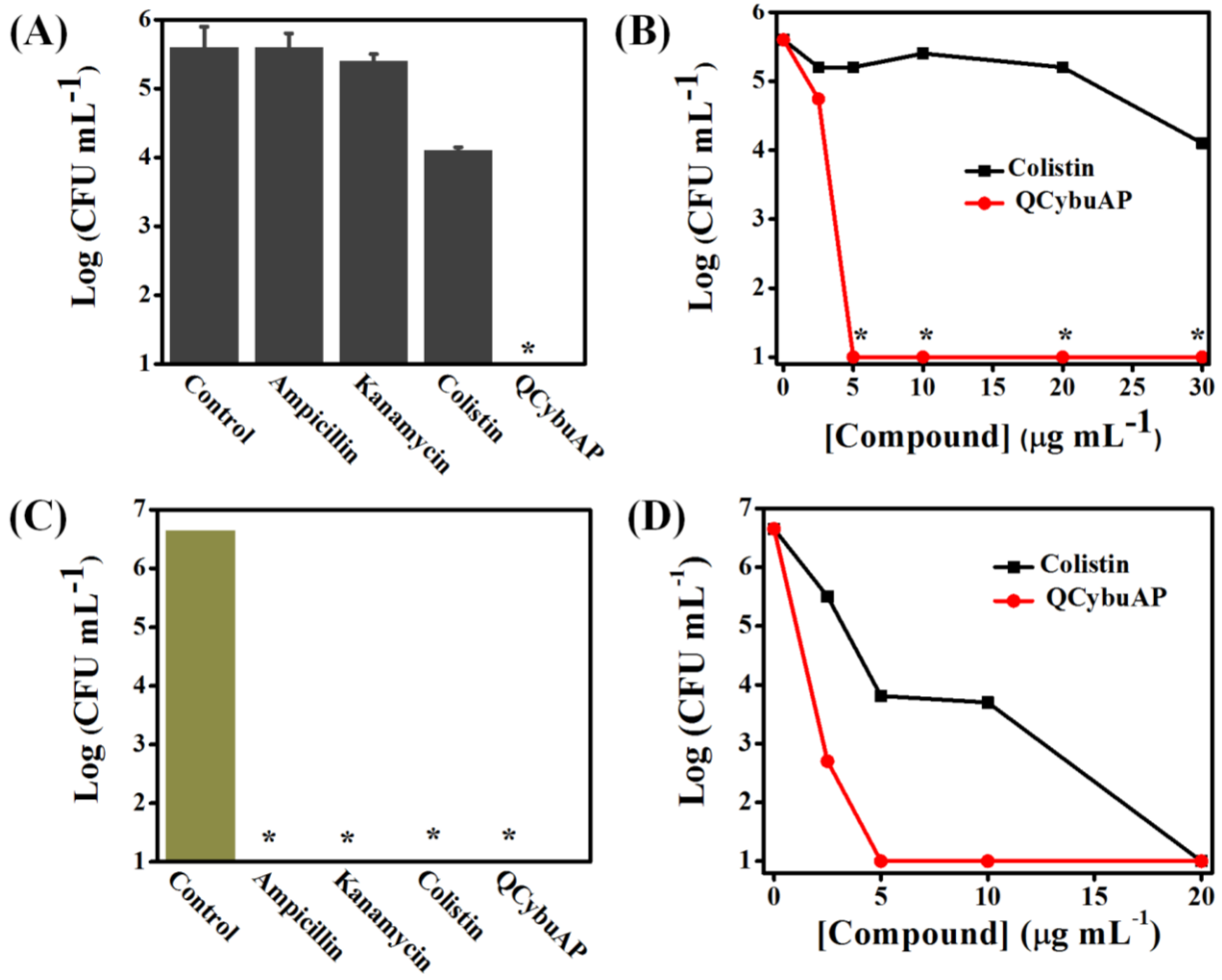

Figure 5.3: Antibacterial activity of antibiotics and cationic polymer (QCybuAP) against *E. coli* persister and actively growing cells after 2 h treatment. (A) Ampicillin (100 μg mL^{-1}), kanamycin (100 μg mL^{-1}) and colistin (30 μg mL^{-1}) do not kill whereas QCybuAP (5 μg mL^{-1}) completely eliminates *E. coli* persisters. (B) Concentration dependent killing of persister *E. coli* in presence of QCybuAP and colistin. (C) Against the actively growing cells of *E. coli*, Ampicillin (100 μg mL^{-1}), kanamycin (100 μg mL^{-1}), colistin (30 μg mL^{-1}) and QCybuAP (5 μg mL^{-1}) reduced the bacterial counts down to the detection limit. (D) Concentration dependent killing of active *E. coli* in presence of QCybuAP and colistin. Stars represent the limit of detection.

5.2.3 Mechanistic investigation against persister cells

The membrane-active properties of QCybuAP were determined by measuring the cytoplasmic membrane depolarization and permeabilization against *E. coli* and *S. aureus* persisters. QCybuAP showed concentration dependent dissipation of membrane potential against *E. coli* (Fig. 5.6 A) and *S. aureus* (Fig. 5.6 B) persisters. Even at 5 μg mL^{-1}, the concentration at which

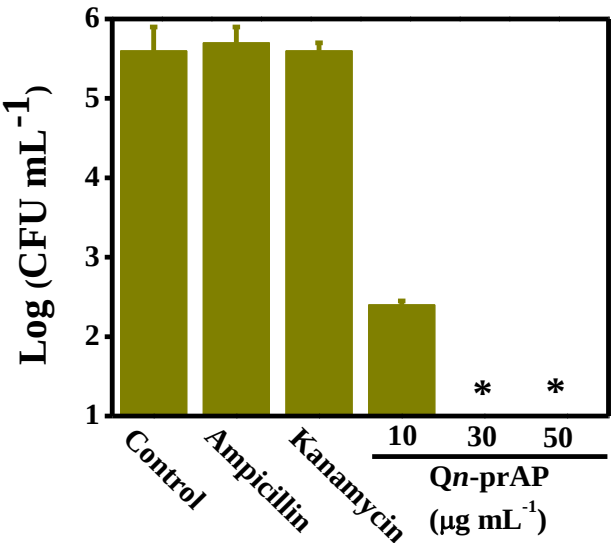

Figure 5.4: Antibacterial activity of antibiotics and cationic polymer (QCybuAP) against *E. coli* persister cells. (A) Ampicillin (100 μg mL^{-1}), kanamycin (100 μg mL^{-1}) do not kill whereas Q*n*-prAP shows concentration dependent (10 μg mL^{-1}, 30 μg mL^{-1} and 50 μg mL^{-1}) elimination of *E. coli* persisters. Stars represent the limit of detection.

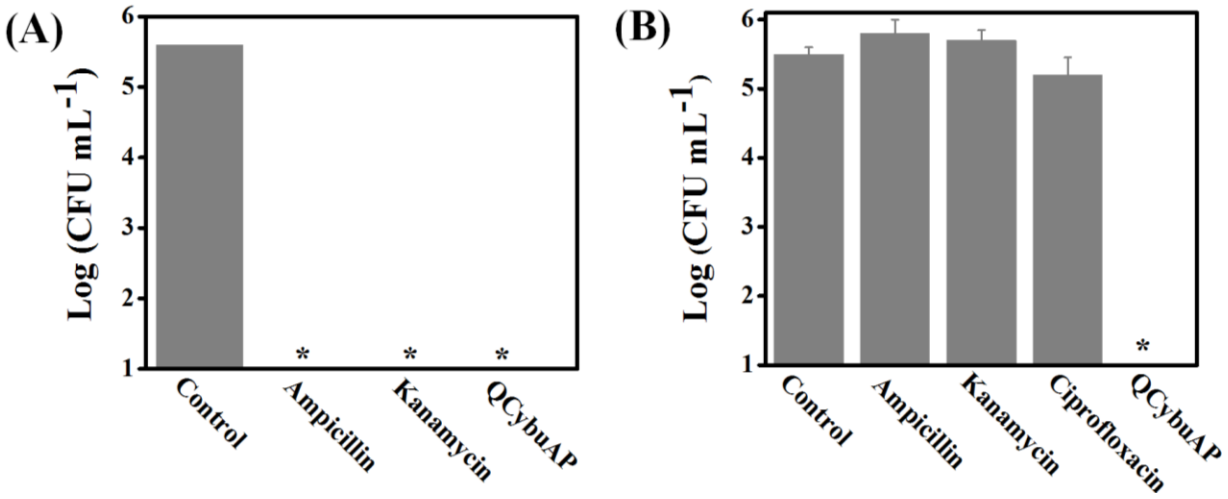

Figure 5.5: Antibacterial activity of antibiotics and cationic polymer (QCybuAP) against actively growing and persister *S. aureus*. (A) Ampicillin (20 μg mL^{-1}), kanamycin (20 μg mL^{-1}) and ciprofloxacin (5 μg mL^{-1}) are ineffective whereas QCybuAP (2.5 μg mL^{-1}) eradicates *S. aureus* persisters. (B) Ampicillin (20 μg mL^{-1}), kanamycin (20 μg mL^{-1}) and QCybuAP (2.5 μg mL^{-1}) eradicates actively growing cells down to the detection limit. Stars represent the limit of detection in the experiment (< 50 CFU/mL).

complete bacterial killing was observed; QCybuAP dissipated the membrane potential of both the bacterial persisters. QCybuAP collapsed the membrane potential even against the actively growing cells of *E. coli* and *S. aureus* as shown in Chapter 4. QCybuAP permeabilized the cell

membrane in concentration dependent manner against *E. coli* and *S. aureus* persisters as shown in Fig. 5.7 A & 5.7 B respectively. More importantly, both QCybuAP and colistin at 20 µg mL^{-1} showed equal extent of membrane permeabilization against actively growing cells of *E. coli* (Fig. 5.6 C). However, against persister *E. coli*, QCybuAP (20 µg mL^{-1}) retained the capability to permeabilize the membranes whereas colistin at the same concentration showed very low extent of membrane permeabilization (Fig. 5.6 D). QCybuAP (20 µg mL^{-1}) also showed membrane permeabilization against actively growing cells of *S. aureus* as shown in Chapter 4.

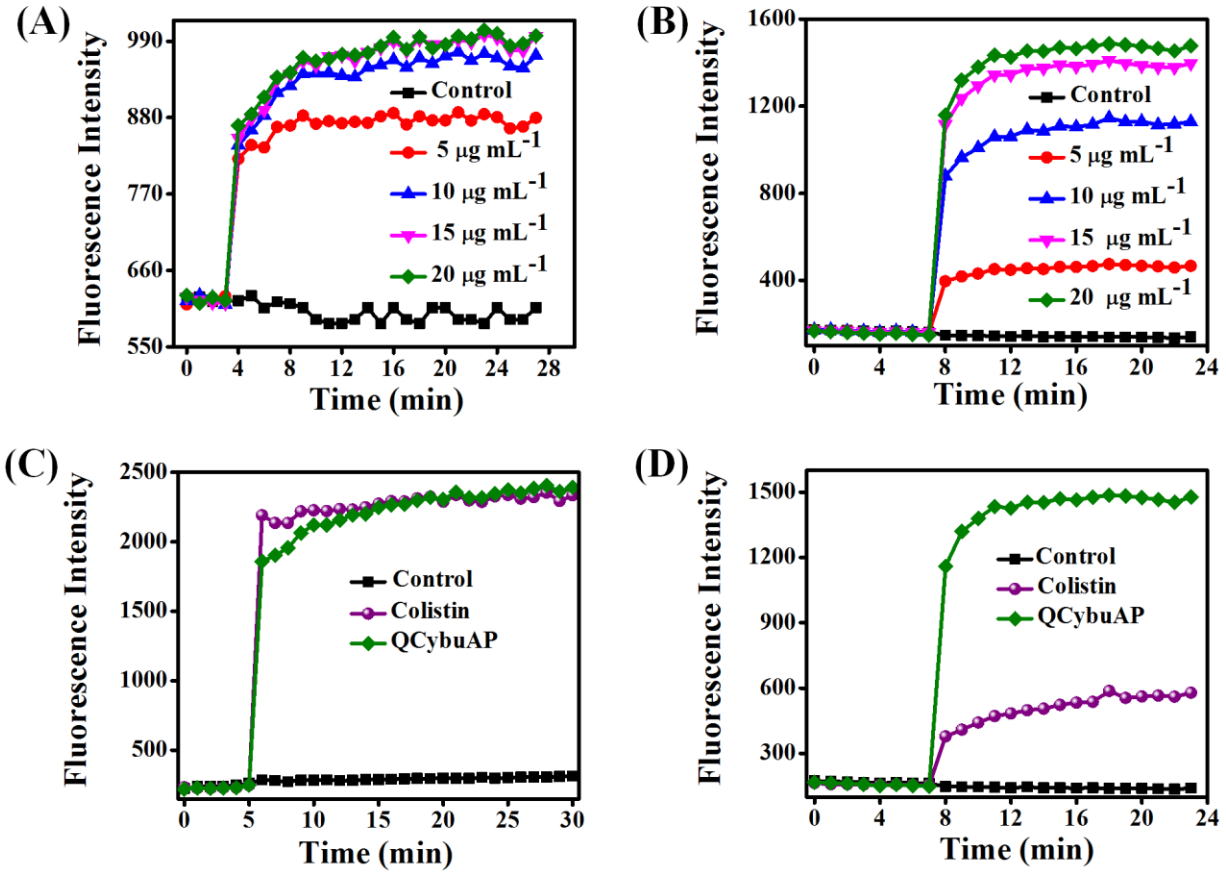

Figure 5.6: Membrane-active properties of QCybuAP against *E. coli*. (a) Concentration dependent increase of membrane depolarization and (b) membrane permeabilization against *E. coli* persisters. Numbers in the parenthesis represent the concentration in µg mL^{-1}; Membrane permeabilization against actively growing (c) and persister (d) *E. coli*. The concentrations used were 20 µg mL^{-1}.

These results suggested that antibiotics targeting the essential bio-synthetic processes in bacteria lose their efficacy in dormant persisters. More importantly, these observations showed that colistin being specific-membrane targeting antibiotic has reduced efficacy against stationary

phase and persister cells compared to actively growing cells. On the contrary, the cationic amphiphilic polymers reported here do not differentiate between the actively growing, stationary phase and persister bacteria and employ membrane-active mechanism of bacterial killing. Sugars [47, 205], basic amino acids[206], acyldepsipeptides[46] and bromofuranones (BF8)[207] have been reported to eradicate the persisters in combination with antibiotics whereas antibiotics such as oritavancin[208] and daptomycin[209] were found to kill the stationary phase cells. Trp/Arg containing AMPs [210], porphyrin derivatives[211], a single chemical compound (C10)[212] and a peptide-tobramycin conjugate (Pentobra)[49] have been demonstrated to eradicate persister cells. The present findings underscore the importance of non-specific targeting of cell membrane for the elimination of bacterial persisters which are the root-cause of antibiotic resistance as well as recalcitrant or chronic infections.

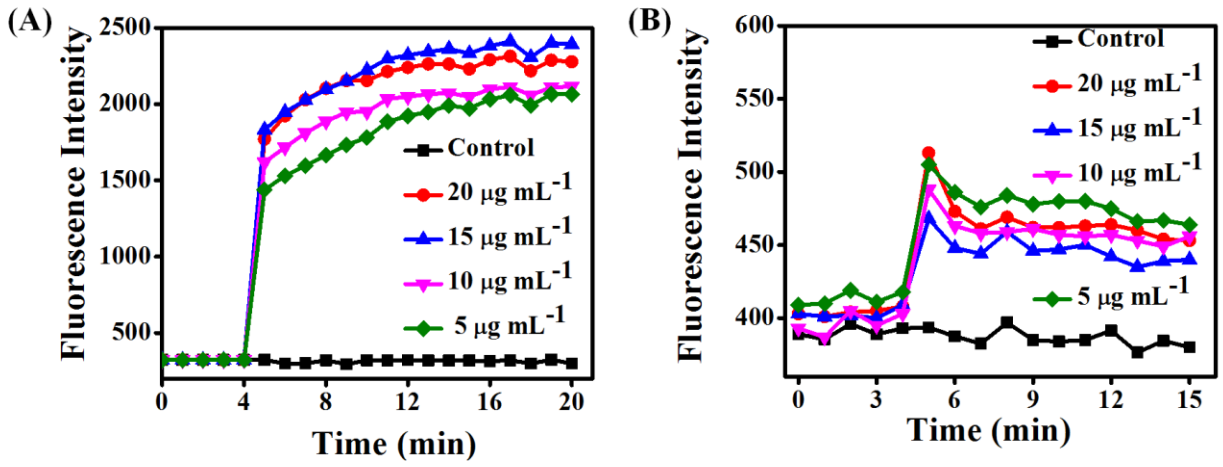

Figure 5.7: Concentration dependent Membrane depolarization (A) and Membrane permeabilization (B) of QCybuAP against *S. aureus* persisters.

5.2.4 Disperse and kill biofilms *in-vitro*

Biofilms contain a concoction of bacteria and extracellular matrix components such as polysaccharides, proteins and extracellular DNA[22]. Conventional antibiotics are ineffective against bacterial biofilms due to the presence of slow or non-growing cells (persisters), diffusion barriers and genetic mutations[24]. Persister formation in biofilms has been found to be favorable in the presence of stress responses like antibiotic treatment, oxidative stress, nutrient limitation and acidic environment (in macrophages)[33].

Mature *A. baumannii* MTCC 1425 and *A. baumannii* R674 (carbapenem resistant clinical isolate) bio-films grown on glass cover slips (for 48 h) were treated with QCybuAP, Q*n*-prAP, tobramycin, colistin and erythromycin (all at 30 μg mL^{-1}) for 24 h. Biofilms stained with 0.1% crystal violet were dissolved in 95% ethanol and absorbance was measured at 520 nm. The crystal violet staining evidently showed that both the polymers had higher disruption properties compared to erythromycin, tobramycin and colistin against both the strains (Fig. 5.8A). Tobramycin (114% and 116%) had increased biomass compared to the untreated control (100%) against both the strains supporting the observation that amino glycosides promote biofilm formation[213]. Colistin and erythromycin showed 30% and 43% reduction in biomass against *A. baumannii* MTCC 1425. Against *A. baumannii* R674, colistin reduced the biomass by 42% compared to the untreated control. Both the polymers, Q*n*-prAP and QCybuAP displayed reduction in biomass by 83% and 84% against *A. baumannii* MTCC 1425. Q*n*-prAP and QCybuAP reduced the biomass of antibiotic-resistant *A. baumannii* R674 biofilms to a great extent by 97% and 98% compared to the untreated biofilms.

Dispersed bacteria upon treatment of biofilms with antibiotics represent a dangerous pool of bacteria that cause more tissue damage and can revert to planktonic condition[214]. Importantly, all biofilm dispersal strategies will need to be accompanied by simultaneous antibiotic treatment to eliminate the planktonic bacterial cells that are liberated after dispersion in order to avoid the spread of infection to other parts of the body[24]. The optical density ($O.D._{600}$) of the bacteria that has got dispersed from the *A. baumannii* biofilms and reverted to the planktonic stage during the 24 h treatment has been measured in the well plates with antibacterial agents (Fig. 5.8 B). Interestingly, colistin, tobramycin, erythromycin and polymers did not allow the growth of planktonic bacteria in the well plates during the 24 h treatment against sensitive strain of *A. baumannii* (MTCC 1425). However, the similar investigations done for biofilms grown from clinical isolate strain of *A. baumannii* R674 showed that the antibiotics did not prevent the growth of planktonic bacteria. Colistin despite being sensitive to *A. baumannii* R674 did not arrest the planktonic growth. On the contrary, in the presence of both Q*n*-prAP and QCybuAP, no planktonic growth of bacteria in the suspending medium was observed in case of both sensitive *A. baumannii* and clinical isolate strains. These results led to the understanding that unlike antibiotics the membrane-active polymers not only disrupted the biofilms but also arrested the planktonic growth of dispersed bacteria from the biofilms.

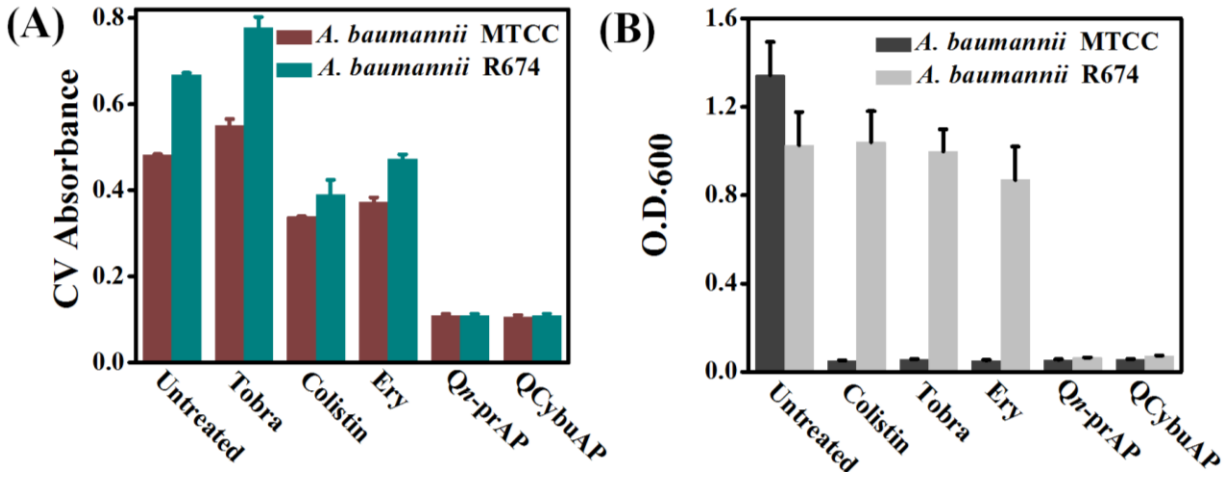

Figure 5.8: Disruption of *A. baumannii* bio-films. (A) Absorbance of the Crystal violet (CV) staining of the bio-films grown on glass cover slips in presence of colistin (30 µg mL^{-1}), Q*n*-prAP and QCybuAP (both at 30 µg mL^{-1}), erythromycin (Ery, 30 µg mL^{-1}), tobramycin (Tobra, 30 µg mL^{-1}). (B) $O.D._{600}$ of the planktonic growth of bacteria due to dispersed cells from the surface established biofilms. Both (A) and (B) correspond to 24 h treated or untreated conditions. *A. baumannii* MTCC 1425 is a sensitive strain and *A. baumannii* R674 is a multi-drug (carbapenem) resistant clinical isolate.

The confocal laser scanning microscopy (CLSM) images of *A. baumannii* MTCC 1425 biofilms stained with SYTO 9 dye clearly demonstrated the dispersal of biofilm in presence of QCybuAP and Q*n*-prAP (both at 50 µg mL^{-1}) compared to erythromycin (30 µg mL^{-1}) (Fig. 5.9). The thickness was found to be 18 µm and 7.6 µm for the untreated and erythromycin treated biofilms respectively. On the other hand, both the Q*n*-prAP and QCybuAP treated biofilms had a lower thickness of 2.4 µm compared to untreated and erythromycin treated biofilms. The enumeration of the bacterial count was performed after the treatment of the biofilms with test compounds and represented as $\log_{10}$(cfu/mL) (Fig. 5.10). Against *A. baumannii* MTCC 1425, colistin and tobramycin showed 2 $\log_{10}$ and 3 $\log_{10}$ reduction compared to the untreated control (10 $\log_{10}$). At the same concentration of 30 µg mL^{-1}, Q*n*-prAP and QCybuAP displayed 4 $\log_{10}$ and 5 $\log_{10}$ reductions. Against the biofilms formed by antibiotic-resistant clinical isolate, *A. baumannii* R674 tobramycin and colistin reduced the bacterial counts by 3 $\log_{10}$ and 5.5 $\log_{10}$ whereas Q*n*-prAP and QCybuAP reduced by 5.5 $\log_{10}$ and 4.5 $\log_{10}$ compared to the untreated (10 $\log_{10}$) control. Taken together, the results suggest that these polymers disperse the biofilms and kill the dispersed bacteria more efficiently than conventional antibiotics. These results suggest that antibiotics are less effective against bio-films. In contrast,

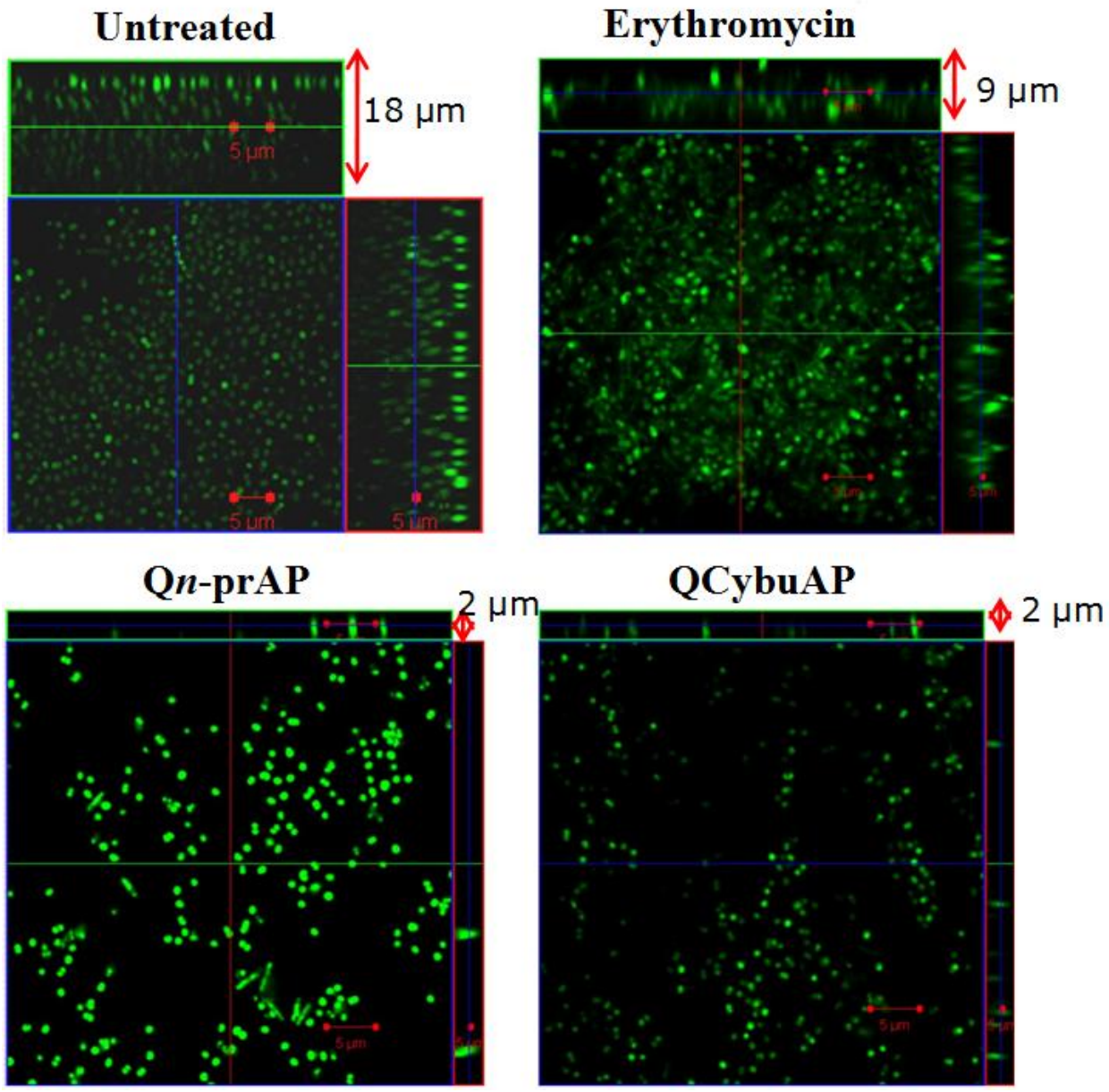

Figure 5.9: *A. baumannii* biofilm disruption properties using confocal laser scanning microscopy (CLSM). Mature biofilms were left untreated or treated with erythromycin (50 µg mL^{-1}), Q*n*-prAP (50 µg mL^{-1}) and QCybuAP (50 µg mL^{-1}) for 24 h and stained with Syto 9 dye. The central pictures show horizontal optical sections (XY), and the flanking pictures show vertical optical sections (YZ and ZX). Images were processed using Zeiss LSM software. Scale bars, 5 µm.

these polymers displayed good ability to disrupt the biofilms. Anti-biofilm efficacy of molecules alone or in combination with antibiotics has extensively been reported[46-48, 194-196]. However, the present findings underscore the importance of membrane-active polymers for the dispersal and

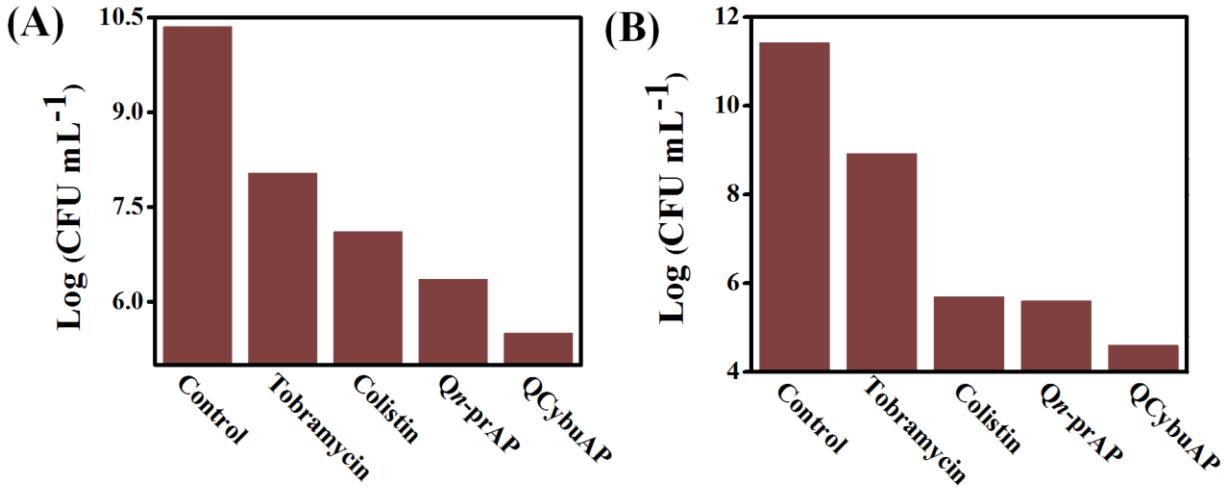

Figure 5.10: *A. baumannii* biofilm disruption properties. Mature biofilms of *A. baumannii* grown on glass cover slips were left untreated or treated with antibiotics and polymers for 24 h. Bacterial count enumeration of *A. baumannii* MTCC 1425 (A) and *A. baumannii* R674 (clinical isolate) biofilms (B).

killing of bacterial bio-films. We believe that these cationic polymers would possess non-specific interactions with negatively charged extracellular matrix components resulting in disruption of *A. baumannii* biofilms but it needs further investigations.

5.2.5 Drug resistance studies

Development of bacterial resistance has been the major drawback of antibiotics due to their target specific mechanism of action. The development of bacterial resistance against polymers was tested in *E. coli* grown over 30 passages using sub-MIC concentrations. Bacteria did not develop resistance to Q*n*-prAP, whereas rapid resistance to tetracycline was observed with a 125 fold increase in MIC over 30 passages (Fig. 5.11 A). *E. coli* developed rapid and high resistance to colistin, an antibiotic with lipopolysaccharide (LPS) as the target in Gram- negative bacteria, with a 250-fold of increase in MIC after 28 passages (Fig. 5.11 A). Gram-negative bacteria are inherently resistant to most of the antibiotics due to exclusion by efflux pumps and formation of biofilms by these bacteria worsens the situation. *A. baumannii* were found to be inherently resistant to erythromycin and rifampicin. The ability to develop bacterial resistance to erythromycin, rifampicin and QCybuAP has been performed against *A. baumannnii* (Fig. 5.11 B). Erythromycin and rifampicin displayed 64-fold of increase in MIC whereas no fold of increase in MIC was observed for QCybuAP against *A. baumannii* even after 28 passages. These

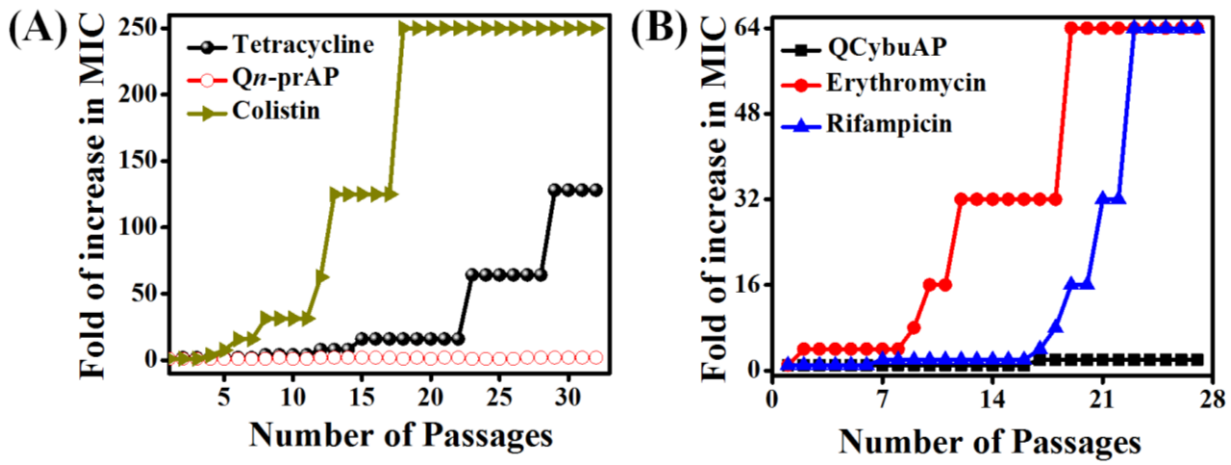

Figure 5.11: Bacterial resistance studies of polymers and antibiotics. (A) *E. coli* developed rapid resistance to colistin and tetracycline but no detectable resistance was observed for Q*n*-prAP even after repeated passages. (B) *A. baumannii* developed rapid and high resistance to erythromycin and rifampicin but not to QCybuAP even after 28 passages.

results suggest that unlike the target-specific antibiotics, non-specific targeting of bacterial cell membrane by these polymers is advantageous as the bacteria find it difficult to develop resistance.

5.2.6 Animal studies

Polymers, unlike small molecules, can act as non-adsorbable drugs that are ideal materials for safe topical treatment[215, 216] of bacterial infections, such as *A. baumannii* burn wound infections. Polymers can be restricted to the site of application due to their relatively low permeation into the skin compared to small molecules. This localization offers unique medical benefits where it is desirable to confine a therapeutic agent from systemic exposure, thereby limiting concerns about toxicity[215].

5.2.6.1 *In-vivo* toxicity

The *in-vivo* toxicity studies of QCybuAP and Q*n*-prAP have been carried out in mice models as described in Chapter 3. A single dose subcutaneous (s.c.) administration of Q*n*-prAP or QCybuAP at 55 mg kg^{-1} did not induce any lethal effects in mice even after 14 days post-treatment.

5.2.6.2 Acute burn wound infection

The *in-vivo* antibacterial efficacy studies were performed in mice using burn wound infection model against *A. baumannii*[217]. Colloquially, *A. baumannii* is referred to as 'Iraqibacter' due to its seemingly sudden emergence in military treatment facilities during the Iraq War[218, 219]. Soldiers in Iraq and Afghanistan reported with traumatic injuries due to gunfire and explosions suffered from chronic and life-threatening *A. baumannii* burn wound infections[220, 221]. Burn wounds were created on the back of the mice using heated brass bars and infected the burn wounds with *A. baumannii* (~10^7 cfu, MTCC 1425). Mice were treated with Q*n*-prAP (50 mg kg^{-1}), QCybuAP (50 mg kg^{-1}) and rifampicin (5 mg kg^{-1}) every 24 h for 5 days (Fig. 5.12 A). Six days post-infection, untreated mice and even rifampicin had a very high bacterial burden of 10-11 log(cfu/g). On the other hand, mice treated with Q*n*-prAP and QCybuAP had significant ($p = 0.001$) decrease of ~3 log(cfu/g) in bacterial burden compared to the untreated mice (Fig. 5.12 B). Skin histolopathology of control mice without treatment showed infiltration of inflammatory cells mostly neutrophils and mononuclear cells (inset) and damage to squamous stratified epithelial cells (Fig. 5.12 C). Rifampicin treated showing moderate regeneration of stratified squamous epithelial cells with sweat gland and sebaceous glands (inset). Q*n*-prAP and QCybuAP treated mice showing regeneration of the skin with squamous epithelial cells with keratin layers, sebaceous gland, sweat gland and hair follicles (inset). These results suggested that the combination of antibiotics and polymers have the potential for the topical treatment of burn wound infections caused by *A. baumannii*.

5.2.6.3. Chronic burn wound infection

Next, the *in-vivo* antibacterial efficacy studies were performed in mice using chronic biofilm burn wound infection model [222] against *A. baumannii*. Burn wounds were created on the back of the mice using heated brass bars and infected (~10^6 cfu) the burn wounds with *A. baumannii* (Fig. 5.13 A). To mimic the condition for the establishment of biofilms, drug treatment started 24 h post-infection by when the bacterial count increased to 8.3×10^7 cfu/g of tissue (day 1). Seven days post infection, the untreated mice had a very high bacterial burden of 9-10 log(cfu/g) of tissue (Fig. 5.13 B). Mice that had recieved QCybuAP (50 mg kg^{-1}) and erythromycin (50 mg kg^{-1}) had decreased bacterial burden of 5 log(cfu/g) compared to the untreated mice. Skin tissue sections were stained with hematoxylin and eosin staining for histopathology analysis (Fig. 5.13

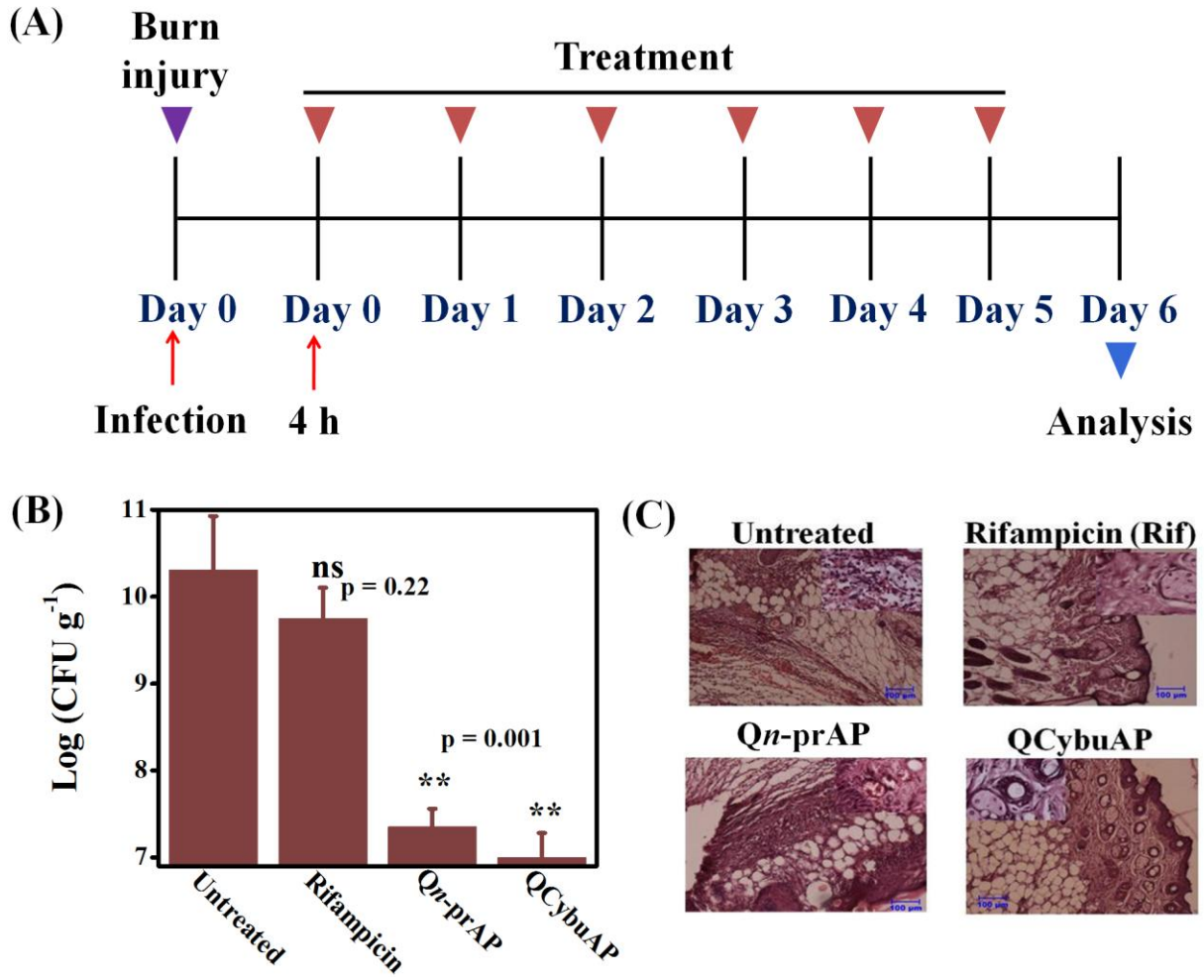

Figure 5.12: *In-vivo* anti-infective studies against *A. baumannii* acute burn wound infection. (A) Experimental plan. Burn wounds were created on the back of mice (n = 4) and infected with 10^7 cfu of *A. baumannii*. (B)Mice were treated with rifampicin (5 mg kg^{-1}), QCybuAP (50 mg kg^{-1}) and Q*n*-prAP (50 mg kg^{-1}). The data are expressed as mean±standard deviation based on values obtained from four mice (n = 4). P value was calculated using Student's *t* test (2 tailed one sample, unpaired distribution) and two stars represent a p value < 0.001. (C) Haematoxylin and Eosin (H & E) staining of the respective skin sections. Scale bar = 100 µm (inset 20 µm).

C). The results also revealed that before commencing the treatment mice had an established infection with numerous bacterial cells with proteinaceous exudates (arrow) along with severe infiltration of inflammatory cells mainly neutrophils which are degenerating (inset) (Fig. 5.13 C). Increase in the bacterial count (8.3×10^7 cfu/g) and the proteinaceous exudates (probably EPS components) reflected the establishment of biofilms on burn wounds[46]. Seven days post-infection, untreated mice showed burn wound area with numerous bacterial cells with proteinaceous exudates (arrow), with severe infiltration of inflammatory cells mainly neutrophils

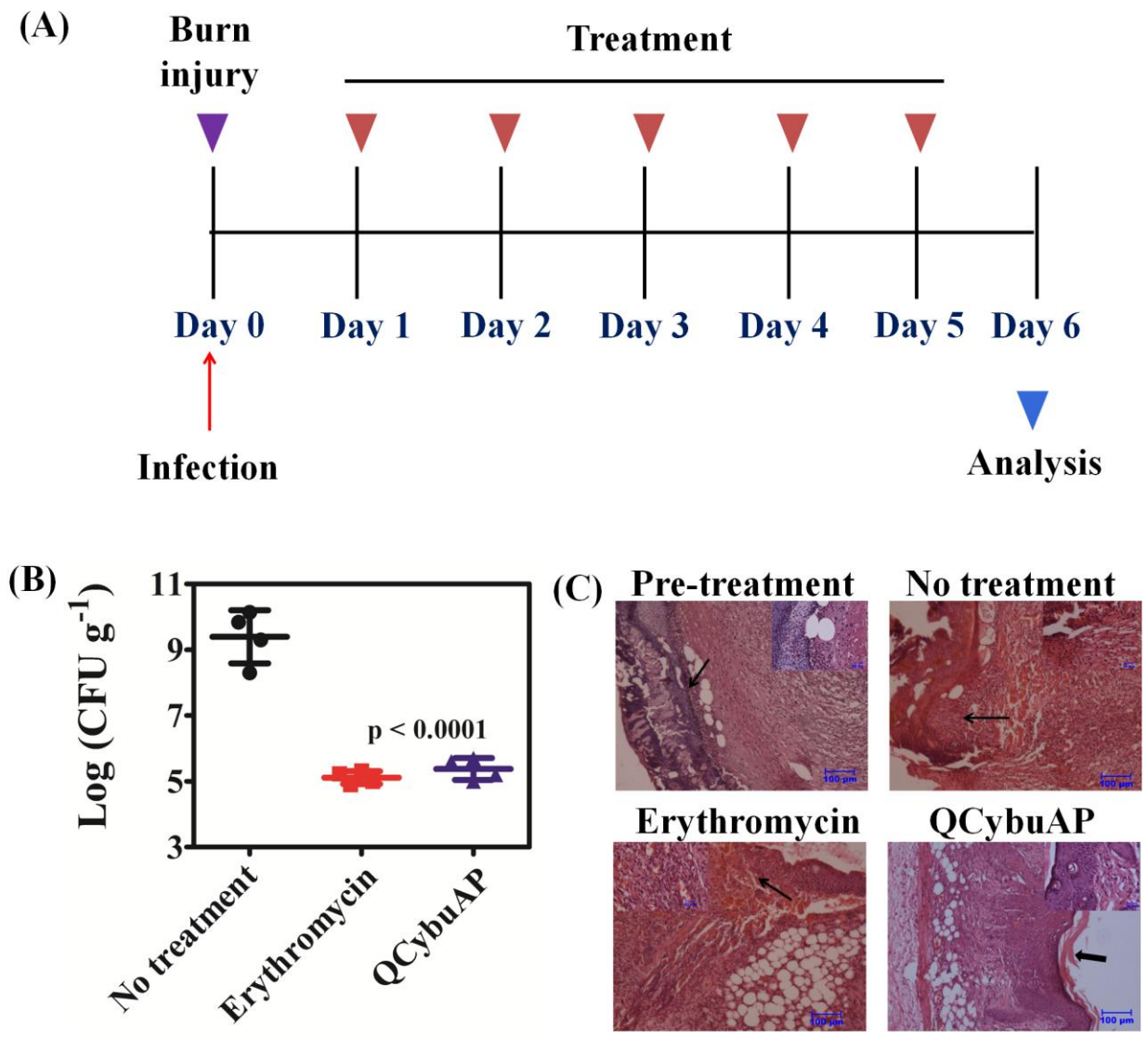

Figure 5.13: *In-vivo* anti-infective activity against *A. baumannii* burn wound biofilm infection. (A) Experimental model. Infected burn wounds were kept untreated for 24 h to allow for the establishment of biofilm. (B) Mice were infected with ~6 log (cfu/mL) that increased to ~7.5 log (cfu/g) on day 2. Mice that were not treated had a very high bacterial burden of 9-10 log(cfu/g) of tissue seven days post-infection. Mice that had recieved erythromycin (50 mg kg^{-1}) and QCybuAP (50 mg kg^{-1}) for 5 days had a decreased bacterial burden of 5 log(cfu/g). P value was calculated using Student's *t* test (2 tailed one sample, unpaired distribution) and a value of $p < 0.05$ was considered significant. (C) Histopathology analysis of Hematoxylin and Eosin (H&E) stained skin tissue sections revealed biofilms in untreated mice, mild recovery in erythromycin treatment and recovery of burn wounds with QCybuAP treatment. Scale bar 100 µm (inset 20 µm).

which are degenerating and attached to the exudates (inset). There was loss of squamous epithelial cell layer, sweat and sebaceous glands, and hair follicles along with architecture of skin

tissue. These results revealed the serious infection condition of mice. Erythromycin treated mice had moderate regeneration of squamous epithelial cell layer over the burn wound area (arrow), with loss of sweat, sebaceous glands and hair follicles. Severe infiltration of neutrophils and red blood cells were seen (inset). QCybuAP treated mice showed regeneration of stratified squamous epithelial cells with hair follicles (inset) sweat gland and sebaceous glands and formation of keratin layer (arrow) (Fig. 5.13 C). Although both erythromycin and QCybuAP had comparable *in-vivo* anti-infective activity, bacteria developed resistance to erythromycin but not to QCybuAP even after repeated passages. The results suggest that these polymers are effective *in-vivo* for the treatment of topical infections caused by Gram-negative biofilms such as formed by *A. baumannii* without the development of bacterial resistance.

5.3 Conclusions

In conclusion, polymeric materials have been shown to disrupt surface established Gram-negative biofilms that have very high ability to persist on artificial surfaces mainly in hospital environments. These polymers also eradicated the slow or non-dividing bacteria as well as dormant bacterial persisters with membrane-active mode of action. More importantly, these polymers decreased the bacterial burden in an acute and chronic burn wound infections of Gram-negative bacteria in mice models whereas the antibiotics were ineffective. However, bacteria developed rapid resistance to conventional antibiotics such as tetracycline, erythromycin and colistin but not to the polymers. These results suggested the potential of these polymeric biomaterials for sterilizing bio-medical device surfaces after the infection has got established and also for the topical treatment of burn wound infections.

5.4 Experimental section

5.4.1 Antibacterial activity against actively growing cells in chemically defined media

5 μL of the -80 °C stock was added to 3 mL of the broth and the culture was grown for 6 h at 37 °C prior to the experiments contained ~10^9 CFU mL^{-1}. Actively growing cells (mid-log phase) were diluted to ~5×10^5 CFU mL^{-1} in M9 media (*E. coli*) or MEM (*S. aureus*). 50 μL of compounds (antibiotics or polymers) were added to a 96 well plate (Polystyrene) containing 150

μL bacterial solutions. The plate was then incubated at 37 °C for a period of 2 h. After 2 h, the bacterial suspension was serially diluted (10 fold) and spot-plated on agar plates. The viable colonies (< 100) were counted after 48 h incubation at 37 °C. The data is represented as percentage of survival of bacteria with respect to the untreated samples.

5.4.2 Antibacterial activity against stationary phase and persister cells

Persister cells were generated by following a literature procedure[46, 47]. 5 μL of the -80 °C stock was added to 3 mL of the culture medium and grown for 6 h at 37 °C. Then the bacterial suspension was diluted to 1:1000 and grown for 16 h to reach stationary phase. 1 ml of this bacterial suspension was treated with 100 μg mL^{-1} (*S. aureus*) and 300 μg mL^{-1} (*E. coli*) of ampicillin sodium for 3h at 37 °C to generate the persister cells. After 3h, the bacteria were centrifuged, washed three-four times and resuspended in M9 media (*E. coli*) or MEM (*S. aureus*) to remove the traces of the antibiotic. Then the bacterial suspension was diluted and spot-plated on LB agar (*E. coli)* or nutrient agar (*S. aureus*) plates for determining the CFU of persister cells.

Stationary phase and persister cells were diluted to ~10^{6-7} CFU mL^{-1} in M9 media (*E. coli*) or MEM (*S. aureus*). 50 μL of compounds (antibiotics or polymers) were added to a 96 well plate (Polystyrene) containing 150 μL bacterial suspension. The plate was then incubated at 37 °C for 2 h. After 2 h, the bacterial suspension was serially diluted (10 fold) and spot-plated on agar plates. The viable colonies (< 100) were counted after 48 h incubation at 37 °C. The data is represented as percentage of survival of bacteria with respect to the untreated samples.

5.4.3 Biofilm disruption assays

5.4.3.1. Crystal violet staining

Cover slips (diameter 13 mm) were chosen as the substrates for conducting the biofilm disruption study. Sterilized cover slips were placed in wells of a 6-well plate. Mid-log phase *A. baumannii* were diluted to ~10^5 CFU mL^{-1} in BM2 media (supplemented with 0.5% glucose as carbon source, 0.5% casaminoacids and 200 μM $FeCl_3$). 2 mL of this bacterial suspension was added to wells containing the cover slips. The plate was incubated under stationary conditions at 30 ºC for 48 h. Afterwards, media was removed and planktonic bacteria were carefully washed with 1X PBS (pH = 7.4) and removed. Biofilm containing cover slips were then placed into

another 6-well plate and 2 mL of test compounds were added to it and allowed to incubate for 24 h. In case of control, 2 mL of media was added instead of compounds. At the end of 24 h, medium was then removed and planktonic cells were removed by washing with 1X PBS. The cover slips were carefully removed from the well and placed into another 6-well plate. For visualizing the disruption of bio-film, 1 mL of 0.1% of crystal violet (CV) was added into the wells and incubated for 10 min. After washing, the crystal violet was dissolved in 95% ethanol and absorbance of crystal violet was measured at 520 nm. Similarly, for bacterial count enumeration, the biofilms containing cover slips were treated with trypsin EDTA for 20 min at 37 ºC, serially diluted and plated on agar plates. Viable bacteria were counted after 24-48 h incubation at 37 ºC.

5.4.3.2. Confocal laser scanning microscopy (CLSM)

As described above, the cover slips after 24 h treatment with the test compounds (including the untreated conditions) were carefully removed from the well, washed and placed on glass slides. The biofilms were stained with 10 µL SYTO9 (3 µM) and imaged using a Zeiss 510 Meta confocal laser-scanning microscope. The orthogonal projections of the images were processed using LSM 5 Image examiner.

5.4.3.3. Dispersed cells

Bacterial suspension in the surrounding media of the biofilm containing cover slip in the well plates after 24 h treatment was collected. The $O.D._{600}$ of this bacterial suspension was measured and 20 µL of this suspension was also spot plated on agar plates to see the viable bacteria.

5.4.4 Animal studies

5.4.4.1 *In-vivo* acute skin infection[217]

Female Balb/c mice (6-8 weeks, 22-25 g) were anesthetized with ketamine-xylazine cocktail, their dorsal surface shaved and cleansed. Six mm diameter burn wounds were created by applying a 120 s- heated brass bar for 10 s. Immediately after injury, burn wounds were infected with a mid-log phase bacterial inoculum of ~10^7 CFU (20 µL of 10^9 CFU mL^{-1}) of *A. baumannii* (MTCC 1425) prepared in PBS. Burn wounds were treated 3-4 h post infection and thereafter

every 24 h for 5 days. Rifampicin stock solution (100 mg mL^{-1}) was prepared in DMSO and further diluted in sterile PBS (pH = 7.4). Polymers were dissolved in sterile PBS (pH = 7.4). Burn wounds were treated with 40 µL of solutions containing rifampicin (5 mg kg^{-1}), Q*n*-prAP (50 mg kg^{-1}), QCybuAP (50 mg kg^{-1}) whereas PBS was used as untreated control. Mice were euthanized 6 days post-injury; the wounded muscle tissue was excised, weighed, and homogenized in 10 mL of PBS. Serial homogenate dilutions were plated and the results were stated as log ($CFU.g^{-1}$) of tissue. Data was plotted using Graphpad prism software and P value was calculated using unpaired Student's *t* test (2 tailed 1 sample, unpaired distribution) between the control group and the treatment group and a value of $P < 0.05$ was considered significant.

5.4.4.2 *In-vivo* chronic biofilm skin infection[46, 222]

Female Balb/c mice (6-8 weeks, 22-25 g) were anesthetized with ketamine-xylazine cocktail, their dorsal surface shaved and cleansed. Six mm diameter burn wounds were created by applying a 120 s heated brass bar for 10 s. Immediately after injury, burn wounds were infected with a mid-log phase bacterial inoculums of 1.6×10^6 CFU (20 µL from 0.8×10^8 CFU mL^{-1}) of *A. baumannii* (MTCC 1425) prepared in PBS. To mimic the condition for the biofilms, burn wounds were left untreated for 24 h. Treatment started 24 h post infection by when the infection has already become established. Burn wounds were treated every 24 h for 5 days. Erythromycin stock solution (100 mg mL^{-1}) was prepared in DMSO and further diluted in sterile PBS (pH = 7.4). QCybuAP was dissolved in PBS. Burn wounds were treated with 40 µL of solutions containing erythromycin (50 mg kg^{-1}), QCybuAP (50 mg kg^{-1}) whereas 5% DMSO was used as untreated control. Mice were euthanized 6 days post-injury; the wounded muscle tissue was excised, weighed, and homogenized in 10 mL of PBS. Serial homogenate dilutions were plated on MacConkey agar (Himedia, India) and the results were stated as log ($CFU.g^{-1}$) of tissue. P value was calculated using unpaired Student's *t* test (2 tailed 2 samples assuming equal variances) between the control group and the treatment group and a value of $P < 0.05$ was considered significant.

5.4.4.3 Histopathology[46]

The portion of skin was collected and fixed in 10 % formalin (10 ml of 40% formaldehyde added to 90 ml of water). The tissues were fixed for 48 h and washed for 1 h in running tap water. Then

dehydration of the tissues was performed with increasing concentrations of ethanol (70%, 90% and 100%; each for 1 h). Then, the tissues were cleared in xylene twice for 1 h. Paraffin embedding was carried by keeping the tissues in melted paraffin at 56º C thrice. Longitudinal and transverse sections (5 µm) were prepared with semiautomatic microtome and placed on glass slide coated with Meyer's egg albumin. Tissue sections were dried by incubating them for 2 h at 40º C. Rehydration of fixed sections was carried in decreasing grades of alcohol (100%, 90%, 70% and 50%; each for 1 h) and then water. The sections were stained with haematoxylin and eosin staining. Then the sections were covered with DPX (SRL, India) mounting medium with cover glass and observed under light microscope (Nikon, Japan) to study the histopathological changes.

Chapter 6

Membrane-active Polymers Potentiate Antibiotics to Gram-negative Superbugs

Abstract

Gram-negative 'superbugs' including New Delhi metallo-beta-lactamase-1 (bla_{NDM-1}) producing pathogens have become world's major public health threats. Development of molecular strategies that can rehabilitate the 'old antibiotics' and halt the antibiotic resistance is a promising approach to target them. In this chapter, membrane-active polymers have been shown to restore the antibacterial efficacy (enhancement by >80-1250 fold) of antibiotics (erythromycin, rifampicin and tetracyclines) towards Gram-negative bacteria including bla_{NDM-1} K. pneumoniae and bla_{NDM-1} E. coli clinical isolates. More importantly, these polymers potentiate antibiotics to eradicate surface established biofilms formed by Gram-negative bacteria. Further, these membrane-active polymers delay the development of bacterial resistance to antibiotics that highlights the potential of this combination approach in clinical settings. Furthermore, membrane-active polymers potentiate antibiotic activity in mice models of Gram-negative burn and surgical wound infections. Organismic studies showed that bacteria had an increased and faster uptake of antibiotics in presence of these polymers which is attributed to the mechanism of re-sensitization. Polymers displayed membrane-active properties such as dissipation of membrane potential and membrane-permeabilization that enabled higher uptake of antibiotics in bacteria. These findings stress the importance of combination approaches of membrane-active molecules and antibiotics to combat MDR Gram-negative superbugs and for the topical treatment of Gram-negative bacterial infections.

(1) Uppu, D. S. *et al.* "Membrane-active Macromolecules Re-sensitize Tetracycline Antibiotics to Gram-negative Clinical Isolates". *PLoS One* **2015**, *10*, e0119422.
(2) Uppu, D. S. *et al.* "Membrane-active Polymers Kill Bacterial Persisters and Potentiate Antibiotics to Biofilms". Manuscript under preparation.

6.1 Introduction

Gram-positive bacteria need more antibiotics but Gram-negative bacteria need antibiotics. Gram-negative bacteria have a paucity of antibiotics that can treat the infections caused by them. The WHO Global Report on Surveillance of Antimicrobial Resistance 2014 says that *E. coli* and *K. pneumoniae* have developed more than 50 % of resistance to commonly used antibacterial drugs in many settings [9]. Of particular concern is the fact that *K. pneumoniae* has developed resistance to carbapenems, the last line of available treatment in all WHO regions [9]. This ongoing explosion of multi-drug resistant Gram-negative 'superbugs' including the New Delhi metallo-beta-lactamase-1 ($bla_{\text{NDM-1}}$) producing bacteria along with the paucity of antibiotics poses an immense threat to the global public health [7, 10]. More importantly, carbepenem resistant bacteria such as $bla_{\text{NDM-1}}$ *E. coli* and $bla_{\text{NDM-1}}$ *K. pneumoniae* have become resistant to the highly toxic and the last resort antibiotic, colistin [11]. Another antibiotic, tigecycline though useful in tissue infections, is less useful in systemic infections. Development of resistance to tigecycline in Gram-negative bacteria being reported in clinical settings is a matter of worry[12]. The emergence of pan-drug resistant Gram-negative bacteria has become a reality, necessitating the exploration for alternative ammunitions to combat them.

Biofilms due to their chronic nature impose a huge burden in healthcare as there are no effective drugs dedicated particularly to treat the infections caused by them. Antibiotics, despite their low activity, are generally prescribed for the treatment of biofilm related infections. Unfortunately, Gram-negative bacteria, unlike Gram-positive bacteria, even in their planktonic condition are resistant to most of the antibiotics. Hence, the formation of biofilms by Gram-negative bacteria leaves us with almost no options for the treatment of infections caused by them. Nosocomial and opportunistic Gram-negative bacteria such as *A. baumannii* pose a serious threat in hospital settings[223-226]. *A. baumannii* has been noted for its apparent ability to survive on artificial surfaces for an extended period of time, therefore allowing it to persist in the hospital environment. This is thought to be due to its ability to form biofilms. *A. baumannii* causes nosocomial infections targeting mainly immuno-compromised patients. The already inadequate antibiotic arsenal for *A. baumannii* due to its inherent and rapidly acquiring drug-resistance makes this bacterium a threat to the global public health. Thus, there is an urgent need to develop materials that can disrupt *A. baumannii* biofilms established on surfaces. The goal was to develop an effective combination approach using membrane-active polymers to restore the

efficacy of antibiotics against Gram-negative bacteria including their biofilms.

One of the promising strategies to target multi-drug resistant (MDR) bacteria is by using either combination of two antibiotics or combination of antibiotics and non-antibiotics/adjuvants [57, 198, 227-239]. The combination of two or more antibiotics has been found to foster the development of bacterial resistance than the individual antibiotics[240]. An ideal combination approach would have at least one agent with lower rate of emergence of bacterial resistance. Molecules targeting the cell membrane of bacteria have been known to possess low propensity for triggering the development of bacterial resistance. It has been found that bacteria do not develop resistance to the cationic-amphiphilic polymers developed in previous chapters. Thus, it would be ideal to entrust these polymers, the role of re-sensitizing the superbugs to the antibiotics using a combination approach.

6.1.1 Role of efflux pumps in potentiating the antibiotics

Gram-negative bacteria are resistant to some of the antibiotics such as tetracycline, erythromycin and rifampicin (all of these are active against Gram-positive bacteria) by excluding them through efflux pumps (mostly RND (resistance nodulation division) family)[6, 7].With the clear involvement of RND transporters in the continuous increase of MDR clinical bacteria, these efflux pumps are considered as "key" drug targets for the development of combination strategies using antibiotic efflux inhibitor[58, 60, 61]. A similar way has been previously used for the development of the combination "β-lactam β- lactamase inhibitor"[227]. Inhibition of the Gram-negative bacteria pump activity may be achieved by[58, 60]

i. Altering regulatory steps that govern the expression of effluxpumps
ii. Inhibiting the functional assembly of the multi-component pump
iii. Collapsing the energy of efflux, direct/specific via an antiporter site or indirect/general via a collapse of energy driven mechanisms of the bacterial transporters
iv. Creating competitive or non-competitive inhibition with a nonantibiotic molecule to the affinity sites of the efflux pump
v. Changing the chemical design of previous antibiotics in order to reduce its affinity for efflux recognition and binding sites or to block the efflux transport.

Efflux through RND-family pumps is driven by the proton motive force, an electrochemical gradient in which the movement of hydrogen ions drives transport of the substrate [61]. The ATP binding cassette (ABC) efflux systems exploit the free energy of ATP hydrolysis to energize transport. Since the activity of the efflux pumps depend on the proton motive force across the bacterial cell membrane, it has been envisaged that the cationic-amphiphilic polymers (Fig. 6.1) which can dissipate the membrane potential might be able to restore the efficacy of these antibiotics (Fig. 6.1). Tt has been hypothesized that the dissipation of membrane potential by these polymers indirectly collapse the efflux energy and inhibit the efflux pump activity thereby provide a backdoor entry for the antibiotics that are otherwise excluded by the efflux pumps [232].

In this chapter, a molecular approach has been developed to rehabilitate the 'old antibiotics' towards Gram-negative superbugs. The mechanistic investigations of re-sensitization, membrane-active properties of polymers and more importantly, the drug resistance studies of tetracycline antibiotics in presence of polymers are reported herein. The ability of the polymers to potentiate the antibiotics to biofilms and *in-vivo* antibacterial activity of the combination approach in mouse burn wound and surgical wound (acute and chronic) infections against Gram-negative superbugs were also studied.

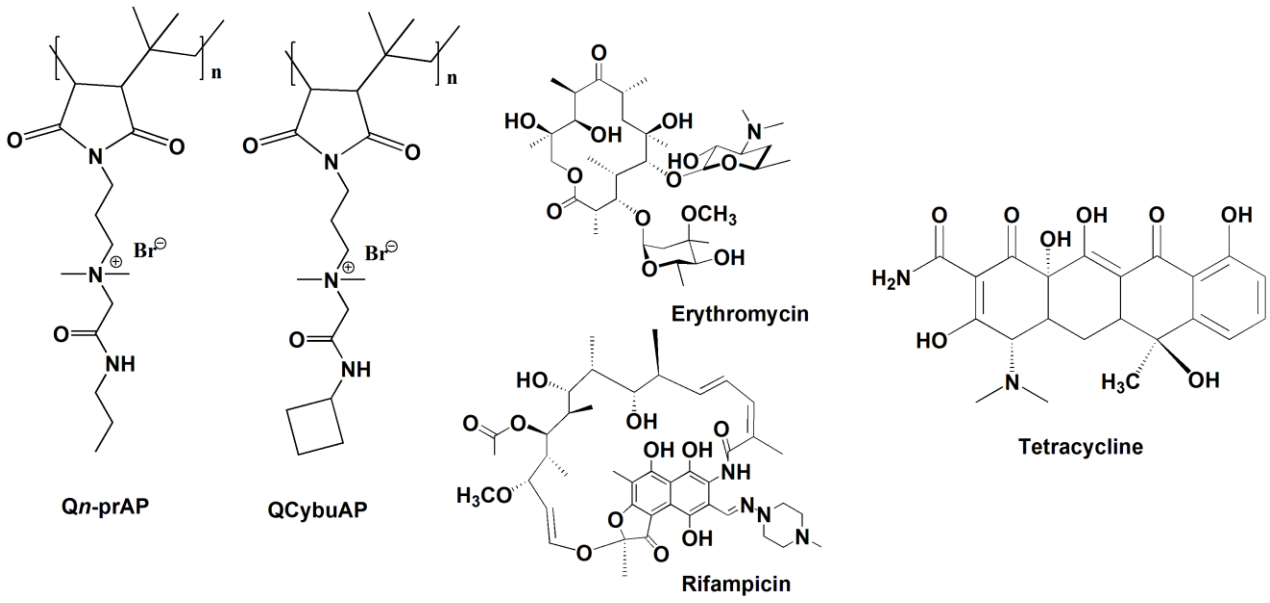

Figure 6.1: Chemical structures of membrane-active polymers that potentiate the antibiotics.

6.2 Results and Discussion

6.2.1 Combination efficacy against Gram-negative bacteria: acquired resistance

Clinical isolates of carbapenem-resistant bacteria (minimum inhibitory concentration, MIC of meropenem >16 μg mL^{-1}) were characterized for bla_{NDM-1} gene (475 bp) using PCR and gel electrophoresis (Fig. 6.2) [241].The bla_{NDM-1} gene was confirmed in *K. pneumoniae* R3934 and *E. coli* R3336 including the positive control *K. pneumoniae* (ATCC-BAA-2146) whereas MDR *K. pneumoniae* R3421 showed negative (Fig. 6.2). The prevalence of bla_{NDM-1} in clinical settings makes the development of alternative strategies imperative.

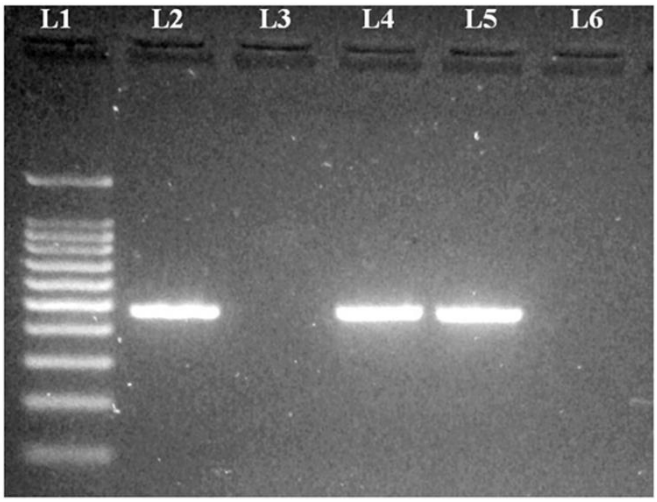

Figure 6.2: Schematic representation of agarose gel (2%) showing the 475 bp amplified product by conventional polymerase chain reaction. Lane 1, 100 bp DNA ladder; Lane 2, positive control- NDM-1 producing *K. pneumoniae* (ATCC-BAA-2146); Lane 3, negative control- *E. coli* (ATCC-25922); Lane 4, *E. coli* R3336 and Lane 5, *K. pneumoniae* R3934 confirm the bla_{NDM-1} gene; Lane 6, multi-drug resistant (MDR) *K. pneumoniae* R3421 which was negative for bla_{NDM-1} gene.

All the three bla_{NDM-1} isolates and the MDR strain are represented here on as R3336, R3934, ATCC2146 and R3421 respectively. All the four isolates were sensitive to tigecycline and colistin only (MIC = 0.5-1 μg mL^{-1}) and were highly resistant to intracellular antibiotics (ciprofloxacin, kanamycin, erythromycin, tetracycline, doxycycline and minocycline) and cell-wall directed antibiotics (ampicillin and meropenem) (Table 6.1). In most of the cases, the MICs of the antibiotics against all the four bacteria were > 250 μg mL^{-1}, the highest concentration tested (Table 6.1). This provides yet another evidence for the high level of multi-drug

Table 6.1: Antibacterial activity of conventional antibiotics in presence or absence of polymers and colistin against clinical isolates.

Antibiotics and bacterial strains	MIC of antibiotic (μg mL^{-1})					
	-Polymers	+Q*n*-prAP (μg mL^{-1})		+Q*n*-prEP (μg mL^{-1})		+Colistin (μg mL^{-1})
		12.5	25	25	50	0.25
bla$_{NDM-1}$ E. coli R3336						
Ampicillin	>250	>100	>100	>100	>100	>100
Meropenem	50	50	50	50	50	100
Ciprofloxacin	125	>100	>100	100	100	100
Erythromycin	>250	>100	>100	>100	>100	>100
Kanamycin	>250	>100	>100	>100	>100	>100
bla$_{NDM-1}$ K. pneumoniae R3934						
Ampicillin	>250	>100	>100	>100	>100	>100
Meropenem	50	50	50	50	25	100
Ciprofloxacin	>250	>100	>100	>100	>100	>100
Erythromycin	>250	>100	>100	>100	>100	1.5
Kanamycin	>250	>100	>100	>100	>100	>100
bla$_{NDM-1}$ K. pneumoniae ATCC-BAA-2146						
Ampicillin	>250	ND	ND	ND	ND	ND
Meropenem	25	ND	ND	ND	ND	ND
Ciprofloxacin	>250	ND	ND	ND	ND	ND
Erythromycin	125	ND	ND	ND	ND	ND
Kanamycin	>250	ND	ND	ND	ND	ND
MDR K. pneumoniae R3421						
Ampicillin	>250	ND	ND	ND	ND	ND
Meropenem	30	ND	ND	ND	ND	ND
Ciprofloxacin	>250	ND	ND	ND	ND	ND
Erythromycin	125	ND	ND	ND	ND	ND
Kanamycin	>250	ND	ND	ND	ND	ND

ND – Not determined

Table 6.2: Antibacterial activity of polymers and colistin against clinical isolates.

Bacterial Strain	MIC (μg mL^{-1})		
	Q*n*-prAP	Q*n*-prEP	Colistin
bla$_{NDM-1}$ E. coli R3336	250	125	0.75
bla$_{NDM-1}$ K. pneumoniae R3934	125	125	1
bla$_{NDM-1}$ K. pneumoniae ATCC-BAA-2146	62.5	125	0.75
MDR K. pneumoniae R3421	125	125	0.75

resistance in clinical settings. The antibacterial activity of polymers alone was also evaluated and found to be marginal against all the four isolates. Q*n*-prAP displayed MIC of 250 µg mL^{-1} against R3336 and 62.5 µg mL^{-1} against ATCC2146 whereas it showed MIC of 125 µg mL^{-1} against both R3934 and R3421 (Table 6.2). On the other hand, Q*n*-prEP showed MIC of 125 µg mL^{-1} against all the four bacteria.

The combination efficacy of eight antibiotics and these two polymers against the isolates has been determined using chequerboard assays. Using the fractional inhibitory concentration (FIC), a combination was called synergistic when the combined FIC of both agents, (the FIC Index; FICI) was ≤ 0.5[242]. In the presence of polymers (at a concentration of 12.5 and 25 µg mL^{-1} for Q*n*-prAP and 25 and 50 µg mL^{-1} for Q*n*-prEP), the MICs of the antibiotics like ampicillin, meropenem, ciprofloxacin, erythromycin and kanamycin did not reduce when tested against the two clinical isolates-R3336 and R3934 (Table 6.1). However, synergistic effect (FICI of ≤ 0.5) of polymers was observed with tetracycline antibiotics (tetracycline, doxycycline and minocycline) against all the four isolates (Table 6.3).

Notably, Q*n*-prAP at 12.5 µg mL^{-1}, which is $1/20^{th}$, $1/10^{th}$ and $1/5^{th}$ of its MIC against R3336, R3934 and R3421 respectively showed high synergy (FICI as low as 0.15) in combination with both doxycycline and minocycline (Table 6.3). At 25 µg mL^{-1}, Q*n*-prAP in combination with doxycycline and minocycline displayed synergy against all the four isolates. On the other hand, Q*n*-prEP at 25 µg mL^{-1} ($1/5^{th}$ of MIC) resulted in synergistic combinations with doxycycline and minocycline against the bla_{NDM-1} strains (ATCC2146, R3336 and R3934). Whereas, at 50 µg mL^{-1}, it showed synergy with doxycycline and minocycline against all the four clinical isolates. Tetracycline showed synergy in presence of Q*n*-prAP against R3336, R3934 and ATCC 2146 whereas in presence of Q*n*-prEP, synergy was observed only against ATCC2146. Next, the combination efficacy of eight antibiotics and colistin was determined against all the four clinical isolates as a control. Colistin at 0.25 µg mL^{-1} (~$1/3^{rd}$ of MIC) displayed synergy (FICI of 0.3 to 0.5) with tetracycline against R3934 and showed synergy with both tetracycline and doxycycline against ATCC2146 (Table 6.3).

The study also demonstrated that polymers re-sensitized all the four isolates to tetracycline antibiotics (Table 6.4). The CLSI breakpoint for the susceptibility of tetracycline antibiotics is ≤ 4 µg mL^{-1}. The MICs of tetracycline antibiotics were brought down to susceptible limits of as low as 0.2-3.1 µg mL^{-1}, resulting in >80-1250 fold of reduction in the presence of

Table 6.3: Synergistic profiles of tetracycline antibiotics in combination with polymers or colistin against MDR and *bla*$_{NDM-1}$ clinical isolates.

Bacterial strains and FIC of Polymers	**FIC[a]**			**FICI[b]**		
	Tetra	**Doxy**	**Mino**	**Tetra**	**Doxy**	**Mino**
bla$_{NDM-1}$ E. coli R3336						
FIC$_{Qn\text{-}prAP}$ = 0.05	0.4	0.1	0.4	0.45	0.15	0.45
FIC$_{Qn\text{-}prAP}$ = 0.1	0.2	0.05	0.1	0.3	0.15	0.2
FIC$_{Qn\text{-}prEP}$ = 0.2	0.8	0.2	0.2	1.0	0.4	0.4
FIC$_{Qn\text{-}prEP}$ = 0.4	0.4	0.05	0.07	0.8	0.45	0.47
FIC$_{Colistin}$ = 0.3	0.8	0.4	0.8	1.1	0.7	1.1
bla$_{NDM-1}$ K. pneumoniae R3934						
FIC$_{Qn\text{-}prAP}$ = 0.05	0.4	0.15	0.15	0.5	0.25	0.25
FIC$_{Qn\text{-}prAP}$ = 0.1	0.2	0.04	0.02	0.4	0.24	0.22
FIC$_{Qn\text{-}prEP}$ = 0.2	0.4	0.1	0.2	0.6	0.3	0.4
FIC$_{Qn\text{-}prEP}$ = 0.4	0.4	0.04	0.03	0.8	0.44	0.43
FIC$_{Colistin}$ = 0.3	0.4	0.2	0.4	0.7	0.5	0.7
bla$_{NDM-1}$ K. pneumoniae ATCC-BAA-2146						
FIC$_{Qn\text{-}prAP}$ = 0.05	0.02	0.01	0.1	0.22	0.21	0.3
FIC$_{Qn\text{-}prAP}$ = 0.1	0.01	0.003	0.01	0.41	0.40	0.41
FIC$_{Qn\text{-}prEP}$ = 0.2	0.05	0.003	0.01	0.25	0.20	0.21
FIC$_{Qn\text{-}prEP}$ = 0.4	0.05	0.0008	0.003	0.45	0.40	0.40
FIC$_{Colistin}$ = 0.3	0.025	0.05	0.4	0.32	0.35	0.7
MDR K. pneumoniae R3421						
FIC$_{Qn\text{-}prAP}$ = 0.05	0.8	0.1	0.1	0.9	0.2	0.2
FIC$_{Qn\text{-}prAP}$ = 0.1	0.14	0.03	0.04	0.34	0.23	0.24
FIC$_{Qn\text{-}prEP}$ = 0.2	1.2	0.5	0.42	1.4	0.7	0.62
FIC$_{Qn\text{-}prEP}$ = 0.4	0.2	0.08	0.08	0.6	0.48	0.48
FIC$_{Colistin}$ = 0.3	0.78	0.42	0.21	1.08	0.72	0.51

[a]Fractional Inhibitory Concentration (FIC) = [X]/MIC$_X$, where [X] is the lowest inhibitory concentration of compound 1 in the presence of the compound 2. [b]FIC index, FICI = FIC$_{compound1}$ + FIC$_{compound2}$. FICs were calculated only for the combination of tetracycline antibiotics and polymers or colistin. Tetra, Doxy and Mino represent tetracycline, doxycycline and minocycline respectively.

polymers (Table 6.4). Q*n*-prAP at 12.5 µg mL^{-1} (1/10th of its MIC) reduced the MIC of doxycycline and minocycline (~10 fold) to 3.1 µg mL^{-1} against R3421 (Table 6.4). Against ATCC 2146, Q*n*-prAP reduced the MIC of doxycycline (> 80 fold) to 3.1 µg mL^{-1} at 1/5th of its MIC (12.5 µg mL^{-1}). Whereas, at 25 µg mL^{-1}, Q*n*-prAP re-sensitized all the four clinical isolates to tetracycline antibiotics (MIC = 0.8-3.1 µg mL^{-1}) with the reduction in the range of > 80-312 fold. On the other hand, Q*n*-prEP at 25 µg mL^{-1} (1/5th of MIC) decreased the MIC of doxycycline

Table 6.4: Antibacterial efficacy of tetracycline antibiotics with or without polymers and colistin against MDR and bla_{NDM-1} clinical isolates.

Antibiotics and bacterial strains	MIC of antibiotic (μg mL^{-1})				
	-Polymers	+Q*n*-prAP (μg mL^{-1})		+Q*n*-prEP (μg mL^{-1})		+Colistin (μg mL^{-1})
		12.5	25	25	50	0.25
bla_{NDM-1} E.coli R3336						
Tetracycline	32	12.5	6.2	25	12.5	25
Doxycyline	62	6.2	3.1	12.5	3.1	25
Minocycline	32	12.5	3.1	6.2	2.2	25
bla_{NDM-1} K. pneumoniae R3934						
Tetracycline	>250	100	50	>100	100	100
Doxycycline	>250	37	9.4	25	9.4	50
Minocycline	62	9.4	1.5	12.5	1.9	25
bla_{NDM-1} K. pneumoniae ATCC-BAA-2146						
Tetracycline	>250	6.2	3.1	12.5	12.5	6.2
Doxycycline	>250	3.1	0.8	0.8	0.2	12.5
Minocycline	62	6.2	0.8	0.8	0.2	25
MDR K. pneumoniae R3421						
Tetracycline	16	12.5	2.3	19	3.1	12.5
Doxycycline	30	3.1	0.8	16	2.3	12.5
Minocycline	30	3.1	1.1	12.5	2.3	6.2

(> 312 fold) and minocycline (~ 77 fold) down to 0.8 μg mL^{-1} against ATCC2146. At 50 μg mL^{-1}, Q*n*-prEP re-sensitized (>300-1250 fold) all the four isolates to tetracycline antibiotics by lowering the MIC to 0.2-3.1 μg mL^{-1}. Over all, Q*n*-prAP showed higher synergistic and re-sensitization profiles at low concentrations than Q*n*-prEP against all the four isolates. The synergistic combination was not only found to be bacteriostatic but also bactericidal, unlike tetracycline antibiotics that are only bacteriostatic in nature. Q*n*-prAP + minocycline (50 μg mL^{-1} + 6.3 μg mL^{-1}) showed bactericidal activity whereas minocycline (6.3 μg mL^{-1}) alone and Q*n*-prAP (50 μg mL^{-1}) alone were devoid of antibacterial activity against R3336 (Fig. 6.3 A). Colistin, at 0.25 μg mL^{-1} showed no re-sensitization of any of the four isolates to tetracycline antibiotics (Table 6.4). Polymers had higher synergistic and re-sensitization profiles than colistin. The synergistic and re-sensitization profiles of polymers and colistin are seen specifically to

tetracycline antibiotics but not with other cell-wall directed or intracellular antibiotics. In presence of either polymers or colistin, synergy was not observed with ampicillin and meropenem as the beta-lactamases found in the MDR and bla_{NDM-1} Gram-negative bacteria degrade them[6]. Within tetracycline antibiotics, it was found that the synergistic and re-sensitization profiles were always way better for doxycycline and minocycline than the first generation antibiotic, tetracycline. Over all, four isolates of Gram-negative superbugs were made susceptible to tetracycline antibiotics in combination with polymers. Even against a tetracycline sensitive strain of *E. coli* (ATCC 25922), Q*n*-prEP at 62.5 µg mL^{-1} ($1/4^{th}$ of its MIC) showed a 2-fold reduction in the MIC of tetracycline (MIC-1.56 µg mL^{-1}).

6.2.2 Combination efficacy against Gram-negative bacteria: inherent resistance

Gram-negative bacteria are inherently resistant to erythromycin and rifampicin (both are active against Gram-positive bacteria) by excluding them through efflux pumps. *E. coli* and *A. baumannii* were found to be inherently resistant to erythromycin (MIC = 38 µg mL^{-1} and 6.2 µg mL^{-1}) and rifampicin (MIC = 8 µg mL^{-1} and 3.1 µg mL^{-1}) (Table 6.5). MICs of QCybuAP and Q*n*-prAP are 25 µg mL^{-1} and 50 µg mL^{-1} against *E. coli* and > 50 against *A. baumannii* respectively. Chequer-board assays have been performed to determine the synergy profiles between these antibiotics and polymers against both the bacteria. These polymers restored the efficacy of antibiotics to as low as 0.1 µg mL^{-1}. At 6.25 µg mL^{-1} and 12.5 µg mL^{-1}, both the polymers decreased the MIC of antibiotics in the range of 0.1-1.6 µg mL^{-1} against *E. coli* and *A. baumannii* (Table 6.5). Both the polymers showed synergistic profiles with erythromycin and rifampicin against *E. coli* and *A. baumannii*. These results suggested that polymers have the potential to restore the efficacy of antibiotics.

6.2.3 Drug resistance studies

Emergence of rapid resistance in bacteria to conventional antibiotics is a major problem and is the primary hurdle for the introduction of new antibiotics in clinical settings. The development of resistance has been investigated in bla_{NDM-1} *E. coli* (R3336) by exposing to sub-MIC doses of Q*n*-prAP, minocycline alone and in combination with Q*n*-prAP over 30 passages (Fig. 6.3 B). Resistance did not develop with the treatment of polymers as observed by the consistent MIC over 30 passages. This data shows that bacteria do not readily develop resistance to membrane-

Table 6.5: Antibacterial efficacy of polymers in combination with antibiotics.

Antibiotics and Bacterial strains	**MIC of antibiotic (μg mL^{-1})**				
	-Polymers	**+QCybuAP** (μg mL^{-1})		**+Q*n*-prAP** (μg mL^{-1})	
		6.25	12.5	6.25	12.5
E. coli					
Erythromycin	38	1.6	0.1	1.6	0.8
Rifampicin	8	0.4	0.1	1.6	0.2
A. baumannii					
Erythromycin	6.2	1.5	0.4	1.5	0.8
Rifampicin	3.1	0.4	0.2	0.8	0.4

active molecules. *Bla*$_{NDM-1}$ *E. coli* (R3336) which was already resistant to minocycline further developed resistance by a 16-fold increase in MIC after 30 passages (Fig. 6.3 B). Once again, it suggests that resistance to tetracycline antibiotics can indeed develop rapidly with sub-MIC treatment. On the other hand, the development of resistance by *bla*$_{NDM-1}$ *E. coli* (R3336) to minocycline was not observed in the presence of Q*n*-prAP (Fig. 6.3B). The MIC of Q*n*-prAP + minocycline (50 μg mL^{-1} + 6.2 μg mL^{-1}) stayed consistent over the 30 passages. Resistance studies performed in tetracycline sensitive *E. coli* (ATCC 2592) also showed similar results wherein the resistance did not develop for the combination of tetracycline and polymers unlike tetracycline alone (Fig. 6.3 C). The MICs of individual agents were as follows: tetracycline (1.56 μg mL^{-1}); Q*n*-prAP (15.6 μg mL^{-1}), Q*n*-prAP + tetracycline (8 + 1) μg mL^{-1}; Q*n*-prEP (250 μg mL^{-1}); Q*n*-prEP + tetracycline (62.5 + 1) μg mL^{-1} and colistin (0.5 μg mL^{-1}). Colistin developed rapid resistance with an increase of MIC by 250 fold by the end of 30 passages. This showed that *E. coli* did not develop resistance to tetracycline antibiotics in presence of polymers.

Gram-negative bacteria are inherently resistant to most of the antibiotics due to exclusion by efflux pumps and formation of biofilms by these bacteria worsens the situation. *A. baumannii* was found to be inherently resistant to erythromycin and rifampicin. The ability to develop bacterial resistance to erythromycin and rifampicin in presence of QCybuAP has been evaluated against *A. baumannnii* (Fig. 6.3 D). Erythromycin and rifampicin displayed 64-fold of increase in MIC whereas no fold of increase in MIC was observed for QCybuAP against *A. baumannii*

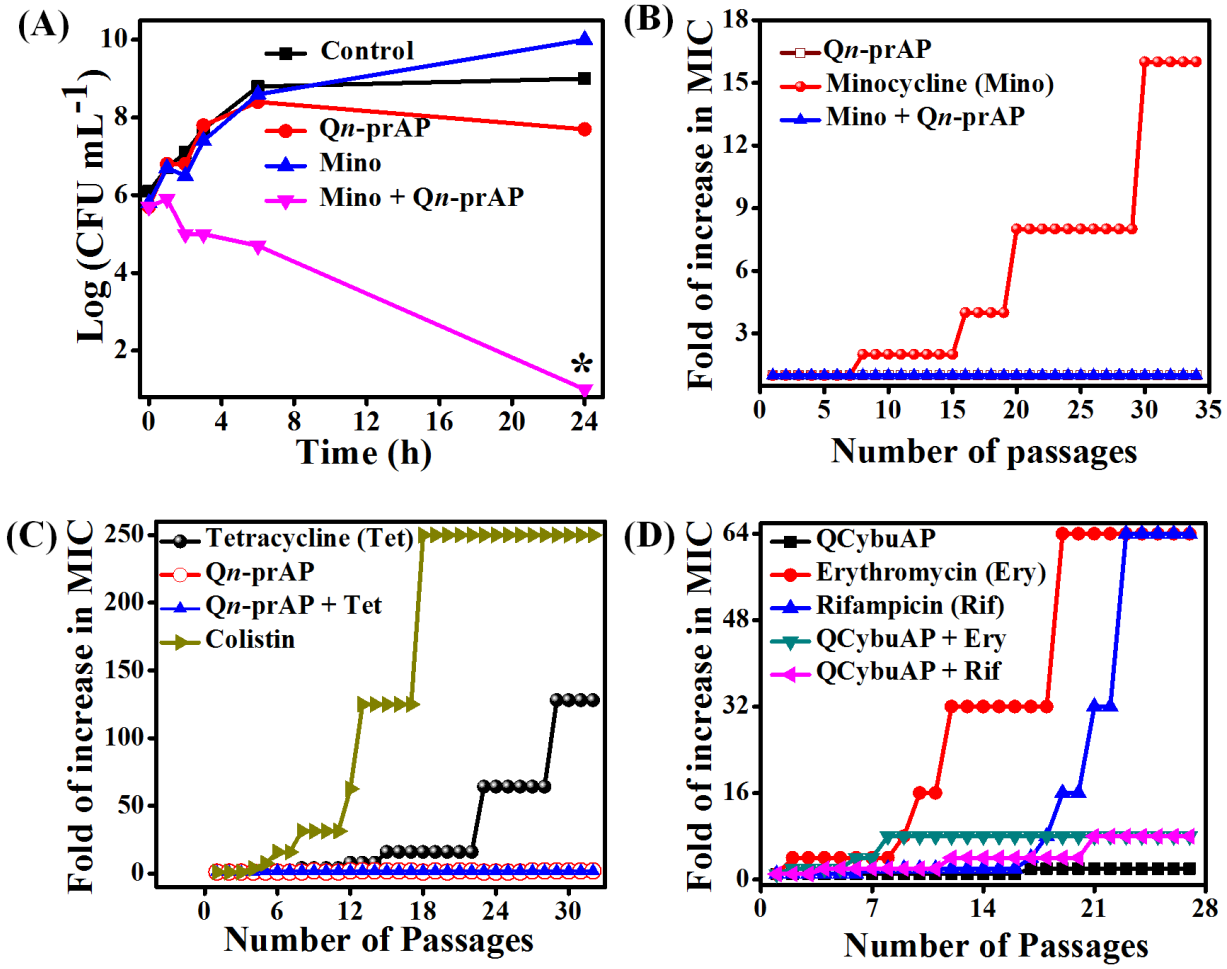

Figure 6.3: Synergy bactericidal activity and development of drug-resistance of polymers and tetracycline antibiotics. (A) The combination of Q*n*-prAP and minocycline (50 µg mL^{-1} + 6.3 µg mL^{-1}) showed synergistic bactericidal activity whereas Q*n*-prAP (50 µg mL^{-1}) alone and minocycline alone (6.3 µg mL^{-1}) were devoid of antibacterial activity (star represents < 50 CFU mL^{-1}, the detection limit of the experiment). (B) Bacteria developed resistance to minocycline alone with increase in MIC up to 400 µg mL^{-1} whereas it did not develop resistance to minocycline (6.2 µg mL^{-1}) in presence of Q*n*-prAP (50 µg mL^{-1}) up to 30 days. Bacteria did not readily develop resistance to Q*n*-prAP. (C) *E. coli* (ATCC 25922) did not develop resistance to polymers. More importantly, resistance against tetracycline alone developed very rapidly but did not develop in presence of Q*n*-prAP. (D) *A. baumannii* developed resistance to erythromycin and rifampicin but not to QCybuAP. QCybuAP delayed bacterial resistance to both the antibiotics.

even after 28 passages (Fig. 6.3 D). Interestingly, in presence of these polymers, *A. baumannii* had low tendency for antibiotic resistance with only 8-fold increase in the MIC of antibiotics at the end of 28 passages. As shown above, these polymers stall the development of bacterial resistance to tetracycline antibiotics in Gram-negative clinical isolates. Since bacteria develop resistance to tetracycline antibiotics primarily due to efflux pumps, these polymers could curb

the resistance development. However, the 8-fold increase in case of erythromycin and rifampicin might be due to their additional genetic mechanisms of resistance such as target site modification or others. Hence, these polymers could delay the development of bacterial resistance to these antibiotics in Gram-negative bacteria. These results suggest that unlike the target-specific antibiotics, non-specific targeting of bacterial cell membrane by these polymers is advantageous as the bacteria find it difficult to develop resistance.

6.2.4 Biofilm disruption in combination with antibiotics

After investigating the combination efficacy in planktonic bacteria, the effect of restoring the antibiotics towards tough-to-kill Gram-negative biofilms established on surfaces has been studied. Established *A. baumannii* MTCC 1425 and *A. baumannii* R674 (multi-drug resistant clinical isolate) bio-films grown on glass cover slips were either treated with QCybuAP, Q*n*-prAP, tobramycin, colistin, erythromycin (Ery), polymer + Ery (all at 30 μg mL^{-1}) or left untreated for 24 h. Biofilms stained with crystal violet were dissolved in 95% ethanol and absorbance was measured at 520 nm. The crystal violet staining evidently showed that both the polymers alone and in combination with erythromycin had higher biofilm disruption properties compared to erythromycin, tobramycin and colistin against both the strains (Fig. 6.4 A). Tobramycin (114% and 116%) had increased biomass compared to the untreated control (100%) against both the strains supporting the observation that amino glycosides promote biofilm formation as previously known in literature [243]. Colistin and erythromycin showed 30%, 43% and 32%, 40% reduction in biomass against *A. baumannii* MTCC 1425 and *A. baumannii* R674 respectively (Fig. 6.4 A). Both the polymers, Q*n*-prAP and QCybuAP alone displayed reduction in biomass by 60-70% whereas in combination with erythromycin they showed 80-90% reduction against *A. baumannii* MTCC 1425 and *A. baumannii* R674 biofilms compared to the untreated biofilms (Fig. 6.4 A).

Dispersed bacteria upon treatment of biofilms with antibiotics represent a dangerous pool of bacteria that cause more tissue damage and can revert to planktonic condition[214]. Importantly, all biofilm dispersal strategies will need to be accompanied by simultaneous antibiotic treatment to eliminate the planktonic bacterial cells that are liberated after dispersion in order to avoid the spread of infection to other parts of the body [24]. Optical density ($O.D._{600}$) of the bacteria that has got dispersed from the *A. baumannii* biofilms and reverted to the planktonic stage during the 24

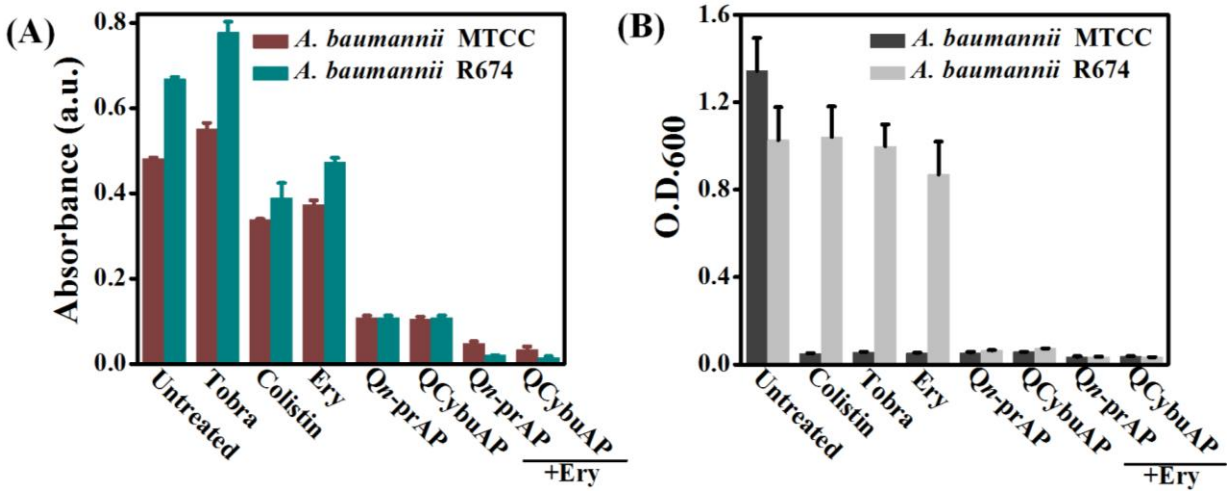

Figure 6.4: Disruption of *A. baumannii* bio-films. (A) Absorbance of the Crystal violet staining of the bio-films grown on glass cover slips in presence of colistin (30 µg mL^{-1}), Q*n*-prAP and QCybuAP (both at 30 µg mL^{-1}), erythromycin (30 µg mL^{-1}), tobramycin (30 µg mL^{-1}), erythromycin + Q*n*-prAP/QCybuAP (30 µg mL^{-1} + 30 µg mL^{-1}). (B) $O.D._{600}$ of the planktonic growth of bacteria due to dispersed cells from the surface established biofilms. Both (A) and (B) correspond to 24 h treated or untreated conditions. *A. baumannii* MTCC 1425 is a sensitive strain and *A. baumannii* R674 is a multi-drug (carbapenem) resistant clinical isolate.

h treatment in the well plates with antibacterial agents has been measured. Interestingly, colistin, tobramycin, erythromycin, polymers and their combination with antibiotics did not allow the growth of planktonic bacteria in the well plates during the 24 h treatment against sensitive strain of *A. baumannii* (MTCC 1425) (Fig. 6.4 B). However, the similar investigations done for biofilms grown from clinical isolate strain of *A. baumannii* R674 showed that the antibiotics did not prevent the growth of planktonic bacteria. Colistin despite being sensitive to *A. baumannii* R674 did not arrest the planktonic growth. On the other hand, polymers alone and in the combination with antibiotics prevented the growth of planktonic bacteria in case of both sensitive *A. baumannii* and clinical isolate strains (Fig. 6.4 B). These results led to the understanding that unlike antibiotics the membrane-active polymers in combination with antibiotics not only disrupted the biofilms but also arrested the planktonic growth of dispersed bacteria from the biofilms.

The confocal laser scanning microscopy (CLSM) images of *A. baumannii* MTCC 1425 biofilms stained with SYTO 9 dye clearly demonstrated the dispersal of biofilm in presence of QCybuAP and Q*n*-prAP (both at 30 µg mL^{-1}) compared to erythromycin (30 µg mL^{-1}) (Fig. 6.5). The effect was more pronounced wherein the combination of polymers and erythromycin

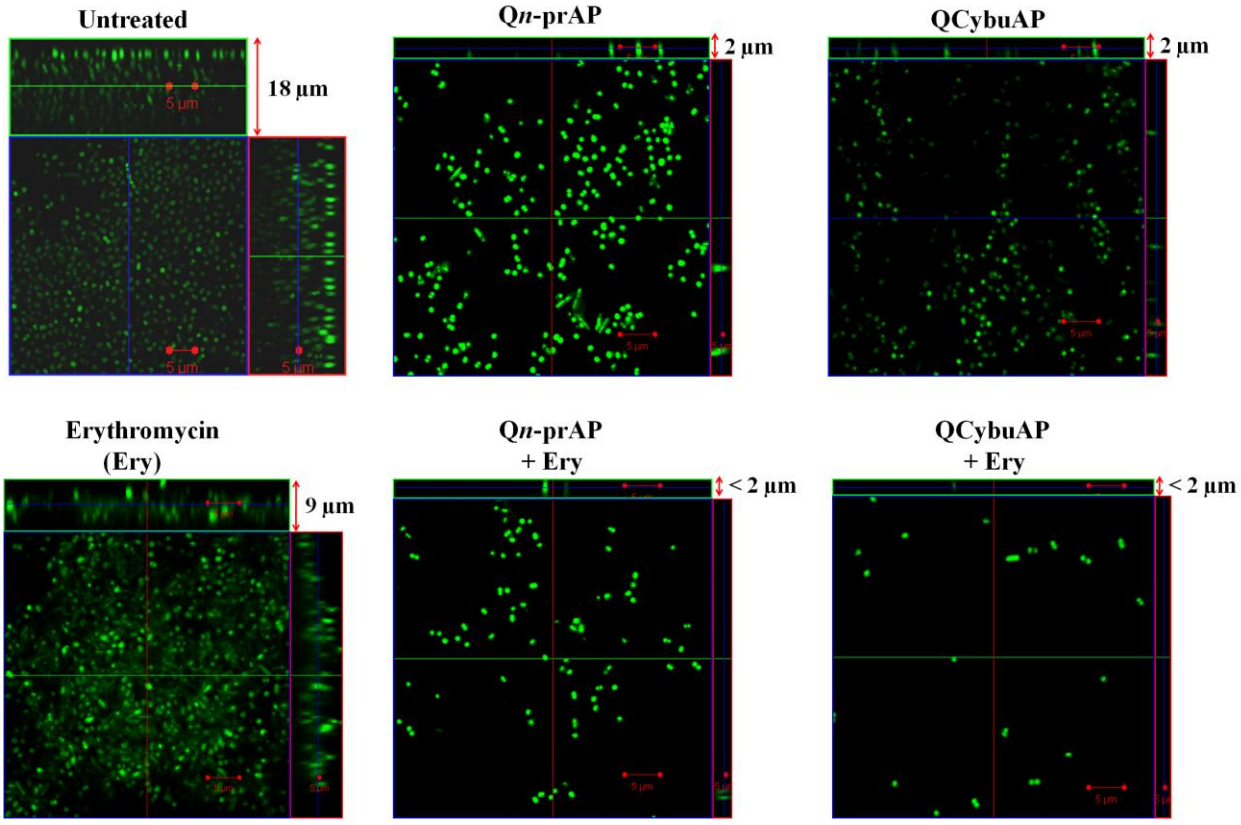

Figure 6.5: *A. baumannii* biofilm disruption properties using confocal laser scanning microscopy (CLSM) stained with Syto 9 dye. Bio-films grown on glass cover slips were either treated with QCybuAP (50 µg mL^{-1}), Q*n*-prAP (50 µg mL^{-1}), erythromycin (50 µg mL^{-1}), erythromycin + QCybuAP (50 µg mL^{-1} + 50 µg mL^{-1}) and erythromycin + Q*n*-prAP (50 µg mL^{-1} + 50 µg mL^{-1}) or left untreated. The central pictures show horizontal optical sections (XY), and the flanking pictures show vertical optical sections (YZ and ZX). Images were processed using Zeiss LSM software. Scale bars, 5 µm.

showed almost complete eradication of bacteria in the biofilms. The orthogonal projections (XY,YZ and ZX) of the biofilms indicated clear differences in reduction of biofilm thickness upon disruption in the presence of polymers. The thickness was found to be 18 µm and 9 µm for the untreated and erythromycin treated biofilms respectively. On the other hand, both the Q*n*-prAP and QCybuAP treated biofilms had a lower thickness of 2.4 µm compared to untreated and erythromycin treated biofilms. Polymers in combination with erythromycin showed a thickness of < 2 µm indicating the presence of single bacterial cells (Fig. 6.5). Mature *E. coli* bio-films were incubated with colistin, QCybuAP, erythromycin, rifampicin, combination of polymers and antibiotics for 24 h. The crystal violet staining evidently showed the disruption of mature *E. coli*

bio-films upon the treatment of combination of polymer and antibiotics than the individual molecules and untreated conditions. Although QCybuAP disrupted *A. baumannii* biofilms, it was inactive against pre-formed *E. coli* bio-films at 50 µg mL^{-1} (Fig. 6.6 A**)**. Colistin too did not show the biofilm eradication properties at 10 µg mL^{-1} against *E. coli* bio-films. However, QCybuAP + erythromycin (50 µg mL^{-1} + 50 µg mL^{-1}) and QCybuAP + rifampicin (30 µg mL^{-1} + 50 µg mL^{-1}) nearly eradicated the pre-formed *E. coli* bio-films. On the other hand, treatment with erythromycin (50 µg mL^{-1}) and rifampicin (30 µg mL^{-1}) did not result in appreciable biofilm disruption (Fig. 6.6 A). Bacterial count enumeration was performed after the treatment of biofilms with the antibacterial agents. QCybuAP + erythromycin (50 µg mL^{-1} + 50 µg mL^{-1}) showed nearly 3 log_{10} reduction in bacterial biomass of *E. coli* bio-films compared to the polymer alone or erythromycin alone and untreated conditions (Fig. 6.6 B). The confocal laser scanning microscopy (CLSM) images stained with Syto 9 dye also clearly demonstrated the complete dispersal of biofilm in the presence of QCybuAP + erythromycin (50 µg mL^{-1} + 50 µg mL^{-1}) compared to the individual molecules and untreated conditions (Fig. 6.6.C). These results showed that the polymers restored the efficacy of antibiotics towards Gram-negative biofilms.

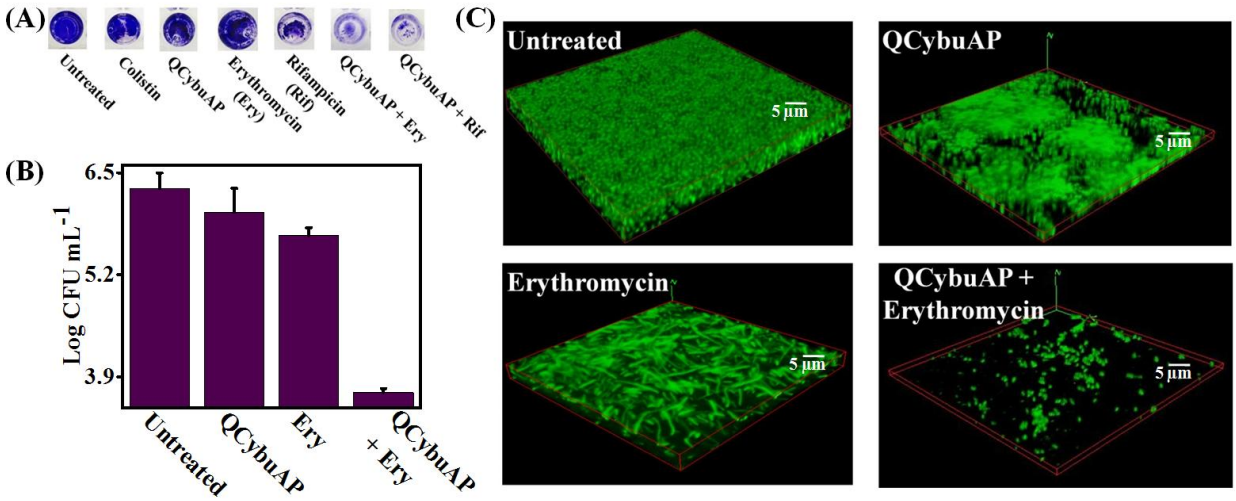

Figure 6.6: Disruption of *E. coli* bio-films. (A) Crystal violet staining of the bio-films grown in polystyrene 96-well plates in presence of colistin (10 µg mL^{-1}), QCybuAP (50 µg mL^{-1}), erythromycin (50 µg mL^{-1}), rifampicin (50 µg mL^{-1}), erythromycin + QCybuAP (50 µg mL^{-1} + 50 µg mL^{-1}) and rifampicin + QCybuAP (50 µg mL^{-1} + 30 µg mL^{-1}). (B) Reduction in bacterial biomass of biofilms grown on glass cover slips. (C) Confocal laser scanning microscopy (CLSM) images of biofilms stained with Syto 9 dye and each image is a 3D reconstruction of z-stack images. Concentrations mentioned in (A) were used for (B) and (C) experiments.

6.2.5 *In-vivo* anti-infective studies

6.2.5.1. *In-vivo* toxicity

The *in-vivo* toxicity studies have been performed as described in Chapter 3. For the combination efficacy of antibiotics and polymers, the mice were given a single i.v. injection of combination of doxycycline and Q*n*-prAP. It was observed that the mice showed no lethal effects after injection of doxycycline + Q*n*-prAP up to 100 mg kg^{-1} + 15 mg kg^{-1} and also doxycycline (100 mg kg^{-1}) alone. This showed that these polymers alone and in combination with antibiotics have low toxicity in mice models and have a good safety profile required for therapeutic applications.

6.2.5.2. Acute burn wound infection

The *in-vivo* antibacterial efficacy studies of combination of polymers and antibiotics were performed in mice using an acute burn wound infection model of *A. baumannii* as described in Chapter 5. Burn wounds were created on the back of the mice using heated brass bars and infected the burn wounds with 10^7 cfu of *A. baumannii* (Fig. 6.7 A). Mice were treated with Q*n*-prAP (50 mg kg^{-1}), minocycline (50 mg kg^{-1}) and Q*n*-prAP + minocycline (50 mg kg^{-1}+ 50 mg kg^{-1}) every 24 h for 5 days. Six days post-infection, untreated mice had an increased bacterial burden of 10 $\log_{10}$ (CFU g^{-1}). Mice treated with Q*n*-prAP showed reduction of 3 $\log_{10}$ of bacterial burden (Fig. 6.7 B). Mice receiving minocycline, a known bacteriostatic antibiotic, showed 3 $\log_{10}$ reductions in bacterial burden. However, mice that had received Q*n*-prAP + minocycline had a high reduction of 6 $\log_{10}$ in the bacterial burden compared to the untreated mice. Histopathological staining of skin tissue sections also revealed that mice treated with Q*n*-prAP + minocycline had recovered from burn wound compared to Q*n*-prAP alone and minocycline alone whereas untreated mice had severe inflammation due to infection (Fig. 6.7 C). Untreated mice showed severe infiltration of inflammatory cells mainly neutrophils and mononuclear cells with congestion of blood vessels (inset) and loss of stratified squamous epithelial cells (arrow). Minocycline and Q*n*-prAP treated mice showed moderate infiltration of inflammatory cells with congestion of blood vessels (inset) and regeneration of stratified squamous epithelial cells with loss of sebaceous and sweat glands (arrow). Q*n*-prAP + Minocycline treated group showed regeneration of the skin with squamous epithelial cells with keratin layers (arrow) and appearance of sebaceous gland, sweat gland and hair follicles (inset).

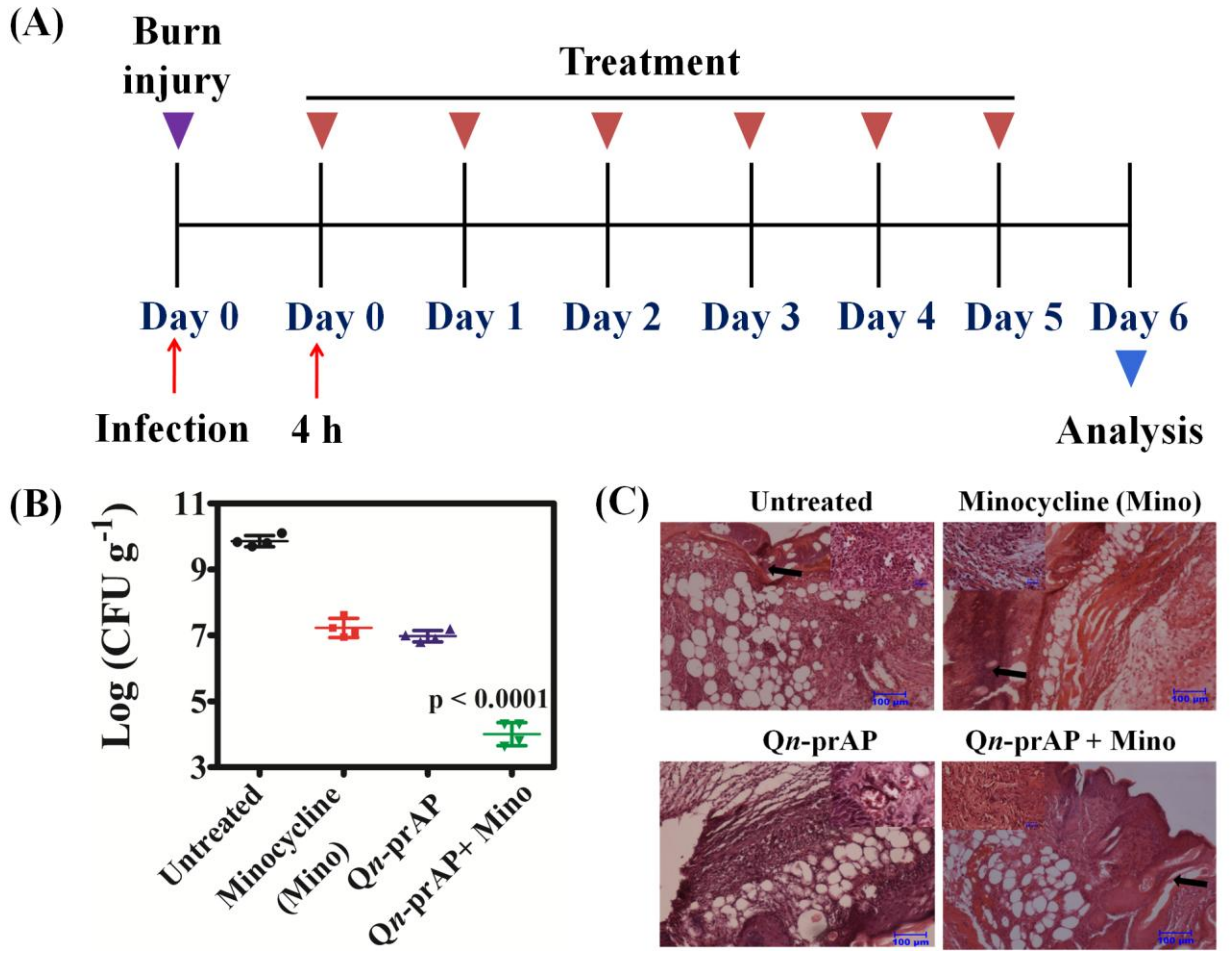

Figure 6.7: *In-vivo* anti-infective studies against *A. baumannii* burn wound infection. Burn wounds were created on the back of mice (n = 4) and infected with 10^7 cfu of *A. baumannii*. Wounds treated every 24 h for 5 days with minocycline (Mino, 50 mg kg^{-1}) and Q*n*-prAP (50 mg kg^{-1}) had 3 log_{10} reduction whereas Q*n*-prAP + Mino (50 mg kg^{-1} + 50 mg kg^{-1}) decreased the bacterial burden by 6 log_{10} reduction compared to the untreated mice. The data are expressed as mean ± standard deviation based on values obtained from four mice (n=4). P value was calculated using Student's *t* test (2 tailed one sample, unpaired distribution) and three stars represent a p value < 0.0001 (D) Haematoxylin and Eosin (H & E) staining of the respective skin sections. Scale bar = 100 µm (inset 20 µm).

In a second *A. baumannii* acute durn wound infection model, mice were treated with QCybuAP (50 mg kg^{-1}), rifampicin (5 mg kg^{-1}) and QCybuAP + rifampicin (50 mg kg^{-1} + 5 mg kg^{-1}) every 24 h for 5 days. Six days post-infection, untreated mice and even rifampicin had a very high bacterial burden of 10-11 log_{10} (Fig. 6.8 A). On the other hand, mice treated with QCybuAP had significant (p = 0.001) decrease of ~3 log_{10} in bacterial burden compared to the untreated mice. More importantly, mice receiving QCybuAP + rifampicin had a very high

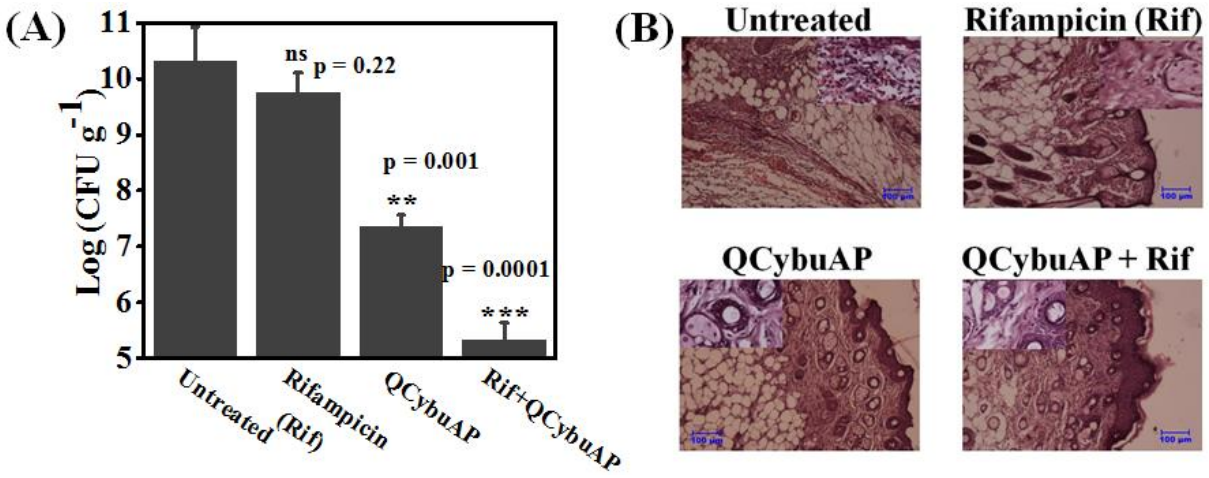

Figure 6.8: *In-vivo* anti-infective activity against *A. baumannii* burn wound infection. (A) Mice were infected with ~7 log(CFU). Mice (n = 4) were treated with rifampicin (5 mg kg^{-1}), QCybuAP (50 mg kg^{-1}) and QCybuAP + rifampicin (50 mg kg^{-1} + 5 mg kg^{-1}). P value was calculated using Student's *t* test (2 tailed one sample, unpaired distribution) and a value of $p < 0.05$ was considered significant. (B) Histopathology analysis of Hematoxylin and Eosin (H&E) stained skin tissue sections. Scale bar 100 µm (inset 20 µm).

significant reduction (p = 0.0001) of 6 log_{10} in the bacterial burden compared to the untreated conditions. Skin histolopathology of control mice without treatment showed infiltration of inflammatory cells mostly neutrophils and mononuclear cells (inset) and damage to squamous stratified epithelial cells (Fig. 6.8 B). Rifampicin treated showing moderate regeneration of stratified squamous epithelial cells with sweat gland and sebaceous glands (inset). QCybuAP treated mice showing regeneration of the skin with squamous epithelial cells with keratin layers, sebaceous gland, sweat gland and hair follicles (inset). QCybuAP + rifampicin treated skin showed recovery from the burn wound with numerous keratin layers, sweat and sebaceous glands and hair follicles (inset). These results suggested that the combination of antibiotics and polymers have the potential for the topical treatment of Gram-negative burn wound infections.

6.2.5.3. Murine Surgical wound infection

The WHO Global Report on Surveillance of Antimicrobial Resistance 2014 shows that *K. pneumoniae* has developed resistance to carbapenems, the last line of available treatment in all WHO regions. Thus, a carbapenemase producing strain of *K. pneumoniae* (KPC) was used in a murine surgical wound infection model for testing the efficacy of polymers in combination with antibiotics. The *bla*KPC gene (DNA fragment at 1011 bp)[244] screening by PCR amplification and

the resulting gel electrophoresis data along with the strain susceptibility data are given in Fig. 6.9 & Table 6.6. Surgical wound were created on the dorsal surface of the mice with 6 mm biopsy punch needles and infected with the multi-drug resistant) carbapenem and tetracycline resistant) *K. pneumoniae*. Wounds were left untreated for 24 h to simulate the conditions for formation of biofilms (Fig. 6. 10 A). Treatment started 24 h post-infection and thereafter every 24 h for 7 days with colistin (5 mg kg^{-1}), tetracycline (100 mg kg^{-1}), Q*n*-prAP (50 mg kg^{-1}) and Q*n*-prAP +

Table 6.6: Antibiotic susceptibility data of *K. pneumoniae*-003259271 (carbapenemase producing strain, KPC) clinical isolate.

Antibiotic	MIC (µg mL^{-1})	Susceptibility
Amikacin MIC	≤16	S
Ampicillin/Sulbactam	>16/8	R
Ampicillin	>16	R
Aztreonam	>16	R
Cefepime	>16	R
Cefotaxime	>32	R
Cefotaxime/K Clavulanate	>4	R
Cefotetan	>32	R
Cefoxitin	NT	NT
Ceftazidime	>16	R
Ceftazidime/K Clavulanate	>2	R
Ceftriaxone	>32	R
Cefuroxime	>16	R
Cephalothin	>16	R
Ciprofloxacin	>2	R
Ertapenem	>4	R
Gemifloxacin	NT	NT
Gentamicin	≤4	S
Imipenem	>8	R
Levofloxacin	>4	R
Meropenem	>8	R
Nitrofurantoin	>64	R
Pipericillin/Tazobactam	>64	R
Piperacillin	>64	R
Tetracycline	>8	R
Tigecycline	≤2	S
Tobramycin	>8	R
Trimethoprim/ Sulfamethoxazole	>2/38	R

S- sensitive, R- resistant, NT- not tested.

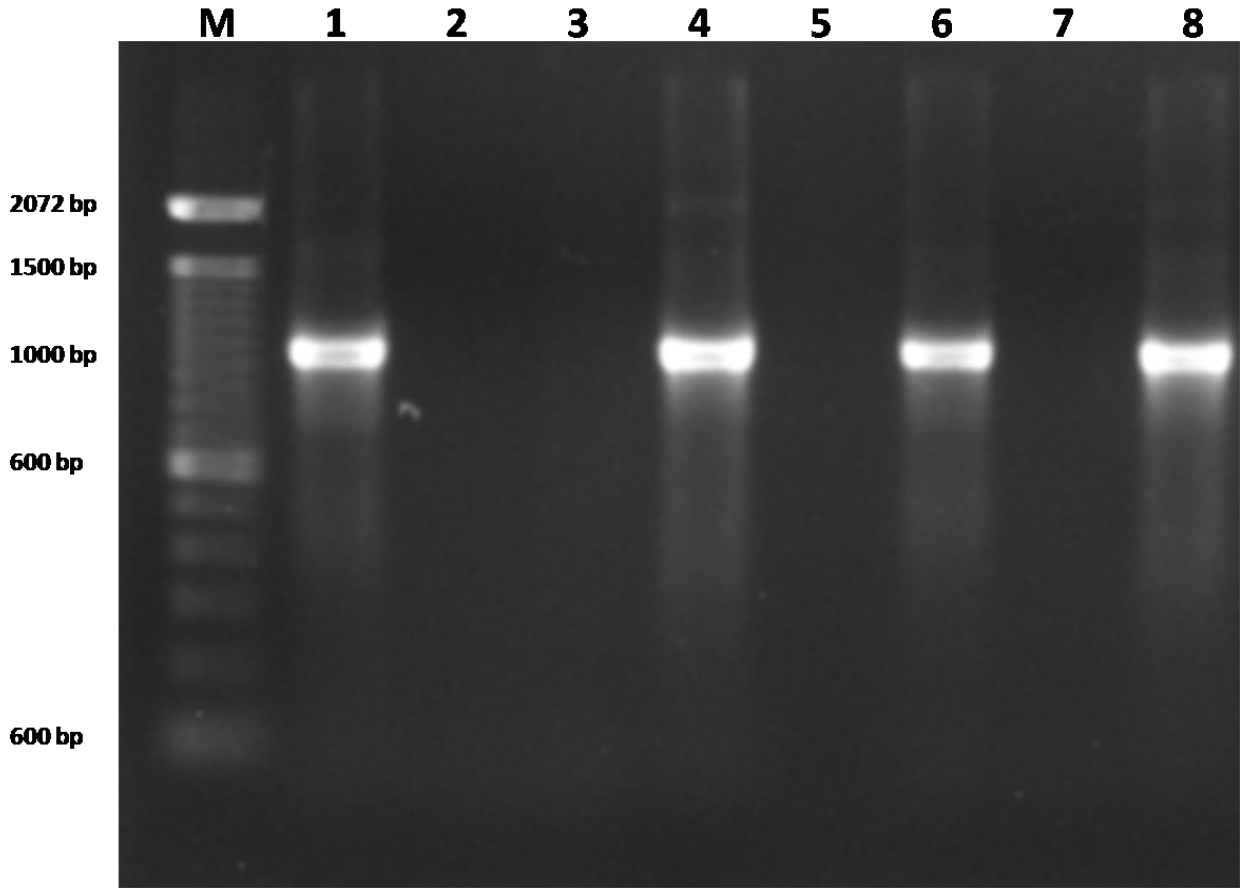

Figure 6.9: Electrophoresis results for the *bla*KPC gene screening by PCR amplification (DNA fragment at 1011bp)[1]. M-100 bp DNA ladder, **Lane 1**, positive control - *K. pneumoniae* IOC4955; **Lane 2**, negative control - *K. pneumonia* ATCC700603; **Lane 3**, Negative clinical isolate - 1; **Lane 4**, 003259271 - *K. pneumoniae*; **Lane 5**, Negative clinical isolate – 2; **Lane 6**, Positive clinical isolate - 1; **Lane 7**, Negative clinical isolate – 3; **Lane 8**, Positive clinical isolate - 2.

tetracycline (50 mg kg^{-1} + 100 mg kg^{-1}). Mice that were left untreated had a very high bacterial burden of 8-9 $\log_{10}$ (Fig. 6.10 B). Tetracycline treatment was found have no effect on the wounds whereas treatment with polymers significantly ($p = 0.001$) reduced the bacterial burden by 3 $\log_{10}$ after 7 days. Interestingly, tetracycline in combination with the polymer reduced the bacterial burden by 5-6 $\log_{10}$ similar to colistin (Fig. 6.10 B).

Histopathology results of the skin infected mice showed clear damage to tissue including little epithelialization, focal inflammation with intense polymorphonuclear (PMNs) and mononuclear cell infiltration, loose irregular connective tissue and initial neovascularisation (Fig.

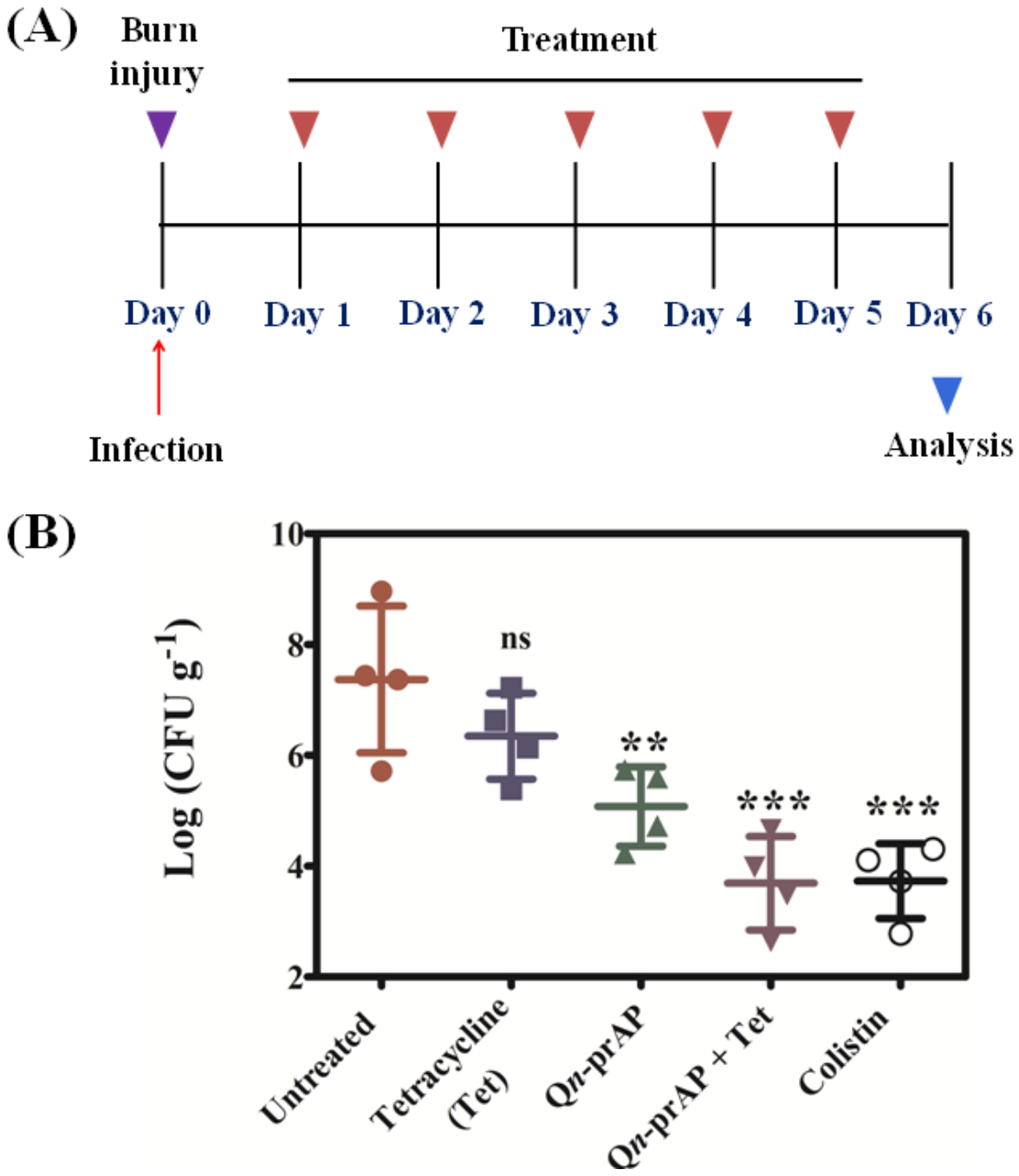

Figure 6.10: *In-vivo* anti-infective activity against *K. pneumoniae* (carbapenem and tetracycline resistant clinical isolate, KPC) surgical wound infection. Mice (n = 4) were infected with ~7 log (CFU). Mice were treated 24 h post-infection with colistin (5 mg kg^{-1}), tetracycline (Tet) (100 mg kg^{-1}), QCybuAP (50 mg kg^{-1}) and QCybuAP + Tet (50 mg kg^{-1} + 100 mg kg^{-1}). A value of $p < 0.05$ was considered significant.

6.11 A & B). Skin histolopathology of mice treated with colistin (Fig. 6.11 B & F), Q*n*-prAP (Fig. 6.11 C & G) and Q*n*-prAP + Tetracycline (Fig. 6.11 D & H) showed a healing process at

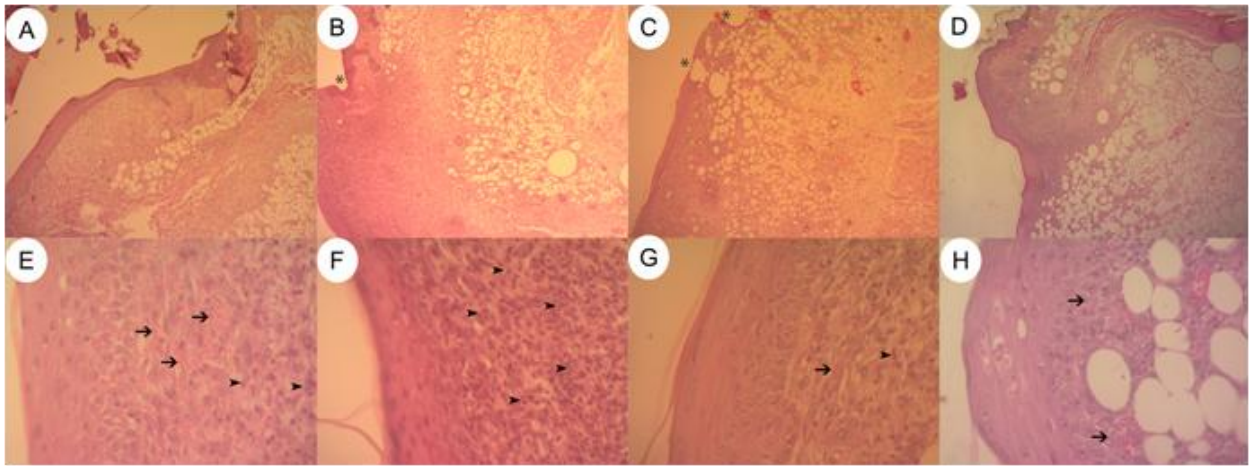

Figure 6.11. Histopathology analyses of mice wounds untreated (A and E) and treated with colistin (B and F), Q*n*-prAP (C and G) and Q*n*-prAP + Tetracycline (D and H). Arrows show blood vessels, arrowhead shows polymorphonuclear infiltration and asterisk shows epithelialization área. All images were perfomed in 5 replicates.

infection site damaged by the pathogen. It has been shown that colistin developed rapid resistance to Gram-negative bacteria including the carbapenem resistant strains (Fig. 6.3 C). On the contrary, bacteria do not develop resistance to the combination of polymer and antibiotic. Thus, this combination of membrane-active polymers in combination with antibiotics has enormous potential for the treatment of Gram-negative infections without developing bacterial resistance.

6.2.6 Mechanism of resensitization of antibiotics

Mechanistic studies were performed in tetracycline resistant $bla_{\text{NDM-1}}$ *E. coli* (R3336) and tetracycline sensitive *E. coli* (ATCC 25922) to understand the mechanism of re-sensitization of tetracycline antibiotics. Tetracycline is fluorescent in aqueous solutions and it is reported that there is an enhancement in its fluorescence as it traverses the bacterial membranes[228, 245]. The uptake of tetracycline (100 μg mL^{-1}) alone was less and slow in $bla_{\text{NDM-1}}$ *E. coli* (R3336) as shown in Fig. 6.12. In presence of the polymers (20 μg mL^{-1}), $bla_{\text{NDM-1}}$ *E. coli* (R3336) had a much higher and faster uptake of tetracycline compared to tetracycline alone (Fig. 6.12). Similarly, the higher uptake was observed even with tetracycline sensitive *E. coli* (ATCC 25922) (Fig. 6.13 A). The mechanism of re-sensitization can be attributed to this enhanced and faster uptake of tetracycline.

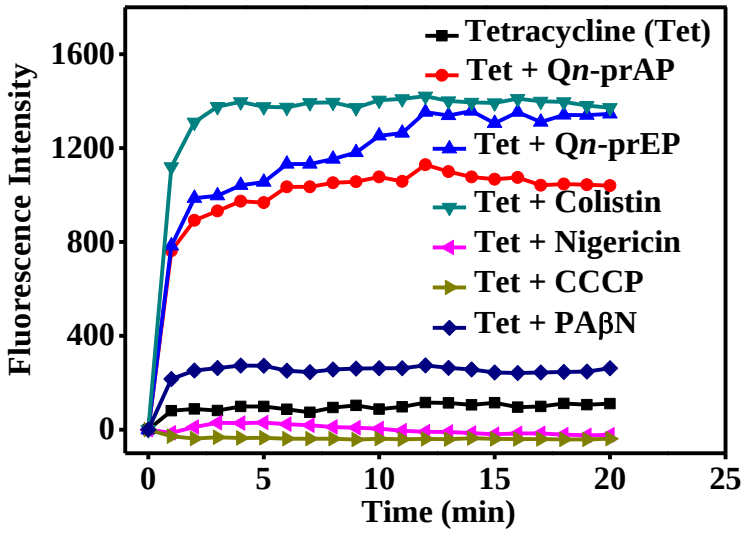

Figure 6.12: Uptake of tetracycline and membrane-active properties of polymers against bla_{NDM-1} *E. coli* (R3336). (A) Uptake of tetracycline by increase in its fluorescence in presence of Q*n*-prAP, Q*n*-prEP (both at 20 μg mL^{-1}), PAβN (50 μg mL^{-1}) and colistin (30 μg mL^{-1}) as well as in the presence of CCCP and nigericin (both at 10 μg mL^{-1}). Tetracycline was used at 100 μg mL^{-1}. Relative fluorescence was calculated by subtracting the fluorescence without the bacteria from the fluorescence of bacteria containing samples.

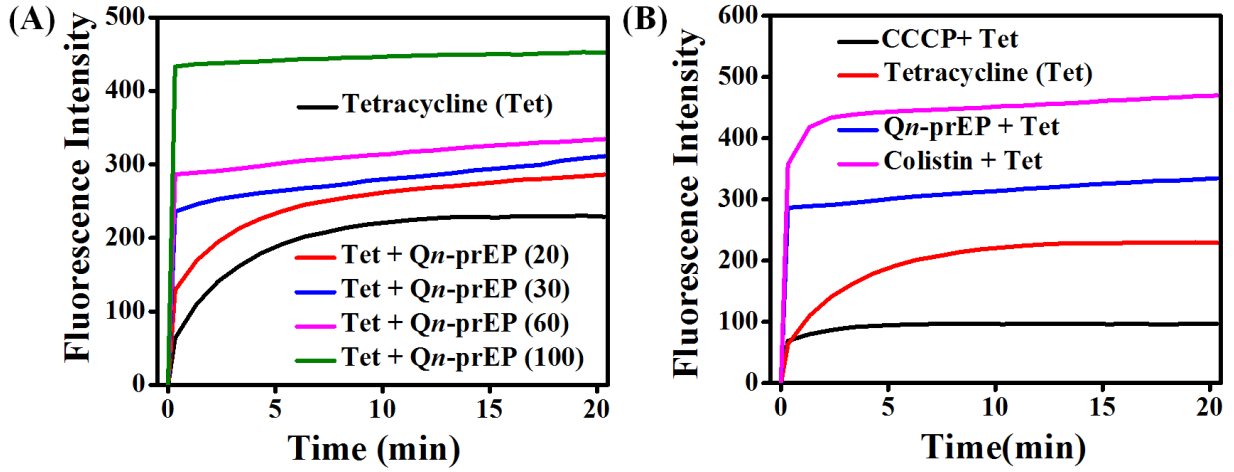

Figure 6.13: Mechanistic studies using tetracycline sensitive *E. coli* (ATCC 25922). (A) *E. coli* had much faster and higher uptake of tetracycline (Tet) in presence Q*n*-prEP (20, 30, 60 and 100 μg mL^{-1}) than tetracycline alone (100 μg mL^{-1}). (B) Colistin and Q*n*-prEP (both at 60 μg mL^{-1}) increased whereas CCCP (5 μg mL^{-1}) decreased the uptake of tetracycline (100 μg mL^{-1}).

In a pursuit to determine the driving force for this higher uptake of tetracycline, the membrane-active properties of cationic amphiphilic polymers has been investigated. The urge to do so stem from the fact that tetracycline is known to accumulate in bacteria through ΔpH

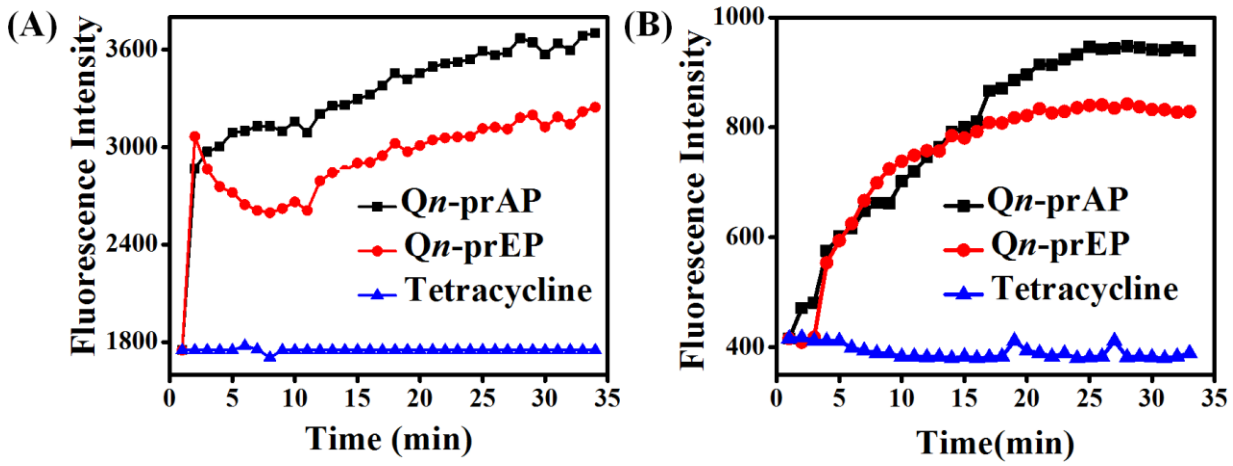

Figure 6.14: Membrane-active properties of polymers against *bla*$_{NDM-1}$ *E. coli* (R3336). (A) Dissipation of membrane potential by increase in the fluorescence of $DiSC_3(5)$ with the treatment of Q*n*-prAP and Q*n*-prEP (both at 100 µg mL^{-1}). (B) Membrane permeabilization by increase in the fluorescence of propidium iodide (PI) with the treatment of Q*n*-prAP and Q*n*-prEP (both at 100 µg mL^{-1}).

(transmembrane pH) gradient[246]. Bacteria maintain an intact proton motive force (PMF) across the cell membrane that is a combination of transmembrane electrical potential (ΔΨ) and ΔpH [247]. Using a fluorescence assay, the cytoplasmic membrane depolarization by polymers in *bla*$_{NDM-1}$ *E. coli* (R3336) has been measured (Fig. 6.14 A). Polymers selectively dissipated the ΔΨ component of the PMF as seen in the increase of fluorescence of $DiSC_3(5)$ when added at 100 µg mL^{-1} (Fig. 6.14 A). Q*n*-prAP showed higher cytoplasmic membrane depolarization than Q*n*-prEP (Fig. 6.14 A). This observation supports the fact that Q*n*-prAP displayed higher synergy and re-sensitization profiles than Q*n*-prEP (Table 6.3 & 6.4). Tetracycline alone did not have any effect on the ΔΨ of bacteria (Fig. 6.14 A). Even against tetracycline sensitive *E. coli* (ATCC 25922), Q*n*-prAP has higher dissipation of membrane potential than Q*n*-prEP as shown in previous chapters. This selective dissipation of ΔΨ by polymers led us to the hypothesis that membrane potential might play a role in the mechanism of re-sensitization.

To support this hypothesis, the uptake studies of tetracycline in *bla*$_{NDM-1}$ *E. coli* (R3336) have been performed in presence of CCCP (carbonyl cyanide *m*-chlorophenyl hydrazone) that is known to abolish PMF and nigericin which is known to selectively dissipate ΔpH [246]. Bacteria in presence of both nigericin and CCCP (both at 10 µg mL^{-1}) had a decreased uptake of tetracycline (Fig. 6.12). Whereas, in presence of polymers (both at 20 µg mL^{-1}) and colistin (30 µg mL^{-1}), increased uptake of tetracycline was observed compared to tetracycline alone (Fig. 6.12). PAβN

(phenyl arginine-β-naphthylamide), a very well known efflux pump inhibitor of Gram-negative bacteria has been shown to restore the efficacy of antibiotics[248]. PAβN at 50 μg mL^{-1}, to a lesser extent, also increased the uptake of tetracycline (Fig. 6.12). Even tetracycline sensitive *E. coli* (ATCC 25922) had a lower uptake in presence of CCCP whereas colistin and polymers had an increased uptake of tetracycline (Fig. 6.13 A). As tetracycline is known to accumulate in the bacteria through ΔpH dependent pathway [246], CCCP and nigericin resulted in a decreased uptake of tetracycline. However, polymers dissipate the ΔΨ component of the PMF that might have to be compensated by an increase in the ΔpH component driving the uptake of tetracycline. It has been reported that CCCP and nigericin inhibits tetracycline accumulation whereas valinomycin, which specifically cancels the ΔΨ, does not inhibit the accumulation [246].

Polymers when added at 100 μg mL^{-1}, increased the permeability of propidium iodide (PI) to bacterial cell membranes as seen by the increase of its fluorescence whereas tetracycline alone does not have any effect on membrane permeability (Fig. 6.14 B). Q*n*-prAP caused higher cytoplasmic membrane permeabilization than Q*n*-prEP which further facilitated the uptake of tetracycline antibiotics (Fig. 6.14 B). Similar results were also observed with tetracycline sensitive *E. coli* (ATCC 25922). Overall, the mechanism of restoring the efficacy can be attributed to the membrane-active properties of polymers that enabled the uptake of tetracycline both in tetracycline resistant and sensitive strains.

Clinically approved drugs (loperamide)[228], 2-aminoimidazoles[229], acyl lysine oligomers (OAKs)[234], polycarbonates[235], silver (Ag^{+})[198], Ianthelliformisamines[238] and cationic cobaltocenium-containing polymers[239] were found to be antibiotic-enhancers against bacteria. These reports taken together with the data, suggest that the synergy to different antibiotics mostly depends on the nature of the membrane-active agent used in combination to them. These observations and mechanistic studies suggest that the synergy is indeed selective to tetracycline antibiotics but not to other intracellular antibiotics like macrolides, fluoroquinolones and aminoglycosides. To a large extent, bacteria develop resistance to tetracycline antibiotics by excluding them through RND-efflux pumps whereas; other intracellular antibiotics have additional major mechanisms of resistance such as target modification and inactivating enzymes[6]. So, it is the membrane-active properties of polymers that increased the uptake of tetracycline antibiotics giving them a backdoor entry into the bacteria that are otherwise excluded through the efflux pumps. However, as shown here and by other reports, since

polymers dissipate the ΔΨ, the uptake of aminoglycosides is not favorable as they need the ΔΨ for their uptake[228]. Despite the fact that membrane-active properties of polymers can facilitate the entry of other intracellular antibiotics, target modification and inactivating enzymes can play a major role in making them ineffective.

In a pursuit to determine the role of efflux pumps in the mechanism of antibiotic resensitization, the antibiotic restoration ability of these polymers and PAβN has been investigated for Linezolid and Vancomycin. Linezolid, an oxazolidinone class of antibiotic, is ineffective against Gram-negative bacteria due to resistance by efflux pumps and other mechanisms. Gram-negative bacteria are also resistant to Vancomycin, a glycopeptide antibiotic, due to inability to cross the additional outer membrane in them. It has been observed that Linezolid and Vancomycin were resistant to *E. coli* with MIC of 100 μg mL^{-1} and >100 μg mL^{-1} respectively (Table 6.7). In presence of both Q*n*-prAP and PAβN, MIC of Linezolid was decreased to 12.5-25 μg mL^{-1} whereas no effect was observed for Vancomycin against *E. coli*. Moreover, the MIC of erythromycin and rifampicin were decreased to 0.1-0.8 μg mL^{-1} in presence of 12.5 μg mL^{-1} and 25 μg mL^{-1} of PAβN towards *E. coli* (MIC of PAβN = 50 μg mL^{-1}). It has been shown that these polymers and PAβN, to a lesser extent increase the uptake of tetracycline antibiotics (efflux pumps are the mechanism of resistance) in Gram-negative bacteria as the mechanism of resensitization (Fig. 6.12). These results indicated two observations: i) these polymers and PAβN restore the efficacy of antibiotics that are excluded by efflux pumps by Gram-negative bacteria and ii) both these agents do not restore the efficacy of antibiotics that possess other mechanisms of resistance for e.g. Linezolid and Vancomycin. These polymers dissipating the transmembrane potential thereby affect the efflux pump activity and also cause the membrane permeabilization. The present results make us believe that these polymers indirectly inhibit the action of efflux pumps (unlike PAβN, a classical efflux pump inhibitor) and restore the efficacy of expunged antibiotics from Gram-negative bacteria [232] but this certainly needs further investigations. Wright and co-workers have elegantly shown that a class of anthracycline derivatives dissipate the membrane potential and inhibit the efflux pump activity of Gram-negative bacteria[249]. These derivatives were shown to potentiate the Gram-positive antibiotics to Gram-negative bacteria.

The highlight of the results is that planktonic Gram-negative bacteria is inherently resistant to erythromycin and rifampicin due to their exclusion by efflux pumps and the polymer

Table 6.7: Antibiotic resensitization in presence of Q*n*-prAP and PAβN in *E. coli*.

Antibiotics	**MIC of antibiotic (μg mL^{-1})**			
	-Polymers	**+Q*n*-prAP** (μg mL^{-1})		**+PAβN[a]** (μg mL^{-1})	
		6.25	12.5	12.5	25
Erythromycin	38	1.6	0.8	0.8	0.4
Rifampicin	8	1.6	0.2	0.4	0.1
Linezolid	100	25	12.5	25	12.5
Vancomycin	>100	>100	>100	>100	>100

[a]PAβN- phenyl arginine β-naphthylamide.

showed efficacy in combination with these antibiotics against tough-to-kill biofilms. The ability of these polymers to disrupt the cell membranes might pave the way for erythromycin and rifampicin that are otherwise excluded from the Gram-negative bacteria due to efflux pumps. These results suggest that antibiotics are less effective against the metabolically inactive persisters as well as biofilms. In contrast, the cationic polymers displayed good activity against actively growing, stationary phase as well as the persister cells of Gram-positive and Gram-negative bacteria at low concentrations with membrane-active mechanism of action. The anti-biofilm activity of the polymer could be achieved in combination with antibiotics. The cationic charge of these polymers might interact with the negatively charged EPS of biofilms thereby weakening the biofilms. In the context of increasing evidence for role of efflux pumps in the tolerance of biofilms[62,232] to antibiotics, the use of efflux pump inhibitors (such as PAβN) alone or in combination with antibiotics has been shown to inhibit/disrupt biofilms. The indirect inhibition of efflux pumps might have resulted in further weakening of the biofilms. Hence, as shown above, the indirect inhibition of efflux pumps due to dissipation of membrane potential by these polymers might have improved the antibiotic efficacy even in biofilms leading to disruption and killing of bacteria. The present findings underscore the importance of non-specific targeting of cell membrane for the elimination of bacterial persisters and eradication of biofilms.

6.3 Conclusions

In conclusion, the current crisis of MDR Gram-negative superbugs coupled with the lack of suitable antibiotics establishes the need for alternative approaches to target them. To address this problem, combination of membrane-active polymers and antibiotics were used. These polymers re-sensitized tetracycline antibiotics with >80-1250 fold of reduction in their MIC towards MDR and *bla*$_{\text{NDM-1}}$ pathogens, *E. coli* and *K. pneumoniae*. Also, the synergistic combination was found to be bactericidal unlike tetracycline antibiotics that are bacteriostatic in activity. Mechanistic studies showed that bacteria had higher uptake of tetracycline in presence of polymers. Bacteria did not develop resistance to polymers, unlike to colistin, and moreover polymers stalled the development of bacterial resistance to antibiotics. Polymers displayed membrane-active properties that had driven the uptake of tetracycline in bacteria. Polymers have strong implications in halting the antibiotic resistance that would otherwise lead to rapid emergence of bacterial resistance. These findings stress the importance of combination approaches of membrane-active molecules and antibiotics to combat MDR Gram-negative superbugs. These polymers potentiated the antibiotics to disrupt and kill the Gram-negative biofilms. More importantly, the polymers in combination with antibiotics reduced the bacterial burden in surgical and burn wound infections caused by Gram-negative bacteria. Collectively, these findings support the potential implications of this combination approach of membrane-active polymer and antibiotics for the topical treatment of Gram-negative bacterial infections.

6.4 Experimental section

6.4.1 Bacterial strains

Clinical samples were from Department of Neuromicrobiology, National Institute of Mental Health and Neuro Sciences, Hosur Road, Bangalore 560029, India and *K. pneumoniae* 003259271 (Hodge test positive, *bla*$_{\text{KPC}}$ positive and *bla*$_{\text{NDM-1}}$ negative) was from Lacen, Laboratorio Central, Brasília, DF, Brazil. Bacterial identification was performed by the Vitek 2 Compact 60 system, bioMerieux, France and Gram-negative bacteria were screened for carbapenem resistance using Kirby-Bauer disc diffusion method (data not shown).

6.4.2 PCR and gel-electrophoresis

The *bla*$_{NDM-1}$ gene was identified using the primers NDM-F (5′-GGG CAG TCG CTT CCA ACG GT-3′) and NDM-R (5′-GTA GTG CTC AGT GTC GGC AT-3′) (Eurofins Genomics India Pvt. Ltd., Bangalore) which amplified an internal fragment of 475 bp using conventional polymerase chain reaction (PCR). The conditions included an initial denaturation step of 5 min at 94 ºC, followed by 30 cycles of 30s at 95 ºC, 30s at 60 ºC and 30s at 72 ºC, and then a final extension step of 5 min at 72 ºC. The PCR products were analyzed in 2% agarose gel, containing 0.05 mg/liter ethidium bromide, at 100V for 1h in 1X Tris Acetate EDTA buffer. A 100 bp DNA ladder was used as a molecular weight marker (SRL Biolit™, Mumbai India). Bands were visualized under UV light and an amplified product corresponding to 475 bp was considered as positive.

6.4.3 Antibacterial activity: chequer board assays

The combination antibacterial efficacy of polymers and antibiotics was measured in nutrient broth using chequer board assays in the following manner. A solution of 25 µL each of antibiotic and polymers was added into each well of a 96 well plate followed by 150 µL of bacterial suspension (~5.0×10^5 CFU mL^{-1}) and incubated at 37 °C for 24 h. Bacterial suspension alone and nutrient broth alone served as controls. Each MIC was a result of two independent experiments.

6.4.4 Bactericidal time-kill kinetics

Briefly, *bla*$_{NDM-1}$ *E. coli* R3336 was grown in nutrient broth at 37 °C for 6 h. Test compounds were inoculated with the aliquots of bacteria resuspended in fresh media at ~1.8×10^5 CFU mL^{-1}. After specified time intervals (0, 1, 2, 3, 6, and 24 h), 20 µL aliquots were serially diluted 10 fold in 0.9 % saline, plated on sterile MacConkey agar plates and incubated at 37 °C overnight. The viable colonies were counted the next day and represented as $\log_{10}$ (CFU mL^{-1}).

6.4.5 Drug resistance study

In brief, the first MIC determination of polymers, tetracycline antibiotics and polymers + tetracycline antibiotics was performed as described above (Antibacterial activity: chequer board assays). Bacteria from triplicate wells at the concentration of one-half MIC were removed and

used to prepare the bacterial dilution (~5.0×10^5 CFU mL^{-1}) for the next experiment. These bacterial suspensions were then used to perform the antibacterial assay that was repeated for 32 passages. The fold of increase in MIC was determined by normalizing the MIC at passage n to that of the first passage (MIC_n/MIC_1).

6.4.6 *K. pneumoniae* surgical wound infection

All procedures including care and handling of animals were approved by the Ethics Committee of the Catholic University of Brasilia (Number 005/13). Female C57BL/6 mice (8-10 weeks old) were obtained from animal facility of the Catholic University of Brasilia. The murine surgical wound infection model was performed as described previously [250-252] with minor modifications. Mice (n = 4 per group) were anesthetized, their dorsal surface shaved and a puncture was performed using 6-mm punch biopsy needles (Stiefel Laboratories, UK) and then 20 µL of clinical isolate of tetracycline-resistant *K. pneumoniae* (carbapenemase producing strain, KPC) suspension (2×10^9 CFU mL^{-1}) was introduced into the puncture wound. Wounds were treated every 24 h with 20 µL of a solution containing 50 mg kg^{-1} of Q*n*-prAP, 100 mg kg^{-1} of tetracycline, 5 mg kg^{-1} of colistin, 100 mg kg^{-1} + 50 mg kg^{-1} of tetracycline + Q*n*-prAP and a group not treated served as negative control. Mice were euthanized 7 days post-surgery and the wounded tissue was excised, weighed, and homogenized in 1 mL of PBS. Serial homogenate dilutions were plated in triplicate on Muller Hinton agar (Himedia, India) and the results were stated as log (CFU g^{-1}) of tissue. P value was calculated using one way ANOVA (Dunnett's Multiple Comparison Test) between the control group and treatment groups and a value of $P < 0.05$ was considered significant. Histopathology was performed as described previously[253].

6.4.7 Uptake of tetracycline[228]

The uptake of tetracycline was measured through enhancement in its fluorescence as it enters the bacterial cell membranes. Bacteria was grown in LB media (OD_{600} ~0.5). The bacteria were harvested, washed and resuspended in 10 mM HEPES (4-(2-hydroxyethyl)-1-piperazineethanesulfonic acid) buffer (pH = 7.2). PAβN, CCCP and nigericin were dissolved in dimethyl sulfoxide (DMSO) and diluted further in 10 mM HEPES. Always, a freshly made tetracycline solution in water was used owing to its low solubility. All the other test compounds were dissolved in water at 4 mg mL^{-1} and diluted further in HEPES. A bacterial suspension of

100 µl in HEPES containing the test drugs at required concentration (100 µl) was taken for the fluorescence measurements in a Corning 96 well black plate with clear bottom. The fluorescence of tetracycline was monitored using a Tecan InfinitePro series M200 Microplate Reader at the excitation of 405 nm and emission was collected at 535 nm at room temperature for 30 min for Figure 6.12. For, Figure 6.13, a bacterial suspension of 2 ml in HEPES containing the test drugs at required concentration (100 µL) was taken for the fluorescence measurements using PerkinElmer LS-55 Luminescence Spectrometer. The fluorescence was measured at the excitation of 405 nm and emission was collected at 535 nm (excitation and emission slit widths at 10 nm) at room temperature for 20 min. The readout is reported as Tet Fluorescence (a.u.) which is the relative fluorescence calculated by subtracting the background from the fluorescence of bacteria containing samples. The fluorescence of tetracycline alone or in presence of polymers without the bacteria was used as the background. We found no quenching of the fluorescence of tetracycline in presence of polymers compared to tetracycline alone without bacteria.

Chapter 7

Endotoxin Neutralization by Cationic-amphiphilic Polymers

Abstract

Bacterial endotoxins such as lipopolysaccharide (LPS) cause sepsis that is responsible for a great amount of mortality worldwide. In this chapter, cationic-amphiphilic polymers that bind and cause LPS neutralization and detoxification are reported. Levels of pro-inflammatory cytokines in human monocytes caused by LPS stimulation were inhibited by more than 80% when co-incubated with these polymers. These reductions were found to be dependent on concentration and more importantly, on the side chain chemical structure due to variations in the hydrophobicity profiles of these polymers. Using fluorescence studies, dynamic light scattering and electron microscopy of LPS, it was obderved that these polymers bind but neither dissociate nor promote LPS aggregation. Binding of polymer to LPS might lead to sort of a pseudo-aggregate formation resulting in LPS neutralization/detoxification. These findings provide an unusual mechanism of LPS neutralization using novel synthetic cationic amphiphilic polymers.

(1) Uppu, D. S. *et al.* "Lipopolysaccharide Neutralization by Cationic Amphiphilic Polymers through Pseudo-aggregate Formation". *Biomacromolecules*. **2016**. Under Revision.

7.1 Introduction

Flourishing bacterial resistance to antibiotics coupled with languishing antibiotic discovery creates an urgent need for the development of new antimicrobial agents which exert novel mechanisms of action[7]. In the past two decades, antimicrobial peptides (AMPs) have received increasing attention due to their broad-spectrum activities and ability to combat multi-drug-resistant microbes[81-85, 93]. Apart from broad spectrum antimicrobial activity, AMPs also possess anti-endotoxin/anti-inflammatory properties. For e.g. AMPs such as LL-37, Indolicidin human lactoferrin-derived peptide[254] and Buforin II bind to bacterial endotoxins (pathogen associated molecular patterns (PAMPs)) such as lipopolysaccharide (LPS) from Gram-negative bacteria that otherwise result in uncontrollable and harmful inflammation leading to sepsis[63, 64, 255-258]. This uncontrolled inflammation is due increased production of pro-inflammatory cytokines such as TNF-α (tumor necrosis factor- α), IL-6 (Interleukin-6) from macrophages/monocytes that cause septic shock[63, 64]. Globally, an estimated 18 million cases of sepsis occur each year resulting in 8 million casualties[65]. Every hour, about 36 people die from sepsis. It causes more deaths than prostate cancer, breast cancer and HIV/AIDS combined. One million children die in the first four weeks of life every year in India and out of these deaths, 190,000 are caused by sepsis. As far as the management modalities are concerned there is no specific treatment available to control sepsis other than antibiotics. However, it has been found that some of the conventional antibiotics fail to control this harmful inflammation and unfortunately some antibiotics even aggravate the sepsis disease condition. The current crisis of antibiotic resistance makes even the little beneficial effects of antibiotics unavailable for the sepsis treatment. Over 30% of neonatal sepsis deaths are attributed to antibiotic resistance[65].

LPS, a major component of the outer membrane of Gram-negative bacteria, contains an O-antigen (O-polysaccharide), core oligosaccharide and Lipid A[63]. The activation mechanism of macrophages by LPS starts when it (through its toxic entity, lipid A) binds with LPS binding protein (LBP), accelerating the binding of LPS to CD14 (primary receptor of LPS). The LPS-CD14 complex initiates intracellular signaling by interacting with the transmembrane protein Toll-like receptor-4 (TLR-4), which activates the NF-κB transcription factor, resulting in the production and secretion of pro-inflammatory cytokines[64]. LPS, a negatively charged hydrophobic molecule, spontaneously self-assembles to form aggregates in aqueous solutions[63, 64]. Recognition of LPS by either soluble or cell surface receptors need the native aggregate

structure of LPS[63, 64]. Most of the amphiphilic molecules (including antimicrobial peptides (AMPs)) reported till now interact with LPS aggregates accompanied by aggregate dissociation[256, 259-266] whereas Polymyxin B (PMB)[267], $rBPI_{21}$[268] and ultrashort AMPs[269] have been shown to promote LPS aggregation and hence inhibits cytokine secretion. Small molecular antibacterials have been shown to possess anti-inflammatory[270-274] or immunomodulatory properties[275-277]. Polyvalent dendrimer glucosamine conjugates with immunomodulatory properties have also been reported[278]. In some of the cases molecular mechanism of inhibiting cytokine secretion has not been investigated. Cationic amphiphilic polymers mimicking the AMPS with potent antibacterial activity and low toxicity have extensively been reported[105, 107]. However, cationic and amphiphilic antibacterial polymers with anti-endotoxin properties, to the best of the knowledge, have not been reported. The advantage of using polymers is due their multivalent (hydrophobic, electrostatic and hydrogen bonding interactions) nature. Amphiphilic polymers with cationic charge, hydrophobicity and amide moieties can efficiently bind to negatively charged hydrophobic LPS thereby prevent its binding to the receptors and hence inhibit cytokine secretion.

In this chapter, cationic-amphiphilic polymers based on poly(isobutylene-alt-*N*-alkyl maleimide) backbone with anti-endotoxin properties are reported. The side chain chemical structure of these amphiphilic polymers has been found to play role in their LPS neutralization and detoxification properties leading to inhibiting cytokine secretion (TNF-α and IL-6) in human monocytes. Interestingly, using fluorescence spectroscopy, dynamic light scattering (DLS) and electron microscopy, it was found that these amphiphilic polymers interact with LPS aggregates but rather do not lead to aggregate dissociation. More importantly, that these polymers significantly decreased bacterial burden and also reduced the infiltration of inflammatory cells near the site of infection in a mouse model of *Acinetobacter baumannii* burn wound infection.

7.2 Results and Discussion

7.2.1 Synthesis

The synthesis of the polymers was as described in Chapter 2 (Q*n*-PenP, Q*n*-prAP, Q*n*-prEP and Q*n*-BEGP) and Chapter 4 (QCybuAP, Q*n*-buenAP, QCyprAP, Q*i*-prAP and Q*n*-buynAP) (Scheme 7.1).

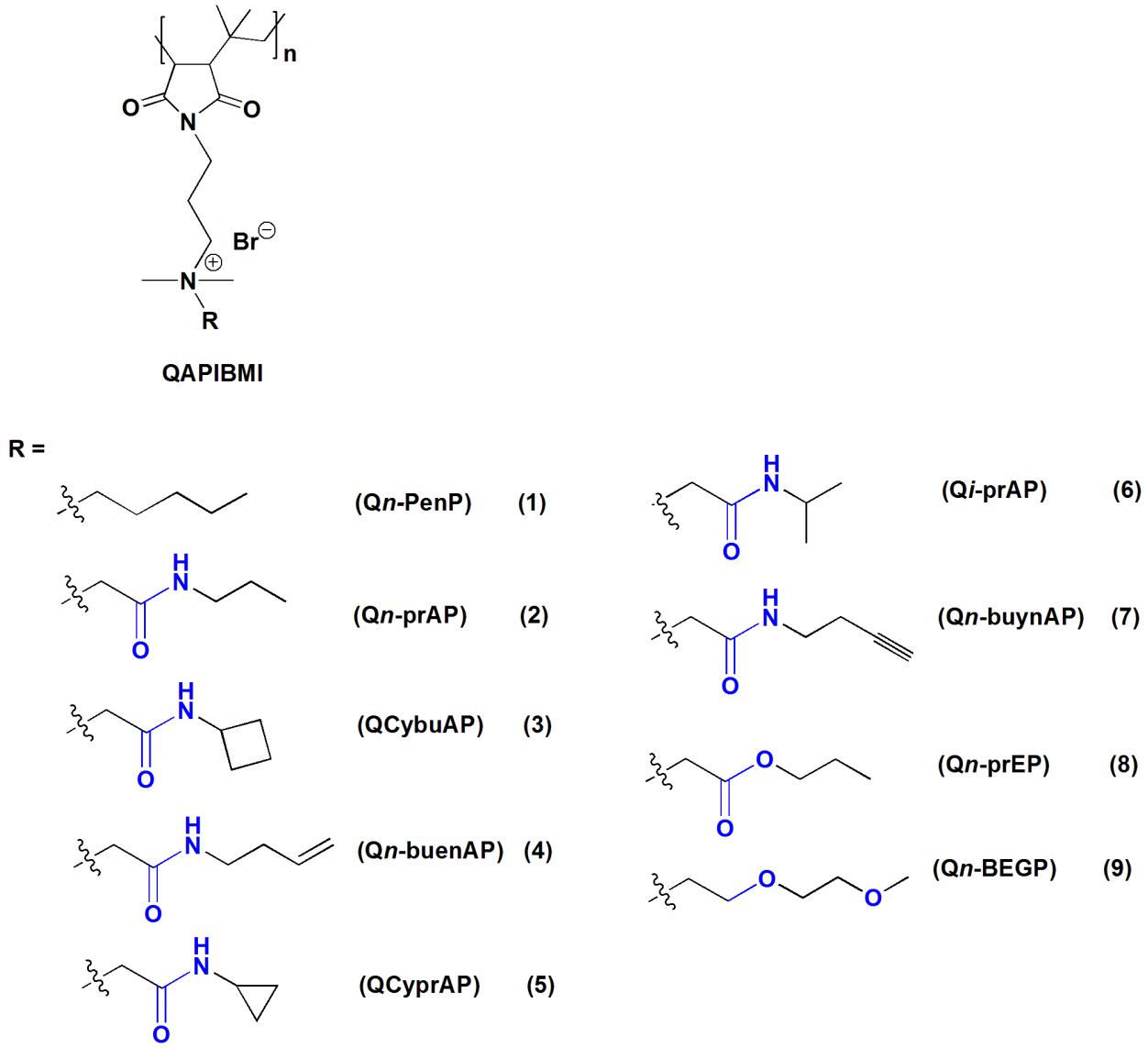

Scheme 7.1: Chemical structures of cationic amphiphilic polymers.

7.2.2 Anti-endotoxin properties

Human peripheral blood mononuclear cells (hPBMCs) were isolated from fresh human blood using Ficoll-Hypaque density centrifugation technique. These are the monocytes circulating in the peripheral human blood that get stimulated by bacterial endotoxins and lead to inflammatory response. Before proceeding with the anti-endotoxin studies, the cytotoxicity of these polymers against hPBMCs was evaluated by measuring the release of lactate dehydrogenase (LDH). Q*n*-PenP had 40% whereas all the other polymers had ~20% release of LDH even at 100 µg mL^{-1}, the highest concentration tested (Fig. 7.1 A). Next, hPBMCs were stimulated with LPS (20 ng

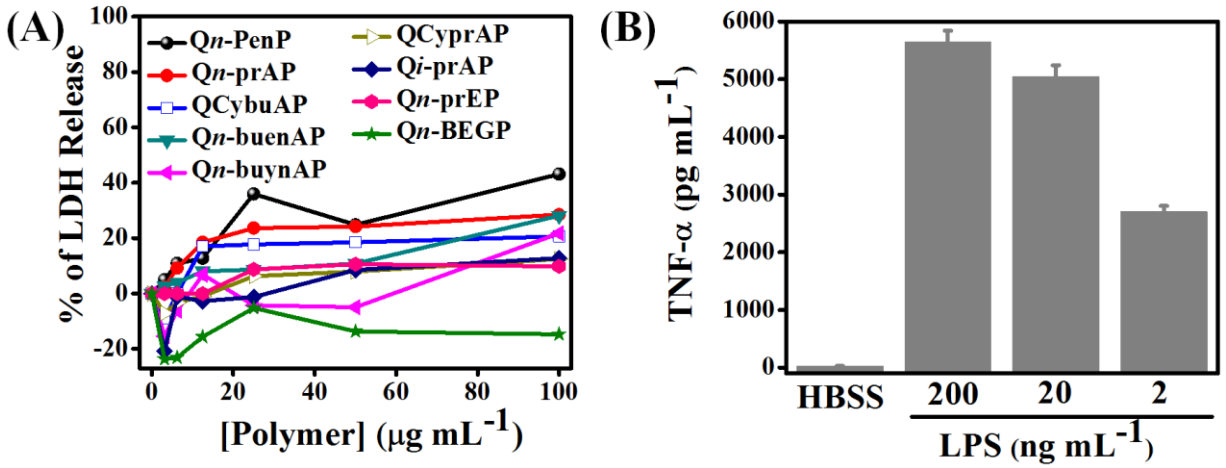

Figure 7.1: (A) Cytotoxicity of human PBMCs measured by the release of lactate dehydrogenase (LDH) due to membrane permeabilization. Percentage of LDH release after treatment with polymers containing different side chain structures. (B) Stimulation of hPBMCs with LPS. Secretion of TNF-α after stimulation with different concentrations of LPS.

mL^{-1}) in the presence and absence of these amphiphilic polymers and the corresponding secretion of pro-inflammatory cytokines, TNF-α and IL-6 were measured using ELISA. LPS from *E. coli* O111:B4, a strain of considerable interest has been used because of its pathogenicity. This strain of *E. coli* was discovered in 1945 to be the main cause of nonspecificgastroenteritis of babies and is still frequently isolated from babies suffering from acute diarrheal episodes[279]. Concentration dependent stimulation of LPS on hPBMCs was studied and it was found that 20 ng mL^{-1} is the minimum concentration that can produce high levels of cytokine response (Fig. 7.1 B). Polymers were used at 10 μg mL^{-1}, 20 μg mL^{-1} and 30 μg mL^{-1}. Polymers alone did not increase the production of cytokines. Amphiphilic polymers with different side chain structures were used to understand their effect towards anti-inflammatory properties.

LPS when co-incubated with 20 μg mL^{-1} of Q*n*-PenP, Q*n*-prAP and QCybuAP (more hydrophobic polymers) had more than 80% inhibition of cytokine secretion compared to LPS alone (Fig. 7.2 A & B). Q*n*-BEGP, the highly hydrophilic polymer, co-treated with LPS had no effect on the inhibition of either of the cytokines. Q*n*-buenAP, QCyprAP, and Q*i*-prAP reduced the LPS induced production of TNF-α by 60-70% and of IL-6 by 30-40%, compared to LPS alone. Co-incubation of LPS with Q*n*-buynAP and Q*n*-prEP though reduced TNF-α secretion by 20-40%, did not inhibit IL-6 production compared to LPS. All the polymers also showed

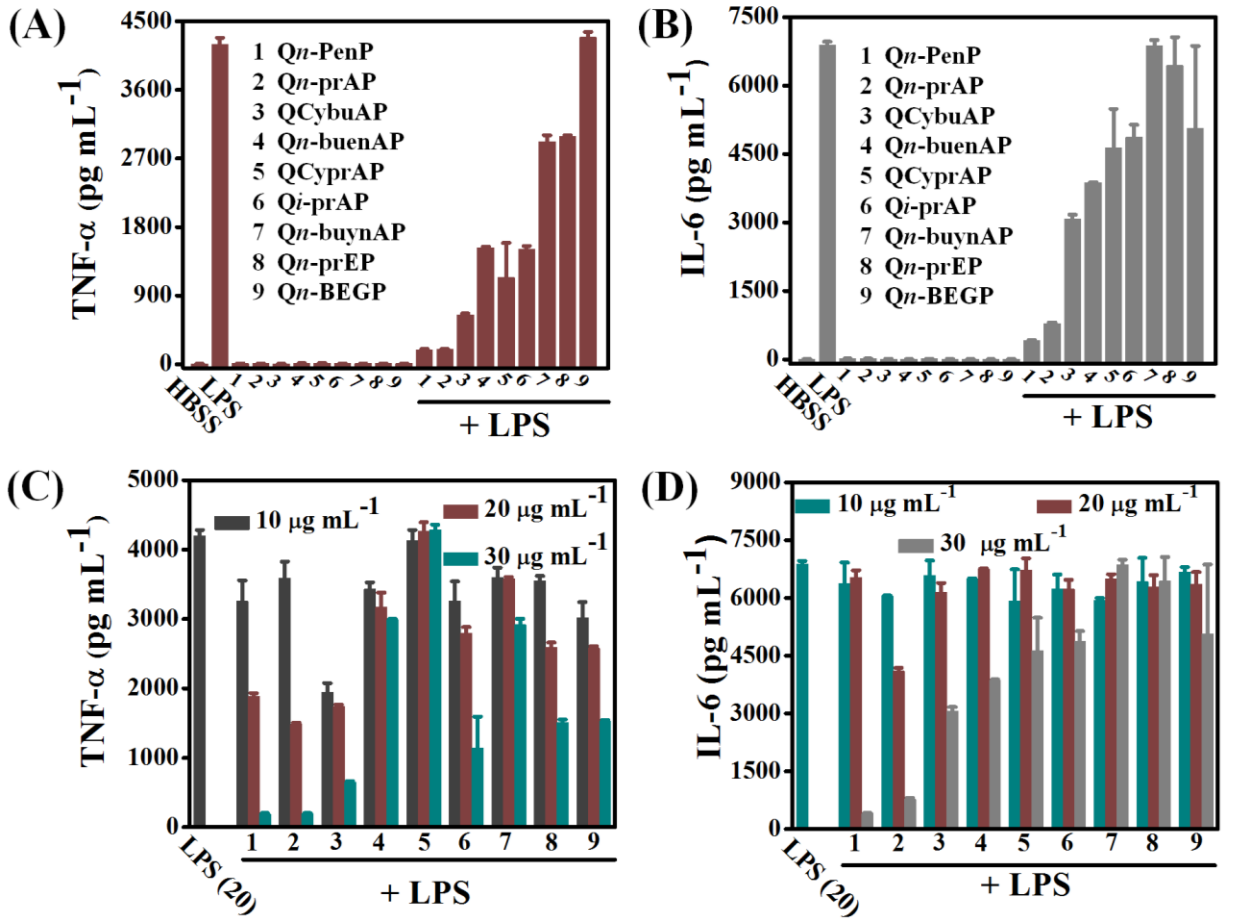

Figure 7.2: Secretion of pro-inflammatory cytokines. Production of TNF-α (A &C) and IL-6 (B & D) after stimulation of hPBMCs with LPS (in the parenthesis 20 ng mL^{-1}) in presence of polymer at 20 μg mL^{-1} and at various concentrations of different side chain structure. Polymers alone were also used as controls. Hank's balance salt solution (HBSS) was used as negative control.

concentration dependent effect on the inhibition of cytokine secretion depending on their side chain structure and the hydrophobicity (Fig. 7.2 C & D). These results suggest that the inhibition of LPS stimulated cytokine secretion is dependent on the hydrophobicity of the polymers, which in turn depends on the side chain chemical structure.

7.2.3 Hydrophobicity profiles

The differences in the anti-inflammatory profiles of all polymers prompted us to determine the variations in their hydrophobicity profiles. The hydrophobicity profiles of the polymers were investigated using reverse-phase high performance liquid chromatography (RP-HPLC) by observing the absorbance at 220 nm on a C-18 column (Fig. 7.3) as described in Chapter 4. The

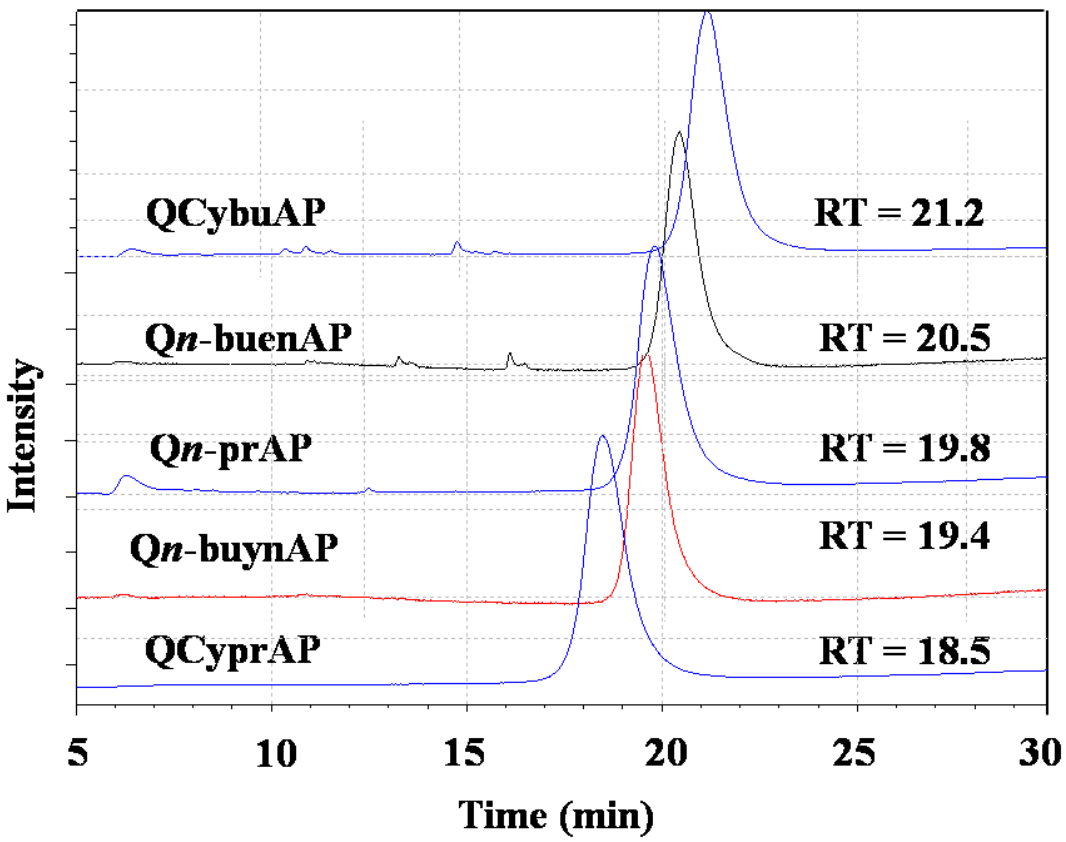

Figure 7.3: Chromatograms (reverse phase-high performance liquid chromatography, RP-HPLC) of polymers having different side chains displaying different retention times (RT).

retention time (RT in min) of the polymers varied with respect to differences in hydrophobicity as well as side chain chemical structure. QCybuAP had high RT of 21.2 min followed by 20.5 min for Q*n*-buenAP. Q*n*-prAP, Q*n*-buynAP and QCyprAP showed RT values of 19.8, 19.4 and 18.5 min. These results suggest that the variations in the side chain structure leads to tunable hydrophobicity of the polymers. The change in the hydrophobicity profiles of these polymers with different sidechain structure, to some extent explains the trends in anti-endotoxin properties.

7.2.4 LPS binding by BODIPY-LPS fluorescence

In a pursuit to determine the binding properties of these polymers to LPS, experiments were performed using BODIPY dye conjugate of LPS (BLPS) (Molecular Probes Inc.). BODIPY conjugate of LPS (BODIPY-LPS) has its fluorescence quenched due to aggregation of LPS. The fluorescence increases in presence of an amphiphilic molecule that can dissociate LPS aggregate structure [280]. The fluorescence of BLPS (0.5 µg mL^{-1}) increased in the presence of 2% sodium

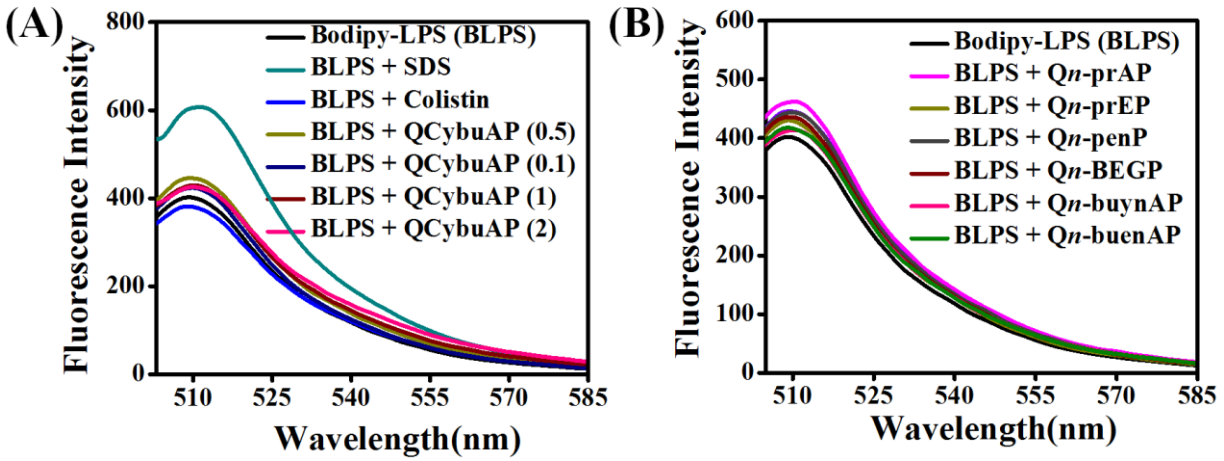

Figure 7.4: LPS binding in presence of amphiphilic molecules. Fluorescence intensity of 0.5 µg mL^{-1} of BLPS measured in presence of sodium dodecyl sulphate (2% SDS), colistin (0.5 mg mL^{-1}), QCybuAP (0.1 mg mL^{-1}, 0.5 mg mL^{-1}, 1 mg mL^{-1}, & 2 mg mL^{-1}) (A) and polymers with different side chain chemical structure (all at 0.5 mg mL^{-1}) (B).

dodecyl sulphate (SDS) whereas it decreased in presence of colistin (Polymixin E) (0.5 mg mL^{-1}) compared to BLPS alone (Fig. 7.4 A). These results indicated that SDS binds and dissociates LPS aggregates and hence increase the fluorescence to a great extent as known in literature [280]. Polymixin derivatives (colistin) were found to bind and promote the aggregation of LPS resulting in a decrease of fluorescence as reported in literature for Polymixin B binding to LPS [267]. On the other hand, fluorescence of BLPS increased in presence of polymers (0.5 mg mL^{-1}) but to a lesser extent compared to SDS (Fig. 7.4 A). The variations in the increase of fluorescence were found to be dependent on the side chain chemical structure (Fig. 7.4 B). Concentration dependent effect of QCybuAP binding to BLPS was also studied. Either increasing or decreasing concentration of QCybuAP from 0.5 mg mL^{-1} decreased the fluorescence of BLPS (Fig. 7.4 A). Polymers bind and cause changes in the aggregate structure of LPS which was evident through increase in fluorescence of BLPS. Thus, these findings led to the understanding that the polymers bind to LPS but whether they dissociated (like SDS) or promoted (like colistin) LPS aggregate structure could not be explained with this experiment.

7.2.5 LPS binding by dynamic light scattering

Further, to probe polymer binding to LPS, Dynamic light scattering (DLS) studies were performed. Polydisperse size distribution of LPS (12.5 µg mL^{-1}) aggregates due to its

spontaneous self-assembly in aqueous solutions was observed (Fig. 7.5). However, co-incubation of LPS and QCybuAP (12.5 μg mL^{-1} + 12.5 μg mL^{-1}) resulted in a monodisperse size distribution with no larger changes in hydrodynamic diameter compared to LPS alone. LPS + Q*n*-PenP, LPS + Q*n*-prAP also had monodisperse size distribution. However, LPS + Q*n*-prEP and LPS + Q*n*-BEGP had polydisperse size distribution as compared to LPS alone. Interestingly, the effect of polymer binding to LPS was studied with respect to light scattering intensity and mean count rate (KCPS (kilo counts per second)) in DLS measurements. These effects were studied for polymers with different side chain chemical structures. The intensity is naturally weighted according to the scattering intensity of each particle fraction which increases as the density or number of particles increase. Light scattering intensity (%) increased to 10% (LPS + Q*n*-PenP) and 12% (LPS + Q*n*-prAP and LPS + QCybuAP) whereas LPS + Q*n*-prEP and LPS + Q*n*-BEGP had same as LPS (8%) (Fig. 7.6 A). This suggests that the particle density increase for LPS co-treated with Q*n*-PenP, Q*n*-prAP and QCybuAP but not those with Q*n*-prEP and Q*n*-BEGP compared to LPS alone. Mean count rate or KCPS in DLS is simply the number of photons detected and is usually stated in a "per second" basis. This is useful for determining the sample quality, by monitoring its stability as a function of time. It was found that the count rates increased in the order of LPS, LPS + Q*n*-PenP, LPS + Q*n*-prAP and LPS + QCybuAP and decreased for LPS + Q*n*-prEP and LPS + Q*n*-BEGP (Fig. 7.6 B). These results indicated that the stability of the LPS aggregates increase in presence of Q*n*-PenP, Q*n*-prAP and QCybuAP but not in presence of Q*n*- prEP and Q*n*-BEGP. The above mechanistic studies suggest that LPS binding by these cationic amphiphilic polymers is the mechanism of LPS neutralization. The variations in binding characteristics of different polymers with different side chain chemical structures also explained the ability of differential inhibition of cytokine secretion in hPBMCs.

7.2.6 Influence of side chain chemical structure in LPS neutralization

Since the cationic charge density of the cationic-amphiphilic polymers is nearly constant, the role of electrostatic interaction in LPS binding may be similar for these polymers with different side chain chemical structures.

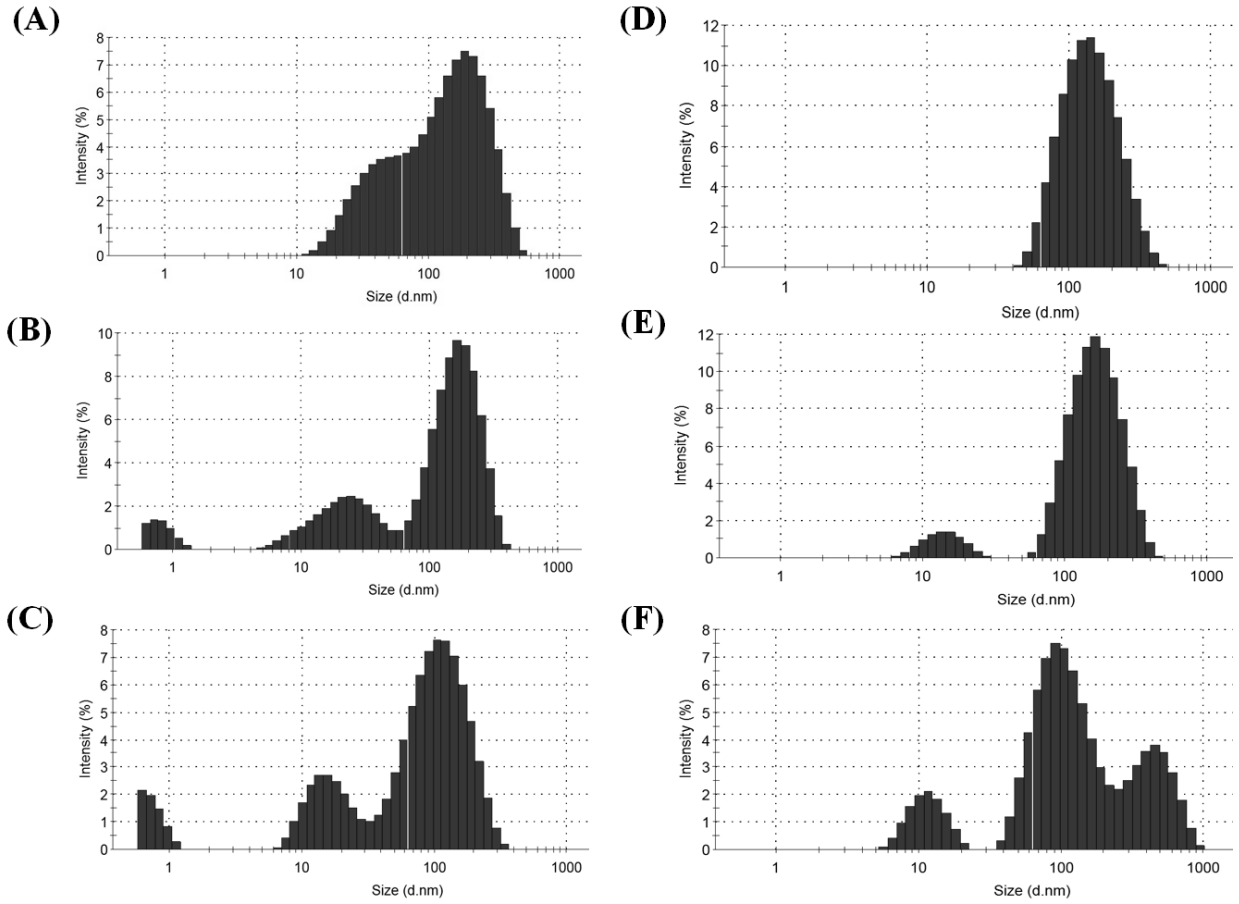

Figure 7.5: LPS binding studies of polymers using dynamic light scattering (DLS) studies. Size distribution of LPS (A), LPS + Q*n*-PenP (B), LPS + Q*n*-prEP, LPS + QCybuAP, LPS + Q*n*-prAP and LPS + Q*n*-BEGP. LPS was used at a concentration of 12.5 µg mL^{-1} and LPS: polymer at 12.5 µg mL^{-1} + 12.5 µg mL^{-1}.

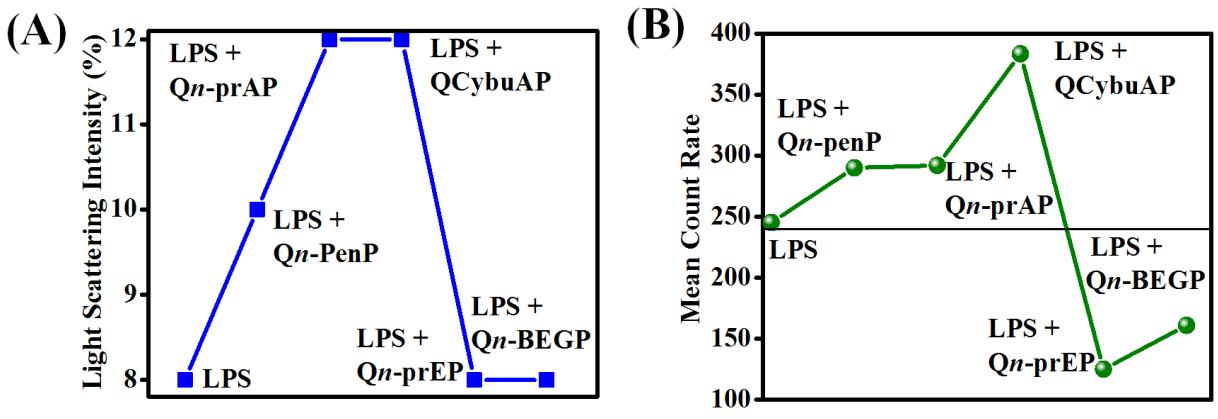

Figure 7.6: LPS binding and dissociation in presence of amphiphilic. Light scattering intensity (A) and mean count rate (KCPS (kilo counts per second)) (B) of LPS alone and in presence of polymers with different side chain chemical structure.

7.2.6.1 Hydrophobic/hydrophilic ratio

The highly hydrophilic polymer, Q*n*-BEGP showed no inhibition of cytokine production due to its inability to bind LPS. Whereas the higher hydrophobic polymers (Q*n*-PenP) and amide moiety containing (Q*n*-prAP, QCybuAP) polymers bind strongly to LPS and thereby inhibit LPS induced cytokine secretion to a great extent in hPBMCs. The weaker LPS binding polymers with ester moieties (Q*n*-prEP) and unsaturation (Q*n*-buynAP) in the side chains due to their reduced hydrophobicity had weaker inhibition of cytokine production. These results suggest that amphiphilicity (hydrophobic/hydrophilic ratio) of these polymers play an important role in LPS binding and neutralization.

7.2.6.2 Role of hydrogen bonding

All the amide side chain containing polymers (Q*n*-prAP, QCybuAP, Q*n*-buenAP, QCyprAP and Q*i*-prAP) showed greater LPS neutralization compared to the corresponding ester polymer, Q*n*-prEP. This indicated the role of strong hydrogen bonding interactions in amide polymers for LPS neutralization compared to that of ester polymers.

Overall, these results suggest that LPS binding by these cationic polymers might have been mediated through a concoction of electrostatic, hydrophobic and hydrogen bonding interactions that are tunable by varying the side chain chemical structure. More importantly, unlike the amphiphilic small molecules/AMPs or PMB/ $rBPI_{21}$/ultrashort AMPs, these polymers bind but neither dissociates nor promotes LPS aggregation (Fig. 7.7). Binding of polymer to LPS might lead to some sort of a pseudo-aggregate formation (Fig. 7.7) and result in LPS neutralization/detoxification. This pseudo-aggregate formation got evident from the BODIPY-LPS binding studies which showed that increase of fluorescence in presence of polymers is less than that of SDS and more than that of colistin. Thus, these polymers bind and transiently dissociate LPS aggregate structure and revert to a stable pseudo-aggregate containing both the oppositely charged macromolecules (anionic LPS and cationic polymer). These conclusions were also supported by DLS studies. The advantage of this mode of binding compared to the LPS disaggregation approach is that the pseudo-aggregate formation might also lead to phagocytosis by the immune cells (e.g. macrophages) thereby completely eliminating the presence or effect of endotoxins.

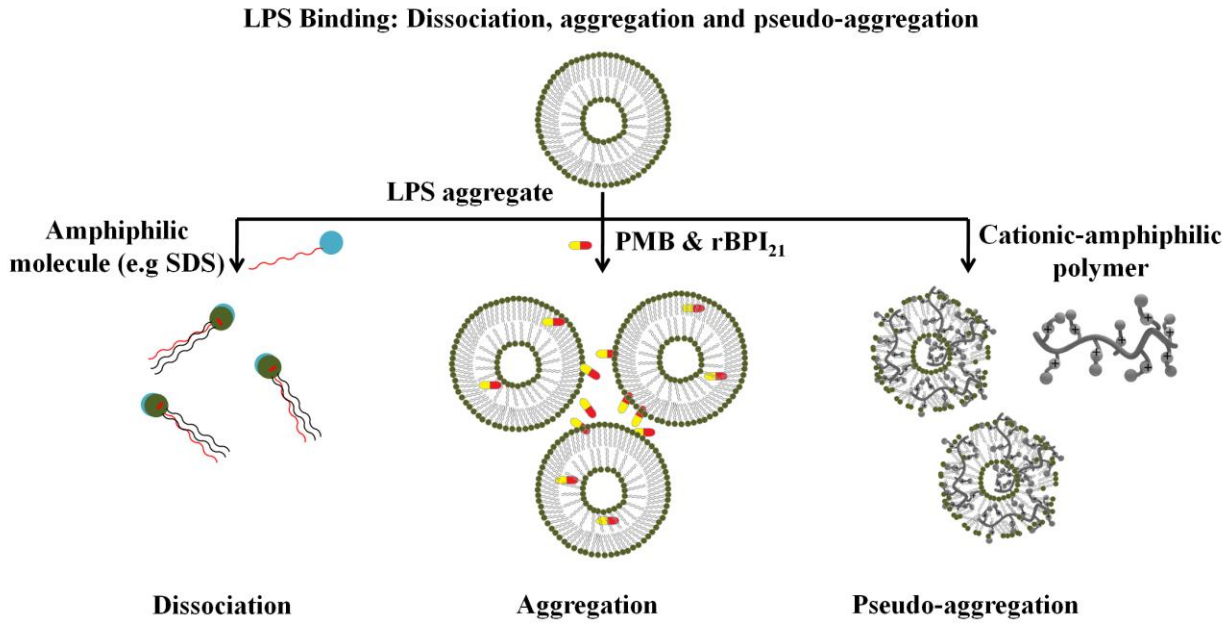

Figure 7.7: Binding of LPS to different molecules and their respective mechanisms of LPS neutralization.

7.2.7 *In-vivo* antibacterial activity and *In-vivo* anti-inflammatory activity

A. baumannii burn wound infection model (Fig. 7.8 A) was used as described in the Chapter 5. Mice treated with Q*n*-prAP, QCybuAP (both at 50 mg kg^{-1}) and erythromycin (20 mg kg^{-1}) showed 3 log_{10}, 3 log_{10} and 6 log_{10} reductions in bacterial burden compared to the untreated mice (10 log_{10}) (Fig. 7.8 B). Q*n*-prAP + Ery (50 mg kg^{-1} + 20 mg kg^{-1}), QCybuAP + Ery (50 mg kg^{-1} + 20 mg kg^{-1}) and colistin (5 mg kg^{-1}) had decreased the bacterial burden down to the detection limits. Both the antibiotics alone decreased the bacterial counts but did not decrease the inflammatory response due to infection. On the otherhand, the polymers alone and in combination with antibiotics decreased both bacterial burden and also reduced the inflammatory response (Fig. 7.8 C). Untreated mice showed burn wound area with numerous bacterial cells with proteinaceous exudates (arrow) along with severe infiltration of inflammatory cells mainly neutrophils which are degenerating (inset). There was loss of squamous epithelial cells, sweat gland, sebaceous gland and hair follicles along with architecture of skin tissue. Erythromycin group showed the process of healing which is evident by presence of fibrous tissue and squamous epithelial cells from the surrounding area (arrow) with severe infiltration of

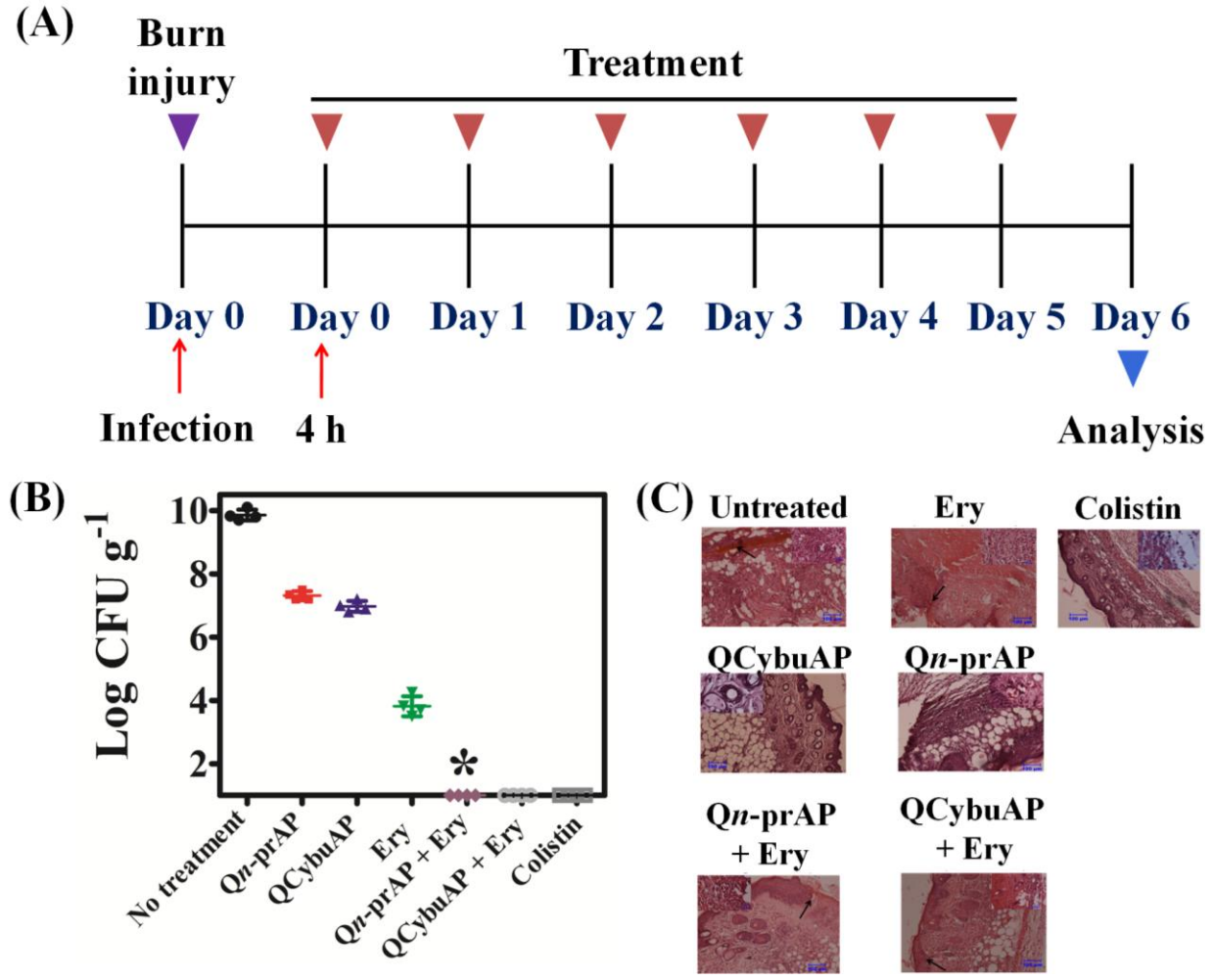

Figure 7.8: *In-vivo* anti-infective studies against *A. baumannii* acute burn wound infection. (A) Burn wounds were created on the back of mice (n = 4) and infected with 10^7 cfu of *A. baumannii*. Mice were treated with erythromycin (20 mg kg^{-1}), QCybuAP (50 mg kg^{-1}), Q*n*-prAP (50 mg kg^{-1}), Q*n*-prAP + Ery (50 mg kg^{-1} + 20 mg kg^{-1}), QCybuAP + Ery (50 mg kg^{-1} + 20 mg kg^{-1}) and colistin (5 mg kg^{-1}). Haematoxylin and Eosin staining of the respective skin sections. Scale bar = 100 µm (inset 20 µm) (B) Bacterial titers of the respective skin tissue sections. Star represents the detection limit.

inflammatory cells mainly neutrophils and also congestion of blood vessels (inset). Q*n*-prAP group showed moderate infiltration of inflammatory cells with congestion of blood vessels (inset) and regeneration of stratified squamous epithelial cells with loss of sebaceous and sweat glands. Q*n*-prAP + Erythromycin treated group showing regeneration of squamous epithelial cell layer over the burn wound area along with fibrous tissue (arrow), appearance of sweat and sebaceous glands, and hair follilces with moderate infiltration of neutrophils in the subepithelial

layer (inset). QCybuAP treated mice showing regeneration of the skin with squamous epithelial cells with keratin layers, sebaceous gland, sweat gland and hair follicles (inset). QCybuAP + Erythromycin showing regeneration of stratified squamous epithelial cells over the burn wound area (arrow) with appearance of hair follicles, sebaceous and sweat glands, along with infiltration of neutrophils beneath the fibrous tissue (inset). Colistin treated skin showing moderate regeneration of squamous epithelial cells with infiltration of inflammatory cells and red blood cells (inset) (Fig. 7.8 C).

7.3 Conclusions

In conclusion, cationic-amphiphilic polymers have been shown to neutralize and detoxify LPS by inhibiting the LPS induced secretion of pro-inflammatory cytokines (TNF-α and Il-6) in human monocytes. These polymers bind LPS aggregates but interestingly lead to a pseudo-aggregate formation that might prevent the recognition and binding of LPS to cell surface receptors thereby resulting in LPS detoxification (Fig. 7.9). This study provides novel synthetic cationic amphiphilic polymers for effective neutralization of bacterial endotoxins (e.g. LPS).

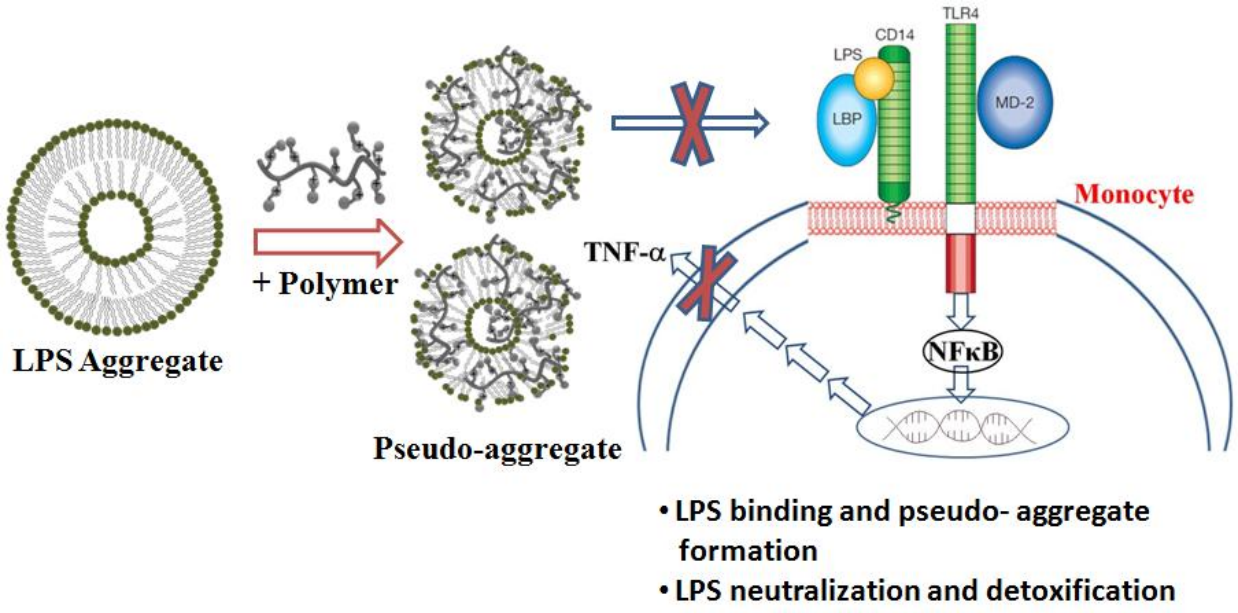

Figure 7.9: Schematic representation of LPS neutralization by cationic amphiphilic polymers. Adapted from reference 64 with the permission from Nature Publishing Group.

7.4 Experimental Section

7.4.1 *In-vitro* cytotoxicity against human PBMCs

Fresh human blood was drawn and human peripheral blood mononuclear cells (PBMCs) were isolated using a standard Ficoll-Hypaque density centrifugation technique and the number of PBMCs (and viability) was determined by trypan blue exclusion. More than 95% of cells were viable. All the media components used were certified and contained low endotoxin levels. After isolation, human PBMCs were resuspended in RPMI 1640 growth medium (with L-glutamine and sodium bicarbonate, Gibco, Life Technologies) supplemented with 10% of heat inactivated and low endotoxin fetal bovine serum (FBS, Life Technologies) and 1% penicillin-streptomycin at 37 °C in a humidified-air atmosphere (5% CO_2/95% air). Human PBMCs (2×10^4) were seeded into 96 well plates and incubated overnight at 37 °C in a humidified-air atmosphere (5% CO_2/95% air). The release of cytosolic LDH was then assessed after 24 h of incubation with polymeric derivatives using concentrations up to 100 μg mL^{-1}.

7.4.2. Stimulation of human PBMCs with LPS

Freshly isolated human PBMCs were seeded into 24- well plates (1×10^6 cells) in 1 mL of RPMI 1640 complete medium. After 3 hr of resting, the cells were stimulated with 20 ng mL^{-1} of *E. coli 0111:B4* LPS (Sigma Aldrich) either in the presence or absence of polymeric derivatives (different concentrations). A control experiment was performed using HBSS (Life Technologies) as vehicle control. The cells were incubated for 18-24 hours and then cell culture supernatants were analyzed for cytokines such as tumor necrosis factor (TNF- α) and interleukin- 6 (IL-6) using the human ELISA kits (BD Biosciences) following the manufacturer's instructions.

7.4.3 BODIPY-LPS fluorescence

Bodipy conjugated LPS (from *E. coli*, Molecular Probes, Life Technologies) was used for studying the interaction with polymers. Stock solution of bodipy-LPS (100 μg/mL) was prepared and diluted to 10 μg/mL in 1X PBS (pH= 7.4). Bodipy-LPS stock solutions were sonicated for 2 min before use. 2 mL of solution was taken in a quartz cuvette containing bodipy-LPS (500 ng/mL) and the test compounds in PBS. Experiments were performed using a λS55 Fluorescence

Spectrophotometer (Perkin Elmer) at an excitation wavelength of 485 nm and emission was collected from 500-700 nm (excitation slit width = 5 nm, emission slit width = 15 nm) at room temperature.

7.4.4 Dynamic light scattering (DLS)

E. coli 0111:B4 LPS and polymers were dissolved in Hank's balanced salt solution (HBSS without Ca^{2+} and Mg^{2+}). Experiments were performed using Zetasizer Nano Z (Malvern Instruments) at room temperature. LPS and the polymers were taken in disposable cuvettes in 2 mL of solution. Data were acquired for 200 scans.

References

1. Morens DM, Folkers GK, & Fauci AS (2008) Emerging infections: a perpetual challenge. *Lancet Infect Dis* 8(11):710-719.
2. Morens DM, Folkers GK, & Fauci AS (2004) The challenge of emerging and re-emerging infectious diseases. *Nature* 430(6996):242-249.
3. Ganguly NK, *et al.* (2011) Rationalizing antibiotic use to limit antibiotic resistance in India. *Ind J Med Res* 134(3):281-294.
4. Laxminarayan R, *et al.* (2013) Antibiotic resistance-the need for global solutions. *Lancet Infect Dis* 13(12):1057-1098.
5. Review on Antimicrobial Resistance. *Antimicrobial Resistance: Tackling a Crisis for the Health and Wealth of Nations.* 2014.
6. Walsh C (2000) Molecular mechanisms that confer antibacterial drug resistance. *Nature* 406(6797):775-781.
7. Blair JM, Webber MA, Baylay AJ, Ogbolu DO, & Piddock LJ (2015) Molecular mechanisms of antibiotic resistance. *Nat Rev Microbiol* 13(1):42-51.
8. McKenna M (2013) Antibiotic resistance: the last resort. *Nature* 499(7459):394-396.
9. Antimicrobial resistance: global report on surveillance. World health Organization. Geneva. 2014.
10. Walsh TR, Weeks J, Livermore DM, & Toleman MA (2011) Dissemination of NDM-1 positive bacteria in the New Delhi environment and its implications for human health: an environmental point prevalence study. *Lancet Infect Dis* 11(5):355-362.
11. Arpin C, *et al.* (2012) NDM-1-Producing Klebsiella pneumoniae Resistant to Colistin in a French Community Patient without History of Foreign Travel. *Antimicrob Agents Chemother* 56(6):3432-3434.
12. Deng M, *et al.* (2014) Molecular Epidemiology and Mechanisms of Tigecycline Resistance in Clinical Isolates of Acinetobacter baumannii from a Chinese University Hospital. *Antimicrob Agents Chemother* 58(1):297-303.
13. Taubes G (2008) The bacteria fight back. *Science* 321(5887):356-361.
14. Center for Disease Dynamics, Economics & Policy. 2015. *State of the World's Antibiotics, 2015.* CDDEP: Washington, D.C.
15. Stewart PS & Costerton JW (2001) Antibiotic resistance of bacteria in biofilms. *Lancet* 358(9276):135-138.
16. Hoiby N, Bjarnsholt T, Givskov M, Molin S, & Ciofu O (2010) Antibiotic resistance of bacterial biofilms. *Int J Antimicrob Agents* 35(4):322-332.
17. Davies D (2003) Understanding biofilm resistance to antibacterial agents. *Nat Rev Drug Discov* 2(2):114-122.
18. Stewart PS (2002) Mechanisms of antibiotic resistance in bacterial biofilms. *Int J Med Microbiol* 292(2):107-113.
19. Obst U, Schwartz T, & Volkmann H (2006) Antibiotic resistant pathogenic bacteria and their resistance genes in bacterial biofilms. *Int J Artif Organs* 29(4):387-394.
20. Ciofu O, Tolker-Nielsen T, Jensen PO, Wang H, & Hoiby N (2015) Antimicrobial resistance, respiratory tract infections and role of biofilms in lung infections in cystic fibrosis patients. *Adv Drug Deliv Rev* 85:7-23.

21. Costerton JW, Stewart PS, & Greenberg EP (1999) Bacterial biofilms: a common cause of persistent infections. *Science* 284(5418):1318-1322.
22. O'Toole G, Kaplan HB, & Kolter R (2000) Biofilm formation as microbial development. *Annu Rev Microbiol* 54:49-79.
23. Hall-Stoodley L, Costerton JW, & Stoodley P (2004) Bacterial biofilms: from the natural environment to infectious diseases. *Nat Rev Microbiol* 2(2):95-108.
24. Bjarnsholt T, Ciofu O, Molin S, Givskov M, & Hoiby N (2013) Applying insights from biofilm biology to drug development - can a new approach be developed? *Nat Rev Drug Discov* 12(10):791-808.
25. Romero D, Aguilar C, Losick R, & Kolter R (2010) Amyloid fibers provide structural integrity to Bacillus subtilis biofilms. *Proc Natl Acad Sci* 107(5):2230-2234.
26. Brackman G & Coenye T (2015) Quorum Sensing Inhibitors as Anti-Biofilm Agents. *Curr Pharm Des* 21(1):5-11.
27. O'Loughlin CT, *et al.* (2013) A quorum-sensing inhibitor blocks Pseudomonas aeruginosa virulence and biofilm formation. *Proc Natl Acad Sci* 110(44):17981-17986.
28. Balaban NQ, Gerdes K, Lewis K, & McKinney JD (2013) A problem of persistence: still more questions than answers? *Nat Rev Microbiol* 11(8):587-591.
29. Amato SM, *et al.* (2014) The role of metabolism in bacterial persistence. *Front Microbiol* 5:70.
30. Balaban NQ, Merrin J, Chait R, Kowalik L, & Leibler S (2004) Bacterial persistence as a phenotypic switch. *Science* 305(5690):1622-1625.
31. Maisonneuve E & Gerdes K (2014) Molecular mechanisms underlying bacterial persisters. *Cell* 157(3):539-548.
32. Lewis K (2010) Persister cells. *Annu Rev Microbiol* 64:357-372.
33. Helaine S, *et al.* (2014) Internalization of Salmonella by Macrophages Induces Formation of Nonreplicating Persisters. *Science* 343(6167):204-208.
34. Pamp SJ, Gjermansen M, Johansen HK, & Tolker-Nielsen T (2008) Tolerance to the antimicrobial peptide colistin in Pseudomonas aeruginosa biofilms is linked to metabolically active cells, and depends on the pmr and mexAB-oprM genes. *Mol Microbiol* 68(1):223-240.
35. Wu H, Moser C, Wang HZ, Hoiby N, & Song ZJ (2015) Strategies for combating bacterial biofilm infections. *Int J Oral Sci* 7(1):1-7.
36. Chen M, Yu Q, & Sun H (2013) Novel strategies for the prevention and treatment of biofilm related infections. *Int J Mol Sci* 14(9):18488-18501.
37. Campoccia D, Montanaro L, & Arciola CR (2013) A review of the biomaterials technologies for infection-resistant surfaces. *Biomaterials* 34(34):8533-8554.
38. Campoccia D, Montanaro L, & Arciola CR (2013) A review of the clinical implications of anti-infective biomaterials and infection-resistant surfaces. *Biomaterials* 34(33):8018-8029.
39. Banerjee I, Pangule RC, & Kane RS (2011) Antifouling Coatings: Recent Developments in the Design of Surfaces That Prevent Fouling by Proteins, Bacteria, and Marine Organisms. *Adv Mater* 23(6):690-718.
40. Tasso M, *et al.* (2009) Antifouling potential of Subtilisin A immobilized onto maleic anhydride copolymer thin films. *Biofouling* 25(6):505-516.

41. Kazemzadeh-Narbat M, *et al.* (2013) Multilayered coating on titanium for controlled release of antimicrobial peptides for the prevention of implant-associated infections. *Biomaterials* 34(24):5969-5977.
42. Fischer M, *et al.* (2015) Multilayer hydrogel coatings to combine hemocompatibility and antimicrobial activity. *Biomaterials* 56:198-205.
43. Statz AR, Meagher RJ, Barron AE, & Messersmith PB (2005) New peptidomimetic polymers for antifouling surfaces. *J Am Chem Soc* 127(22):7972-7973.
44. O'Loughlin CT, *et al.* (2013) A quorum-sensing inhibitor blocks Pseudomonas aeruginosa virulence and biofilm formation. *Proc Natl Acad Sci U S A* 110(44):17981-17986.
45. Taglietti A, *et al.* (2014) Antibiofilm activity of a monolayer of silver nanoparticles anchored to an amino-silanized glass surface. *Biomaterials* 35(6):1779-1788.
46. Conlon BP, *et al.* (2013) Activated ClpP kills persisters and eradicates a chronic biofilm infection. *Nature* 503(7476):365-370.
47. Allison KR, Brynildsen MP, & Collins JJ (2011) Metabolite-enabled eradication of bacterial persisters by aminoglycosides. *Nature* 473(7346):216-220.
48. de la Fuente-Nunez C, *et al.* (2015) D-Enantiomeric Peptides that Eradicate Wild-Type and Multidrug-Resistant Biofilms and Protect against Lethal Pseudomonas aeruginosa Infections. *Chem Biol* 22(2):196-205.
49. Schmidt NW, *et al.* (2014) Engineering persister-specific antibiotics with synergistic antimicrobial functions. *ACS Nano* 8(9):8786-8793.
50. Nait Chabane Y, *et al.* (2014) Virstatin inhibits biofilm formation and motility of Acinetobacter baumannii. *BMC Microbiol* 14:62.
51. Hurdle JG, O'Neill AJ, Chopra I, & Lee RE (2011) Targeting bacterial membrane function: an underexploited mechanism for treating persistent infections. *Nat Rev Microbiol* 9(1):62-75.
52. Silhavy TJ, Kahne D, & Walker S (2010) The Bacterial Cell Envelope. *Cold Spring Harb Perspect Biol* 2(5).
53. Cabeen MT & Jacobs-Wagner C (2005) Bacterial cell shape. *Nat Rev Microbiol* 3(8):601-610.
54. Tommasi R, Brown DG, Walkup GK, Manchester JI, & Miller AA (2015) ESKAPEing the labyrinth of antibacterial discovery. *Nat Rev Drug Discov* 14(8):529-542.
55. Epand RM, Walker C, Epand RF, & Magarvey NA (2015) Molecular mechanisms of membrane targeting antibiotics. *Biochim Biophys Acta*.
56. Yarlagadda V, Konai MM, Manjunath GB, Ghosh C, & Haldar J (2015) Tackling vancomycin-resistant bacteria with 'lipophilic-vancomycin-carbohydrate conjugates'. *J Antibiot* 68(5):302-312.
57. Velkov T, *et al.* (2014) Teaching 'old' polymyxins new tricks: new-generation lipopeptides targeting gram-negative 'superbugs'. *ACS Chem Biol* 9(5):1172-1177.
58. Pages JM, Masi M, & Barbe J (2005) Inhibitors of efflux pumps in Gram-negative bacteria. *Trends Mol Med* 11(8):382-389.
59. Marquez B (2005) Bacterial efflux systems and efflux pumps inhibitors. *Biochimie* 87(12):1137-1147.
60. Pages JM & Amaral L (2009) Mechanisms of drug efflux and strategies to combat them: Challenging the efflux pump of Gram-negative bacteria. *Biochim Biophys Acta* 1794(5):826-833.

61. Langton KP, Henderson PJF, & Herbert RB (2005) Antibiotic resistance: multidrug efflux proteins, a common transport mechanism? *Nat Prod Rep* 22(4):439-451.
62. Piddock LJ (2006) Multidrug-resistance efflux pumps - not just for resistance. *Nat Rev Microbiol* 4(8):629-636.
63. Cohen J (2002) The immunopathogenesis of sepsis. *Nature* 420(6917):885-891.
64. Aderem A & Ulevitch RJ (2000) Toll-like receptors in the induction of the innate immune response. *Nature* 406(6797):782-787.
65. Uppu DS, Ghosh C, & Haldar J (2015) Surviving sepsis in the era of antibiotic resistance: are there any alternative approaches to antibiotic therapy? *Microb Pathog* 80:7-13.
66. Yarlagadda V, Akkapeddi P, Manjunath GB, & Haldar J (2014) Membrane Active Vancomycin Analogues: A Strategy to Combat Bacterial Resistance. *J Med Chem* 57(11):4558-4568.
67. Yarlagadda V, Samaddar S, Paramanandham K, Shome BR, & Haldar J (2015) Membrane Disruption and Enhanced Inhibition of Cell-Wall Biosynthesis: A Synergistic Approach to Tackle Vancomycin-Resistant Bacteria. *Angew Chem Int Ed Engl* 54(46):13644-13649.
68. Gabriel GJ, Som A, Madkour AE, Eren T, & Tew GN (2007) Infectious Disease: Connecting Innate Immunity to Biocidal Polymers. *Mater Sci Eng R Rep* 57(1-6):28-64.
69. Epand RM & Epand RF (2011) Bacterial membrane lipids in the action of antimicrobial agents. *J Pep Sci* 17(5):298-305.
70. Lee DK, Bhunia A, Kotler SA, & Ramamoorthy A (2015) Detergent-Type Membrane Fragmentation by MSI-78, MSI-367, MSI-594, and MSI-843 Antimicrobial Peptides and Inhibition by Cholesterol: A Solid-State Nuclear Magnetic Resonance Study. *Biochemistry* 54(10):1897-1907.
71. Bechinger B (1999) The structure, dynamics and orientation of antimicrobial peptides in membranes by multidimensional solid-state NMR spectroscopy. *Biochim Biophys Acta* 1462(1-2):157-183.
72. Sheehan JC, Mania D, Nakamura S, Stock JA, & Maeda K (1968) The structure of telomycin. *J Am Chem Soc* 90(2):462-470.
73. Iwamoto K, *et al.* (2007) Curvature-dependent recognition of ethanolamine phospholipids by duramycin and cinnamycin. *Biophys J* 93(5):1608-1619.
74. Hamamoto H, *et al.* (2015) Lysocin E is a new antibiotic that targets menaquinone in the bacterial membrane. *Nat Chem Biol* 11(2):127-U168.
75. Tiller JC, Liao CJ, Lewis K, & Klibanov AM (2001) Designing surfaces that kill bacteria on contact. *Proc Natl Acad Sci* 98(11):5981-5985.
76. Haldar J, An D, Alvarez de Cienfuegos L, Chen J, & Klibanov AM (2006) Polymeric coatings that inactivate both influenza virus and pathogenic bacteria. *Proc Natl Acad Sci U S A* 103(47):17667-17671.
77. Haldar J, Weight AK, & Klibanov AM (2007) Preparation, application and testing of permanent antibacterial and antiviral coatings. *Nat Proto* 2(10):2412-2417.
78. Kenawy el R, Worley SD, & Broughton R (2007) The chemistry and applications of antimicrobial polymers: a state-of-the-art review. *Biomacromolecules* 8(5):1359-1384.
79. Schaer TP, Stewart S, Hsu BB, & Klibanov AM (2012) Hydrophobic polycationic coatings that inhibit biofilms and support bone healing during infection. *Biomaterials* 33(5):1245-1254.

80. Shai Y (1999) Mechanism of the binding, insertion and destabilization of phospholipid bilayer membranes by alpha-helical antimicrobial and cell non-selective membrane-lytic peptides. *Biochim Biophys Acta* 1462(1-2):55-70.
81. Hancock RE & Sahl HG (2006) Antimicrobial and host-defense peptides as new anti-infective therapeutic strategies. *Nat Biotechnol* 24(12):1551-1557.
82. Zasloff M (2002) Antimicrobial peptides of multicellular organisms. *Nature* 415(6870):389-395.
83. Brogden KA (2005) Antimicrobial peptides: pore formers or metabolic inhibitors in bacteria? *Nat Rev Microbiol* 3(3):238-250.
84. Wimley WC (2010) Describing the mechanism of antimicrobial peptide action with the interfacial activity model. *ACS Chem Biol* 5(10):905-917.
85. Yeaman MR & Yount NY (2003) Mechanisms of antimicrobial peptide action and resistance. *Pharmacol Rev* 55(1):27-55.
86. Hancock REW, Nijnik A, & Philpott DJ (2012) Modulating immunity as a therapy for bacterial infections. *Nat Rev Microbiol* 10(4):243-254.
87. Mookherjee N, Chow LNY, & Hancock REW (2012) Immunomodulatory Cationic Peptide Therapeutics: A New Paradigm in Infection and Immunity. *Small Wonders: Peptides for Disease Control* 1095:1-19.
88. Bowdish DME, Davidson DJ, & Hancock REW (2006) Immunomodulatory properties of defensins and cathelicidins. *Antimicrobial Peptides and Human Disease* 306:27-66.
89. Hilchie AL, Wuerth K, & Hancock REW (2013) Immune modulation by multifaceted cationic host defense (antimicrobial) peptides. *Nat Chem Biol* 9(12):761-768.
90. Easton DM, Nijnik A, Mayer ML, & Hancock REW (2009) Potential of immunomodulatory host defense peptides as novel anti-infectives. *Trends Biotechnol* 27(10):582-590.
91. Hancock RE (2000) Cationic antimicrobial peptides: towards clinical applications. *Expert Opin Investig Drugs* 9(8):1723-1729.
92. Czaplewski L, *et al.* (2016) Alternatives to antibiotics-a pipeline portfolio review. *Lancet Infect Dis*.
93. Ghosh C & Haldar J (2015) Membrane-Active Small Molecules: Designs Inspired by Antimicrobial Peptides. *ChemMedChem* 10(10):1606-1624.
94. Wenzel M, *et al.* (2014) Small cationic antimicrobial peptides delocalize peripheral membrane proteins. *Proc Natl Acad Sci U S A* 111(14):E1409-E1418.
95. Xiong M, *et al.* (2015) Helical antimicrobial polypeptides with radial amphiphilicity. *Proc Natl Acad Sci U S A* 112(43):13155-13160.
96. Porter EA, Wang X, Lee HS, Weisblum B, & Gellman SH (2000) Non-haemolytic beta-amino-acid oligomers. *Nature* 404(6778):565.
97. Patch JA & Barron AE (2003) Helical peptoid mimics of magainin-2 amide. *J Am Chem Soc* 125(40):12092-12093.
98. Tew GN, *et al.* (2002) De novo design of biomimetic antimicrobial polymers. *Proc Natl Acad Sci U S A* 99(8):5110-5114.
99. Liu D, *et al.* (2004) Nontoxic membrane-active antimicrobial arylamide oligomers. *Angew Chem Int Ed Engl* 43(9):1158-1162.
100. Radzishevsky IS, *et al.* (2007) Improved antimicrobial peptides based on acyl-lysine oligomers. *Nat Biotechnol* 25(6):657-659.

101. Niu YH, *et al.* (2012) Lipo-gamma-AApeptides as a New Class of Potent and Broad-Spectrum Antimicrobial Agents. *J Med Chem* 55(8):4003-4009.
102. Ghosh C, *et al.* (2014) Small Molecular Antibacterial Peptoid Mimics: The Simpler the Better! *J Med Chem* 57(4):1428-1436.
103. Hoque J, *et al.* (2015) Membrane Active Small Molecules Show Selective Broad Spectrum Antibacterial Activity with No Detectable Resistance and Eradicate Biofilms. *J Med Chem* 58(14):5486-5500.
104. Konai MM, Ghosh C, Yarlagadda V, Samaddar S, & Haldar J (2014) Membrane active phenylalanine conjugated lipophilic norspermidine derivatives with selective antibacterial activity. *J Med Chem* 57(22):9409-9423.
105. Engler AC, *et al.* (2012) Emerging trends in macromolecular antimicrobials to fight multi-drug-resistant infections. *Nano Today* 7(3):201-222.
106. Li P, Li X, Saravanan R, Li CM, & Leong SSJ (2012) Antimicrobial macromolecules: synthesis methods and future applications. *RSC Adv* 2(10):4031-4044.
107. Ganewatta MS & Tang CB (2015) Controlling macromolecular structures towards effective antimicrobial polymers. *Polymer* 63:A1-A29.
108. Liu RH, *et al.* (2014) Tuning the Biological Activity Profile of Antibacterial Polymers via Subunit Substitution Pattern. *J Am Chem Soc* 136(11):4410-4418.
109. Lee MW, *et al.* (2014) Two interdependent mechanisms of antimicrobial activity allow for efficient killing in nylon-3-based polymeric mimics of innate immunity peptides. *Biochim Biophy Acta* 1838(9):2269-2279.
110. Sgolastra F, Deronde BM, Sarapas JM, Som A, & Tew GN (2013) Designing Mimics of Membrane Active Proteins. *Acc Chem Res* 46(12):2977-2987.
111. Kuroda K & DeGrado WF (2005) Amphiphilic polymethacrylate derivatives as antimicrobial agents. *J Am Chem Soc* 127(12):4128-4129.
112. Takahashi H, Palermo EF, Yasuhara K, Caputo GA, & Kuroda K (2013) Molecular design, structures, and activity of antimicrobial peptide-mimetic polymers. *Macromol Biosci* 13(10):1285-1299.
113. Dizman B, Elasri MO, & Mathias LJ (2004) Synthesis and antimicrobial activities of new water-soluble bis-quaternary ammonium methacrylate polymers. *J Appl Polym Sci* 94(2):635-642.
114. Punia A, He E, Lee K, Banerjee P, & Yang NL (2014) Cationic amphiphilic non-hemolytic polyacrylates with superior antibacterial activity. *Chem Commun* 50(53):7071-7074.
115. Sambhy V, Peterson BR, & Sen A (2008) Antibacterial and hemolytic activities of pyridinium polymers as a function of the spatial relationship between the positive charge and the pendant alkyl tail. *Angew Chem Int Ed Engl* 47(7):1250-1254.
116. Nederberg F, *et al.* (2011) Biodegradable nanostructures with selective lysis of microbial membranes. *Nat Chem* 3(5):409-414.
117. Chan JLMW, *et al.* (2014) Chemically modifiable N-heterocycle-functionalized polycarbonates as a platform for diverse smart biomimetic nanomaterials. *Chem Sci* 5(8):3294-3300.
118. Li P, *et al.* (2012) Cationic peptidopolysaccharides show excellent broad-spectrum antimicrobial activities and high selectivity. *Adv Mater* 24(30):4130-4137.
119. Li P, *et al.* (2011) A polycationic antimicrobial and biocompatible hydrogel with microbe membrane suctioning ability. *Nat Mater* 10(2):149-156.

120. Song A, Walker SG, Parker KA, & Sampson NS (2011) Antibacterial studies of cationic polymers with alternating, random, and uniform backbones. *ACS Chem Biol* 6(6):590-599.
121. Abd-El-Aziz AS, *et al.* (2015) Antimicrobial Organometallic Dendrimers with Tunable Activity against Multidrug-Resistant Bacteria. *Biomacromolecules* 16(11):3694-3703.
122. Al-Ahmad A, *et al.* (2013) Nature-Inspired Antimicrobial Polymers - Assessment of Their Potential for Biomedical Applications. *Plos One* 8(9).
123. Chattopadhyay S, Heine ET, Keul H, & Moller M (2014) Multifunctional Poly(Vinyl Amine)s Bearing Azetidinium Groups: One Pot Preparation in Water and Antimicrobial Properties. *Macromol Biosci* 14(8):1116-1124.
124. Chen CZ, *et al.* (2000) Quaternary ammonium functionalized poly(propylene imine) dendrimers as effective antimicrobials: structure-activity studies. *Biomacromolecules* 1(3):473-480.
125. Costanza F, *et al.* (2014) Investigation of antimicrobial PEG-poly(amino acid)s. *RSC Adv* 4(4):2089-2095.
126. Engler AC, *et al.* (2011) Effects of Side Group Functionality and Molecular Weight on the Activity of Synthetic Antimicrobial Polypeptides. *Biomacromolecules* 12(5):1666-1674.
127. Ganewatta MS, *et al.* (2014) Bio-inspired resin acid-derived materials as anti-bacterial resistance agents with unexpected activities. *Chem Sci* 5(5):2011-2016.
128. He Y, Heine E, Keusgen N, Keul H, & Moller M (2012) Synthesis and characterization of amphiphilic monodisperse compounds and poly(ethylene imine)s: influence of their microstructures on the antimicrobial properties. *Biomacromolecules* 13(3):612-623.
129. Hu K, *et al.* (2013) A Critical Evaluation of Random Copolymer Mimesis of Homogeneous Antimicrobial Peptides. *Macromolecules* 46(5):1908-1915.
130. Jiang YJ, *et al.* (2013) Acid-Activated Antimicrobial Random Copolymers: A Mechanism-Guided Design of Antimicrobial Peptide Mimics. *Macromolecules* 46(10):3959-3964.
131. King A, *et al.* (2014) High antimicrobial effectiveness with low hemolytic and cytotoxic activity for PEG/quaternary copolyoxetanes. *Biomacromolecules* 15(2):456-467.
132. Krumm C, *et al.* (2014) Antimicrobial Poly(2-methyloxazoline) s with Bioswitchable Activity through Satellite Group Modification. *Angew Chem Int Ed* 53(15):3830-3834.
133. Locock KE, *et al.* (2013) Guanylated polymethacrylates: a class of potent antimicrobial polymers with low hemolytic activity. *Biomacromolecules* 14(11):4021-4031.
134. Melo LD, *et al.* (2011) Structure-activity relationship for quaternary ammonium compounds hybridized with poly(methyl methacrylate). *ACS Appl Mater Interfaces* 3(6):1933-1939.
135. Mi L & Jiang S (2014) Integrated antimicrobial and nonfouling zwitterionic polymers. *Angew Chem Int Ed Engl* 53(7):1746-1754.
136. Palermo EF, Lee DK, Ramamoorthy A, & Kuroda K (2011) Role of cationic group structure in membrane binding and disruption by amphiphilic copolymers. *J Phys Chem B* 115(2):366-375.
137. Paslay LC, *et al.* (2012) Antimicrobial poly(methacrylamide) derivatives prepared via aqueous RAFT polymerization exhibit biocidal efficiency dependent upon cation structure. *Biomacromolecules* 13(8):2472-2482.

138. Pranantyo D, *et al.* (2015) Tea stains-inspired initiator primer for surface grafting of antifouling and antimicrobial polymer brush coatings. *Biomacromolecules* 16(3):723-732.
139. Sharma A, *et al.* (2015) Cell Penetrating Synthetic Antimicrobial Peptides (SAMPs) Exhibiting Potent and Selective Killing of Mycobacterium by Targeting Its DNA. *Chem Eur J* 21(9):3540-3545.
140. Strassburg A, *et al.* (2015) Nontoxic, Hydrophilic Cationic Polymers-Identified as Class of Antimicrobial Polymers. *Macromol Biosci*.
141. Stratton TR, Rickus JL, & Youngblood JP (2009) In vitro biocompatibility studies of antibacterial quaternary polymers. *Biomacromolecules* 10(9):2550-2555.
142. Tejero R, Lopez D, Lopez-Fabal F, Gomez-Garces JL, & Fernandez-Garcia M (2015) High Efficiency Antimicrobial Thiazolium and Triazolium Side-Chain Polymethacrylates Obtained by Controlled Alkylation of the Corresponding Azole Derivatives. *Biomacromolecules* 16(6):1844-1854.
143. Timofeeva LM, Kleshcheva NA, Moroz AF, & Didenko LV (2009) Secondary and tertiary polydiallylammonium salts: novel polymers with high antimicrobial activity. *Biomacromolecules* 10(11):2976-2986.
144. Wang J, *et al.* (2012) Robust antimicrobial compounds and polymers derived from natural resin acids. *Chem Commun* 48(6):916-918.
145. Wang M, Zhou C, Chen J, Xiao Y, & Du J (2015) Multifunctional biocompatible and biodegradable folic acid conjugated poly(epsilon-caprolactone)-polypeptide copolymer vesicles with excellent antibacterial activities. *Bioconjug Chem* 26(4):725-734.
146. Wang Y, Chi EY, Schanze KS, & Whitten DG (2012) Membrane activity of antimicrobial phenylene ethynylene based polymers and oligomers. *Soft Matter* 8(33):8547-8558.
147. Wang Y, Xu J, Zhang Y, Yan H, & Liu K (2011) Antimicrobial and hemolytic activities of copolymers with cationic and hydrophobic groups: a comparison of block and random copolymers. *Macromol Biosci* 11(11):1499-1504.
148. Yang X, *et al.* (2014) Long hydrophilic-and-cationic polymers: a different pathway toward preferential activity against bacterial over mammalian membranes. *Biomacromolecules* 15(9):3267-3277.
149. Yuan WZ, Wei JR, Lu H, Fan L, & Du JZ (2012) Water-dispersible and biodegradable polymer micelles with good antibacterial efficacy. *Chem Commun* 48(54):6857-6859.
150. Popescu I, Suflet DM, Pelin IM, & Chitanu GC (2011) Biomedical Applications of Maleic Anhydride Copolymers. *Rev Roum Chim* 56(3):173-188.
151. Duncan R (2003) The dawning era of polymer therapeutics. *Nat Rev Drug Discov* 2(5):347-360.
152. Verheul RJ, van der Wal S, & Hennink WE (2010) Tailorable thiolated trimethyl chitosans for covalently stabilized nanoparticles. *Biomacromolecules* 11(8):1965-1971.
153. Bohrisch J, Schimmel T, Engelhardt H, & Jaeger W (2002) Charge interaction of synthetic polycarboxybetaines in bulk and solution. *Macromolecules* 35(10):4143-4149.
154. Lin CAJ, *et al.* (2008) Design of an amphiphilic polymer for nanoparticle coating and functionalization. *Small* 4(3):334-341.
155. Wiegand I, Hilpert K, & Hancock RE (2008) Agar and broth dilution methods to determine the minimal inhibitory concentration (MIC) of antimicrobial substances. *Nat Proto* 3(2):163-175.

156. Spellberg B, *et al.* (2008) The epidemic of antibiotic-resistant infections: a call to action for the medical community from the Infectious Diseases Society of America. *Clin Infect Dis* 46(2):155-164.
157. David MZ & Daum RS (2010) Community-associated methicillin-resistant Staphylococcus aureus: epidemiology and clinical consequences of an emerging epidemic. *Clin Microbiol Rev* 23(3):616-687.
158. Cohen ML (2000) Changing patterns of infectious disease. *Nature* 406(6797):762-767.
159. Chambers HF & Deleo FR (2009) Waves of resistance: Staphylococcus aureus in the antibiotic era. *Nat Rev Microbiol* 7(9):629-641.
160. Gold HS & Moellering RC, Jr. (1996) Antimicrobial-drug resistance. *N Engl J Med* 335(19):1445-1453.
161. Ge YG, *et al.* (1999) In vitro antibacterial properties of pexiganan, an analog of magainin. *Antimicrob Agents Chemother* 43(4):782-788.
162. McKay GA, *et al.* (2009) Time-kill kinetics of oritavancin and comparator agents against Staphylococcus aureus, Enterococcus faecalis and Enterococcus faecium. *J Antimicrob Chemother* 63(6):1191-1199.
163. Choi H, Chakraborty S, Liu R, Gellman SH, & Weisshaar JC (2014) Medium effects on minimum inhibitory concentrations of nylon-3 polymers against E. coli. *PLoS One* 9(8):e104500.
164. Hussain M, Hastings JG, & White PJ (1991) A chemically defined medium for slime production by coagulase-negative staphylococci. *J Med Microbiol* 34(3):143-147.
165. Hoque J, *et al.* (2012) Cleavable cationic antibacterial amphiphiles: synthesis, mechanism of action, and cytotoxicities. *Langmuir* 28(33):12225-12234.
166. Strahl H & Hamoen LW (2010) Membrane potential is important for bacterial cell division. *Proc Natl Acad Sci* 107(27):12281-12286.
167. Wiberg KB & Laidig KE (1987) Barriers to Rotation Adjacent to Double-Bonds .3. The C-O Barrier in Formic-Acid, Methyl Formate, Acetic-Acid, and Methyl Acetate - the Origin of Ester and Amide Resonance. *J Am Chem Soc* 109(20):5935-5943.
168. Pawar DM, *et al.* (1998) E and Z conformations of esters, thiol esters, and amides. *J Am Chem Soc* 120(9):2108-2112.
169. Jenkins CL, Vasbinder MM, Miller SJ, & Raines RT (2005) Peptide bond isosteres: Ester or (E)-alkene in the backbone of the collagen triple helix. *Organic Letters* 7(13):2619-2622.
170. Sreekanth V & Bajaj A (2013) Fluorescence (fluidity/hydration) and calorimetric studies of interactions of bile acid-drug conjugates with model membranes. *J Phys Chem B* 117(7):2123-2133.
171. Sreekanth V & Bajaj A (2013) Number of free hydroxyl groups on bile acid phospholipids determines the fluidity and hydration of model membranes. *J Phys Chem B* 117(40):12135-12144.
172. Klocek G, Schulthess T, Shai Y, & Seelig J (2009) Thermodynamics of melittin binding to lipid bilayers. Aggregation and pore formation. *Biochemistry* 48(12):2586-2596.
173. Wieprecht T, Apostolov O, Beyermann M, & Seelig J (2000) Membrane binding and pore formation of the antibacterial peptide PGLa: thermodynamic and mechanistic aspects. *Biochemistry* 39(2):442-452.

174. Yang L, *et al.* (2008) Mechanism of a prototypical synthetic membrane-active antimicrobial: Efficient hole-punching via interaction with negative intrinsic curvature lipids. *Proc Natl Acad Sci U S A* 105(52):20595-20600.
175. Seelig J (1997) Titration calorimetry of lipid-peptide interactions. *Biochim Biophys Acta* 1331(1):103-116.
176. Gabriel GJ, *et al.* (2008) Interactions between Antimicrobial Polynorbornenes and Phospholipid Vesicles Monitored by Light Scattering and Microcalorimetry. *Langmuir* 24(21):12489-12495.
177. Faig A, *et al.* (2015) Biscationic Tartaric Acid-Based Amphiphiles: Charge Location Impacts Antimicrobial Activity. *Langmuir* 31(43):11875-11885.
178. Ivanov I, *et al.* (2006) Characterization of nonbiological antimicrobial polymers in aqueous solution and at water-lipid interfaces from all-atom molecular dynamics. *J Am Chem Soc* 128(6):1778-1779.
179. Baul U, Kuroda K, & Vemparala S (2014) Interaction of multiple biomimetic antimicrobial polymers with model bacterial membranes. *J Chem Phys* 141(8):084902.
180. Movasaghi Z, Rehman S, & Rehman IU (2007) Raman spectroscopy of biological tissues. *Appl Spectroscop Rev* 42(5):493-541.
181. Mantsch HH, Martin A, & Cameron DG (1981) Characterization by infrared spectroscopy of the bilayer to nonbilayer phase transition of phosphatidylethanolamines. *Biochemistry* 20(11):3138-3145.
182. Barnett M, Bushby SR, & Wilkinson S (1964) Sodium Sulphomethyl Derivatives of Polymyxins. *Br J Pharmacol Chemother* 23:552-574.
183. Choi HS, *et al.* (2007) Renal clearance of quantum dots. *Nat Biotechnol* 25(10):1165-1170.
184. Phillips JC, *et al.* (2005) Scalable molecular dynamics with NAMD. *J Comput Chem* 26(16):1781-1802.
185. Klauda JB, *et al.* (2010) Update of the CHARMM all-atom additive force field for lipids: validation on six lipid types. *J Phys Chem B* 114(23):7830-7843.
186. Vanommeslaeghe K & MacKerell AD (2012) Automation of the CHARMM General Force Field (CGenFF) I: Bond Perception and Atom Typing. *J Chem Inform Model* 52(12):3144-3154.
187. Vanommeslaeghe K, Raman EP, & MacKerell AD (2012) Automation of the CHARMM General Force Field (CGenFF) II: Assignment of Bonded Parameters and Partial Atomic Charges. *J Chem Inform Model* 52(12):3155-3168.
188. MacKerell AD, *et al.* (1998) All-atom empirical potential for molecular modeling and dynamics studies of proteins. *J Phys Chem B* 102(18):3586-3616.
189. Feller SE, Zhang YH, Pastor RW, & Brooks BR (1995) Constant-Pressure Molecular-Dynamics Simulation - the Langevin Piston Method. *J Chem Phys* 103(11):4613-4621.
190. Lipnick RL, *et al.* (1995) Comparison of the up-and-down, conventional LD50, and fixed-dose acute toxicity procedures. *Food Chem Toxicol* 33(3):223-231.
191. Gough KM (1989) Theoretical-Analysis of Molecular Polarizabilities and Polarizability Derivatives in Hydrocarbons. *J Chem Phys* 91(4):2424-2432.
192. Chakraborty S, *et al.* (2013) Effects of Cyclic vs. Acyclic Hydrophobic Subunits on the Chemical Structure and Biological Properties of Nylon-3 Co-Polymers. *ACS Macro Lett* 2(8).

193. Amato SM & Brynildsen MP (2014) Nutrient Transitions Are a Source of Persisters in Escherichia coli Biofilms. *PLoS One* 9(3).
194. Hoque J, *et al.* (2015) Selective and broad spectrum amphiphilic small molecules to combat bacterial resistance and eradicate biofilms. *Chem Commun* 51(71):13670-13673.
195. Konai MM, Adhikary U, Samaddar S, Ghosh C, & Haldar J (2015) Structure-Activity Relationship of Amino Acid Tunable Lipidated Norspermidine Conjugates: Disrupting Biofilms with Potent Activity against Bacterial Persisters. *Bioconjug Chem*.
196. Barraud N, *et al.* (2012) Cephalosporin-3 '-diazeniumdiolates: Targeted NO-Donor Prodrugs for Dispersing Bacterial Biofilms. *Angew Chem Int Ed* 51(36):9057-9060.
197. Hazer DB, *et al.* (2012) The efficacy of silver-embedded polypropylene-grafted polyethylene glycol-coated ventricular catheters on prevention of shunt catheter infection in rats. *Childs Nerv Syst* 28(6):839-846.
198. Morones-Ramirez JR, Winkler JA, Spina CS, & Collins JJ (2013) Silver enhances antibiotic activity against gram-negative bacteria. *Sci Transl Med* 5(190):190ra181.
199. Peng L, *et al.* (2011) Inhibition of Acinetobacter baumannii biofilm formation on a methacrylate polymer containing a 2-aminoimidazole subunit. *Chem Commun* 47(17):4896-4898.
200. Fukushima K, *et al.* (2013) Supramolecular high-aspect ratio assemblies with strong antifungal activity. *Nat Commun* 4:2861.
201. Li Y, *et al.* (2013) Broad-spectrum antimicrobial and biofilm-disrupting hydrogels: stereocomplex-driven supramolecular assemblies. *Angew Chem Int Ed Engl* 52(2):674-678.
202. Liu R, *et al.* (2015) Nylon-3 polymers active against drug-resistant Candida albicans biofilms. *J Am Chem Soc* 137(6):2183-2186.
203. McLeod GI & Spector MP (1996) Starvation- and Stationary-phase-induced resistance to the antimicrobial peptide polymyxin B in Salmonella typhimurium is RpoS (sigma(S)) independent and occurs through both phoP-dependent and -independent pathways. *J Bacteriol* 178(13):3683-3688.
204. Soon RL, *et al.* (2011) Different surface charge of colistin-susceptible and -resistant Acinetobacter baumannii cells measured with zeta potential as a function of growth phase and colistin treatment. *J Antimicrob Chemother* 66(1):126-133.
205. Barraud N, Buson A, Jarolimek W, & Rice SA (2013) Mannitol enhances antibiotic sensitivity of persister bacteria in Pseudomonas aeruginosa biofilms. *PLoS One* 8(12):e84220.
206. Lebeaux D, *et al.* (2014) pH-Mediated Potentiation of Aminoglycosides Kills Bacterial Persisters and Eradicates In Vivo Biofilms. *J Infect Dis* 210(9):1357-1366.
207. Pan JC, Song FC, & Ren DC (2013) Controlling persister cells of Pseudomonas aeruginosa PDO300 by (Z)-4-bromo-5-(bromomethylene)-3-methylfuran-2(5H)-one. *Bio Med Chem Lett* 23(16):4648-4651.
208. Belley A, *et al.* (2009) Oritavancin kills stationary-phase and biofilm Staphylococcus aureus cells in vitro. *Antimicrob Agents Chemother* 53(3):918-925.
209. Mascio CT, Alder JD, & Silverman JA (2007) Bactericidal action of daptomycin against stationary-phase and nondividing Staphylococcus aureus cells. *Antimicrob Agents Chemother* 51(12):4255-4260.

210. Chen X, Zhang M, Zhou CH, Kallenbach NR, & Ren DC (2011) Control of Bacterial Persister Cells by Trp/Arg-Containing Antimicrobial Peptides. *Appl Environ Microbiol* 77(14):4878-4885.
211. Ooi N, *et al.* (2010) XF-70 and XF-73, novel antibacterial agents active against slow-growing and non-dividing cultures of Staphylococcus aureus including biofilms. *J Antimicrob Chemother* 65(1):72-78.
212. Kim JS, *et al.* (2011) Selective Killing of Bacterial Persisters by a Single Chemical Compound without Affecting Normal Antibiotic-Sensitive Cells. *Antimicrob Agents Chemother* 55(11):5380-5383.
213. Mah TF, *et al.* (2003) A genetic basis for Pseudomonas aeruginosa biofilm antibiotic resistance. *Nature* 426(6964):306-310.
214. Chua SL, *et al.* (2014) Dispersed cells represent a distinct stage in the transition from bacterial biofilm to planktonic lifestyles. *Nat Commun* 5:4462.
215. Dhal PK, Polomoscanik SC, Avila LZ, Holmes-Farley SR, & Miller RJ (2009) Functional polymers as therapeutic agents: concept to market place. *Adv Drug Deliv Rev* 61(13):1121-1130.
216. Li J, Yu F, Chen Y, & Oupicky D (2015) Polymeric drugs: Advances in the development of pharmacologically active polymers. *J Control Release*.
217. McConnell MJ, Actis L, & Pachon J (2013) Acinetobacter baumannii: human infections, factors contributing to pathogenesis and animal models. *FEMS Microbiol Rev* 37(2):130-155.
218. Dijkshoorn L, Nemec A, & Seifert H (2007) An increasing threat in hospitals: multidrug-resistant Acinetobacter baumannii. *Nat Rev Microbiol* 5(12):939-951.
219. O'Shea MK (2012) Acinetobacter in modern warfare. *Int J Antimicrob Agents* 39(5):363-375.
220. Murray CK (2008) Epidemiology of infections associated with combat-related injuries in Iraq and Afghanistan. *J Trauma* 64(3 Suppl):S232-238.
221. Jones A, *et al.* (2006) Importation of multidrug-resistant Acinetobacter spp infections with casualties from Iraq. *Lancet Infect Dis* 6(6):317-318.
222. Lebeaux D, Chauhan A, Rendueles O, & Beloin C (2013) From in vitro to in vivo Models of Bacterial Biofilm-Related Infections. *Pathogens* 2(2):288-356.
223. Rodriguez-Bano J, *et al.* (2008) Biofilm formation in Acinetobacter baumannii: associated features and clinical implications. *Clin Microbiol Infect* 14(3):276-278.
224. Pour NK, *et al.* (2011) Biofilm formation by Acinetobacter baumannii strains isolated from urinary tract infection and urinary catheters. *FEMS Immunol Med Microbiol* 62(3):328-338.
225. Longo F, Vuotto C, & Donelli G (2014) Biofilm formation in Acinetobacter baumannii. *New Microbiol* 37(2):119-127.
226. Espinal P, Marti S, & Vila J (2012) Effect of biofilm formation on the survival of Acinetobacter baumannii on dry surfaces. *J Hosp Infect* 80(1):56-60.
227. King AM, *et al.* (2014) Aspergillomarasmine A overcomes metallo-beta-lactamase antibiotic resistance. *Nature* 510(7506):503-506.
228. Ejim L, *et al.* (2011) Combinations of antibiotics and nonantibiotic drugs enhance antimicrobial efficacy. *Nat Chem Biol* 7(6):348-350.

229. Worthington RJ, Bunders CA, Reed CS, & Melander C (2012) Small molecule suppression of carbapenem resistance in NDM-1 producing Klebsiella pneumoniae. *ACS Med Chem Lett* 3(5):357-361.
230. Ribeiro SM, *et al.* (2015) Antibiofilm peptides increase the susceptibility of carbapenemase-producing Klebsiella pneumoniae clinical isolates to beta-lactam antibiotics. *Antimicrob Agents Chemother* 59(7):3906-3912.
231. Gill EE, Franco OL, & Hancock REW (2015) Antibiotic Adjuvants: Diverse Strategies for Controlling Drug-Resistant Pathogens. *Chem Biol Drug Des* 85(1):56-78.
232. Kaneti G, Meir O, & Mor A (2015) Controlling bacterial infections by inhibiting proton-dependent processes. *Biochim Biophys Acta*.
233. Taylor PL, Rossi L, De Pascale G, & Wright GD (2012) A forward chemical screen identifies antibiotic adjuvants in Escherichia coli. *ACS Chem Biol* 7(9):1547-1555.
234. Goldberg K, *et al.* (2013) Sensitization of gram-negative bacteria by targeting the membrane potential. *FASEB J* 27(9):3818-3826.
235. Ng VW, Ke X, Lee AL, Hedrick JL, & Yang YY (2013) Synergistic co-delivery of membrane-disrupting polymers with commercial antibiotics against highly opportunistic bacteria. *Adv Mater* 25(46):6730-6736.
236. Sakoulas G, *et al.* (2014) Ceftaroline restores daptomycin activity against daptomycin-nonsusceptible vancomycin-resistant Enterococcus faecium. *Antimicrob Agents Chemother* 58(3):1494-1500.
237. Harris TL, *et al.* (2014) Small molecule downregulation of PmrAB reverses lipid A modification and breaks colistin resistance. *ACS Chem Biol* 9(1):122-127.
238. Pieri C, *et al.* (2014) New Ianthelliformisamine Derivatives as Antibiotic Enhancers against Resistant Gram-Negative Bacteria. *J Med Chem* 57(10):4263-4272.
239. Zhang JY, *et al.* (2014) Antimicrobial Metallopolymers and Their Bioconjugates with Conventional Antibiotics against Multidrug-Resistant Bacteria. *J Am Chem Soc* 136(13):4873-4876.
240. Pena-Miller R, *et al.* (2013) When the Most Potent Combination of Antibiotics Selects for the Greatest Bacterial Load: The Smile-Frown Transition. *Plos Biol* 11(4).
241. Manchanda V, *et al.* (2011) Development of TaqMan real-time polymerase chain reaction for the detection of the newly emerging form of carbapenem resistance gene in clinical isolates of Escherichia coli, Klebsiella pneumoniae, and Acinetobacter baumannii. *Ind J Med Microbiol* 29(3):249-253.
242. Odds FC (2003) Synergy, antagonism, and what the chequerboard puts between them. *J Antimicrob Chemother* 52(1):1.
243. Hoffman LR, *et al.* (2005) Aminoglycoside antibiotics induce bacterial biofilm formation. *Nature* 436(7054):1171-1175.
244. Yigit H, *et al.* (2001) Novel carbapenem-hydrolyzing beta-lactamase, KPC-1, from a carbapenem-resistant strain of Klebsiella pneumoniae. *Antimicrob Agents Chemother* 45(4):1151-1161.
245. Dockter ME, Trumble WR, & Magnuson JA (1978) Membrane lateral phase separations and chlortetracycline transport by Bacillus megaterium. *Proc Natl Acad Sci U S A* 75(3):1319-1323.
246. Yamaguchi A, Ohmori H, Kaneko-Ohdera M, Nomura T, & Sawai T (1991) Delta pH-dependent accumulation of tetracycline in Escherichia coli. *Antimicrob Agents Chemother* 35(1):53-56.

247. Kashket ER (1985) The proton motive force in bacteria: a critical assessment of methods. *Annu Rev Microbiol* 39:219-242.
248. Lamers RP, Cavallari JF, & Burrows LL (2013) The efflux inhibitor phenylalanine-arginine beta-naphthylamide (PAbetaN) permeabilizes the outer membrane of gram-negative bacteria. *Plos One* 8(3):e60666.
249. Cox G, Koteva K, & Wright GD (2014) An unusual class of anthracyclines potentiate Gram-positive antibiotics in intrinsically resistant Gram-negative bacteria. *J Antimicrob Chemother* 69(7):1844-1855.
250. Fensterseifer IC, *et al.* (2015) Effects of cyclotides against cutaneous infections caused by Staphylococcus aureus. *Peptides* 63:38-42.
251. Steinstraesser L, *et al.* (2012) Innate defense regulator peptide 1018 in wound healing and wound infection. *PLoS One* 7(8):e39373.
252. Jacobsen F, *et al.* (2005) Activity of histone H1.2 in infected burn wounds. *J Antimicrob Chemother* 55(5):735-741.
253. Lima TB, *et al.* (2011) In Vivo Effects of Cagaita (Eugenia dysenterica, DC.) Leaf Extracts on Diarrhea Treatment. *Evidence-Based Complementary and Alternative Medicine*.
254. Zhang GH, Mann DM, & Tsai CM (1999) Neutralization of endotoxin in vitro and in vivo by a human lactoferrin-derived peptide. *Infect Immun* 67(3):1353-1358.
255. Rosenfeld Y & Shai Y (2006) Lipopolysaccharide (Endotoxin)-host defense antibacterial peptides interactions: role in bacterial resistance and prevention of sepsis. *Biochim Biophys Acta* 1758(9):1513-1522.
256. Rosenfeld Y, Papo N, & Shai Y (2006) Endotoxin (lipopolysaccharide) neutralization by innate immunity host-defense peptides. Peptide properties and plausible modes of action. *J Biol Chem* 281(3):1636-1643.
257. Andra J, Koch MH, Bartels R, & Brandenburg K (2004) Biophysical characterization of endotoxin inactivation by NK-2, an antimicrobial peptide derived from mammalian NK-lysin. *Antimicrob Agents Chemother* 48(5):1593-1599.
258. Gough M, Hancock REW, & Kelly NM (1996) Antiendotoxin activity of cationic peptide antimicrobial agents. *Infect Immun* 64(12):4922-4927.
259. Rosenfeld Y, Lev N, & Shai Y (2010) Effect of the hydrophobicity to net positive charge ratio on antibacterial and anti-endotoxin activities of structurally similar antimicrobial peptides. *Biochemistry* 49(5):853-861.
260. Ong ZY, Gao SJ, & Yang YY (2013) Short Synthetic beta-Sheet Forming Peptide Amphiphiles as Broad Spectrum Antimicrobials with Antibiofilm and Endotoxin Neutralizing Capabilities. *Adv Funct Mater* 23(29):3682-3692.
261. Li P, Wohland T, Ho B, & Ding JL (2004) Perturbation of lipopolysaccharide (LPS) micelles by Sushi 3 (S3) antimicrobial peptide - The importance of an intermolecular disulfide bond in S3 dimer for binding, disruption, and neutralization of LPS. *J Biol Chem* 279(48):50150-50156.
262. Wei L, *et al.* (2013) Structure and function of a potent lipopolysaccharide-binding antimicrobial and anti-inflammatory peptide. *J Med Chem* 56(9):3546-3556.
263. Brandenburg K, *et al.* (2004) Structural polymorphism and endotoxic activity of synthetic phospholipid-like amphiphiles. *Biochemistry* 43(13):4039-4046.

264. Zorko M & Jerala R (2008) Alexidine and chlorhexidine bind to lipopolysaccharide and lipoteichoic acid and prevent cell activation by antibiotics. *J Antimicrob Chemother* 62(4):730-737.
265. Bowdish DME, Davidson DJ, Scott MG, & Hancock REW (2005) Immunomodulatory activities of small host defense peptides. *Antimicrob Agents Chemother* 49(5):1727-1732.
266. Larrick JW, *et al.* (1995) Human CAP18: a novel antimicrobial lipopolysaccharide-binding protein. *Infect Immun* 63(4):1291-1297.
267. Domingues MM, *et al.* (2012) Biophysical characterization of polymyxin B interaction with LPS aggregates and membrane model systems. *Biopolymers* 98(4):338-344.
268. Domingues MM, Castanho MA, & Santos NC (2009) rBPI(21) promotes lipopolysaccharide aggregation and exerts its antimicrobial effects by (hemi)fusion of PG-containing membranes. *PLoS One* 4(12):e8385.
269. Chih YH, *et al.* (2015) Ultrashort Antimicrobial Peptides with Antiendotoxin Properties. *Antimicrob Agents Chemother* 59(8):5052-5056.
270. Murugan RN, *et al.* (2013) De novo design and synthesis of ultra-short peptidomimetic antibiotics having dual antimicrobial and anti-inflammatory activities. *PLoS One* 8(11):e80025.
271. Findlay B, Mookherjee N, & Schweizer F (2013) Ultrashort cationic lipopeptides and lipopeptoids selectively induce cytokine production in macrophages. *PLoS One* 8(2):e54280.
272. Li Y, *et al.* (2014) Lipidated cyclic gamma-AApeptides display both antimicrobial and anti-inflammatory activity. *ACS Chem Biol* 9(1):211-217.
273. Som A, *et al.* (2012) Identification of Synthetic Host Defense Peptide Mimics That Exert Dual Antimicrobial and Anti-Inflammatory Activities. *Clin Vac Immunol* 19(11):1784-1791.
274. Padhee S, *et al.* (2014) The Development of Antimicrobial a- AApeptides that Suppress Proinflammatory Immune Responses. *Chem Bio chem* 15(5):688-694.
275. Scott MG, *et al.* (2007) An anti-infective peptide that selectively modulates the innate immune response. *Nat Biotechnol* 25(4):465-472.
276. Thaker HD, *et al.* (2012) Synthetic mimics of antimicrobial peptides with immunomodulatory responses. *J Am Chem Soc* 134(27):11088-11091.
277. Guchhait G, *et al.* (2015) Amphiphilic tobramycins with immunomodulatory properties. *Angew Chem Int Ed Engl* 54(21):6278-6282.
278. Shaunak S, *et al.* (2004) Polyvalent dendrimer glucosamine conjugates prevent scar tissue formation. *Nat Biotechnol* 22(8):977-984.
279. Coleman WG, Jr., Goebel PJ, & Leive L (1977) Genetic analysis of Escherichia coli O111:B4, a strain of medical and biochemical interest. *J Bacteriol* 130(2):656-660.
280. Yu B & Wright SD (1996) Catalytic properties of lipopolysaccharide (LPS) binding protein. Transfer of LPS to soluble CD14. *J Biol Chem* 271(8):4100-4105.

List of Publications

PhD Thesis Publications

1. **Uppu DSSM**, Akkapeddi P, Manjunath GB, Yarlagadda V, Hoque J and Haldar J. (2013) Polymers with Tunable Side-chain Amphiphilicity as Non-hemolytic Antibacterial Agents. *Chem Commun* 49(82): 9389-9391.

2. **Uppu DSSM**, Manjunath GB, Yarlagadda V, Konai MM, Kaivyil JE, Ravikumar R and Haldar J (2015). Membrane-active Macromolecules Re-sensitize Tetracycline Antibiotics to Gram-negative Clinical Isolates. *PLoS One* 10(3): e0119422.

3. **Uppu DSSM**, Samaddar S, Ghosh C, Paramanandam K, Shome BR and Haldar J. (2016) Amide Side Chain Amphiphilic Polymers Disrupt Surface Established Bacterial Biofilms and Protect Mice from Chronic Acinetobacter baumannii Infection. *Biomaterials* 74, 131-143.

4. **Uppu DSSM** and Haldar J. (2016) Lipopolysaccharide Neutralization by Cationic Amphiphilic Polymers through Pseudo-aggregate Formation. *Biomacromolecules*. Under revision.

5. **Uppu DSSM**, Bhowmik M, Samaddar S and Haldar J. (2016) Cyclization and Unsaturation rather than Isomerization of Side Chains Governs the Selective Antibacterial Activity of Cationic-amphiphilic Polymers. *Chem Commun* Under revision.

6. **Uppu DSSM**, Konai MM, Baul U, Singh P, Siersma T, Samaddar S, Hoque J, Vemparala S, Hamoen LW, Paramanandham K, Shome BR, Narayana C and Haldar J. An Essential Role for Hydrogen Bonding in Bacterial Membrane Interactions. Under review.

7. **Uppu DSSM**, Samaddar S, Konai MM, Fensterseifer ICM, Farias-Junior C, Franco OL and Haldar J. Membrane-active Molecules Kill Bacterial Persisters and Potentiate Antibiotics to Biofilms. Under preparation.

Other publications

1. Hoque J, Akkapeddi P, Yarlagadda V, **Uppu DSSM**, Kumar P, and Haldar J. (2012) Cleavable Cationic Antibacterial Amphiphiles: Synthesis, Mechanism of Action, and Cytotoxicities. *Langmuir* 28(33): 12225-122234.

2. Ghosh C, Manjunath GB, Akkapeddi P, Yarlagadda V, Hoque J, **Uppu DSSM**, Konai MM, and Haldar J. (2014) Small Molecular Antibacterial Peptoid Mimics: the simpler the better! *J Med Chem* 57(4): 1428–1436.

3. Hoque J, Akkapeddi P, Yadav V, Manjunath GB, **Uppu DSSM**, Konai MM, Yarlagadda V, Sanyal K and Haldar J. (2015) Broad spectrum antibacterial and antifungal polymeric paint materials: synthesis, structure-activity relationship and membrane-active mode of action. *ACS Appl Mater Interfaces* 7(3): 1804-1815.

4. Ghosh C, Manjunath GB, Konai MM, **Uppu DSSM**, Paramanandham K, Shome BR and Haldar J. (2015) Aryl-alkyl-lysines: Agents that kill planktonic cells, persister cells, biofilms of MRSA and protect mice from skin-infection. *PLoS One* 10(12): e0144094.

5. Ghosh C, Manjunath GB, Konai MM, **Uppu DSSM**, Paramanandham K, Shome BR, Ravikumar R, and Haldar J. (2015) Aryl-alkyl-lysines: Membrane active small molecules active against murine model of burn infection. *ACS Infect Dis* DOI:10.1021/acsinfecdis.5b00092.

Patents

1. **Uppu DSSM**, Akkapeddi P, Manjunath GB and Haldar J. Nanoparticle compositions of antibacterial compounds and other uses thereof. *WO2014006601A3, EP20152870186A2, US20150238521A1*. National Phase Applications have been filed in USA, Europe and South Korea.

Book Chapters

1. **Uppu DSSM**, Hoque J and Haldar J. (2014) Engineered Polymers and Organic-inorganic Hybrids as Antimicrobial Materials for Water Disinfection. Aquananotechnology: Global Prospects, *CRC Press-Taylor and Francis Group*.
2. **Uppu DSSM**, Ghosh C and Haldar J. (2015) Alternative Strategies to Target Quorum Sensing (QS): Combination of QS Inhibitors with Antibiotics and Nanotechnological Approaches. Quorum Sensing vs Quorum Quenching: A battle with no end in sight, *Springer*.

Review

1. **Uppu DSSM**, Ghosh C and Haldar J. (2015) Surviving sepsis in the era of antibiotic resistance: Are there any alternative approaches to antibiotic therapy? *Microb Pathog* 80: 7-13.